

**PROBABILISTIC SAFETY ANALYSIS USING TRAFFIC
MICROSCOPIC SIMULATION**

Carlos Miguel Lima de Azevedo

Supervisor: Doctor João Paulo Lourenço Cardoso

Co-Supervisors: Doctor Moshe E. Ben-Akiva

Doctor Filipe Manuel Mercier Vilaça e Moura

**Thesis approved in public session to obtain the PhD Degree in
Transportation Systems**

Jury final classification: Pass with Merit

Jury

Chairperson: Chairman of the IST Scientific Board

Members of the Committee:

Doctor Luís Guilherme de Picado Santos

Doctor Carlos Manuel Robalo Lisboa Bento

Doctor João Paulo Lourenço Cardoso

Doctor José Pedro Maia Pimentel Tavares

Doctor João António de Abreu e Silva

Doctor Luís Miguel Garrido Martinez

INSTITUTO SUPERIOR TÉCNICO**PROBABILISTIC SAFETY ANALYSIS USING TRAFFIC
MICROSCOPIC SIMULATION**

Carlos Miguel Lima de Azevedo

Supervisor: Doctor João Paulo Lourenço Cardoso

Co-Supervisors: Doctor Moshe E. Ben-Akiva

Doctor Filipe Manuel Mercier Vilaça e Moura

**Thesis approved in public session to obtain the PhD Degree in
Transportation Systems**

Jury final classification: Pass with Merit

Jury

Chairperson: Chairman of the IST Scientific Board

Members of the Committee:

Doctor Luís Guilherme de Picado Santos, Full Professor of the Instituto Superior Técnico, University of Lisbon;

Doctor Carlos Manuel Robalo Lisboa Bento, Associate Professor (with Habilitation) of the Faculty of Science and Technology of the University of Coimbra;

Doctor João Paulo Lourenço Cardoso, Principal Investigator (Habilitation to Research Coordination) of the National Laboratory of Civil Engineering;

Doctor José Pedro Maia Pimentel Tavares, Assistant Professor of the Faculty of Engineering of the University of Porto;

Doctor João António de Abreu e Silva, Invited Assistant Professor of the Instituto Superior Técnico, University of Lisbon;

Doctor Luís Miguel Garrido Martinez, Invited Assistant Professor of the Instituto Superior Técnico, University of Lisbon.

INSTITUIÇÕES FINANCIADORAS

Abstract

Traffic microscopic simulation applications are currently a common tool in road system analysis and several application attempts to safety performance assessment have been recently carried out. However, current most common approaches still ignore causal relationships between different levels of vehicle interactions or accident types, lacking for a physical representation of the accident phenomena itself.

A new generic probabilistic safety assessment framework for traffic microscopic simulation tools is proposed. The probability of a specific accident occurrence is assumed to be estimable by an accident propensity function, composed by a deterministic safety score component and a random component. The formulation of the safety score component may be specified depending on the type of occurrence and on the simulation features. The generic model is then specified for the case of urban motorways for no-accident events and three types of accidents: rear-end, lane-changing and run-off-road accidents.

To deal with the lack of available trajectory data for different occurrence types, artificial trajectories from a calibrated microscopic simulation tool are used. These trajectories are obtained following a comprehensive calibration effort: extracting trajectories for a generic scenario, calibration of the simulation tool using the collected trajectories, and re-calibration of the simulation model using aggregate data for each event selected at replication. An advanced method for automatic extraction of vehicle trajectories using aerial imagery is presented, in order to collect the detailed traffic variables. A global sensitivity analysis based calibration is proposed to deal with uncertainty in the detailed calibration of complex models.

The parameters of the safety model are estimated using artificial vehicle trajectory data calibrated for the Portuguese A44 motorway and using the **MITSIMLab** simulator. With this study it is shown how traffic microsimulation tools may replicate detailed traffic statistics that are essential to explain different accident phenomenon and how the quality of this replication is strongly linked to the simulation modelling formulation, the calibration methodology and the available data.

Key-words: traffic microscopic simulation; road safety; probabilistic assessment; driving behaviour modeling; surrogate safety measures; discrete choice; global sensitivity analysis; calibration; vehicle tracking; remote sensing.

Resumo

As aplicações de simulação microscópica de tráfego representam, hoje em dia, uma ferramenta importante na análise de sistemas de transporte. Recentemente, várias tentativas de aplicação destes recursos para a avaliação do desempenho em segurança rodoviária foram concretizadas. No entanto, as abordagens mais comuns ainda carecem da explicitação de relações causa-efeito, não só relativamente às diferentes interações entre veículos como também na representação física da ocorrência de vários tipos de acidentes.

Neste estudo é proposto um novo modelo genérico de avaliação probabilística da segurança rodoviária para integração em ferramentas de simulação microscópica de tráfego. A probabilidade de ocorrência de um determinado evento é definida em função de uma componente determinística, designada por grau de segurança, e de uma componente aleatória. O grau de segurança é especificado consoante o tipo de ocorrência, tendo em conta as características específicas do simulador utilizado. Este modelo genérico é pormenorizado para as auto-estradas urbanas considerando os eventos de não-acidente e três tipos de acidentes: colisões traseiras, colisões laterais associadas a mudanças de via e despistes.

Visto não existirem ainda dados de trajetórias de veículos para diferentes tipos de ocorrência, na estimação do modelo proposto foram utilizadas trajetórias artificiais geradas através de um simulador microscópico de tráfego. Estes dados foram obtidos após um processo de calibração avançada: extração de trajetórias para um cenário genérico, calibração do simulador com base nestas trajetórias, e nova calibração do modelo para cada um dos eventos a replicar. Para o efeito foram desenvolvidos um algoritmo de extração automática de trajetórias de veículos registados em imagens aéreas e um método inovador de calibração de modelos complexos baseado em análise de sensibilidade global.

Os parâmetros do modelo de segurança são estimados usando dados recolhidos para a auto-estrada A44, em Portugal, e usando o simulador de tráfego MITSIMLab. É demonstrado o potencial da simulação microscópica em replicar estatísticas detalhadas de tráfego, essenciais na modelação de diferentes tipos de acidente, e a sua dependência relativamente à especificação do modelo de simulação, metodologia de calibração e dados disponíveis.

Palavras-chave: simulação microscópica de tráfego; segurança rodoviária; análise probabilística; modelação do comportamento do condutor; indicadores de segurança; modelos discretos; análise de sensibilidade; calibração; seguimento de veículos; sensor remoto.

Acknowledgements

I would like to express my sincere gratitude to Prof. João Cardoso and Prof. Moshe Ben-Akiva for their continuous guidance, support and friendship. It has been a privilege to work with both of them and have the opportunity to learn from their vast knowledge. I am also thankful to Prof. Filipe Moura whom interest and guidance was a source of inspiration.

Dr. Biagio Ciuffo from the Joint Research Center deserves a very special thanks as his helpful guidance for more than a year allowed to acquire a strong knowledge in uncertainty analysis. Some parts of this thesis were joint work with Biagio and under the EU Commission's Cost Action TU0903 (Multitude). His technical and practical insights for making the complex things tractable were invaluable for the presented and future research. Also, this dissertation could not be completed without the generous help of Prof. João Costeira and Dr. Manuel Marques from the Institute for Systems and Robotics at IST, without whom I would not have discovered the potential and fun of image processing.

I am thankful to my colleagues from the National Laboratory of Civil Engineering (LNEC) who helped me in the arduous task of collecting and processing a considerable amount of data: José Gil, Cristina Sousa, Cristina Cabral, Paulo Miranda, Francisco Cavaleiro, José Carmo, Óscar López, Ivan Lopes and Acácio Monteiro. A special thanks to the Portuguese National Grid Initiative and namely to João Martins and Gonçalo Borges for the use of one of the most advanced computational infrastructures for research in Portugal; to Ge Qiao from ETH Zurich for his precious help on the EE design; and to Lu Lu from MIT for providing part of the code used in the WSPSA calibration.

I am grateful to LNEC and to the Department of Transportation for hosting me, providing the resources used in this research, and funding my scholarship jointly with the Fundação para a Ciência e Tecnologia through the MIT Portugal Program. I am also thankful to InfoPortugal, S.A. for the precious help in the aerial image collection,

especially to Alexandre Gomes for the help in the data processing and for distracting me when I first saw the size of the aircraft we had to fly in; to José Luís Almeida Garret from LNEC for developing the electronic trigger used in the sequential photo shooting; and to Ascendi, S.A. for providing the traffic data used in this thesis.

The guidance and motivation from my close friends at LNEC, Sandra Vieira, André Paixão, Elisabete Arsénio, Francesca De Chiara, Carlos A. Roque, Sofia Azeredo and Simona Fontul also deserve my heartfelt acknowledgments. Thanks also to Prof. João Barros from University of Porto and Prof. Tomer Toledo from Technion Israel Institute of Technology for their crucial motivation and advice regarding my career and research.

I must admit that my personal and professional experience during my stays at the Massachusetts Institute of Technology (MIT) could not have been better. I am grateful to MIT for hosting and supporting this research and to my colleagues and friends from Boston that helped me in so many ways during this long process: Maya Abou Zeid for your friendship and clear and enthusiastic guidance; Li Qu for helping me during my my first steps with simulation; Ásbjörg Kristinsdóttir for turning the dream of living in the best neighbourhood of Boston and with best flatmate ever into reality; my very good friends Travis Dunn, Christopher Grilo and Tina Xue whom helped me become so passionate about the US; Varun Pattabhiraman and Vikrant Vaze thanks for your constant cheerful and interested attitude; Ana Laura, João Zeferino and João Pita for keeping Portugal closer during my stay in America; and a very special thanks to my friend Alda Metrass for being my closest comrade during this five year project. I was also fortunate to have an amazing group of old friends back home who were always there: Rodrigo, Carlos, Roberto, Rafa and Luís Miguel.

I could not have reached this point in my life without the love and care of my family. I am grateful to my mother Cremilda, who showed me that happiness and dreams in life are always attainable, and to my dad Rui that always supported, guided and cared about me during this tough years; to my dearest sister Inês for being the best sister ever and always encouraging me to take the most challenging options without fear; to my brother-in-law Pedro for always making me think ahead; and my little brother Marc and Elsa for making family time the best ever.

Above all, I am grateful to my beloved Tânia who has been my best friend and companion since the very beginning.

Contents

1	Introduction	20
1.1	Motivation	20
1.2	Objectives	23
1.3	Thesis Outline	24
2	Literature Review	26
2.1	Safety modelling	26
2.1.1	A short historical perspective on safety modelling	26
2.1.2	Accident frequency models	27
2.1.3	Accident injury-severity models	33
2.1.4	Accident probability models	39
2.1.5	Surrogate safety indicators	43
2.1.6	Probabilistic frameworks	53
2.2	Traffic Microscopic Simulation	54
2.2.1	Driving behaviour models	54
2.2.2	Data used for estimation and calibration	67
2.2.3	Simulation tools	67
2.3	Safety studies using simulation	70
2.4	Simulation applications in Portugal	75
2.5	General comments	78
3	Modelling Framework	80
3.1	General modelling assumptions	80
3.2	General model structure	81
3.3	Model components	84

3.3.1	Rear-end (RE) conflicts	84
3.3.2	Lane change (LC) conflicts	87
3.3.3	Run-off-road (ROR) events	89
3.4	Estimation framework	91
3.5	Model limitations and possible enhancements	97
4	The Case Study	101
4.1	General description of the pilot site	101
4.2	Sensor Data	103
4.3	Demand Data	108
4.4	Incident Data	120
4.5	Other Data	123
4.6	Comments	124
5	Trajectory Extraction	125
5.1	General Aspects	125
5.2	Image-based Trajectory Extraction Methods	128
5.2.1	Static observations	128
5.2.2	Dynamic observations	129
5.2.3	Image processing algorithms for vehicle tracking	131
5.3	Data Collection System	133
5.4	Image Processing	134
5.5	Vehicle Tracking	138
5.5.1	Graph construction	140
5.5.2	The k -shortest disjoint paths algorithm	144
5.6	Results	147
5.7	Discussion	149
6	Microsimulation Application	152
6.1	MITSIMLab	152
6.2	Sensitivity Analysis	155
6.2.1	Sensitivity analysis in traffic micro-simulation studies	155
6.2.2	A multi-step global sensitivity analysis	158
6.2.3	Variance-based methods on the Sobol decomposition of variance . .	160

6.2.4	Sensitivity analysis using aggregated data	163
6.2.5	Sensitivity analysis using detailed trajectory data	169
6.3	Calibration of Sensitive Parameters	186
6.3.1	A Kriging metamodel approach	187
6.3.2	Testing the calibration using aggregated data	188
6.3.3	Testing the calibration using trajectory data	193
6.4	Event-specific Calibration	201
6.4.1	Weighted-Simultaneous Perturbation Stochastic Approximation . .	202
6.4.2	WSPSA test	205
6.5	Concluding remarks	210
7	Safety Modelling Results	212
7.1	Data for estimation	212
7.1.1	Accident event starting times	212
7.1.2	Sampling	213
7.1.3	Simulation parameter values	214
7.1.4	Artificial Data generation	217
7.1.5	Modelling assumptions	219
7.2	Results	222
7.2.1	The Aggregated Model (AM)	223
7.2.2	The Disaggregated Model (DM)	226
7.3	Validation	228
7.4	General Comments	229
8	Conclusions	232
8.1	Research Summary	232
8.2	Directions for Future Research	235
	Bibliography	240
	A Integrated driving behaviour model	264
	B Driving Behaviour Model Parameters List & Numbering	271
	C Changes in MITSIM code	280

List of Figures

2-1	Estimated total accidents per million vehicle miles of travel by traffic flow regimes plotted in standardized space of (x) median speed vs. (y) variation in speeds in left and interior lanes (Golob et al., 2004).	43
2-2	The safety pyramid (Hydén, 1987)	45
2-3	Time-space diagram for a typical left-turn conflict (Allen et al., 1978). . . .	47
2-4	The Wiedemann psycho-physical model	59
2-5	Two-step calibration approach (Huang et al., 2013)	74
3-1	Model structure for motorway accident occurrence	83
3-2	Rear-end Interaction	84
3-3	Vehicle interaction in car-following behaviour	86
3-4	Lateral Interaction	88
3-5	Run-off-road event	90
3-6	Estimation framework	95
4-1	A44 network and data collection stations.	103
4-2	Five minutes loop sensor data for 2007.	107
4-3	Monitored sections for stopping time measurements	111
4-4	Average stopping times at different intersections	112
4-5	Sampling at entry and exit stations	116
4-6	Seed OD dynamic matrix for light vehicles (am period)	119
4-7	Sample of the GIS accident database	123
5-1	Sample of a part of an aerial image taken by the Digicam camera	134
5-2	Rosin's Uni-modal Threshold (adapted from Rosin (2001))	136
5-3	Image processing steps	138
5-4	Generic multiple object tracking (adapted from Berclaz et al. (2011)) . . .	140

5-5	Dual graph construction	142
5-6	Suurballe General Framework	146
5-7	Empirical CDF of traffic variables	148
5-8	Tracking results for lane 1 (left) and 2 (right) in the S-N direction	150
5-9	Tracking results for lane 1 (left) and 2 (right) in the S-N direction	151
6-1	Multi-step Sensitivity Analysis Framework	158
6-2	Group analysis bar plots of first (white) and total (black) order sensitivity indices based on the Theil coefficient, using counts (left) and speed (right) profiles	165
6-3	Final analysis bar plots of total order sensitivity indices on the Theil coefficient, using counts (left) and speed (right) profiles	167
6-4	Counts vs. speed Theil inequality coefficient	169
6-5	Group analysis bar plots of first (white) and total (black) order sensitivity indices on the Theil coefficient of trajectory based MoP (1)	172
6-6	Group analysis bar plots of first (white) and total (black) order sensitivity indices on the Theil coefficient of trajectory based MoP (2). Grey lines are the 90% confidence intervals.	173
6-7	Convergence of total order sensitivity indices on the Theil coefficient of speed and TTC trajectory based MoP	176
6-8	Absolute mean $\mu_{EE_i}^*$ vs. standard deviation σ_{EE_i} example	179
6-9	Ranking of the 56 parameter subset based on the μ_{EE}^* value for all 11 computed GoF	180
6-10	Final analysis bar plots of first (white) and total (black) order sensitivity indices on the Theil coefficient of trajectory based MoP (1)	183
6-11	Final analysis bar plots of first (white) and total (black) order sensitivity indices on the Theil coefficient of trajectory based MoP (2)	184
6-12	Counts vs. speed Theil inequality coefficient values for the simulated and Kriging estimates	189
6-13	Simulated (grey) vs. true (black) counts (top) and average speed (bottom) (1)	190
6-14	Simulated (grey) vs. true (black) counts (top) and average speed (bottom) for the loop-based calibration	191

6-15	CDF for different detailed traffic variables for the 30 best combinations of the loop-based calibration (grey) and real data (black)	192
6-16	CDF in the right lane of two-lane sections, grade between 0 and +2%, speed-limit over 100 km/h and light traffic for the 30 best combinations of the loop-based calibration (grey) and real data (black)	193
6-17	CDF in the left lane of two-lane sections (w/ acc. lane), grade lower than -2%, speed-limit over 100 km/h and low traffic for the 30 best combinations of the loop-based calibration (grey) and real data (black)	194
6-18	Theil inequality coefficient values for the simulated and Kriging estimates for different output pairs	195
6-19	Simulated (grey) vs. true (dark) counts (top) and average speed (bottom) for the 30 best combinations of the trajectory-based calibration (grey) and real data (black)	196
6-20	CDF for different detailed traffics variables for the 30 best combinations of the trajectory-based calibration (grey) and real data (black)	198
6-21	CDF in the right lane of two-lane sections, grade between 0 and +2%, speed-limit over 100 km/h and light traffic for the 30 best combinations of the trajectory-based calibration (grey) and real data (black)	199
6-22	CDF in the left lane of two-lane sections (w/ acc. lane), grade lower than -2%, speed-limit over 100 km/h and low traffic conditions for the 30 best combinations of the trajectory-based calibration (grey) and real data (black)	199
6-23	WSPSA test performance for a specific event calibration	208
6-24	WSPSA test performance for a specific event calibration	209
7-1	Accident occurrence detection example	213
7-2	Histogram of accident time record delays and log-normal fit	213
7-3	Distribution of the RMSNE reduction rates for counts (green) and average speed (blue) during the events calibration	215
7-4	Distribution of calibrated parameters for accident (red) and non-accident (grey) events	216
7-5	Distribution of simulated variables for accident (red) and non-accident (grey) occurrences	220

A-1	Structure of the integrated driving behaviour model	265
-----	---------------------------------------------------------------	-----

List of Tables

2.1	Simulation Tools and its models	68
2.2	Simulation Tool Features (extended from Gettman and Head (2003a)) . .	69
4.1	Errors in the speed database	104
4.2	Time-series errors	105
4.3	DSA parameters	106
4.4	Map of OD stations coverage for plate number collection	111
4.5	Main statistics for the Seed OD optimisation	118
4.6	Weighting of the objective function (light vehicles, a.m. period)	118
4.7	Accident database description	121
5.1	RMSPE (%) for different weights combination and MoP	143
6.1	Best Theil's Inequality Coefficient values for both trajectory-based and sensor-based calibrations	200
6.2	Test calibration setup	207
7.1	Events sampling	214
7.2	Statistics of variables related to artificial trajectories for the 5 min before accident occurrences	218
7.3	Statistics of variables related to artificial trajectories for the 5 min before non-accident occurrences	218
7.4	Estimation results for the AM Model	224
7.5	Estimation results for the DM Model	226
7.6	Probability ratios	229
7.7	Summary of predictive performance (%)	229
B.1	List of MITSIMLab driving behaviour parameters	272

B.2	Numbering of parameters for the SA using loop-based data	276
B.3	Numbering of parameters for the SA using trajectory-based data	278

Chapter 1

Introduction

1.1 Motivation

Road accidents have long been identified as one of the major causes of death and injury in the world. Each year nearly 1.25 million people die as a result of a road traffic accidents, summing up to more than 3000 deaths each day (WHO, 2013). These figures will continue to rise despite recent efforts and achievements in the traditionally motorized countries, particularly due to the increasing car ownership and use in developing countries. In fact, the number of road fatalities in the European Union dropped from 57,691 deaths to an estimated 30,108 deaths between 1999 and 2011. In the United States, the U.S. Department of Transportation's National Highway Traffic Safety Administration (NHTSA) reported a total of 32,367 highway deaths in 2011, marking the lowest level since 1949 (NHTSA, 2012). These figures are still not satisfactory and several national and international efforts are being made to make our roads safer. The World Health Organization, for example, defined as goal for this decade to stabilize and reduce the increasing global trend in road traffic fatalities, saving an estimated 5 million lives until 2020 (WHO, 2011). In Europe, the EU Commission also has set as target halving the overall number of road deaths in the European Union by 2020 starting from 2010 (EUCommission, 2010). In Portugal 29,867 corporal accidents were recorded in 2012 by the National Road Safety Authority (ANSR) summing up to 573 deaths, 2,060 severe injuries and 36,190 slight injuries (ANSR, 2013). These statistics are the lowest values since 1975 but, although the positive effect of multiple national road safety efforts are undeniable, these recent figures have also been affect by the economic conditions of the past years.

Along with these uncomfortable statistics, road transportation research and policy has also struggled to reduce congestion. Congestion in the EU is estimated to affect 10 % of the road network, and yearly costs amount to 0.9-1.5 % of the EU GDP (CEMT/ITF, 2007). For the US, the Texas A&M Transportation Institute (TTI) estimated a congestion cost of 121 billion USD for 2011, due to mainly additional fuel consumption and 5.5 billion additional hours in traffic (Schrang et al., 2012). Furthermore, the two phenomenons (accidents and congestion) are related. Induced congestion may result from accidents and a complex "accidents related to congestion" phenomenon comes into play, namely due to both a sudden reduction in speed and a higher vehicle interaction exposure. Nevertheless, traffic incidents have been identified as a major contributor to congestion. In 2006, the National Traffic Incident Management Coalition (NTIMC) estimated that traffic incidents are the cause of about one-quarter of the congestion on all roadways in the US, and that for every minute a freeway lane is blocked due to an incident, there is an increase of 4 minutes in travel delay time (NTIMC, 2006).

The use of Intelligent Transportation Systems (ITS) has long been identified as one key solution to reduce congestion and accident rates in existing road networks. For example, early German figures reported that variable speed limits (VSL) reduced the number of accidents by 30 % and increased capacity by 5 to 10 % by stabilising traffic flow (BMV BW, 1998). More recently, the TTI calculated that in 2007, on the roads where improved incident management procedures were implemented (in a total of 272 out of the 439 monitored urban areas) the resulting reduction in incident-related congestion saved 143.3 million hours and \$3.06 million (Schrang et al., 2012). Currently, several international and national road safety programs scheduled a specific ITS deployment and research agenda. The EU Commission, for example, has committed to "further assess the impact and benefits of co-operative systems to identify most beneficial applications and recommend the relevant measures for their synchronised deployment" within its latest safety program (EU Commission, 2010). With the increased confidence on the benefits of such measures, the interest in quantifying its effects and optimize its design grew rapidly. It is assumed that the costs and public acceptance associated with the test and the implementation of these transportation systems is typically high, especially if safety impacts are at stake. Field experiments are therefore implemented only sparingly and the resulting conclusions are generally limited to the specific conditions observed at the experimented site.

Traffic microscopic simulation tools have been widely applied and its development has been significantly intensified in the recent years. It is now accepted as the main tool for the design of several ITS solutions and for its assessment by transportation researchers and practitioners. These tools incorporate several driving behaviour models that simulate vehicle movements, drivers decisions and road agent interactions at a very detailed level. The level of detail considered in driving behavior models is particularly critical when disaggregated relations between vehicles are more important than the aggregate traffic flow characteristics, such as in detailed safety assessments (Toledo, 2003). The driving behavior models typically include acceleration, lane-changing, route choice models and even more detailed features such as courtesy yielding or target gap selection models that were estimated based on a few (typically just one) sets of trajectory data. Due to the complex nature of traffic systems, to the level of detail reached by several proposed models and to the limited data used for its estimation, the calibration task has gained an increased importance in the application of microscopic simulation tools. However, it is well established by the research community that the calibration task of such complex models is as crucial as it is challenging. In fact, in traffic applications several aspects affect the calibration performance: the measure of performance chosen to depict traffic behaviour, the nature of the available data, the sub-set of parameters used in the calibration task, the specific traffic simulation model applied, the traffic scenario to be simulated, etc (Punzo and Ciuffo, 2009). As a consequence of this complexity, most studies did not investigate these issues in depth; instead the main focus has been on the performance of the optimization algorithm. More importantly, in such studies, algorithm performances are evaluated in terms of convergence time or model fitting by directly calibrating models against real traffic data making it hard to evaluate if a satisfactory control over the full set of uncertainty sources was achieved.

The difficulty in replicating detailed traffic variables in traffic microscopic simulation tools has also hampered its application to safety analysis, especially when compared with network traffic performance analysis. In fact, there is a clear gap between the solid research on classical accident statistical analysis (such as accident frequency and injury-severity modelling) and the very recent developments in safety assessment using simulation. Surrogate safety models and a few real-time accident probability models are the two main research streams that have emerged very recently with satisfactory

results, especially as regards intersections, where the importance of vehicle interactions is more straightforwardly recognized. However, surrogate safety assessment methods are originally based in traffic conflict techniques and a robust link between conflicts and the estimation of accident occurrence is still not available (Tarko et al., 2009). On the other hand, real-time accident probability models are typically formulated using aggregated data, especially from traffic sensing technology, such as loops and cameras, and therefore, do not account for vehicle driver interactions specifically.

The research presented in this dissertation explores how microscopic simulation models can replicate detailed traffic data and if the generated data can be used in probabilistic safety assessments.

1.2 Objectives

The main focus of this research is to extend the knowledge on the use of traffic microscopic simulation tools to model accident probability. To this aim, the test of advanced calibration and data collection methods in the replication of vehicle interactions and the development of a general framework for accident probability estimation in a traffic microscopic simulation environment is presented. The following five specific main objectives are covered in this work:

- *Understand the true potential of driving behaviour models for the replication of driving mechanisms and measurements of relevant statistics of vehicle interactions.* By first reviewing the theory behind several state-of-the-art safety modelling approaches, the capability of different advanced driving behaviour formulations to model detailed vehicle interactions is analysed, considering not only their estimation frameworks but also several existing case study applications;
- *Develop a method for robust and efficient collection of vehicle interaction data and test its usefulness in the calibration task.* The lack of detailed vehicle trajectory data has been one of the major obstacles in the development of detailed driving behaviour models and only a few sets are available worldwide. However, with the recent developments in image processing and aerial remote sensing, the (computational and budgetary) resources needed for such task are now much more accessible. This document will explore the application of advanced methods and innovative

algorithms to collect the first trajectory data set for Portugal;

- *Develop a calibration framework to evaluate the uncertainty* of the full set of driving behaviour model parameters, for different optimization performance measures and different types of traffic data. This fundamental aspect in traffic simulation has been often neglected by previous studies, where very simple calibration methods have led to uncontrolled systems and uncertain results. In the current study, the treatment of uncertainty of complex models is discussed and an innovative approach for global calibration is proposed and tested for different objective functions, input data sets and goodness-of-fit measures;
- *Develop an integrated modelling framework for probabilistic safety assessment* of different types of accidents, based on detailed microscopic vehicle interactions. Within this objective, a flexible probabilistic structure allowing for the integration of different vehicle interactions potentially leading to multiple types of accidents is developed. During this process, two key aspects are used as main strategies: an homogeneous formulation, for modelling consistency, and the possibility of specifying diversified components to allow for different accident phenomena;
- *Estimate and test a specific accident probability model formulation for urban motorways*. All methods developed under the previous research efforts are applied to a specific case study, using real data collected for the urban motorway A44, in the region of Porto, Portugal, and the simulation tool **MITSIMLab**.

1.3 Thesis Outline

The present dissertation is structured in eight chapters. In Chapter 2 the main road safety modelling and traffic microscopic simulation research developments are presented. A special attention is given to real-time accident probability models and surrogate safety measures proposed in recent years. A detailed overview of driving behaviour models and integrated simulation platforms is also presented and the state-of-practice in applying traffic simulation for safety assessment is analysed.

In Chapter 3 a conceptual framework for probabilistic safety assessment based on simulated vehicle interactions from microscopic traffic simulation is presented. The general safety concepts assumed for modelling formulation are discussed and the model compo-

nents for the specific case of urban motorways are presented. Finally, a framework for its estimation is also presented.

Chapter 4 presents the urban motorway case study used for model estimation and the steps needed for its appropriate simulation in a traffic microscopic simulation environment. The extensive traffic and safety data collection campaign carried out in this study is also described. This Chapter is complemented by Chapter 5, in which trajectory data collection methods recently developed are discussed and a recent method for object tracking is adapted and applied to the case of vehicle tracking using aerial remote sensing.

In Chapter 6 the calibration process of microscopic simulation tools is carefully followed through. A specific advanced microscopic simulation tool is presented and its selection for the application in the presented case study is discussed. An innovative sensitivity analysis-based method is used to simultaneously assess the influence and estimate the most appropriate values of all its driving behaviour model parameters. The replication of observed variables is then validated and an advanced calibration algorithm is tested in the simultaneous demand-supply calibration for artificial data generation.

In Chapter 7 the results of the estimation of the probabilistic model proposed in Chapter 3 are presented and validated.

Finally, Chapter 8 summarizes the major contributions of this research along with general conclusions and recommendations on the use of simulation tools for safety assessment.

Chapter 2

Literature Review

The task of using microscopic simulation for safety assessment presents itself as a complex problem. In fact, besides the complexity inherent from the accident occurrence mechanisms, simulation platforms are sophisticated frameworks typically relying in a multitude of stochastic sub-models originally designed to replicate traffic operations. In this Chapter important notions on how the traffic engineering research community has modelled accidents is firstly discussed, with a special emphasis on real-time accident probability models and surrogate safety indicators. Subsequently, a detailed overview of driving behaviour models and integrated simulation platforms is presented. Lastly, the bridge between these two research streams is analyzed and the state-of-the-art in applying traffic simulation for safety assessment is dissected.

2.1 Safety modelling

2.1.1 A short historical perspective on safety modelling

Since the well known Ladislaus Bortkiewicz's "Law of Small Numbers" (Bortkiewicz, 1898), where the Poisson distribution was used in the description of number of men killed by horse kicks in the Prussian Army, many statistical models were developed for rare events and accident analysis. However, it took a few decades to see the birth of the first models depending on a set of specific individual attributes (Pólya, 1930). According to this first model, the probability of another accident increases with the number of accidents which have already occurred. This accident proneness theory launched the accident frequency modelling in the field of behavioural psychology, in the late 40's and early 50's,

and the first road accident models soon came forth, such as the study presented by Smeed (Smeed, 1949), where the distribution of “accident proneness” amongst different British driver communities was analysed. These first models were based on probabilistic models, where an accident was considered to be a combination of events, each with a specific probability and a distribution. During the next decades, the normal regression model, the Poisson regression model, the analysis of variance and correlation methods were largely used for road accident frequency estimation. The traffic volume was foremost used as independent variable; then, detailed variables started to be specified in models formulation, such as road characteristics (Lundy, 1964), weather or traffic conditions (Jones and Goolsby, 1970). As these models were being developed, researchers identified the need for different model architectures according to the specific purpose of their studies: assessment of particular safety measures effectiveness, general aggregate accident frequency estimation, local-specific or type-specific accident estimation, etc. In this section, the state-of-the-art of five safety modelling streams are briefly described, with a focus on driving behaviour related variables: accident frequency models, accident injury-severity models, accident probability models and surrogate safety indicators.

2.1.2 Accident frequency models

With the absence of detailed vehicle dynamics data (such as trajectories) and driving behaviour information that would better enable a thorough identification of cause-effect relationships in accident analysis, researchers have framed their novel safety analytic approaches to a limited set of factors that relate to the aggregate number of registered accidents at specific space and/or time units. In two recent and comprehensive literature reviews (Lord et al., 2010b, Elvik, 2011) several different statistical approaches for modelling accident frequency data were documented and a briefly description is presented in this section.

Regression models

The most common approach in accident frequency modelling formulates the interaction between road geometry, traffic characteristics (namely the annual average daily traffic, AADT) and accident frequencies by means of general linear regression models. The

general formula may be specified as:

$$h(y_i) = \sum_j \beta_j X_{ij} \quad (2.1)$$

where h is called the link function between the expected value of the dependent variable $E[y_i]$ and a linear regression by a monotonic function that specifies the statistical nature of the model, X_i are the independent variables and β_j are the model parameters to be estimated. Maximum likelihood estimation and Bayesian methods are the two most common estimation methods used for this type of models. The main differences within this modelling technique rely on the chosen distribution specified for the regression model and the independent variables available.

Poisson regression: As referred earlier the Poisson distribution (see equation 2.2) and its extensions have been widely used for several decades.

$$\Pr(y_i) = e^{-E[y_i]} \cdot \frac{E[y_i]^{y_i}}{y_i!} = e^{y_i \beta_j X_{ij} - e^{\beta_j X_{ij}} - \log(y_i!)} \quad (2.2)$$

where $P(y_i)$ is the probability of entity i having y_i accidents and $E[y_i]$ is the expected number of accidents which is formulated as a function of explanatory variables $E[y_i] = e^{\beta_j X_{ij}}$. Researchers have often found that accident data exhibit characteristics that make the application of the simple Poisson regression (as well as some extensions of the Poisson model) problematic. In fact, Poisson models cannot handle over and under-dispersion and they may result in biased estimates when dealing with small samples.

Negative-binomial regression: The Negative-binomial (or Poisson-gamma) model is an extension of the Poisson model that accepts over-dispersion in the data. This presence of greater variability in a data set is assumed when the variables variance is higher than its average value and may be linked to many different aspects: accident probability variability, data aggregation, temporal correlations, measurement errors or omitted variables in the model formulation. This is a common characteristic of the accident frequency variable resulting in the inadequacy of the Poisson applications which, by definition, restricts the variance and average values to be equal. The Negative-binomial is derived by rewriting the Poisson parameter as $E[y_i] = e^{\beta_j X_{ij} + \varepsilon_i}$, where e^{ε_i} is a gamma-distributed error term

with mean 1 and variance α (Lord, 2006). The probability $\Pr(y_i)$ can be re-written as:

$$\Pr(y_i, \alpha) = \frac{\Gamma(y_i + \alpha^{-1})}{\Gamma(\alpha^{-1}) y_i!} \left(\frac{\alpha^{-1}}{E[y_i] + \alpha^{-1}} \right)^{\alpha^{-1}} \left(\frac{E[y_i]}{E[y_i] + \alpha^{-1}} \right)^{y_i} \quad (2.3)$$

where α is the dispersion parameter of the negative-binomial distribution and Γ is the gamma function. Both Poisson and Negative-binomial models have been widely used by the research community and in policy analysis. In Portugal, these models have been applied for many different traffic scenarios, ranging from two-way two-lane single carriageway highways (Cardoso, 1996), motorways (Azeredo Lopes and Cardoso, 2009), intersections (Gomes et al., 2012) and urban roads (Ferreira and Couto, 2013).

Poisson-log-normal regression: The Poisson-log-normal approach is similar to the negative binomial model, but using a log-normal distributed e^{ε_i} . One of its main features, is that it accounts for correlation between observations, for example, from the same site. In practice, omitted variables (such as sight distances) may simultaneously affect all accident count observations for a particular road segment. Although the Poisson-log-normal potentially offers more flexibility than the negative-binomial, the model estimation process is more complex due to its non-closed form, resulting in the need of full Bayesian methods for its estimation, such as the Markov Chain Monte Carlo (MCMC). For mathematical details and implementation the reader may refer to Ma et al. (2008).

Zero-inflated Poisson and zero-inflated Negative-binomial: Zero-inflated models have been developed to handle data characterized by a significant amount of zeros or more zeros than one would expect in a traditional Poisson or Negative-binomial model. These models are constructed by specifying the probability of an entity being in zero or non-zero states by means of binary logit (or probit) models (see Lambert (1992) for the derivation of the maximum likelihood estimator).

$$\Pr(y_i, p_i) = \begin{cases} 0 & \text{with probability } p_i \\ \Pr_{Poisson}(y_i) & \text{with probability } (1 - p_i) \end{cases} \quad (2.4)$$

$$\Pr(y_i, p_i) = \sum_{y_i=0} \log \left(e^{\text{logit}(p_i)} + \exp \left(-e^{\beta_j X_{ij}} \right) \right) + \sum_{y_i>0} \left(y_i \beta_j X_{ij} - e^{\beta_j X_{ij}} \right) - \sum_{i=1}^n \log(1 + \text{logit}(p_i)) - \sum_{y_i>0} \log(y_i!) \quad (2.5)$$

Conway–Maxwell–Poisson regression: The Conway–Maxwell–Poisson distribution is a generalization of the Poisson distribution (Conway and Maxwell, 1962). Its main advantage is related to data characterized by under-dispersion but only a few uni-variate studies may be found in the literature (Lord et al., 2010a):

$$\Pr(y_i, v) = \frac{E[y_i]^{y_i}}{(y_i!)^v} \cdot \frac{1}{\sum_{j=0}^{\infty} \frac{E[y_i]}{(j!)^v}} \quad (2.6)$$

with $v \geq 0$ as distribution parameter. When $v = 1$, the distribution becomes the standard Poisson distribution and as $v \rightarrow \infty$, the distribution approaches a Bernoulli distribution.

Gamma regression: Similarly to the zero-inflated Poisson model, the gamma model proposed by (Oh et al., 2006) is also characterized by a dual-state formulation. This model can handle over-dispersion and under-dispersion and reduces to the Poisson model when the variance is roughly equal to the mean of the number of accidents. Still, very few applications can be found in the literature:

$$\Pr(y_i = j, \alpha) = \text{Gam}(\alpha j, E[y_i]) - \text{Gam}(\alpha j + \alpha, E[y_i]) \quad (2.7)$$

$$\text{with } \text{Gam}(\alpha j, E[y_i]) = \begin{cases} 1 & \text{for } j = 0 \\ \frac{1}{\Gamma(\alpha j)} \int_0^{E[y_i]} u^{\alpha j - 1} e^{-u} du & \text{for } j > 0 \end{cases} \quad (2.8)$$

where the dispersion parameter is α ; there is under-dispersion if $\alpha > 1$, over-dispersion if $\alpha < 1$, and equi-dispersion if $\alpha = 1$, which reduces the gamma probability to the Poisson model.

Generalized additive models

The generalized additive model was developed with the purpose of mixing properties of generalized linear models through an additive framework. It specifies a distribution and a link function h relating the expected value of the distribution to predictor variables, and

attempts to fit functions f_j to satisfy:

$$h(y_i) = \sum_j \beta_j f_j(X_{ij}) \quad (2.9)$$

The functions f_j may be fit using parametric or non-parametric functions. Only a few examples of these methods applied to accident data are available in the literature (see for example Xie and Zhang, 2008).

Random-effects models

Random-effects models were applied in the context of accident frequency modelling primarily to account for spatial and/or temporal correlation among observations. In random effects models, the common unobserved effects are assumed to be distributed over the spatial/temporal units according to some predefined distribution and the shared unobserved effects with no correlation with explanatory variables. An example of a random-effects model using the Poisson distribution is to consider in equation 2.2, $E[y_i] = e^{\beta_j X_{ijk} + \eta_k}$ where y_i is the expected number of accidents for entity i belonging to a spatial or temporal group k (El-Basyouny and Sayed, 2009, Lord et al., 2010b).

Negative multinomial models

The problem of correlation among observations was also analysed by means of negative multinomial models. Using the negative-binomial structure for example, the specific $E[y_i] = e^{\beta_j X_{ij} + \varepsilon_i}$ is now specified and the e^{ε_i} component is now linked to a spatial or temporal group (Shina and Washington, 2012).

Random-parameters models

In random-parameters models each parameter of the model may vary across each of the individual observations in the data set, typically by means of predefined distributions, accounting for unobserved heterogeneity between entities. In such models, each parameter β_j is specified as $\beta_j = \beta_j^0 + \varphi_j$, where φ_j is a randomly distributed term. Despite the more complex estimation procedure (typically using Bayesian methods) the random-parameters models have already been applied extensively to accident frequency data (Lord et al., 2010b).

Multivariate models

When modelling different types of accidents separately using the above mentioned univariate models, the results ignore the dependencies that exist between them. Multivariate models explicitly account for the correlation between different severity levels or type of accidents, resulting in a more complex estimation procedure (Lord et al., 2010b). These models also have been applied frequently during the past years, with a wide variety of structures and statistical distributions (bivariate vs. multivariate, Poisson vs. negative-binomial, etc).

Other recent modelling approaches

Duration models (models that consider the conditional probability of an accident happening at some time $t + \Delta$ given that it has been time t since the last accident occurred (Washington et al., 2010), Markov switching models (Malyshkina and Mannering, 2009) and several artificial intelligence models (such as neural (Abdelwahab and Abdel-Aty, 2002), Bayesian network models (Xie et al., 2007) or support vector machines (Li et al., 2008)) may also be found in the literature, with an increasing application in accident frequency modelling, thanks to rising computational power availability. All these non-classical methods have their own estimation particularities and the reader is referred to the above mentioned references for application details.

The (low) attention to driving behaviour variables

All the above mentioned models mainly used a static measure of traffic flow data as main traffic variable, such as average annual daily traffic (AADT), that alone captures some irrelevant effect of driving behaviour, but rather should be considered as an exposure measurement. There has been a clear dominance of road design characteristics in the independent variables used in model specification. In some studies, measurements of average speeds, 85th speed percentiles and speeding rates have also been used with success (Corby and Saccomanno, 1997). Cardoso (1996), for example, used several speed distribution percentiles for modelling accident frequency on tangents; Cardoso (1996) modelled accidents frequency on horizontal curves using the speed variation on the approaching curves. This consists in a clear improvement but requires data that is not typically available for every road entity. Although it is "still reasonable to believe that the longer it takes to

stop a vehicle, the larger is the probability of accident involvement" (Hauer, 2009), many research studies still discuss the best formulation alternative to the well known U-shaped curve of the speed-accident frequency relationship (Solomon, 1964).

All these questions and findings motivated many authors to analyse different short-term variation of traffic flow and speed in the analysis of motorway accidents, especially aiming at real-time applications (see section 2.1.4).

2.1.3 Accident injury-severity models

Typically using detailed accident data from police reports, a large research stream has been focused in modelling the consequences of a road accident. Instead of specifying accident count models, these models focus on the discrete nature of accident itself. In a recent review, Savolainen et al. (2011) classified these models on the type of specification of the discrete dependent variable: bivariate (e.g., injury vs. non-injury) or multivariate (e.g., fatality, serious injury, light injury or no injury) treated as both ordinal or nominal (i.e., unordered). A short note should be added to the importance in considering the influence of under-reporting of accident records in, not only injury-severity models, but also other safety models, as these typically generate biased samples for estimation (Savolainen et al., 2011).

Binomial models

The most common binomial methods found in the literature are the classical binary logit and binary probit models. These simple type of regression analysis are used for predicting the outcome of a binary dependent variable based on one or several explanatory variables. The probabilities describing the possible outcomes of a single trial are modeled, as a function of the explanatory variables, using a logistic function (for the logit model, equation. 2.10) or the normal distribution (for the probit model, Esq. 2.11).

$$\Pr(Y = y_i) = p_i^{y_i} (1 - p_i)^{1-y_i} = \left(\frac{1}{1 + e^{-\beta X}} \right)^{y_i} \left(1 - \frac{1}{1 + e^{-\beta X}} \right)^{1-y_i} \quad (2.10)$$

$$\Pr(Y = y_i) = \Phi(\beta X) \quad (2.11)$$

where, Φ is the cumulative distribution function (CDF) of the standard normal distribution, X is the vector of independent variables and β the vector of parameters to be

estimated, with $y_i = \{1, 0\}$.

To account for within-accident correlations, when addressing injuries from the same accident for example, simultaneous binary models and Bayesian hierarchical binomial models have been used.

Ordered multinomial models

It is well accepted by the research community that vehicle interaction severities are ordinal by nature (Hydén, 1987). To account for the ordinal nature of injury data several ordered probability models have been widely applied. This modelling extension assumes an observed dependent variable $y^* = \beta X + \varepsilon$ for the categorisation of the observed dependent variable y_i :

$$y_i = \begin{cases} 0 & \text{if } y^* \leq \mu_0 \\ 1 & \text{if } \mu_0 < y^* \leq \mu_1 \\ \vdots & \vdots \\ n & \text{if } y^* \geq \mu_n \end{cases} \quad (2.12)$$

$$\Pr(y_i > j) = \frac{e^{\beta X_i - \mu_j}}{1 + e^{\beta X_i - \mu_j}} \quad \text{with } j = 0 \dots n \quad (2.13)$$

where X is the vector of independent variables, μ are threshold parameters to be jointly estimated with the model parameters β and n is the highest integer ordered response. Similarly to the binomial models, different modelling structures are derived from different natures of the adopted error term ε , and further extensions have also been proposed to account for within-accident correlations using simultaneous estimation (Eluru et al., 2010), for heteroskedasticity (different error variances, see equation 2.14) and for the violation of the parallel regression assumption (different parameters for different severity levels, see equation 2.15 (Quddus et al., 2010)):

$$\Pr(y_i > j) = \frac{e^{\frac{\beta X_i}{\sigma_n} - \mu_j}}{1 + e^{\frac{\beta X_i}{\sigma_n} - \mu_j}} \quad \text{with } j = 0 \dots n \quad (2.14)$$

$$\Pr(y_i > j) = \frac{e^{\beta_j X_i - \mu_j}}{1 + e^{\beta_j X_i - \mu_j}} \quad \text{with } j = 0 \dots n \quad (2.15)$$

where X is a vector of explanatory variables, σ_n is the error variance, which can be parametrized as a function of X and β_j is a vector of parameters to be estimated that

can now depend on the level j .

Bayesian, mixed and random parameter ordered models may also be found in the literature (Savolainen et al., 2011).

Unordered multinomial models

If one ignores the ordinal nature of the accident severity phenomenon, unordered multinomial models may be used in accident injury-severity data which typically present different statistical proprieties than its ordered counterparts. Such approach is especially useful in accident-type modelling, where each value of the discrete dependent variable is an accident type (run-off-road, side collision, rear-end collision...).

Multinomial logit models: By generalizing the logistic regression to allow more than two discrete outcomes, the multinomial logit models uses a linear predictor function S that aims at scoring each possible outcome of the dependent variable:

$$S_{ij} = \beta_j X_{ij} + \varepsilon_{ij} \quad (2.16)$$

where β_j is the vector of estimable parameters, X_{ij} is a vector of observable characteristics (driver, vehicle, roadway, and environmental factors) for observation i affecting the possible outcome j , and ε_{ij} is a disturbance term that accounts for unobserved effects. If the error term is assumed to be independently and identically distributed (IID) as generalized extreme value (GEV) distribution, the multinomial logit model can be specified as (McFadden, 1981):

$$\Pr(y_i = j) = \frac{e^{\beta_j X_{ij}}}{\sum_j e^{\beta_j X_{ij}}} \quad (2.17)$$

This model does not allow correlation among alternatives. Such correlation causes a violation of the model's independence of irrelevant alternatives (IIA) property (Ben-Akiva and Lerman, 1985), which might be a statistical property missing in both injury-severity and accident-type modelling. One of the main benefits found in the application of such method is that, in the presence of accident under-reporting, all parameters will still be unbiased except for the constant term (Washington et al., 2010).

Joint logit models: This modelling technique allows for shared observed attributes between the possible dependent variable outcomes when considering multidimensional

outcomes. By multidimensional outcome sets in safety analysis, one may consider, for example, a model to estimate both the accident type and the injury-severity level:

$$S_{jl} = \beta_{jl}X_{jl} + \beta_lX_l + \beta_jX_j + \varepsilon_{lj} \quad (2.18)$$

where β_j is the estimable vector parameter for outcome type j in one outcome set 1, β_l is the estimable vector parameter for outcome type l in one outcome set 2, and $\beta_{jl}X_{ij}$ is the estimable vector parameter for the specific combination of type j and l (the coefficient for observation i was omitted for better readability). The advantage of such approach is the easy derivation of marginal and conditional probabilities (see Ben-Akiva and Lerman, 1985, for its formulation).

Nested logit models: When the multidimensional outcome sets share unobserved attributes, the nested logit model is an appropriate generalization of the joint logit model (Ben-Akiva, 1973).

$$S_{jl} = \beta_{jl}X_{jl} + \beta_lX_l + \beta_jX_j + \varepsilon_{lj} + \varepsilon_l + \varepsilon_j \quad (2.19)$$

The structure of the nested logit overcomes the IIA limitation of multinomial logit models (for details on the formulation of marginal and conditional probabilities see (Ben-Akiva and Lerman, 1985)). To estimate a nested logit model, injury-severity levels are partitioned into nests that are comprised of severity outcomes that share some unobserved elements specific to only those outcomes (Patil et al., 2012).

Multinomial probit models The multinomial probit models also allows for shared unobserved attributes between outcome sets. Unlike the nested logit structure, this formulation allows for all error term components to have a non zero variance. Its main drawback is that it typically requires more computational resources than the previous logit structures. Again, in the probit formulation the errors terms are defined as normally distributed instead of GEV distributed (Yamamoto et al., 2008).

Mixed logit models: Mixed logit models address the limitations of the multinomial logit by allowing for random coefficients and correlation in unobserved factors (McFadden and Train, 2000). Unlike the multinomial logit and probit, its error terms are not limited

to GEV and normal distributions:

$$S_{ij} = \beta_i X_{ij} + \varepsilon_{ij} + \eta_{ij} \quad (2.20)$$

where η_{ij} is a random error term with zero mean for observation i affecting the possible outcome j and ε_{ij} is the error term that is IID, and does not depend on the estimable parameters or the data.

The mixed logit is a generalization of the multinomial structure which allows the parameter vector β_i to vary across each observation, allowing for heterogeneity in effects. Estimation methods typically require simulation and Monte-Carlo approaches (Ye and Lord, 2010).

Other modelling approaches

Finally, non-classical approaches such as Markov switching models (Malyshkina and Mannering, 2009), artificial neural network (ANN) models (Abdelwahab and Abdel-Aty, 2001, Delen et al., 2006) and classification and regression tree approaches (Chang and Wang, 2006) may also be found in the literature. Unfortunately, the comparison of different injury-severity modelling techniques was not well documented until very recently. One of the few exceptions is the study of Abdelwahab and Abdel-Aty (2002) where a nested logit model approach was tested against an ANN for accident severity (and location) prediction in the vicinity of toll plazas. For accident location modelling, the nested logit model had better performance, classifying correctly 66.6% and 63.8% of the accident locations for the estimation and testing data sets, respectively. For accident severity however, the estimated ANN resulted in better performance than the nested logit model, by correctly classifying 82.6% and 79.2% of the estimation and testing data sets. However, in the last year, the research community has delivered a few more studies focusing in the assessment of different modelling approaches: Ye and Lord (2014) examined the effects of sample size on three commonly used crash severity models: multinomial logit, ordered probit and mixed logit models; Yasmin and Eluru (2013) compared several ordered response and unordered response models in the context of crash severity. The alternative modeling approaches considered for the comparison exercise include: the ordered logit, generalized ordered logit, mixed generalized ordered logit, multinomial logit, nested logit, ordered generalized extreme value logit and mixed multinomial logit model, pointing the latter as

a strong modeling technique for driver injury severity.

The importance of detailed driving behaviour variables

Despite the distinct injury-severity units used for the specification of the dependent variable (by accident, by passenger...), the reviewed models considered several different driver, vehicle and road environment independent variables:

- driver age, gender, alcohol consumption, and safety equipment usage;
- vehicle type and the number of vehicles involved in the accident;
- horizontal road curvature, number of lanes, road category, surface characteristics and conditions and junction control;
- vehicle maneuvering prior to crash;
- speed limit, day of the week, time of day, AADT, weather and traffic conditions.

The consideration of such variables depends directly on its availability in the accident records database or in complementary databases used in each case study. Yet, the uncertainty associated with each of these variables has disparate magnitudes, as vehicle maneuvering related variables are generally not measurable and the estimation of dynamic parameters depends on the quality of police investigation.

When reviewing the results of several injury-severity studies, Christoforou et al. (2010) stated that the main influencing factors regarding accident severity were, in general, common to all studies: older driver/passenger age, intoxication rate, head-on-collisions, accident with heavy vehicles and motorcycles, poor lighting conditions, atypical vertical and/or horizontal curvature, urban environment and speeding. However, these studies also report conflicting findings on some factors such as gender, road surface conditions and traffic flow. Quddus et al. (2010) suggested that the level of traffic congestion does not affect the severity of road accidents on the M25 motorway in London. On the contrary, Christoforou et al. (2010) used a random parameters ordered probit model in an injury-severity data set for the A4-A86 junction in Paris and concluded that there was a significant relationship between the severity outcome and the traffic characteristics at the time of the accident: traffic volume with a positive effect and speeds with a differential effect with respect to traffic volume. These inconclusive results regarding the generic quantification of traffic variables' influence in accident severity justifies a more detailed

study of the processes underlying such events, by using detailed trajectories collected on-site, estimated trajectories from accident reconstruction or large naturalistic data sets.

2.1.4 Accident probability models

With the development of many infrastructure-based ITS, such as variable message signs, ramp metering and variable speed limits, research efforts have been dedicated to identify, in real-time, traffic scenarios that might be used as accident precursors. Models developed with this aim are referred as (real-time) accident probability models and, typically, make use of real-time traffic data collected by sensing technologies (generally from loop detectors), road geometric characteristics and, in some cases, weather conditions.

The first steps in detailed traffic characteristics for accident occurrence analysis were based on accident frequency studies modelling techniques (Persaud and Dzbik, 1993). In Lee et al. (2002) and Lee et al. (2003), for example, a set of accident precursors were formulated and used as independent variables in a Poisson accident probability model using a log-linear analysis. The proposed model expressed accident frequency as a function of a variety of traffic and environmental characteristics as follows:

$$E[A_{rate}] = \frac{E[y_i]}{EXP^\beta} = f\left(\theta \prod_i \lambda_i\right) \quad (2.21)$$

where λ_i are accident precursors, $E[y_i]$ is the expected number of accidents, EXP is an exposure measure and θ and β are model parameters. By using such functional relationship, the model was estimated using actual accident data. The calculation of accident precursors accounts for several traffic variables such as lane-based average speed, average flow, average occupancy and average coefficients of temporal and spatial speed and flow variation. Weather, road characteristics and time-of day were also considered as "external control factors". It should be noted that accident precursors and external control factors are categorical variables, whereas exposure (traffic flow and road segment length) was assumed as a continuous variable. From the results, the increase in both types of speed variation (along and across lanes) were identified as important accident precursors.

Currently, the majority of the modelling approaches are in-line with the injury-severity modelling methods, and some examples are given in the next sections.

Binomial and Multinomial regression

In one of the earlier efforts, Madanat and Liu (1995) developed two binary logit models to predict two types of freeway incidents: vehicle accident and overheating vehicle incidents for the Borman Expressway, in northwest Indiana, USA. The results indicated that travelling on merging sections, visibility factors, and rain were the significant variables affecting the accident prediction.

Oh et al. (2001) used Bayesian classifiers to categorize two possible traffic scenarios for a 14.8 km stretch of the I-880 freeway in Hayward, California: accident and non-accident traffic scenarios. Statistics (average and standard deviation) of speed, volume and occupancy distributions were estimated for the upstream loop detectors in 5-minute intervals during 30 minutes before an accident occurrence. The results showed that the standard deviation of speed, five-minute before the accident occurrence, was the most significant factor.

In Abdel-Aty et al. (2004) a matched case-control logistic regression was used to model accident likelihood. In such approach, for each accident in the database, non-traffic flow variables, such as location, time of day, and day of the week, were selected as control variables and a sub-population of non-accident cases was selected using these matching factors. When using such approach, it is assumed that there are N strata with 1 accident and m non-accidents in stratum $j = \{1, 2, \dots, N\}$. The conditional likelihood for the j^{th} stratum is the probability of the observed data given the total number of observations and the number of accidents observed in the stratum. Let $\Pr_j(X_{ij})$ be the probability that the i^{th} observation (with $i = 0, 1, \dots, m$) in the j^{th} stratum is an accident. X_{ij} is a vector of k traffic flow variables X_1, X_2, \dots, X_k . This crash probability $\Pr_j(X_{ij})$ may be modeled by using a linear logistic regression model using equations 2.16 and 2.17. Different alternative specific constants (β_0 not associated with any X_{ij}) will capture the effect of variables used to form strata on the probability of accident. To account for the stratification in the analysis of the observed data, the model is estimated using a conditional maximum likelihood. The variation in speed at the downstream station and the average occupancy at the station upstream of the accident location, 5 to 10 min before the occurrence, were found to be the most influencing variables. A similar method was afterwards used in Abdel-Aty and Pemmanaboina (2006) with additional weather historical data, which was firstly categorized by means of principal component analysis.

Lee and Abdel-aty (2008) estimated a two-level nested logit model for accident occurrence in different ramp types and configurations, using 5 min loop-based traffic flow data before each accident occurrence and 5 years of ramp accident data for Interstate 4 in Orlando, Florida, USA. The effects of all factors other than ramp type, ramp configuration, and traffic flow parameters were controlled by grouping ramps with similar characteristics through cluster analysis.

Lee and Ph (2009) used a Bayesian logistic regression model to estimate the probability of occurrence of sideswipe and rear-end accidents given that an accident had occurred. By using the Bayesian approach, the coefficient of each parameter is estimated based on the combined information of a prior value and the observed data. The prior values were assumed to follow a normal distribution with mean equal to the best available point estimate of each parameter, and the maximum likelihood estimates were used as starting values for a Markov Chain simulation-based estimation.

Xu et al. (2013a) used a sequential logit model to capture the impacts of different traffic flow parameters on the accident likelihood at various accident levels: accident vs. non accident, damage only vs. (possible) injury accidents and fatal vs. other injury accidents. At each stage, a binary logit model was used to fit a sub-sample that excluded the observations of a certain level used in the previous stage.

Artificial Intelligence and Data Mining techniques

With the increase availability of computational resources and the interest to apply these models in real-time traffic monitoring, researchers also focused on developing numerical methods that typically have high fitting and replication performances, but do not help explaining the accident occurrence process itself.

Pande and Abdel-aty (2006) used classification trees to identify potential traffic variables to include in an artificial neural networks modelling framework (ANN). Classification trees can be used to automatically rank the input variables based on the strength of their contribution to the tree (dependent variable). In later developments, the authors opted for random forests for the variable selection task, a collection of multiple tree classifiers, avoiding the instability of unique tree classifiers in handling missing values (Abdel-aty et al., 2008, Hassan and Abdel-Aty, 2013).

(Hossain and Muromachi, 2012) proposed a Bayesian network to predict accident on a Japanese urban motorway densely equipped with detectors. They applied a random multinomial logit, a recently introduced hybrid of conventional multinomial logit and random forest methods that can handle interval data, to identify and rank the most important predictors from a large variable space. A Bayesian network was then used to estimate the real-time accident probability model. Rather than building a model focusing on the problem, Bayesian networks model the system using estimated probabilities, which can then be used to make predictions about events. It is structured as a directed acyclic graph (DAG) which illustrates the factorization of a joint probability distribution over the variables that are represented by the nodes of the DAG. The study identified that the traffic conditions in the upstream and the downstream 250m sections as well as the difference in traffic flow parameters on these locations have a high impact in the prediction output. As average performance, the method resulted in 66% success rate in capturing hazardous traffic conditions with 20% false positives.

(Xu et al., 2013b) used genetic programming (GP) to develop a real-time accident probability model for the I-880N motorway in California, USA. The random forest technique was used to select the variables that affect crash risk under uncongested and congested traffic conditions. The GP model was then developed for each traffic state based on the selected candidate variables and its performance compared against a binary logit model. Then, using the GP approach, they recorded an increase of detection performance by 8.2% and 4.9% for uncongested and congested traffic conditions respectively. However, as a result of the intrinsic nature of this modelling approach, no insights on the underlying mechanism of the accident phenomenon were added to the current state-of-knowledge.

Golob et al. (2004) relied on (linear and non-linear) spatial statistical techniques to analyse the traffic variables influence on accident occurrence. The method was based on Principal Component Analysis (PCA) in order to identify the most significant variables from a set of original traffic flow variables, a cluster analysis for grouping traffic variables in traffic regimes, and a Nonlinear (nonparametric) Canonical Correlation Analysis (NLCCA) was used to relate the identified principal components to three accident characteristics: type (rear end, sideswipe or hit object, number of vehicles involved), location (e.g. left lane, interior lanes, right lane, shoulder) and severity (injuries and fatalities per vehicle). A large data set of more than one thousand accidents on six major motorways

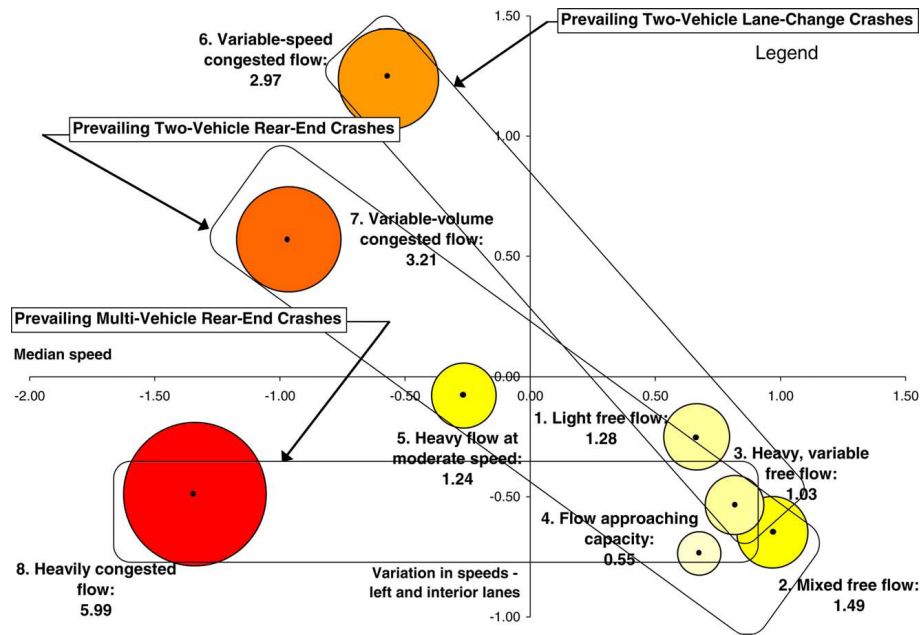


Figure 2-1: Estimated total accidents per million vehicle miles of travel by traffic flow regimes plotted in standardized space of (x) median speed vs. (y) variation in speeds in left and interior lanes (Golob et al., 2004).

in Orange County, California, for the year 1998 was used along with 30s-lane-based loop sensor data for the 30 min preceding each accident. This methodology resulted in bi-plots (see Figure 2-1) with the relationships as to which types of accident are more likely under different types of traffic flow regimes, and several interesting conclusions were extracted from the analysis: run-off-road accidents were identified with low-volume conditions and relatively high speeds; left lane collisions were more likely correlated with volume effects; right lane collisions are more closely tied to speed variations in adjacent lanes; collision type was best-explained with median speed and to left-lane and interior-lane variations in speed.

2.1.5 Surrogate safety indicators

All the previous modelling streams rely on the availability of historical accident records. In the last section however, some of the documented efforts in matching short-term traffic data with accident records lead to the development of pre-processing methods to first identify the traffic variables that may influence the accident occurrence. These efforts are related to both, modelling simplification and extracting new insights in the intrinsic mechanisms of the accident phenomenon. In fact, as the modelling framework steps away from aggregated structures, the interest in understanding the explanatory role of

detailed traffic and driving behaviour variables increases substantially, especially for more congested scenarios.

The first attempts were proposed in the late 60's (Perkins and Harris, 1967) and in the past couple of decades a research stream has focused its attention on the potential use of detailed data about vehicle interactions, such as conflicts, as accident precursors. In fact, as accidents are considered rare events and it is hard to isolate the effect of many factors affecting its occurrence, conflicts have been used as an alternative estimator of system safety. This definition is based on the assumption that the expected number of accidents occurring on a system is proportional to the number of conflicts and, if it is used for systems' comparison, that the coefficients or proportionalities (between conflicts and accidents) will be the same on the systems compared. The accident risk is said to be "a measure of the probability of a potential accident event to result in an accident" (Hauer, 1982):

$$\text{Risk of system } A = \frac{\text{Safety of system } A}{\text{Exposure of system } A} \quad (2.22)$$

This framework may also be applied in conflict analysis (considering accident occurrence as the consequence in risk formulation):

$$\text{Probability of accident from conflict} = \frac{\text{Safety of system } A}{\text{Number of conflicts in } A} \quad (2.23)$$

The conflict event has been defined considering that the probability of accident occurrence given that a specific conflict has occurred is the same on all systems being compared. It is due to this property that for two systems A and B , the ratio of safety levels is equal to the ratio of the conflict rates. It is therefore incongruous to think of a properly defined conflict event as a measuring exposure alone. The whole purpose of risk estimation is to describe the differences between two systems in terms of their characteristic risks R_A and R_B . This is generally the preferred utility of surrogate indicators. If two systems A and B have the same exposure (N), the entire difference in their safety would now be reflected in the risks R_A and R_B . Therefore, a properly defined unit of exposure can never serve as a conflict event by itself because it would allow R to be different from system to system, thereby rendering the basic premise of the conflict method (Hauer, 1982).

This accident-conflict proportionality is based on the concept of safety continuum of traffic events proposed by Hydén (1987) (see Figure 2-2). This theoretical concept

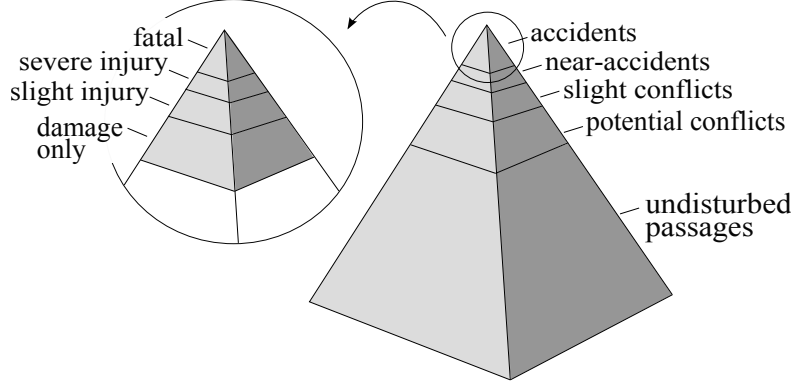


Figure 2-2: The safety pyramid (Hydén, 1987)

provides a bottom-up and more rational approach to safety research as opposed to the traditional top-down perspective of safety given by accident frequency (Cunto, 2008), and defines conflict as "an observable situation in which two or more road users approach each other in space and time to such an extent that there is a risk of collision if their movement remain unchanged"(Hydén, 1987). One of the main difficulties in using conflicts for modelling purposes is the lack of practical definitions and measurement standards for all possible vehicle interactions. For this purpose several (time-based, deceleration-based and dynamic (Cunto, 2008)) safety performance indicators (or measures) were proposed in the literature (Laureshyn et al., 2010).

Time based indicators

TTC - Time-to-Collision: The TTC is defined as "the time required for two vehicles to collide if they continue their present speeds and on the same path" (Hayward, 1971) and is given by equation 2.24 for two vehicles travelling in same direction.

$$TTC_{n,t} = \frac{(X_{n-1,t} - X_{n,t}) - L_{n-1,t}}{V_{n,t} - V_{n-1,t}} \quad (2.24)$$

where X_n , X_{n-1} are the longitudinal positions and V_n , V_{n-1} the longitudinal speeds of the subject and leading vehicle respectively, L_{n-1} is the leading vehicle, all at time t . For vehicles traveling in different directions but with colliding trajectories, the TTC can be expressed as:

$$TTC_{n,t} = \frac{D_{n,t}}{V_{n,t}} \quad (2.25)$$

where D_n is the distance between the projected point of collision and vehicle n . Although variations of TTC are related to drivers reaction time, the definition of TTC thresholds from empirical data is typically based in measurements after the evasive action is performed. Several values for TTC_{\min} threshold may be found in the literature but the value of 1.5s is often considered (van der Horst, 1990). It is worth pointing out that different speed-distance combinations, and therefore accident occurrence probabilities, may result in the same TTC value. Hydén (1987) simplified the continuous computation of TTC at every time t , and proposed the TTA (time-to-accident) which only measures the TTC at the moment the evasive action takes place. A ranking of different severity levels was then proposed under the Traffic Conflict Technique (TCT) framework based on the TTA and the estimated conflict speed.

ET - Encroachment Time: ET is the time that a conflicting vehicle occupies the conflict area (Allen et al., 1978).

PET - Post Encroachment Time: The PET is defined as the time difference between the moment a conflicting vehicle leaves the area of potential collision and the moment the subject vehicle arrives the collision area (Cooper, 1983). Although this indicator may also be computed for the rear-end collision scenarios it is typically suited for angled collisions situations (Gettman and Head, 2003b).

IAPT - Initially Attempted Post-Encroachment Time: Similarly to the PET, the IAPT uses the estimated arrival time of the subject vehicle at the conflict area regarding its movement at the time the encroachment has ended (Allen et al., 1978).

GT - Gap Time: GT is the time difference between the estimated arrival time of the subject vehicle when the vehicle reaches the conflict area and the time the conflicting vehicle needs to cross the area (Allen et al., 1978).

All these encroachment related indicators more suited for conflicts at intersections are represented in Figure 2-3.

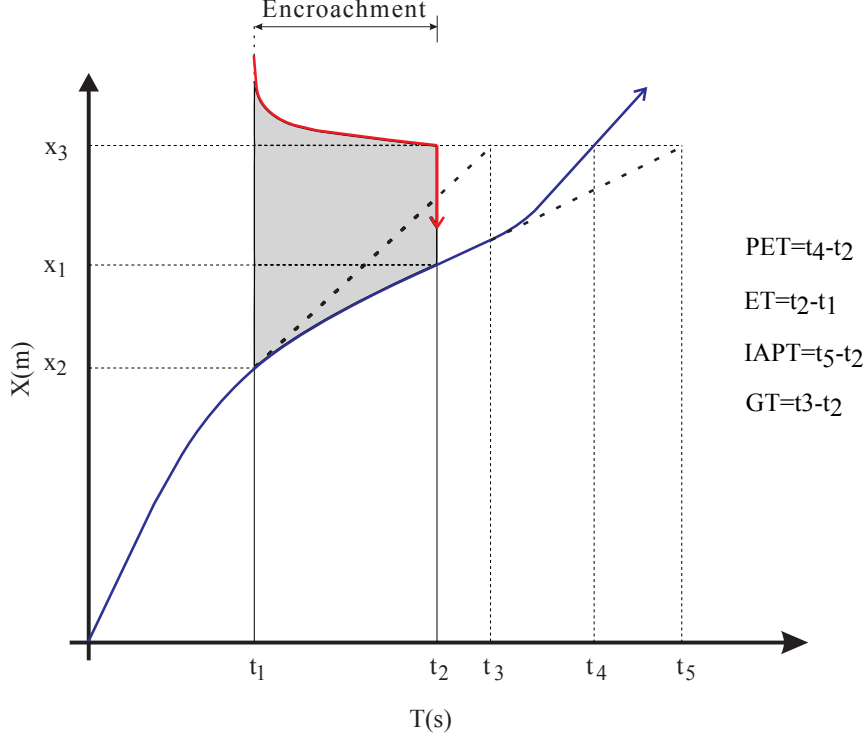


Figure 2-3: Time-space diagram for a typical left-turn conflict (Allen et al., 1978).

Deceleration-based Indicators

Speed influence in traffic conflict severity and possible severity of the resulting crash is not appropriately accounted in all above mentioned surrogate indicators. As previously mentioned, speed is also an important variable to consider in accident occurrence (as it may affect driver perception and evasive manoeuvres) and vehicles' speed differential is a key factor in the accident severity outcomes. To overcome this gap, several indicators that account for the deceleration rate have been proposed.

DRAC - Deceleration Rate to Avoid Crash: Cooper and Ferguson (1976) defined the DRAC as the required deceleration rate to avoid a collision if the conflicting target vehicle maintains its speed and trajectory. Similarly to the TTC, this indicator may be computed at any time t :

$$DRAC_{n,t} = \frac{(V_{n,t} - V_{n-1,t})^2}{2|(X_{n-1,t} - X_{n,t}) - L_{n-1}|} \quad (2.26)$$

where X_n , X_{n-1} are the longitudinal positions and V_n , V_{n-1} the longitudinal speeds of the subject and leading vehicles, respectively and L_{n-1} is the leading vehicle length, all measured at time t . For vehicles travelling in different directions but with coliding

trajectories, the DRAC may be formulated as:

$$DRAC_{n,t} = \frac{V_{n,t}^2}{2D_{n,t}} \quad (2.27)$$

where D_n is the distance between the projected point of collision and vehicle n . McDowell et al. (1983), for example, used four different DRAC thresholds of $\{1.5, 3.0, 4.5, 6.0\}$ (m/s^2) to classify different conflict severities in gap acceptance manoeuvres. The main difficulties in calculating such indicator are the need for both detailed trajectory data and specifications of different thresholds, which depend on vehicle and environmental variables (e.g., vehicle type, pavement condition...).

PSD - Proportion of Stopping Distance: The PSD was proposed by Allen et al. (1978) and is defined as the ratio between the remaining distance to the potential collision point and the minimum acceptable stopping distance:

$$PSD_n = \frac{RD_n}{MSD_n} \quad (2.28)$$

where RD_n is the remaining distance to the potential conflict point (m), MSD_n the acceptable minimum stopping distance $= V_n/2D_n$ (m), with V_n as the speed (m/s) and D_n as the acceptable maximum deceleration rate (m/s^2) for vehicle n . The PSD is computed at the time the conflicting vehicle enters the conflict area.

CI - Crash Index: Ozbay et al. (2008) modified the original TTC after considering the acceleration/deceleration of the two vehicles during the course of conflicting paths. Researchers in this study deemed TTC or the modified TTC (MTTC) as a measure of probability of the occurrence of a conflict; they also use the energy which might be transferred during the collision to measure its severity. Based on these concepts, a crash index was proposed as follows:

$$CI_n = \frac{(V_n + a_n \cdot MTTC)^2 - (V_{n-1} + a_{n-1} \cdot MTTC)^2}{2} \cdot \frac{1}{MTTC} \quad (2.29)$$

where CI_n is the crash index for vehicle n ; V_n , V_{n-1} and a_n , a_{n-1} are the longitudinal speeds and acceleration rated of the subject and leading vehicle, respectively; and $MTTC$ is the modified TTC which accounts for different motion combinations (see Ozbay et al.

(2008) for the detailed formulation).

Dynamic indicators

More recently, several indicators were proposed, which added an exposure component in some of the previous formulations.

TET: Time Exposed Time-to-Collision Minderhoud and Bovy (2001) defined the TET for a vehicle n as the sum of all time intervals that this vehicle had $TTC < TTC^{min}$:

$$TET_n = \sum_{t=0}^T \delta_n(t) \cdot \tau_{sc}$$

$$\delta_i(t) = \begin{cases} 1 & \text{if } 0 \leq TTC_{n,t} \leq TTC^{min} \\ 0 & \text{otherwise} \end{cases} \quad (2.30)$$

where TET_n is the time exposed time-to-collision for vehicle n and for a given threshold TTC^{min} , T is the total number of observed step sizes, and τ_{sc} is the step size of computed trajectories (e.g.: 0.1s).

TIT - Time Integrated Time-to-Collision: Minderhoud and Bovy (2001) also proposed the TIT (s^2), which is defined by:

$$TIT = \int_T^0 (TTC^{min} - TTC_{n,t}) dt \quad (2.31)$$

where TTC^{min} is a predefined threshold.

Similarly to the previously described indicators, different thresholds should be specified for both TET and TIT, depending on the type of vehicle and pavement conditions.

TIDSS - Time Integrated Difference between Space distance and Stopping distance: The Japanese Society of Traffic Engineers (Japan Society of Traffic Engineers, 2005), defined DSS (Difference between Space distance and Stopping distance) as:

$$DSS_n = S - SS = \left(\frac{V_n^2}{2\mu g} + \Delta X \right) - \left(V_{n-1}\tau + \frac{V_{n-1}^2}{2\mu g} \right) \quad (2.32)$$

where S is the space distance (m), SS the stop distance (m), V_n the speed of following vehicle (m/s), V_{n-1} the speed of the leading vehicle (m/s), μ the friction coefficient, g

is the gravity acceleration (m/s^2) , ΔX the gap between leading vehicle and following vehicle (m) and τ the driver reaction time (sec).

Similarly to the TIT, Okamura et al. (2011) proposed an integrated DSS, the TIDSS, as:

$$TIDSS = \sum_{n=1}^N \int_T^0 (DSS^{min} - DSS_{n,t}) dt \quad (2.33)$$

where DSS^{min} is a predefined threshold. Here, there is no a-priory need for different thresholds specified for each vehicle type or observed pavement condition, as these factors are considered in the pavement surface friction coefficient μ .

UD - Unsafe Density Parameter: Torday et al. (2003) proposed the UD as a surrogate safety indicator for car-following situations based on a unity called "unsafety" ($us_{n,t}$):

$$us_{n,t} = \Delta V_t \cdot V_{n,t} \cdot R_d \quad (2.34)$$

where $us_{n,t}$ is the "unsafety" unit for vehicle n at time t , V is the speed of the following vehicle, ΔV is the speed differential of the car-following vehicle pair, R_d is a ratio of deceleration rates, such that:

$$R_d = \begin{cases} b/b_{max} & \text{if } b > 0 \\ 0 & \text{otherwise} \end{cases} \quad (2.35)$$

b is the deceleration rate of the leading vehicle and b_{max} is the possible maximum deceleration rate. The "unsafety" unit is then used to compute the UD parameter for every network segment over time:

$$UD = \frac{\sum_{t=1}^T \sum_{n=1}^N us_{n,t} \cdot \Delta t}{T \cdot L} \quad (2.36)$$

where Δt is the time step, T the total observation time, N the total number of vehicles and L is the segment length. Besides the need for different thresholds (b_{max}), two other main drawbacks of such formulation are: the limitation of conflicts to the leading vehicle breaking situations; and the lack of mathematical meaning for the "unsafety" unit $us_{n,t}$. (Cunto, 2008).

CPI - Crash Potential Index: Cunto (2008) proposed an indicator based on the

DRAC with the extension of two important vehicle interactions features: the maximum available deceleration rate and the time exposed to the interaction. The maximum available deceleration rate (MADR) is a stochastic component introduced to account for different vehicle categories under different pavement conditions (e.g. dry/wet). The CPI is defined as the probability that a given vehicle DRAC exceeds its maximum available deceleration rate (MADR) during a given time interval. The MADR was assumed to be normally distributed with average of $0.86g$ and $0.51g$ for cars and trucks, respectively, with standard deviation of $0.14g$:

$$CPI_n = \frac{\sum_{t=0}^T \Pr \left(MADR_{(a_1, \dots, a_k)} \leq DRAC_{n,t} \right) \cdot \Delta t \cdot b}{T} \quad (2.37)$$

where CPI_n is the crash potential index for vehicle n , $DRAC_{n,t}$ is the deceleration rate to avoid the crash (m/s^2), $MADR_{(a_1, \dots, a_k)}$ is a normally distributed variable (m/s^2), (a_1, \dots, a_k) are a set of traffic and environmental variables, Δt is the time step, T is the total travel time for vehicle n , and b a binary state variable (1 if a vehicle interaction exists and 0 otherwise).

Combined Surrogates Indicators Lareshyn et al. (2010) proposed a theoretical framework to categorize all traffic encounters into a severity hierarchy based on existing safety surrogate indicators. As an important component, this framework used a set of surrogate indicators including TTC, time advantage (a measure similar to PET), a supplement parameter (T_2) to time advantage, GT, and vehicle speed. T_2 represents the time needed for the conflicting vehicle to reach the potential collision point and tries to bring the influence of possible evasive manoeuvres into the assessment framework. This framework improved the ability of the existing set of indicators to describe the process of an encounter event and to classify its severity. The encounter process defined in that study is a continuous interplay between road users who may be on and off the collision course from time to time. During each encounter process, different indicators were used to describe the severity of an encounter.

The relation between surrogates and accident occurrence frequency

One of the main limitations of using surrogate safety indicators is the correct estimation of this link to true accident measurements such as accident records. This difficulty has mo-

tivated the research community to develop several models to estimate accident frequency from traffic conflicts.

Gettman et al. (2008) established a correlation between conflicts and accidents by developing a regression equation to estimate average yearly accident frequencies at an intersection as a function of the average hourly conflict frequencies. Using a traditional volume-based aggregate accident frequency model for intersections to estimate the expected number of accidents (independent variable), non-linear regression was then used to calculate the link between expected accident frequency and traffic conflicts counts. It was assumed that accidents followed a negative binomial distribution while the simulated conflicts followed a Poisson distribution:

$$E[y] = 0.0119 \cdot X^{1.419} \quad (2.38)$$

where $E[y]$ is the number of accidents per year and X is the number of conflicts per hour.

In Liu (2010) a simple generalized linear model (GLM) using simulated traffic conflicts, average flow rates and speeds as independent variables was fitted to assess the effectiveness of truck lane restriction strategies. The traffic data used for estimation was collected on the I-66, I-64 and I-81 highways in Virginia, USA, and the accident data was spanned across 5 years, totalizing 1 822 accident records. Different formulations and surrogate indicators were used, but the final formulation proposed by the author relied just in the number of TTC conflicts:

$$E[y] = 0.0124 \cdot X_{TTC} + 0.0354 \quad (2.39)$$

where $E[y]$ is the number of accidents per year and X_{TTC} is the number of conflicts per hour.

Although this models form an important bridge between surrogate indicators an accident outcomes, the modelling approach ignores the main intrinsic mechanisms that relate these two variables. Furthermore, few authors have focused their attention on the analysis of potential correlations in the simultaneous use of multiple surrogate indicators.

2.1.6 Probabilistic frameworks

While accident probability models just try to estimate the probability of a specific accident occurrence using a statistical model, probabilistic frameworks try to represent all cause-effect relationships of the driving task and the traffic scenario that may lead to the accident event. Such approach has a higher potential in replicating the intrinsic nature of the accident mechanism and, ultimately, would not depend on safety records itself. On the other hand, probabilistic frameworks depend on much more detailed information as the distribution and relationships between all variables at stake are needed (e.g.: evasive manoeuvres probabilities for different situations, mechanical features for different vehicles or pavement conditions for different scenarios).

Until recently, complex probabilistic approaches were mainly applied in psychological studies based in data collected by driving simulation and instrumented vehicle experiments, with small dissemination in real large-scale applications (see Section 2.2.1). With the increase availability of (site-based and infrastructure-based) naturalistic data, insights on the underlying mechanisms of conflicts generation are now possible and the first probabilistic safety assessments were carried out in recent years with very promising results.

Songchitruksa and Tarko (2006) proposed an Extreme Value (EV) approach to build up relationships between occurrence of right-angle accidents at urban intersections and frequency of traffic conflicts measured by using PET as accident proximity variable. This approach first estimates the risk of accident conditional on traffic conflicts based on observed PETs and its EV threshold. The accident frequency was then computed as a product of the frequency of traffic conflicts and the estimated conditional likelihood of accident occurrence. A major improvement of this study is that it links the probability of accident occurrence to the frequency of conflicts estimated from observed variability of accident proximity, using a probabilistic framework and without using accident records.

Saunier and Sayed (2008) developed a comprehensive probabilistic framework for automated road safety analysis based on motion prediction. For a given interaction between two vehicles, possible trajectories are estimated in a probabilistic framework and the collision probability for a given interaction between two road users can be computed at a given instant by summing the collision probability over all possible motions that lead to a collision, given the vehicle states. This requires the ability to generate for each road user at any instant a distribution of its possible future positions given its current and

previous positions. The proposed approach relied on a system to detect directly motion patterns and traffic conflicts by using a Hidden Markov Model-based semi-supervised machine learning technique. The motion pattern probabilities are computed by matching all trajectories over a given period through longest common sub-sequence similarity and can be updated continuously in a real-time application as traffic patterns change over time. For each future position, the conditional probabilities of collision were estimated.

Wang et al. (2010) propose an incident tree model and an incident tree analysis method for the identification of potential characteristics of accident occurrence in a quantified risk assessment framework. The main steps of the incident tree methodology implementation are: to identify the causation related to the accident occurrence process; determine the contents of the accident prevention; describe the dynamic mechanism of the accident occurrence; analyze occurrence-consequence of accident and potential impacts; and assess the likelihood of the accident formation and time frame of incidents occurrence. The approach was applied to the case of run-off-road accidents. The main drawbacks of such method is that it depends on information (probabilities) about all incident scenarios, possible failures and potential impacts, and its absence of comprehensive formulation of the relationships between variables.

2.2 Traffic Microscopic Simulation

2.2.1 Driving behaviour models

Micro-simulation models aim at replicating detailed vehicle motions and interactions by modelling agent decisions such as route choice, accelerations, decelerations and lane changes. These models are implemented as synchronous applications that update the kinematic parameters of each entity (driver-vehicle units, public transportation, management systems and even pedestrians) at every simulation time step. Similar to other transportation simulators, the design of microscopic models is based on a demand and supply equilibrium representation. Traffic demand input is formulated either by defining it in terms of input flows and turning proportions at intersections or, for larger networks, in terms of origin–destination (OD) matrices that will rely on route-choice models for network assignment (Barceló, 2010). Most current microscopic simulators iteratively perform the following generic process:

1. Calculate initial shortest paths for each OD pair on the pre-defined initial link costs;
2. Calculate path flow rates according to a route-choice model dependent on the initial costs for each OD pair;
3. Assign the flows along the paths in accordance with the supply parameters;
4. Collect statistics according to a predefined data collection plan;
5. Update link costs;
6. Go back to step 2.

In microscopic traffic simulation the supply implementation (step 3) relies on the specification of the network configuration, the traffic management algorithms and the driving behaviour model. In this Chapter, we focus the attention on the operational (acceleration and gap acceptance) and short-term tactical (lane changing) driving models. For a comprehensive review on all driving behaviour components used in simulation the reader should refer to Hranac et al. (2004a).

Car-following acceleration models

Models describing how one vehicle follows another were developed primarily in the 1950's with the development of the first car-following models (Reuschel, 1950, Pipes, 1953). Based on the concept of safe headway distance, defined as "the length of a car between the subject vehicle and the vehicle ahead for every ten miles per hour of speed at which the subject vehicle is traveling", this car-following theory leads to a minimum safe distance headway that increases linearly with speed, reproducing appropriately real measurements. This collision avoidance modelling stream gave birth to multiple car-following models during the next decades. Numerous car-following models were proposed since then and are still being developed nowadays. In this section, the six main groups of car-following models are briefly presented: stimulus-response models, collision-avoidance models, linear models, psycho-physical models, fuzzy-logic-based models, optimum velocity models and cellular automata models.

Stimulus-response models: Significant research was undertaken in the late 1950s by the General Motors Group in the USA, based on pioneer field experiments. This research led to the formulation of the car-following models in the form of a stimulus-response

equation (Gazis et al., 1961). The response was formulated as the lagged reaction of a driver to the motion of the vehicle in front of him. As for the dominant stimulus, they specified the relative speed between leading and following vehicle:

$$a_n(t) = c(v_n(t))^m \frac{\Delta v_{n,n+1}(t - \tau)}{(\Delta x_{n,n+1}(t - \tau))^l} \quad (2.40)$$

where a_n is the acceleration of vehicle n at time t , v_n is the speed of the vehicle, Δx and Δv are the relative spacing and speeds, respectively, between the n^{th} and $(n - 1)^{th}$ vehicles, computed at an earlier time $t - \tau$, where τ is the driver reaction time, and m , l and c are the constant parameters to be estimated.

To account for a more heterogeneous formulation several variations of equation 2.40 were proposed during the following years, mainly, by introducing different stimulus-response sub-models and by specifying alternative acceleration and deceleration equations (Ozaki, 1993). Ahmed (1999) proposed a non-linear stimulus by introducing a traffic state variable (traffic density), while Siuhi and Kaseko (2010) calibrated separate sub-models for acceleration and deceleration using individual vehicle trajectory data collected on Interstate 101 in California. However, with the development of an increased number of sub-models, the calibration becomes especially complex and significantly different parameter values for distinct traffic scenarios have been reported in the literature (Brackstone and McDonald, 1999).

Collision-avoidance models: Collision avoidance models were firstly formulated as such by Kometani and Sasaki (1959). It is based on a safe following distance (required to avoid collision with the vehicle ahead) as a function of the speeds of the follower and leader vehicles and the driver's reaction time.

$$\Delta x(t - \tau) = \alpha v_{n-1}^2(t - \tau) + \beta_1 v_n^2(t) + \beta v_n(t) + b_0 \quad (2.41)$$

where v_n is the speed of the following vehicle, v_{n-1} is the speed of leading vehicle; Δx is the relative distance between vehicle n and $(n-1)$; τ is the driver reaction time and α , β , β_1 and b_0 are the model parameters to be calibrated. The Gipps (1981) model, one of the most widely applied models, is based on this formulation. A similar four parameter single regime model integrating the basic Pipes model with adjustments from

Greenshields' macroscopic flow theory was developed by Van Aerde et al. (1992).

As more field measurements were carried out, new insights on driving behavior variability were gathered. When analysing highway traffic video data to study the effect of environmental variables on drivers' car-following behavior, Chen (1995) concluded that the assumption that drivers follow a leading vehicle at a safe distance is frequently not respected. Similarly, Hidas (1998) proposed a model where drivers in a car-following state tend to follow closer than a "safe distance", adjusting their acceleration in function of a desired headway. More recently, Tordeux et al. (2010) developed a continuous car following model in which the interaction between a following vehicle and its predecessor is based on a heterogeneous safety time gap.

Having in mind the modelling of trajectories for traffic scenarios in the discontinuity between free-flow and congestion and to better replicate the traffic hysteresis phenomena (different loops in the congested part of speed–density curves (Cassidy and Bertini, 1999)), Treiber et al. (2000) develop the IDM (Intelligent Driver Model) car-following equation:

$$a_n(t) = \alpha_n \left[1 - \left(\frac{v_n}{v_n^0} \right)^\delta - \left(\frac{s^*(v_n, \Delta v)}{s_n^0} \right)^2 \right] \quad (2.42)$$

$$s^*(v_n, \Delta v) = s^0 + v_n T + \frac{v_n \Delta v}{2\sqrt{ab}} \quad (2.43)$$

where for vehicle n , v_n denotes its speed and Δv is the speed difference between the follower and vehicle directly in front of him. The model parameters are the desired speed (the speed the vehicle would drive at in free-flow traffic conditions) v_n^0 , the free traffic minimum spacing (a minimum net distance that is kept even at a complete stand-still in a traffic jam) s_n^0 , the desired time headway T to the vehicle in front, the acceleration parameter a and the braking deceleration b , and a constant parameter δ . However, the IDM and its recent developments (Kesting et al., 2010) have only recently been applied.

Linear models: Helly (1961) proposed a linear model that included several terms for the adaptation of the acceleration $a_n(t)$:

$$a_n(t) = C_1 \Delta v(t - \tau) + C_2 (\Delta x(t - \tau) - D_n(t)) \quad (2.44)$$

$$D(t) = \alpha + \beta v(t - \tau) + \gamma a_n(t - \tau) \quad (2.45)$$

where $D(t)$ is a desired following distance, v is the speed of the follower vehicle n , Δv and Δx are respectively the distance and relative speed between vehicle n and $(n - 1)$, τ is the driver's reaction time, and α , β , γ , C_1 and C_2 are the model parameters. This model had its origins in the Gazis model described previously and was further improved by several authors, who introduced new components to the equation. The model was found to present a good fit to observed data.

Although the calibrated parameter values did not vary much in existing studies compared to the Gazis model, it was mainly applied on low speed traffic urban networks (Brackstone and McDonald, 1999). An advantage of the Helly model, however, is the specific incorporation of an error component, formulated as a possible rejection of the computed acceleration when Δx differs substantially from its expected value.

Psycho-physical models: The previous models assume that the following vehicle reacts to arbitrarily small changes in the relative speed to the front vehicle. They also assume that the following driver reacts to actions of the front driver even if the headway gap is large. These limitation may be overcome by extending the car-following model with additional regimes, such as free flow models, emergency decelerations, etc. A different approach was taken by Wiedemann (1974) who derived the so-called psycho-physical spacing models based on two main assumptions:

1. Under large spacings, the driver of a following vehicle is not influenced by the amount of speed difference.
2. Under small spacings, there are combinations of relative speeds and distance headways for which there is, as in 1, no response from the driver of the following vehicle, because the relative motion is too small.

With this framework, thresholds or action points where the driver changes behavior are specified, typically, by means of relative space-speed graphs (see Figure 2-4). In the uninfluenced driving regime (dark gray area in Figure 2-4), the follower is trying to reach its desired speed. When the perception threshold of speed difference at long distance (SDV) has been surpassed the follower enters the closing process regime. In this regime, the driver detects a slower vehicle in front of him and, after a given delay, starts to decelerate (light grey area in Figure 2-4). The driver's deceleration goal is to reach a desired minimum following distance, ABX, and at keeping the same speed as the leading driver. However,

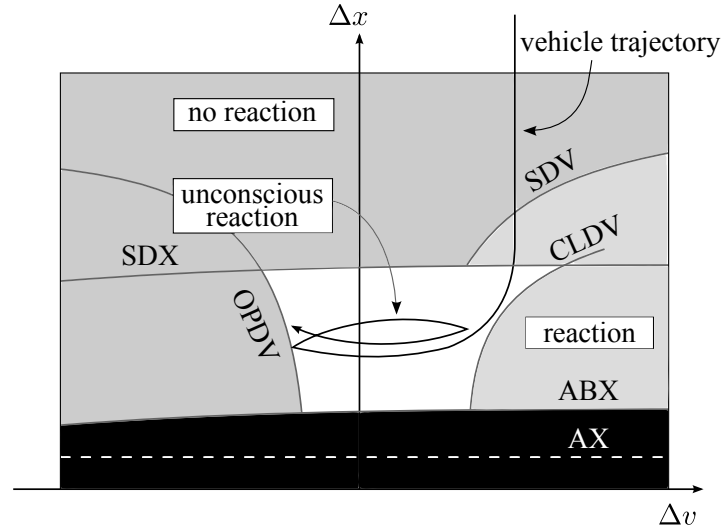


Figure 2-4: The Wiedemann psycho-physical model

the acceleration is applied unconsciously with very low oscillating levels. The following process is delimited by two perceptual thresholds for small speed differences at short, decreasing and increasing distances (CLDV and OPDV) and two thresholds corresponding to the minimum desired distance at low speed differences and the perception of growing distance in the following process (ABX and SDX) (white area in Figure 2-4). These models have been integrated in commercial software and applied in many simulation case studies (Fritzsche, 1994, Wiedemann, 1991). Similarly to previous modelling streams, many extensions and enhancements to the previously describe specification may be found in the literature, such as the calibration of the Wiedemann model to non-lane based behavior (Mathew and Radhakrishnan, 2010).

Fuzzy-based models: Fuzzy logic-based models use fuzzy sets to quantify decision alternatives, generally formulated by logical rules (Kikuchi and Chakroborty, 1992), for example, by checking if the the subject vehicle is driving "too close" to the front vehicle. Instead of knowing their exact motion parameters (speed, headway, gaps...) as in earlier described models, in fuzzy logic-based models, drivers are assumed to only be able to check qualitatively its range (as very low, low, moderate, high, or very high), and change their behavior accordingly. The fuzzy sets may overlap each other, using probabilistic density functions in the decision process. These models have not been as used as the previous research streams, but a few estimation and application studies are referred in the literature (McDonald et al., 1997).

Optimum velocity models: Optimal velocity models formulate the acceleration as a function of the difference between the velocity of the vehicle $v_n(t)$ and an optimal (targeted) velocity v_0 . Bando et al. (1995) assumed that the acceleration that a driver applies is proportional to the deviation of his/her actual speed from a desired speed, which depends on the distance to the leading vehicle. The model is expressed by:

$$a_n(t) = \alpha [v_0(\Delta x(t)) - v_n(t)] \quad (2.46)$$

$$v_0(\Delta x(t)) = \tanh(\Delta x(t) - 2) + \tanh(2) \quad (2.47)$$

where, $v_0(\Delta x(t))$ is the desired speed for a given space headway. Similarly, Newell (2002) formulated the car-following behaviour in a very simple framework, where the trajectory of a following vehicle is essentially the same as that of its leader, with a time-space translation and the inclusion of a desired speed. It was concluded that this model is able to replicate first-order macroscopic traffic flow variables, but fails to replicate detailed heterogeneous behaviors (Treiber et al., 2000).

Cellular automaton models: Cellular Automaton models use a grid-based space system to represent all types of behaviors. Car-following behavior has however been the center of driving behavior cellular automaton modelling because of the focus on traffic stability phases by its research community. Cellular automaton models have attracted much interest in the physics community as they provide a computationally efficient method for the simulation of large scale networks (Nagel and Schreckenberg, 1992). However they are not well suited for a detailed description of motion features due to the lack of a precise coordinates estimation framework.

Multi-regimes acceleration models

The collision avoidance model proposed by Gipps (1981) is also applicable to free-flow behavior. In fact, the model determines a maximum applicable acceleration based on both a minimum safe headway and the driver's desired speed. Using Gipps framework, five other models were formulated separately for five different situations, under which the driver should apply the most constraining acceleration: desired speed acceleration, free-flow acceleration, starting acceleration, car-following acceleration and emergency de-

celeration. Yang (1997) also developed a multi-regime acceleration model, but using the stimulus-response framework. The driver is assigned to one of three regimes (emergency, car-following and free-flowing) based on its current time headway. Another multi-regime acceleration model based on the stimulus-response framework was developed by Zhang et al. (1998). Toledo et al. (2007) developed an integrated model that accounts for accelerations of drivers who are adapting their side gaps to facilitate lane changing among other regimes. Finally Kosonen (1999) proposed a model based on a set of crisp rules where a limited set of perception and driving errors were integrated in a discrete implementation of a multi-regime model (Koskinen et al., 2009).

Lane change and Merging Models

Lane-changing behavior has not been studied as extensively as car-following behavior by the microsimulation community, but interest in this field has grown recently with the increasing computational capability to deal with more complex models and widespread access to multi-lane trajectory data sets.

Lane-changing models span both operational and tactical behaviors. Recent literature separates lane changing and lane selection to separate the physical act of changing lanes from the more tactical selection of lanes for route choice considerations. As lane changing models have evolved over time, they have increasingly added tactical components to what were previously strictly operational models. The general framework for lane-changing models consists of a decision process to: (a) consider a lane-change, (b) choose a lane, (c) search for an acceptable gap and (d) select a trajectory for the lane change.

Although the first documented lane changing logic is the model proposed in **TEXAS** (Rioux, 1977), the driving framework proposed by Gipps (1981) presented a clear representation of the lane-changing decision process intended for use in microsimulation. The balance between the necessity, the possibility and the desirability of a lane change was formulated considering three main factors: a desired speed, the correct lane for an intended downstream turning maneuver (if any) and the distance to the intended turn. Since then, several other lane-changing models have been developed for microsimulators. Following Rahman et al. (2013) classification these lane-changing models are categorized into four groups: rule-based models, discrete-choice models, artificial intelligence models, and incentive-based models.

Rule-based models: Gipps' model is a rule-based model. In its necessity-possibility-desirability framework, he included several factors, such as the availability of safety gaps, the location of permanent obstructions, the intent of turning movement, the presence of heavy vehicles, and a speed advantage. Furthermore, all these factors are considered in different ways for three spatial zones, which are related to the distance to the intended turn. Gipps' model structures the lane-changing process as a decision tree with a series of fixed conditions typically encountered on urban arterials, and the final output of this rule-based triggered event is a binary choice model (i.e., change vs. not change). Several enhancements to the basic Gipps model have been made (Liu et al., 1999, Barceló and Casas, 2003). However, the variability regarding individual driver behavior is not incorporated in the original model.

Halati et al. (1997) developed another (rule-based) lane-changing model where lane-change decisions are classified as mandatory lane-changing (MLC), discretionary lane-changing (DLC), and random lane-changing (RLC). MLC are related to route choice decisions or lanes drops. DLC are applied when the driver chooses to move to a faster lane. RLC is applied when there is no journey related reason, to account for stochasticity. Similarly to the Gipps' model, motivation, advantage, and urgency are considered. These three major factors are formulated as motion and spatial variables, such as the availability of acceptable gaps in the target lane, distance to exit, or number of lane changes to exit. Acceptable gaps are modeled utilizing the deceleration required by the subject vehicle to avoid crashing into its lead vehicle in the target lane. Hidas (2002) developed a very similar framework, but added a courtesy-forced lane changing for creating gaps when these are not available. In this courtesy-forced lane-changing mode, the subject vehicle sends a "courtesy" signal to the vehicles in the target lane asking for a replacement of their current leader by the signal sender and, thus, forcing the creation of gaps. Zhang et al. (1998) extended Halatis' model by including a probability for the lane change action, reflecting the real-world behavior that drivers do not always change lane even if it does benefit them.

In Van Aerde et al. (1992) DLC are considered by computing the potential speeds in both adjacent lanes (if available) and comparing those speeds to a pre-specified threshold distribution for decision making. In this model, vehicle's lateral movements are not simulated during the lane change but both lanes are considered occupied during part of the

manoeuvre (Rioux, 1977, Van Aerde et al., 1992). Similarly, Kosonen (1999) included an DLC model of lane changing based on computation of the traffic pressure (which depends on desired speed) into a general rule-based framework.

Cellular automaton (Nagel and Schreckenberg, 1992) models and the game theory framework proposed by Kita (1999) may also be classified as rule-based models.

Discrete-choice-based models: Yang et al. (1999) modeled MDL and DLC in a probabilistic framework based on utility theory models. The decision whether to respond to an MLC is modeled using a binary logit model, and DLC was modelled depending on traffic variables from the current and target lanes. Ahmed (1999) proposed a dynamic discrete choice model to capture heterogeneity in driving characteristics across the driving population and extended the discrete choice modelling to DLC and a forced merging model (FM). Lane-changing decisions were modelled as a three-step process: lane change action decision (see equation 2.48), target lane choice, and gap acceptance decision. If a MLC situation does not apply or the driver chooses not to respond to it, a decision whether to consider a DLC is made. This decision process is modeled in two steps using logit models. First, drivers examine their satisfaction with the driving conditions of the current lane, which is affected by the difference between the current speed of the subject vehicle and its desired speed and other traffic variables (heavy vehicles, tailgating...). Then, gap acceptance is modeled probabilistically as a function of critical lead and lag gaps.

$$P_n^{LC}(t) = \frac{1}{1 + \exp(-\beta^{LC} X_n^{LC}(t) - \alpha^{LV} v_n)} \quad (2.48)$$

where $P_n^{LC}(t)$ is the probability of executing a lane change manoeuvre for driver n at time t , with $LC = \{MLC, DLC, FM\}$, X_n^{LC} is the vector of explanatory variables affecting the decision to change lane, β^{LC} the corresponding vector of modelling parameters, v_n the driver-specific random term and α_{LC} its parameter.

Toledo et al. (2007) developed an integrated lane-changing framework to account for both a short-term goal and a short-term plan. The short-term goal is defined as a target lane and the short-term plan as a target gap; both are integrated with an acceleration model to facilitate the application of his/her short-term plan. Furthermore, this model structure allows state dependency in decisions made over time (e.g. persistence) to be directly captured through appropriate specification of the choice probabilities at the var-

ious levels. For example, the probability of targeting a lane-change may depend on the lane-change goal in previous time steps. Using part of Ahmed sub-models, the implementation of this general framework captured the inter-dependencies and correlations among the various decisions made by the same driver into an econometric framework of random utility choice models.

Choudhury (2007) introduced latent plans in the discrete-choice-based lane-change decision process to account for the possibility of choosing lanes with lower utility values in the short term, looking for the highest utility ones at the highest level of lane changing decision. This framework is extremely interesting when facing a large number of lanes or dedicated lanes such as high occupancy vehicles (HOV) lanes. The author also proposed a choice-based framework for different merging tactics in the decision framework, considering that the merging driver may choose between normal gap acceptance, merge through courtesy or decide to force in.

Artificial intelligence models: Similarly to the fuzzy acceleration models, fuzzy-logic-based lane-changing models are integrated into an "if-then" structure. In McDonald et al. (1997) lane change decision is formulated as a simple structure based on the average lane speed. Das et al. (1999) formulated Yangs' lane-changing model as fuzzy rules to consider the distance to the next exit or merge point and the required number of lanes to change.

ANN were also used in lane-change modeling (Hunt and Lyons, 1994, Tomar et al., 2010). These models are completely data driven and fundamentally different from the rule-based and discrete choice-based models. Although researchers can specify some network parameters, such as the number of inputs, hidden neurons and layers, they have very low control over the model structure, yet giving good fitting values against existing data.

Incentive-based models: Kesting et al. (2007) proposed a lane-changing model based on two criteria: incentive and safety. In their MOBIL (Minimizing Overall Braking Decelerations Induced by Lane-changes) model, the incentive criterion measures the attractiveness of a given lane, and the safety criterion measures the risk associated with lane changing, both formulated in terms of acceleration variations. The computed values are then compared against a threshold value for final decision making. In Schakel et al. (2012) model, the driver's desire to follow a route is considered to account, for example, for the propensity of drivers to avoid the rightmost lane to bypass the interference from exiting

and entering traffic on a multi-lane highway.

Modelling other driving behaviour maneuvers

Besides these two traditional main processes (acceleration and lane-change), special attention has recently been given to the modelling of more complex driving issues and processes on motorways, such as reaction time, driving errors, behavior under heterogeneous flow, detailed infrastructure characteristics, and vehicle lateral control.

Despite the large number of studies on driving reaction times using controlled experiments (such as laboratory and driving simulators) and on-site measurements, available simulators just recently stepped away from the simulation time-step dependency. In Yang et al. (1999), for example, driving decisions such as acceleration and lane-changing are made at time resolutions that are integer multipliers of the simulation step size. This simplified representation of reaction time resulted in the need for "emergency deceleration" regimes or "safety headways" to avoid vehicle overlaps, and improvements as regards modelling its variability were reported as necessary (Green, 2000, Gasser et al., 2007). Treiber et al. (2006) proposed an interesting improvement of the car-following model to mitigate these limitations by integrating spatial and temporal anticipation in drivers' estimation of variables.

Like the recent model proposed by Mehmood and Easa (2009), many behavioral studies relate reaction-time with the driving scenario and driver characteristics. These, however, would only be possible to integrate with more complex road agent models with cognitive frameworks such as the ones proposed by Kosonen (1999), Archer (2001), Xin et al. (2008), Koskinen et al. (2009). Basak et al. (2013) proposed a framework for modelling a per-agent tunable reaction-time to capture more realistic behavior in common traffic situations. They have demonstrated the improved realism in regards shockwaves, deceleration at intersections, and acceleration from stop-lines. These recent modeling streams try to bring the knowledge on information processing developed by psychology research (Wickens and Hollands, 1999) to traffic simulation tools. Besides the already mentioned studies by the reader is referred to the research by Boer et al. (1998), Boer and Hoedemaeker (1998) on driver attention modeling, as well as a recent review of driver state modelling in the context of collision avoidance and psychological modelling by Markkula et al. (2012). Salvucci (2006) also used the cognitive architecture to model a general driver

behavior framework. This cognitive architecture works as a modular framework with a set of buffers, written to and read from by both the various action sub-models and the central if-then production rules acting as a central bottleneck for cognition. This cognitive architecture has been used to model and reproduce a large number of experimental results. Fuller proposed several models, starting with a model based on avoidance of potential adverse consequences (Fuller, 1984), followed by the task-capability interface (Fuller, 2000), both based on psychological modelling and recently implemented in a multi-agent real-time simulation environment developed at TNO, in the Netherlands (Absil, 2008). All these models raise the potential for stepping away from accident-free simulation, a key factor of criticism on the use of traffic simulation as a safety analysis tool. Without these developments, the assessment of Intelligent Transportation Systems such as Advanced Driver Assistance Systems in large scale networks may always be biased. The question now remains if the wide-spread of increasingly fast developing technologies will be faster or slower than the modelling improvements available for simulation assessment.

Regarding heterogeneous behaviors associated with different vehicle types, most simulation tools simply resort to the method of assigning appropriate driver-vehicle unit (DVU) values based on the effect of the vehicle type. This approach ignores non-conventional behaviors and distinct lateral movement patterns evidenced by some vehicle categories, such as motorcycles. Some models however, allow specific vehicle classes to occupy the same lane as cars (PTV, 2009). Only recently frameworks for incorporating motorcycle driving behaviour into general traffic simulation models have been proposed (Hemakom et al., 2008).

With the raise of traffic efficiency and safety concerns in recently motorized countries, improvements to step away from non-lane based models have been recently proposed, with the development of strip-based models, general coordinate models and grid-models. As these frameworks rely in a different formulation of the network itself, none has been yet integrated into full detailed simulation tools and calibrated for different traffic scenarios. As we focus in traditional motorway simulation, non-lane based models were not considered in the current review. The interested reader should refer to Hranac et al. (2004a) for more details.

In lane-based flow models, lateral placement in lane is not represented. The notable exception is the **TWOPAS**, a microscopic computer simulation model for two-lane, two-way

highways. This model simulates traffic operations on highways by reviewing the position of each vehicle on a simulated roadway at 1 s intervals (St. John and Harwood, 1998). Oketch (2000) developed a modified lane-based model that allows gradual lane change maneuvers instead of instantaneous lane-changing, but wheel steering was not modelled in detail. The already mentioned psychological/cognitive human models typically integrate wheel steering models (Salvucci, 2006). Finally, specific overpassing behaviour such as the one modelled by Farah and Toledo (2010) for two-way roads are not typically modelled in motorway simulation, as these behaviours are captured by the typical-lane changing model.

2.2.2 Data used for estimation and calibration

The estimation of detailed driving behaviour models has systematically relied on very detailed data. Typically, vehicle trajectories and driver and/or vehicle characteristics are collected in the traffic scenarios of interest. Aggregated traffic data and environmental variables are also collected and are a key aspect when analysing the applicability and transferability of the estimated models. In the past, these data collection campaigns have been carried out under specific conditions and, sometimes, tightly controlled scenarios. The research community has now focused its attention on the collection of large naturalistic data sets, as both intra and inter driving behavior differences are better captured (Higgs, 2012). In Chapter 5 a detailed review of methods used for trajectory extraction is presented.

2.2.3 Simulation tools

With the above review, it is clear that, although some of the basic principles used for microscopic traffic simulation are based on similar reasoning, not all models are intended to simulate the same set of scenarios. Even in that case, different outputs should always be expected for detailed variables such as trajectories, considering their distinct specification and all the differences in stochasticity modelling. Panwai and Dia (2005) compared a set of car-following models, including those proposed by Wiedemann (1991), Fritzsche (1994) and Barceló and Casas (2003), and differences in speed and headway were recorded by an instrumented vehicle. Hidas (2005a) compared three different simulation tools, **AIMSUN**, **Paramics** and **VISSIM**, regarding their car-following, gap acceptance and lane-changing

Table 2.1: Simulation Tools and its models

Simulator	Car-following	Lane-change & Merging
AIMSUN	Gipps (1981)	Barceló and Casas (2003)
ARTEMIS	Hidas (1998)	Hidas (2002)
CORSIM	Zhang et al. (1998)	Halati et al. (1997)
DRACULA	Gipps (1981)	Liu et al. (1999)
HUTSIM	Koskinen et al. (2009)	Kosonen (1999)
Integration	Van Aerde et al. (1992)	Rakha and Zhang (2004)
MITSimLab	Ahmed (1999)	Toledo et al. (2007), Choudhury (2007)
Q-Paramics	Fritzsche (1994)	Duncan (2000)
VISSIM	Wiedemann (1991) ¹	Willman (1978), Sparmann (1979) ²

¹ for urban roads, VISSIM uses Wiedemann (1974)

² many of the documented publications of Willmann and Sparmann are published in German and brief descriptions of the algorithm are only available in literature from other authors.

models specifications and parameters, and also the outputs of a theoretical experiment in a two-lane freeway scenario. However, these three simulation tools belong to the short group of integrated platforms available for fast implementation and that have been successfully used in a variety of transportation projects. This type of integrated platforms represent by far the large majority of simulation applications worldwide, and just three of them account for a share of 67% of the practitioners and researchers preference (TU0903-Cost Action, 2012). With the increased use of such platforms in network efficiency studies and also in safety analysis, it is important to understand how they represent detailed behaviours, and how they replicate detailed traffic data, such as trajectories. It is also relevant to develop frameworks to assess their output quality from a safety perspective.

To better understand the modelling differences between the main integrated simulation tools, their link to the behavioral models detailed in the last section is presented in Table 2.1. It's worth pointing out that some of the implemented models might not follow exactly their original formulation. In Table 2.2 some of the additional features available on these platforms that may be of interest in the analysis of detailed traffic variables such as trajectories are assessed. The availability of the model source-code (SC) is a key aspect, as its analysis may help to understand fully the behavioral interactions modelled. It is worth to point out that in the last couple of years three leading commercial software houses released a set of tools allowing for multiple changes in the specification of several sub-models and algorithms of their products. AIMSUN released its Software Development Kit (SDK) enabling the specification in C++ of alternative major behavioural models.

Table 2.2: Simulation Tool Features (extended from Gettman and Head (2003a))

Simulator	SC	VRT	CY	SDL	DEM
AIMSUN	no	yes	yes	yes	no
ARTEMIS	no	no	yes	ni	yes
CORSIM	yes	no	yes	yes	no
DRACULA	no	no	yes	no	no
HUTSIM	no	yes	ni	ni	yes
Integration	no	no	no	no	no
MITSimLab	yes	yes	yes	yes	no
Q-Paramics	no	yes	ramps	no	no
VISSIM	no	yes	ramps	yes	no

SC: source-code available; VRT: variable reaction time; CY: courtesy yielding model

SDL: sight distance limits; DEM: driver error modelling; ni: no information.

VISSIM-API allows the user to specify a signal control policy and part of the driving behaviour model, through the specification of .dll files. Finally, Q-Paramics was extended with a number of plug-ins developed at the University of California, Irvine, for the user control over the traffic management systems.

In Table 2.2, VRT represents a variable driver reaction time (VRT) modelling feature that allows for a representation of heterogeneous driver decision making and is a key aspect for the replication of the stochastic process of human decision. The courtesy yielding modelling (CY) has an important role in avoiding abnormal decelerations especially in busy motorway simulation. The sight-distance limits (SDL) models control drivers’ “look-ahead” distance when making decisions (for each individual driver or driver type) allowing for a more accurate modelling of drivers’ situation awareness. Lastly, the driver error modelling (DEM) introduces the possibility of implicitly represent some human erroneous processes (e.g.: perception error).

Other integrated models are also available for motorway microscopic simulation. The SUMO (Krajzewicz et al., 2002) platform is of particular interest due to its open-source formulation (such as MITSimLab) and its constant enhancement by the actual research community. The commercial platform TransModeler, one of the most applied tools in the USA, is based on the MITSimLab driving behaviour framework. Unfortunately, the commercial software Cube DynaSIM (CubeDynamics, 2013) has less documentation on its core models than the other reviewed models. Finally, freeway simulators such as ARCHISIM (Champion et al., 2001), FOSIM (Dijker, 2012), SITRA (Breheret, 2003), ATMO-MARS (Klunder et al., 2006) and TRITONE (Astarita et al., 2012) have a narrower focus on particular

research applications or are still in developing stage.

A final note on **S-Paramics** is also appropriate. The **Paramics** project started in 1992 at the University of Edinburgh. However, the project originated two distinct development streams: **Q-Paramics** (Quadstone) and **S-Paramics** (SIAS). The latter has, unfortunately, less documentation on the structure and model parameters than the former.

2.3 Safety studies using simulation

Microsimulation environments have long been a seemingly attractive tool for testing safety related solutions, thanks to the high level of detail regarding the road geometric representation, the driver and vehicle heterogeneous characteristics, the vehicle motion description and the flexibility for testing multiple traffic management algorithms, especially when expensive infrastructure interventions are at stake (Archer, 2001).

One of the most important developments regarding the use of surrogate safety indicators by microscopic simulation applications for intersection safety assessment was carried out by the U.S. Federal Highway Administration (Gettman and Head, 2003a). In this comprehensive study, a comparison of the application of nine microscopic simulation packages (**CORSIM**, **SIMTRAFFIC**, **VISSIM**, **HUTSIM**, **Q-Paramics**, **TEXAS**, **AIMSUN**, **WATSIM**, and **Integration**) for intersection safety assessment was presented. This evaluation relied on several factors that ranged from modelling specifications to practical aspects such as trajectory extraction from the simulators. At the time, the authors did not state any preference regarding any of the simulation packages but, **VISSIM** was deemed able to support most features required for better safety studies. This research resulted in a larger project (Gettman et al., 2008) with the purpose of developing a general post-processing tool for computing surrogate indicators from simulation-based trajectories: the Surrogate Safety Assessment Model (SSAM). SSAM computes six surrogate measures used as frequency and severity safety indicators: TTC, PET, DR (deceleration rate) for conflict probability assessment; MaxS (Maximum of the speeds of the two vehicles involved in the conflict event) and DeltaS (Maximum relative speed of the two vehicles involved in the conflict event) for conflict severity assessment.

Torday et al. (2005) used **AIMSUN** to investigate the occurrence of potential rear-end collisions in motorways. The UD surrogate safety initiator (see equation 2.36) was proposed

and tested against three years of accident data obtained from a 7 km freeway segment in Geneva, Switzerland.

Archer (2005b) investigated the potential use of the microsimulation package VISSIM for safety assessment. His study focused on the estimation of traffic conflicts at 3 leg stop controlled intersections using microscopic simulation. The simulation experiment was designed to consider 3 different two-hour time intervals: morning peak, off-peak, and afternoon peak periods. A total of 20 simulation runs for each time interval were performed. It is worth noting that Archer formally attempted to calibrate and validate VISSIM with respect to three measures of performance (MOP): time gap distribution, traffic flow and speed. Four surrogate safety indicators were tested in this study: TTC, PET, TTA and DRAC. Observed measures of TTC, PET, and DRAC were manually extracted from a 6 hours video recording and TTA values were obtained from 18 hours of a conflict survey. After analysing the results, Archer suggested that, in general, the simulation experiment shows a reasonable level of consistency in conflict frequencies and severities, as regards all four surrogate safety indicators tested. Furthermore, differences between simulated and observed safety measurements were hypothesized to be due to the nature of microscopic models which are not able to fully emulate the complex road user behaviour and vehicle performance when subject to risky situations. The authors concluded that, in theory, microscopic traffic models have the potential to account for important factors that heavily influence accident occurrence, including different behavioural aspects of drivers and individual pair-wise vehicle interactions.

Lee et al. (2006) used a log-linearly estimated accident probability model to identify accident precursors (see Section 2.1.4) based on loop sensor data, and simulated the effect of VSL on a 4.7 km stretch of the Gardiner Expressway in Toronto, Canada. VSL scenarios were simulated in Q-Paramics, but only two key parameters (the mean headway factor and the mean reaction time) were calibrated. Using the same approach, Samimi and Hellinga (2012) tested the sensitivity of the categorization of the accident precursors studied by Lee et al. (2006) on the effects of VSL using Q-Paramics.

Ozbay et al. (2008) used Q-Paramics to validate a surrogate safety indicator (CI) through comparison between simulated indicators and real accident records. This validation was carried out for a 10.7 km stretch without interchanges of the New Jersey Turnpike, USA. Real accident records between 1996 and 2005 for this section were used,

comprising more than 1000 records with data such as accident type, time, location, and vehicle characteristics. Only rear-end and sideswipe accident records were considered in the analysis. To get statistically robust results from the simulation experiments the authors performed several replications using different random seeds. However, no details on the calibration procedure are described in the paper. Both temporal and spatial predictions of the modified-TTC and the CI performed well in comparison with the observed accident frequencies on-site.

Pirdavani et al. (2010) used **S-Paramics** to compute PET values at a single unsignalized intersection experiment for different traffic volume and speed limit conditions. As expected, the results showed that PET values dropped substantially after increasing the speed limit on both conflicting legs. Furthermore, the safety level deterioration was observed following the traffic volume increase (but still within uncongested levels). This study was a theoretical experiment and no calibration was performed with real data.

Dijkstra et al. (2010) used **S-Paramics** to compute TET values for a large network comprising a total of 569 junctions in the west of The Netherlands. Accidents with only motor vehicles involved and that occurred in the 6:00 to 10:00 a.m. weekdays period were selected. The simulator was calibrated for this morning peak-period for an average weekday. Generalized linear models assuming either the negative-binomial or the Poisson distributions for different log-linear specification were developed for the relation between accidents and TET conflicts. Although the results suggested that there was a statistical relationship between observed accidents and calculated conflicts, many practical issues regarding the computation of TET for different scenarios and the uncertainty on the calibration and modelling assumptions were raised by the authors.

In Duong et al. (2010) **VISSIM** was used to test left-turn lane offsets at intersections. Two intersections were designed with and without the left-turn lane offset and assessed by means of TTC and PET based conflicts. However, the main benefit of left-turn lane offsets is the improvement in the line-of-sight regarding opposing vehicles, which are not appropriately modelled in **VISSIM**.

Liu (2010) calibrated six driving behaviour parameters of **Q-Paramics** to match collected headway distributions (during 1 min intervals) on weekday peak hours for three highway stretches (I-66, I-64 and I-81 in the USA) with the purpose of specifying guidelines for selecting truck lane restriction strategies using the safety surrogate indicator

TTC.

Ariza (2011) used a calibrated model of the waterfront area of the City of Toronto, Canada, in **Q-Paramics** to assess the suitability of using SSAM surrogate safety indicators to estimate intersection and arterial collision frequencies. This assessment was carried out using a linear regression model and a generalized linear model with a negative binomial error structure. The model predictions were compared to volume-based aggregate model predictions and historical data from Toronto, Canada. A negative-binomial generalized linear model was used and fitted to the same arterial and intersection data set used to fit the conflict-based models. Using such method, the author concluded that the predictions generated by a conflict-based model were comparable to the aggregate ones for intersections, but failed to predict accident frequencies for arterials.

Bevrani and Chung (2011) used **AIMSUN** to validate the distribution of several surrogate safety indicators on a straight stretch of the Pacific Motorway in Brisbane, Australia. The real data used for validation was extracted from loop detectors that collected information for each individual vehicle. A calibration process based on capacity, speed and headway data was conducted. However, no details of this calibration process are described in the paper. The results showed that all critical safety indicators were highly underestimated by the model when compared with the observed distributions.

Very recently, Huang et al. (2013) tested **VISSIM** in the replication of SSAM surrogate safety indicators. A two stage calibration approach based on genetic algorithms and using the mean absolute percent error (MAPE) as goodness-of-fit measure was adopted (see Figure 2-5). The first-stage calibration focused on calibrating the **VISSIM** simulation model to reproduce performance measures such as volume, speed and headways, and the second-stage focused on adjusting crucial parameters in **VISSIM** and SSAM (surrogate safety indicators thresholds) to replicate the conflict counts. A sensitivity analysis reduced the number of parameters to be calibrated to four (three for the **VISSIM** car-following model and one for the SSAM TTC threshold). Field data were collected at ten signalized intersections in Nanjing, China by means of a radar gun (sampled speeds) and 80 hours of video recordings (weekday peak traffic flow and traffic conflicts counts at 15 min time intervals by trained observers). The authors underlined the importance of appropriate calibration procedures, as the MAPE value for total conflicts was reduced from 43% to 24%, after model calibration. More specifically, the MAPE value was reduced from 24%

to 16% for rear-end conflicts, from 70% to 23% in the case of crossing conflicts, and from 85% to 79% for lane-change conflicts.

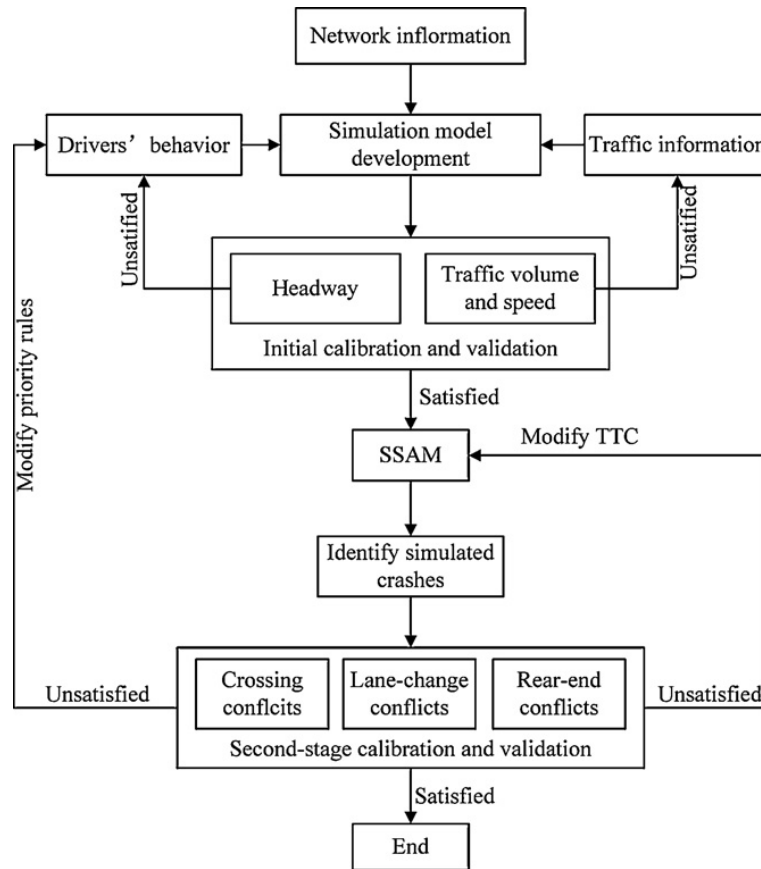


Figure 2-5: Two-step calibration approach (Huang et al., 2013)

Okamura et al. (2011) used *Q-Paramics* with a new driving behaviour model (Xin et al., 2008) that accounts for perception errors, to assess the safety benefits of installing a driving support system. The authors used the TIDSS to evaluate the adaptive cruise control system (ACC) and automated platoon system (APS) for heavy trucks on the Tokyo metropolitan expressway in Japan. With this aim, several simulation scenarios with different installation rates of ACC and APS were simulated and the relations between installation rate, safety indicators, and traffic flow rate on the TIDSS were analyzed. The driving behaviour parameters were set randomly based on distributions obtained by the Japan Automobile Research Institute and the Japanese Industrial Standards in real car-following measurements.

Besides these efforts using surrogate safety indicators, it is worth pointing out that some researchers opted for the use of accident probability models to perform the safety assessment of microsimulation experiments. Abdel-aty et al. (2006) tested the effect of

variable speed limits on Interstate 4 in Florida, using **Q-Paramics** simulation platform and a matched case-control logistic regression for accident likelihood prediction (Abdel-Aty et al., 2004). Later, the authors calibrated a nested logit model (Abdel-aty et al., 2007) and an ANN accident probability model (Abdel-aty and Gayah, 2010) to estimate the effect of ramp metering on accident frequency, using **Q-Paramics**. The models were estimated using 5 min aggregated traffic variables from loop detectors spaced every 800 m throughout the pilot road length.

Along the years, all the above applications clearly evolved to finer descriptions of the driving behavior and the accident phenomenon itself. While this process has required more detailed data collection and calibration efforts, the success of the few applications of both surrogate safety measures and detailed aggregated probabilistic models have given the first insights on how the detailed analysis of accidents can be done in simulation. This evolution was also documented in a very recent and comprehensive review by Young et al. (2014), where some of the above mentioned studies are also analysed. From the review, the authors also clearly pointed out the need of analysing the probabilistic nature of the link between conflict and accidents and generalising the models to accommodate for different types of accidents.

2.4 Simulation applications in Portugal

Only in the past ten years, microscopic simulation was established as an assessment tool in Portugal. The large majority of studies referenced in the literature are related to the analysis of the expected impact of particular infrastructure-based or vehicle-based ITS solutions on traffic performance. Unfortunately, no significant methodological improvement regarding safety analysis using traffic microscopic simulation tools or driving behaviour modelling was found. However, some interesting research studies regarding particular applications of simulation platforms may be singled out:

- Launched within the study of an innovative ITS solution for network efficiency, the intermittent bus-lanes (Viegas, 2007), the University of Lisbon has recently studied how dynamic changes in traffic network topology by means of real-time ITS may affect the system's performance (Geraldes and Viegas, 2010). In both studies, the simulation platform **AIMSUN** and its SDK were used.

- Vilarinho (2012) compared a set of goodness-of-fit (GoF) measures in the sensitivity analysis of a set of **AIMSUN** parameters for a case study in Porto, Portugal, against aggregated traffic data. The results of this sensitive analysis pointed out the GEH statistic as the best GoF measure. The importance of sensitivity analysis to the appropriate use of simulation applications and a detailed discussion of candidate methods for this analysis are presented in Chapter 6.
- The **DIVERT** is a microscopic simulation platform dedicated to vehicular networks and developed over the recent years at the University of Porto. Although its driving behaviour models are not as developed as those in current state-of-the-art integrated microscopic simulation tools, its flexibility as open-source software, its potential to deal with large scale networks and the integration with network communication simulators lays ground for interesting and non-traditional relevant applications (Fernandes et al., 2010).
- A set of roundabout simulation studies has been carried out at the University of Coimbra. In one of the most recent studies within this research stream, Vasconcelos et al. (2012) developed a gap-acceptance model for microscopic simulation of roundabouts. The model was calibrated using video-extracted trajectories collected at a one-lane urban roundabout and validated against conventional methods.
- Teixeira (2010) was the first documented study in Portugal that tried to assess the safety performance of roundabouts by means of surrogate safety indicators. The **VISSIM** platform and the **SSAM** tool were used for simulating a roundabout in the city of Aveiro. Four different demand scenarios were simulated for the default configuration, and a reduced posted speed limit scenario, a scenario with more aggressive driving parameters and a scenario with reduced speed distribution close to the existing pedestrian crossings. The calibration of the **VISSIM** base scenario relied only in aggregated data (counts) collected on-site, and aimed at correctly replicate the daily traffic variability. The aggressive driving scenario was based on the safe distance in queue (three parameters), lane-changing (two parameters) and gap acceptance models (two parameters). Unfortunately, these parameters were altered to groundless values without a meaningful relative variation and all at the same time, thus, not accounting for possible interactions. Furthermore, the **SSAM** threshold parameters were not calibrated although roundabouts were not

used in SSAM original estimation. The resulting surrogate safety performance was compared with aggregated accident frequency model estimates from a calibrated model for New Zealand for roundabouts (Turner et al., 2009). The lane-change conflicts detected by SSAM showed a good correlation with estimates of aggregated accident frequencies. An alternative roundabout design was also tested, to correct the current layout that did not comply national regulations, but the conclusions regarding safety performance benefits were not unequivocal.

- In a similar approach Habtemichael and Picado Santos (2013b) linked VISSIM to SSAM and performed two separate sensitivity analysis of car-following and lane-changing models. The experimental design was based on a one-at-time (OAT) approach and four levels were considered for each of the 10 car-following parameters in the first analysis, and the 11 parameters of the lane-changing model in the second analysis. Although some known simulation concerns were addressed, such as multiple runs for stochasticity control, the authors opted to narrow down the sensitivity analysis by ignoring parameter interactions and by limiting the number of parameters considered, which may lead to biased results and affect any conclusions regarding transferability (see discussion in Chapter 6). The authors then tested SSAM conflict statistics for different VSL configurations in a 7 km stretch of the motorway A5 in Lisbon, Portugal, using VISSIM (Habtemichael and Picado Santos, 2013a). Calibration was carried out by tuning just a single car-following parameter (desired headway), using average loop sensor speed and counts by 5 min intervals regarding the GEH statistic for the morning peak hour. For correlating simulated vehicle conflicts with real accidents, 12 simulations each representing two different hours of a typical weekday were conducted to represent daily variability. The statistical analysis relied on a total of 447 accidents registered on the A5 stretch for a 5 year period. A log-quadratic equation regression was then estimated based on 2 hour aggregated data, for both simulated conflicts and real accidents, resulting in good fitting statistics. Finally, different compliance of VSL levels and VSL configurations were simulated and assessed. Later, the authors used the same approach to assess the impact of different simulated "high risk drivers" by testing different parameter values that may be relate to risky behaviours, such as headway time for tailgating or desired speed for speeding (Habtemichael and Picado Santos, 2013c).

As Bonsall et al. (2005) referred, the choice of appropriate GoF measures is a key aspect. When relying in a calibration process based on the headway time parameter alone, occupancy related measures should be preferred to aggregate loop-base counts or speeds. Besides, no disaggregated calibration using detailed traffic variables was performed, resulting in a (non-validated) initial set of parameters. The authors also related the accident occurrence to (hourly) weekday average sensor data. Although it forms a better approach than daily averages, a direct association between each accident and the traffic conditions for the specific day of the occurrence is preferred. Finally, the approach used two-vehicle accidents only and no reference is made as to whether run-off lane triggered accidents were treated separately, as they are a different accident phenomenon.

2.5 General comments

The development of safety assessment methods has been consistent and sustained by continuous improvements in data collection methods and in computational performances. The state-of-the art has clearly defined the current limitations of all classic modelling streams described earlier. However, the availability of detailed trajectory data has raised several questions regarding the accident phenomenon and created a source for potential improvements in the development of surrogate safety indicators and probabilistic models. Although particular reviewed simulation studies successfully managed to estimate surrogate safety performance, especially regarding intersections, the development of probabilistic models form a promising path towards aggregate safety data independence in the estimation process (but not validation).

The most recent driving behaviour model formulations allow for several improvements (especially in car following behaviour) such as decoupling the simulation step from reaction times, adding look-ahead abilities, making the estimation of the leader's deceleration more flexible, accounting for anticipation and supporting multiple regime decisions. With all the experiments reported in the literature, one may assume that the modelling state-of-the-art provides reasonable aggregate results in uncongested conditions and, for some models, in congested conditions as well. However, some models still fail to provide satisfactory results in the transitions from uncongested to congested. Furthermore, even

considering that the number of sub-models and their parameters has been growing significantly, results at the disaggregated level, such as detailed vehicle interactions, are not always well replicated. In fact, implementing non-accident-free models including cognitive and driving error modelling structures seems to be the coming step to improve disaggregated results reliability and to provide a more general framework compatible with accident occurrence.

Along with these innovative modelling frameworks, the research community has also focused on developing models and procedures to correctly apply the existing and widely disseminated simulating platforms for safety assessments. The replication of individual trajectories still requires and generally misses a great calibration effort. The selection of calibration algorithms and their measures of performance (MOP) for safety assessment are also key aspects. Due to the model (accident-free) specification, using the traditional aggregated network MOP such as traffic counts alone, may result in inappropriate safety-related driving behaviour parameters (Bonsall et al., 2005). During the calibration of VISSIM for the safety assessment of the US Highway 101, for example, Duong (2009) compared two genetic algorithm calibration processes using a multi-criteria MOP using counts, occupancy and speed against a single-criteria MOP based on the surrogate indicator CPI. As expected the single-criteria procedure provided the best estimates of the surrogate indicator, good estimates of speed, but poor results for traffic volume. On the other hand, the multi-criteria procedure resulted in reasonable measures of safety performance and the best results for the other aggregated measurements.

In any calibration procedure for innovative modelling research and new solutions testing, it is important to understand how the microscopic simulation tool and its driving behaviour models are structured. If the uncertainty on such knowledge is not considered, modelling formulation and practical results may be weak and seriously biased, compromising their usefulness.

With the above, it is clear that research efforts regarding the better replication of detailed traffic statistics by microscopic simulators and the development of probabilistic safety models are needed.

Chapter 3

Modelling Framework

In this Chapter, a conceptual framework for probabilistic safety assessment using microscopic traffic simulation tools is presented. This framework aims at bringing a probabilistic structure for the estimation of accident occurrence probability by means of artificial data generated by microscopic traffic simulation tools. In the first section, general concepts and the main assumptions considered for the modelling formulation are presented. Subsequently, the general modelling framework and the specific model components for urban motorways are presented. The estimation framework is presented in section 3.4 and the main limitations of the proposed model are discussed in the final section.

3.1 General modelling assumptions

In the literature review presented in Chapter 2 the need for probabilistic models that could be integrated in microscopic simulation tools was clearly identified. The specification of such model has to consider the limitations of driver behaviour models used in generic simulation tools, namely its intrinsic accident-freedom specification, while being able to link the simulation outputs to accident occurrence probability.

The accident-freedom specification has influence on two important aspects to consider in safety modelling formulation:

- All simulated trajectories are constrained by this assumption and appropriate replications of both accident and near accident trajectories are not expected;
- Only real accident-free trajectories should be needed for its estimation and calibration.

As reviewed in Chapter 2, the link between accident occurrence and traffic variables has been achieved either by estimating the probabilities of all possible trajectories or, more frequently, by fitting a regression model using a linear combination of aggregated traffic variables or surrogate safety indicators. In the first approach, the probabilities may, in fact, be directly computed, avoiding the use of aggregate safety data, but either accident and near-accident trajectories or driving error models are needed for the appropriate probability estimation. When opting to estimate accident frequency using a linear combination of aggregate traffic variables or safety surrogate indicators, two main problems may arise: absence of a causal relationship between different levels in the safety pyramid, and statistical problems of aggregation due to the use of aggregate traffic and safety records. In the next section mathematical representations of cause-effect mechanisms between detailed traffic variables and the probability of different types of accidents are proposed. Even though the driver error process is not modelled in simulation tools, those representations may be developed assuming that, similarly to the safety continuum theory (see Figure 2-2), traffic characteristics are directly related to the accident occurrence probability.

Furthermore, the proposed model does not only aims at estimating the accident occurrence probability, but also to estimate the accident type itself. Here, ordered (hierarchical) architectures are not suitable and interactions between outcomes should still be expected. Side (or angled) collisions, for example, are triggered by inadequate lateral movements and, although they are expected to be more frequent in lane-drop or merging areas, they may also be related to lateral evasive manoeuvres to avoid rear-end-collisions. Similar manoeuvre interactions may also be formulated for run-off-road and rear-end accidents.

3.2 General model structure

It is first assumed that the state of a vehicle n at time t can be viewed as a discrete variable whose state outcome k can be different types of accident or no accident at all. An individual outcome k among all possible outcomes K is considered to be predicted if its probability $\Pr_{n,t}(k)$ is maximum. As in previous research studies, the main difficulty is how to estimate $\Pr_{n,t}(k)$. This probability should be a function of specific observed variables characterizing the interaction between vehicles (Songchitruksa and Tarko, 2006). Such consideration steps away of the assumption of a fixed coefficient model converting

the surrogate event frequency into accident frequency, typically used in the traffic conflict technique. Thus, the probability for a specific accident involving vehicle n to occur at time t is assumed to be estimable by a specific accident propensity (or proximity) measure, with a specific formulation for each type of accident (Tarko et al., 2009):

$$\Pr_{n,t}(k) \sim U_k \quad (3.1)$$

In our proposed model, each accident propensity function U_k , is considered to have a (deterministic) safety score (V_k) component and a random component (ε):

$$U_k = V_k(X, \beta) + \varepsilon \quad (3.2)$$

where X is the vector of explanatory variables, β is the vector of unknown parameters to be estimated and ε_i is the random term (the terms n and t were omitted for simplicity). The assumption of the deterministic safety score component agrees with the more recent research stream where detailed interaction variables directly affect the accident occurrence probability itself. The random component ε is assumed to represent the unobserved effects involved in the determination of the outcome; whether these are derived from a random process in the occurrence of a specific event outcome or caused by a lack of knowledge of this process.

As it is common in safety modelling research, the accident phenomenon relies on many different variables, such as: network and road characteristics, traffic system management state, environmental variables, vehicle characteristics and driver (and passenger) characteristics:

$$V_k(n, t) = f_k(X_{n,t}, X_{n',t}, X_{D,t}, X_S) \quad (3.3)$$

where for any vehicle n in the system, the safety score $V_k(n, t)$ can be computed at each time-step t , dependent on the k accident-type specific scoring function f_k , which depends itself on: $X_{n,t}$, the driver-vehicle unit n specific variables at time t ; $X_{n',t}$, the variables at time t for the interaction between n and a conflicting driver-vehicle unit n' ; $X_{D,t}$, the dynamic environmental variables at time t (e.g.: weather, variable speed limit, lighting conditions, etc); and X_S , the static environmental variables (e.g.: geometrics, road signs, etc).

Note that driver characteristics are typically not considered in traffic simulation tools,

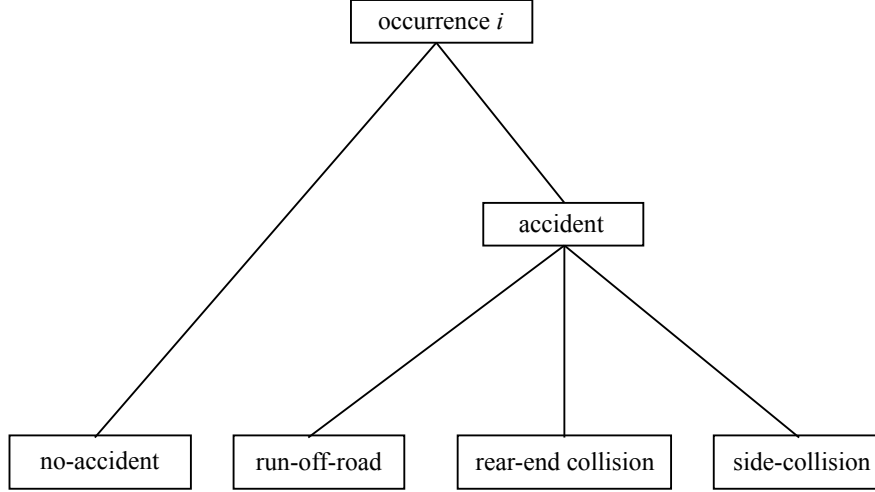


Figure 3-1: Model structure for motorway accident occurrence

which substantially limits the number of available variables $X_{n,t}$. Such variables are typically used in accident-severity modelling based on detailed accident reports, allowing for the consideration of drivers' risk perception surrogates and risk-taking variables. Although these variables are absent in simulation, some unobserved driver specific variables may still be considered in the safety modelling framework (see discussion in section 3.5). Finally, as the accident phenomenon differs for distinct types of accidents, it is expected that the formulation of the safety scoring function f_k will depend on the type of outcome k .

In the present model we push the formulation of each function f_k to represent a cause-effect relationship, to simultaneously deal with different types of accident outcomes and to consider a disaggregated probability for any vehicle state (n, t) observation (instead of the existing aggregate formulation used in real-time accident probability models).

In the present document, the above general formulation is restricted to a specific set of accidents that typically occur on busy urban motorways: rear-end accidents, side collisions during a lane-change manoeuvres and run-of-road accidents. It is clear that these three different outcomes correspond to very distinct phenomena. However, it is also clear that these three outcomes may be related, namely if one considers accident outcomes following an evasive action from different risky interactions (see Figure 3-1).

3.3 Model components

In this section the safety scoring function formulations for the three types of interactions considered are presented: rear-end (RE) conflicts, lane-change (LC) conflicts and run-off-road (ROR) events.

3.3.1 Rear-end (RE) conflicts

When facing rear-end interactions (typically when the subject vehicle is in a car-following state) the probability of a collision should depend on two important aspects: the subject vehicle braking requirements to avoid a RE collision and the maximum available braking power. The subject vehicle braking requirements during a vehicle interaction is represented by the difference between the relative acceleration, $\Delta a(n, t)$, and the deceleration rate required to avoid crash, $DRAC(n, t)$, estimated using Newtonian physics for every time interval:

$$\Delta a_+^{need}(n, t) = \max(0, DRAC(n, t) + \Delta a(n, t)) \quad (3.4)$$

$$\Delta a_-^{need}(n, t) = \min(0, DRAC(n, t) + \Delta a(n, t)) \quad (3.5)$$

$$DRAC(n, t) = \frac{[v(n, t) - v(n-1, t)]^2}{2[x(n-1, t) - x(n, t) - l(n-1)]} \quad (3.6)$$

where $\Delta a^{need}(n, t)$ is the needed deceleration to reach the $DRAC$ for the subject vehicle n at time t , $\Delta a(n, t) = a(n, t) - a(n-1, t)$ is the acceleration difference between the subject vehicle and its leader, and $v(n, t)$, $x(n, t)$ and $l(n)$ are the speed, longitudinal position and length of the subject vehicle (see Figure3-2).

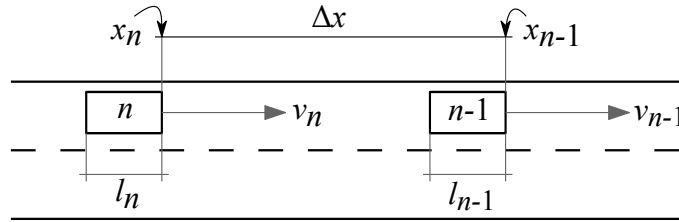


Figure 3-2: Rear-end Interaction

The split of the needed deceleration rate into its positive ($\Delta a_+^{need}(n, t)$) and negative ($\Delta a_-^{need}(n, t)$) components allows for the consideration of different parameters associated with different safety conditions: when the relative speeds are increasing or decreasing.

The advantage of considering the needed deceleration add-on (Δa^{need}) instead of just the *DRAC* (as in previous surrogate safety indicator formulations) is the introduction of the current acceleration state, making the simulated probability of RE collisions dependent on the simulated accelerations, relaxing the hypothesis of constant speed used by *DRAC*. Now, for the same *DRAC* values, different probabilities may be obtained for different relative accelerations and will directly depend on how far the relative acceleration of the subject vehicle is from the *DRAC*.

In Figure 3-3 a pair of vehicles in a theoretical car-following situation is illustrated. It is important to note that this illustration does not represent reality (as it has strong discontinuities in the acceleration function), but easily illustrates the benefits of the proposed formulation. It is assumed that the leading vehicle has a constant speed of 25 m/s up to $t = 14$ s. Then, her/his driver decelerates at a rate of -2 m/s^2 to a stopped state at $t = 26$ s. The following vehicle starts 35 m behind, with a speed of 20 m/s and accelerating with a rate of 1.5 m/s^2 , trying to catch up. At $t = 7$ s, her/his driver starts to decelerate at a constant rate of -1 m/s^2 . At $t = 19$ s it starts to decelerate with a rate of -2.5 m/s^2 , reaching a stopping at $t = 27$ s and a 2m gap spacing. The top figure indicates the vehicles' relative distance, speed and acceleration until stopping time. The bottom figure represents the *DRAC*, Δa , Δa^{need} and the rate $RA^{need} = \Delta a^{need}/TTC$. The light red area represents situations where the *DRAC* > 0 , but with a higher relative deceleration rate, and therefore a safer situation when compared to the dark red area where following vehicle haven't adjusted its acceleration yet.

The value of Δa^{need} is easily interpreted: the negative values represent safer values, for which the vehicle is already applying a deceleration rate greater than *DRAC* ($v_n > v_{n-1} \wedge \Delta a < DRAC$). We further improve this simple formulation by dividing the needed additional acceleration Δa^{need} by the *TTC*. By introducing the *TTC*, one considers not only how much additional deceleration is needed, but also how long the driver has to apply it. The Δa^{need} will then depend on the available time for adjustment, considering the available spacing and the relative speeds, resulting in a relative needed deceleration ratio RA^{need} :

$$RA^{need}(n, t) = \frac{\Delta a^{need}(n, t)}{TTC(n, t)} \quad (3.7)$$

where Δa^{need} is the needed deceleration rate defined by equations 3.4 and 3.5, $TTC(n, t)$

is the time-to-collision given by:

$$TTC(n, t) = \frac{x(n-1, t) - x(n, t) - l(n-1)}{(v(n, t) - v(n-1, t))} \quad (3.8)$$

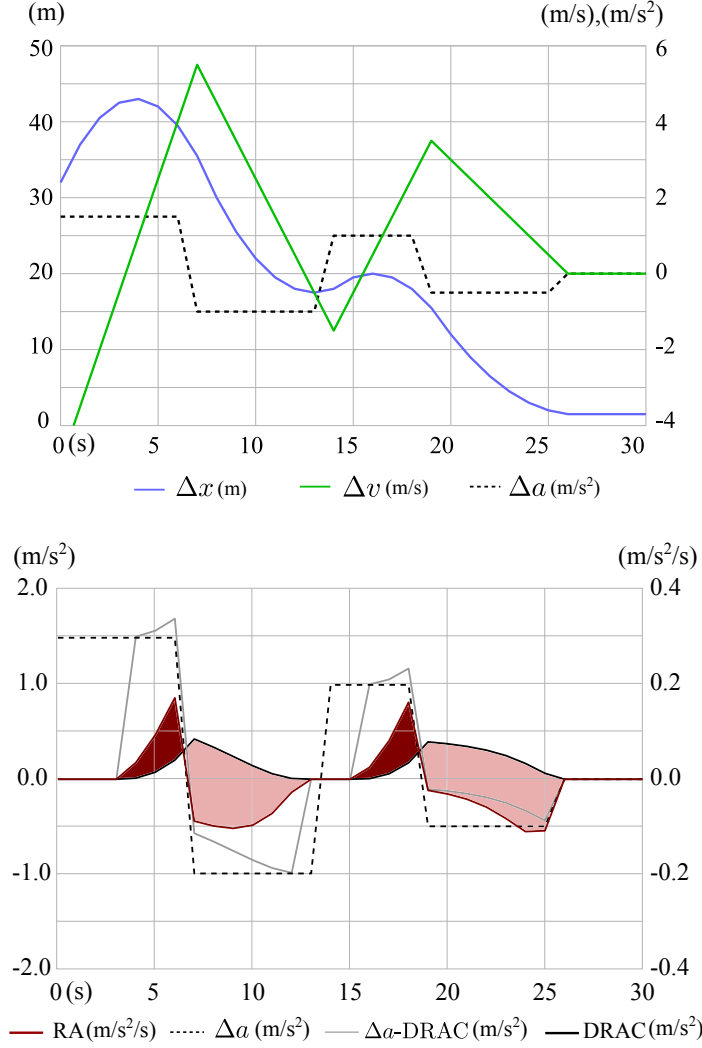


Figure 3-3: Vehicle interaction in car-following behaviour

Finally, similarly to the CPI described in section 2.1.5, a measure of the maximum available deceleration rate is also considered. It allows to consider heterogeneous safety conditions regarding different vehicle categories and different pavement conditions (e.g. dry/wet) that are expected to influence the deceleration performance during an event that requires a specific *DRAC* level:

$$\Delta a^{lim}(n, t) = DRAC(n, t) - (\mu_{long}(n, t) + d)g \quad (3.9)$$

$$\mu_{long}(n, t) = f_{\mu_{long}}(v(n, t), \alpha^{type}, \alpha^{wet}) \quad (3.10)$$

where $\Delta a^{lim}(n, t)$ is the maximum available deceleration for vehicle n at time t , $DRAC(n, t)$ is the deceleration rate required to avoid crash, d is the grade rate (m/m), g is the gravitational acceleration of 9.81 m/s^2 and $\mu_{long}(n, t)$ is the maximum available longitudinal friction coefficient for vehicle n at time t , which depends on the speed of the vehicle itself $v(n, t)$ and on two factors that account for the vehicle type α^{type} and the pavement condition α^{wet} . This simplified formulation of the friction coefficient is due the limited number of variables available in the simulated environment. Similarly to the previous variables, the rate $RA^{lim} = \Delta a^{lim}/TTC$ is use in the safety score function to also account for the time-to-collision.

The systematic component for RE collisions may now be formulate as:

$$V^{RE}(n, t) = \beta_0^{RE} + \beta_1^{RE} RA_+^{need}(n, t) + \beta_2^{RE} RA_-^{need}(n, t) + \beta_3^{RE} RA^{lim}(n, t) \quad (3.11)$$

where RA_+^{need} and RA_-^{need} are the positive and negative components of the relative needed deceleration ratio computed using $\Delta a_+^{need}(n, t)$ and $\Delta a_-^{need}(n, t)$ respectively; $RA^{lim}(n, t)$ is the maximum available deceleration ratio; and β_0^{RE} , β_1^{RE} , β_2^{RE} and β_3^{RE} are the estimable parameters.

3.3.2 Lane change (LC) conflicts

The lane change action decision is typically modelled by means of gap acceptance models (Toledo et al., 2007) or, alternatively, by acceleration variation models (Kesting et al., 2007). Along with the available gaps and longitudinal accelerations, one should also expect that the probability of lane-change collisions also depend on vehicle lateral movements. However, from Chapter 2, it was clear that the large majority of the current microsimulation tools do not provide this modelling feature. Therefore, surrogate measures depending on lateral movements (such as the time to lane crossing proposed by van Winsum et al. (1999) or the PET used by Zheng et al. (2013)) cannot be used.

The gap acceptance is generally modelled separately regarding the lead and the lag gaps on the target lane (see Figure3-4). This disaggregation is of special interest as different parameters may be computed to account for the “blind spot” effect (Chovan et al., 1994). The available gap sizes when a subject vehicle wants to change lanes are a

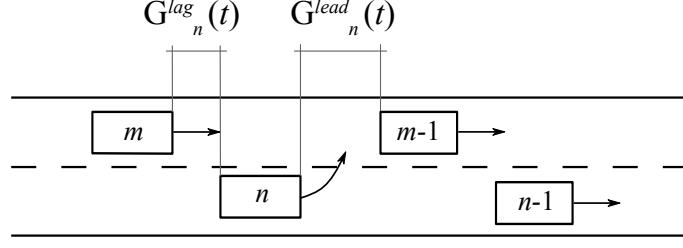


Figure 3-4: Lateral Interaction

key aspect to considered in modelling the probability of a collision during a lane-change.

It is known that the lane changing process becomes increasingly difficult as the speed differences between the subject vehicle and the lead and lag vehicles in the target lane increases (Hidas, 2005b). To account for these factors, in the proposed formulation for the LC accident probability, the safety score is specified in terms of relative gap variation:

$$RG^{gap}(n, t) = \frac{\Delta v_{tl}^{gap}(n, t)}{G^{gap}(n, t)} \quad (3.12)$$

where $G^{gap}(n, t)$ is the gap in meters and $\Delta v_{tl}^{gap}(n, t)$ represents the speed difference between the subject vehicle and the lead (or lag) vehicle on the target lane in m/s :

$$\begin{aligned} \Delta v_{tl}^{lead}(n, t) &= (v(m_{tl}^{lead}, t) - v(n, t)) \\ \Delta v_{tl}^{lag}(n, t) &= (v(n, t) - v(m_{tl}^{lag}, t)) \end{aligned} \quad (3.13)$$

where $v(m_{tl}^{lead}, t)$ and $v(m_{tl}^{lag}, t)$ are the speed of the lead and lag vehicle m or the lead vehicle $m - 1$ in the target lane, respectively. Again, the split of the relative gap variation into its positive ($RG_+^{gap}(n, t)$) or negative ($RG_-^{gap}(n, t)$) values allows for the consideration of different parameters associated with different safety conditions, i.e. for gaps that are either increasing or decreasing, respectively.

$$RG_+^{gap}(n, t) = \max \left(0, \frac{\Delta v_{tl}^{gap}(n, t)}{G^{gap}(n, t)} \right) \rightarrow RG_+^{gap}(n, t) \geq 0 \quad (3.14)$$

$$RG_-^{gap}(n, t) = \min \left(0, \frac{\Delta v_{tl}^{gap}(n, t)}{G^{gap}(n, t)} \right) \rightarrow RG_-^{gap}(n, t) \leq 0 \quad (3.15)$$

Following the above formulation a gap with a higher relative shrinking rate ($RG_-^{gap}(n_1, t_1) < RG_-^{gap}(n_2, t_2) < 0$), for example, should have a higher impact on the LC conflict probability ($\Pr_{n_1, t_1}(LC) > \Pr_{n_2, t_2}(LC)$) and, therefore, its parameter estimate should be $\beta < 0$.

The systematic component for LC collisions may now be formulate as:

$$V^{LC}(n, t) = \beta_0^{LC} + \beta_1^{LC} RG_+^{lag} + \beta_2^{LC} RG_-^{lag} + \beta_3^{LC} RG_+^{lead} + \beta_4^{LC} RG_-^{lead} \quad (3.16)$$

where RG^{gap} is the relative gap variation (with $gap = \{lead, lag\}$) and β_0^{LC} , β_1^{LC} , β_2^{LC} , β_3^{LC} and β_4^{LC} are the estimable parameters.

3.3.3 Run-off-road (ROR) events

ROR events are assumed as being primarily related to individual vehicle dynamics rather than interaction related variables. This assumption is especially true under free-flow scenarios (Davis et al., 2006). However, ROR may also result from evasive manoeuvres due to risky lane-changing or car-following decisions.

Vehicle dynamics in traffic simulation models are represented in a much simplified manner when compared with the detail movements description currently achieved with accident reconstruction models. This significantly limits the potential for a ROR modelling framework. The vehicle lateral movement, the true road geometric characteristics (such as transition curves), the pavement surface characteristics, and the vehicle detailed physical and mechanical attributes are generally not available. However, some relevant variables that may potentially be useful for the analysis of ROR events are still used in microsimulation tools, such as vehicle speed, general road geometrics and the generic vehicle type.

In the proposed framework, the safety score of a ROR event is assumed to be linked to the difference between the current lateral acceleration begot by vehicle n and a site specific critical lateral acceleration. First, as vehicle lateral movements and the true road geometrics are not modelled, the vehicle path in curve elements is assumed as a simple circular path and the vehicle yaw equal to the curve bearing (see Figure 3-5).

The lateral acceleration of vehicle n , $a^{lat}(n, t)$, is therefore derived from its current speed and the curve radius R (m):

$$a^{lat}(n, t) = \frac{v(n, t)^2}{R} \quad (3.17)$$

Although the majority of the simulation tools do not provide information on lateral movement during a lane change, it is expected that this type of manoeuvres will also

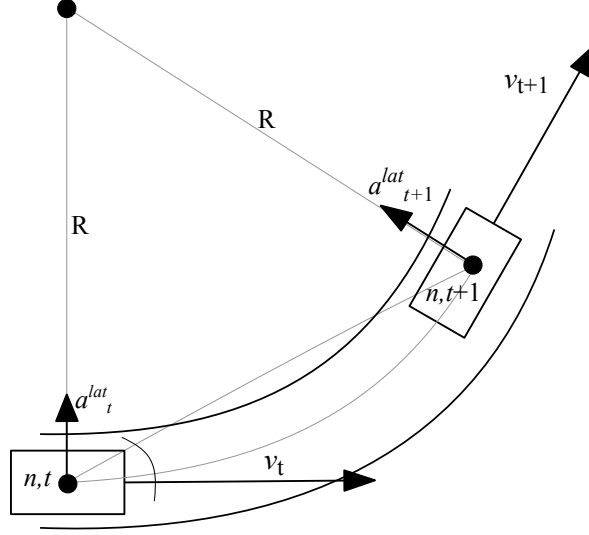


Figure 3-5: Run-off-road event

affect the ROR event probability. Chovan et al. (1994) presented a kinematic model of lane change maneuvers as a sine function for lateral acceleration:

$$a_{lc}^{lat}(n, t) = A \sin(\omega t) = \frac{2\pi x^{lc}}{t_{lc}^2} \sin\left(\frac{2\pi}{t_{lc}} t\right) \quad (3.18)$$

where $a_{lc}^{lat}(n, t)$ is the instantaneous lateral acceleration, $A = 2\pi x^{lc} / (t_{lc})^2$ is the peak acceleration, $\omega = 2\pi / t_{lc}$ is the maximum frequency for the lane change trajectory, t_{lc} is the total time to complete a lane change and x^{lc} is the intended lane change distance. Using test track data, Chovan et al. (1994) considered peak lateral acceleration values of $0.4g$, $0.55g$ and $0.7g$ for mild, moderate, and aggressive steering manoeuvres, respectively. As detailed lane change models such as the one formulated by equation 3.18 are typically not available in microscopic traffic simulation platforms, a generic peak acceleration add-on for lane change of $0.5g$ was adopted and integrated in equation 3.17. With this integration of lane change lateral acceleration in the final ROR safety score, one may account for a potential increased probability of this type of accidents in straight road sections with high frequency of lane changes (lane drop, merging area, etc):

$$a^{lat}(n, t) = \frac{v(n, t)^2}{R} + 0.5\delta^{lc}g \quad (3.19)$$

where $v(n, t)$ is the vehicle speed (m/s), g is the constant gravitational acceleration of $9.81 m/s^2$, R is the curve radius (m) and $\delta^{lc}(n, t)$ is a dummy variable to account for lane change in curves ($\delta^{lc}(n, t) = 1$ if the vehicle is performing a lane change, 0 otherwise).

The maximum allowed lateral acceleration $a_{cr}^{lat}(n, t)$ directly depends on the critical lateral friction coefficient μ_{lat} and the road super-elevation e (m/m):

$$a_{cr}^{lat}(n, t) = (\mu_{lat}(n, t) + e)g \quad (3.20)$$

where g is the constant gravitational acceleration of 9.81 m/s^2 . Similarly to its longitudinal component, the values of the maximum lateral friction coefficient, μ_{lat} , also depend on the vehicle speed itself $v(n, t)$, on the pavement condition (wet/dry), α^{wet} , and on the type of vehicle, α^{type} .

$$\mu_{lat}(n, t) = f_{\mu_{lat}}(v(n, t), \alpha^{type}, \alpha^{wet}) \quad (3.21)$$

The safety score function may now be formulated in terms of the the positive (unsafe) and negative (safe) components of the difference between the current lateral acceleration of vehicle n and the critical lateral acceleration:

$$V^{ROR}(n, t) = \beta_0^{ROR} + \beta_1^{ROR}\Delta a_+^{lat}(n, t) + \beta_2^{ROR}\Delta a_-^{lat}(n, t) \quad (3.22)$$

where $\Delta a^{lat}(n, t) = a^{lat}(n, t) - a_{cr}^{lat}(n, t)$, both acceleration terms defined by equations 3.19 and 3.21 respectively.

3.4 Estimation framework

The general model presented in section 3.2 still needs a statistical formulation for its estimation. As previously stated, the explanatory variables of one type of accident may influence the occurrence of others and evasive manoeuvres may create correlations between different accident outcomes. When modelling multiple discrete outcomes, the multinomial nested logit model (NL) proposed by Ben-Akiva (1973) has advantages over the simple multinomial logit model, because it can simultaneously estimate the influence of independent variables on (more than one) dependent variables and allows for the error terms to be correlated, therefore allowing for the violation of the IIA property (see Chapter 2).

Let us assume that the set of outcomes $k \in K$ may be partitioned into two non-overlapping subsets denoted as m_1 and m_2 called nests, representing the subset m_1 for the no-accident event alone, $m_1 = \{k_0\}$, and m_2 for all types of accident events $m_2 = \{k_1, \dots, k_K\}$ (see Figure 3-1). Two distinct levels are considered: a first level, which

characterises the type of accident outcome (level k), and a second (higher) level that characterizes if an accident occurs or not (level m). The error component of equation 3.2 may now be re-written as:

$$\varepsilon_k = \varepsilon_m + \varepsilon_{mk} \quad (3.23)$$

To allow for correlated alternatives, the NL model assumes that: ε_m and ε_{mk} are independent for all k within a nest (which in this case is nest m_2); the accident propensity for the accident outcome (of any type) is $U_{m_2} = \max_{k \in m_2} U_k$; the term ε_{mk} is an independent and identically GEV distributed with scale parameter μ^k ; and ε_m is distributed so that $\max_{\{m_1, m_2\}} U_m$ is GEV distributed with scale parameter μ^m (Ben-Akiva and Lerman, 1985). It is worth pointing out that the general formulation of multinomial discrete models is closely linked to the discrete choice model formulation where the accident propensity (U_k) is referred as utility. Due to the specific model formulation, only the ratio of the two scale parameters μ^m / μ^k can be calculated during the estimation process (Ben-Akiva and Lerman, 1985). It is however possible to normalize one of them to one. If $\mu^m = 1$ the model is normalized at the top level of the NL.

The probability of outcome k at time t for a vehicle n , $\Pr_{n,t}(k)$, in the NL specification, is composed of the nest probability $\Pr_{n,t}(m)$ as well as the alternative specific probability $\Pr_{n,t}(k|m)$ (Ben-Akiva and Lerman, 1985):

$$\Pr_{n,t}(k) = \Pr_{n,t}(k|m) \Pr_{n,t}(m) \quad (3.24)$$

$$\Pr_{n,t}(m) = \frac{\exp [(\beta_m X_m + L_m)]}{\sum_{m_l \in M} \exp [(\beta_{m_l} X_m + L_{m_l})]} \quad (3.25)$$

$$\Pr_{n,t}(k|m) = \frac{\exp [(\beta_{m,k} X_{m,k}) \mu^k]}{\sum_{k \in K_m} \exp [(\beta_{m,k} X_{m,k}) \mu^k]} \quad (3.26)$$

where $\Pr_{n,t}(m)$ is the unconditional (marginal) probability of vehicle n at time t to fall in nest m ; $\Pr_{n,t}(k|m)$ is the conditional probability of vehicle n at time t to have the outcome k conditioned on nest m ; m_l is the outcome set of nest l ; μ_k is the scale parameter to be estimated along with the parameter vector $\beta = [\beta_m, \beta_{m,k}]$. L_m is the inclusive value (*logsum*) representing the expected value of the attributes from nest m :

$$L_m = \frac{1}{\mu^k} \ln \left[\sum_{k \in K_m} \exp [(\beta_{m,k} X_{m,k}) \mu^k] \right] \quad (3.27)$$

The correlation between alternatives can now be computed as:

$$corr(U_i, U_j) = \begin{cases} 1 - \left(\frac{1}{\mu^k}\right)^2 & \text{if } i, j \in m_2 \\ 0 & \text{otherwise} \end{cases} \quad (3.28)$$

The probabilities for non-nested alternatives take a form similar to the multinomial logit model (MNL) probabilities. To be consistent with the NL derivation, the value of the μ^m/μ^k should be greater than 0 and less than 1 (McFadden, 1981). If the estimated value of μ^m is not significantly different from 1, then the NL does not produce a significant improvement when comparing with a simple MNL model.

To directly estimate the proposed model, trajectory data is needed for several observations of all considered outcomes (including all accident types). Unfortunately, a large data set with direct association between trajectories and accident occurrence is still not available. Even in the first naturalistic pilot studies only a few accident and near accidents were detected (see Chapter 5 for a detailed review on trajectory data collection). Although the proposed model is specified individually for any vehicle n at every time t , the philosophy of microscopic simulation applications is to replicate as close as possible real aggregate measurements, even at such detailed level as accelerations, headways or time-to-collisions.

Thus, to estimate the above model (equations 3.24 to 3.27), a new framework is proposed using a set of artificial (simulated) trajectories which are used to generate the detailed relevant variables for each observed event. To this aim a set of critical estimation assumptions must be stated:

1. A well calibrated microscopic simulation model is able to replicate the statistical distribution of detailed traffic variables. The question here is how "well" must be "well calibrated". To give more insight on this subject, kinematic data of vehicle trajectories at a pilot site were collected and used for detailed calibration (see Chapter 5). It is expected that, if one is looking at detailed simulated output (such as acceleration and headways distribution) first the microscopic model must be calibrated appropriately using such data. An extensive description of the calibration task is presented in Chapter 6.
2. Trajectories extracted in a generic day represent the general driving behaviour of traffic. Confidence on this assumption depends on the amount and breath of infor-

mation available for treatment. Environmental factors (such as weather or roadside works) are expected to influence generic driving behaviour parameters. It is expected that part of this variability will be assessed by means of an aggregate calibration, carried out for each specific event, using loop sensor based data.

3. As already stated, a link between detailed traffic variables and accident occurrence is assumed. Even if simulation models are accident free, it is assumed that its description of detailed traffic variables can be linked to the accident probability. This assumption is supported by several previous studies as reported in Chapter 2, namely in sections 2.1.4 and 2.1.5.

Following the above assumptions, a microscopic simulation tool is calibrated once, using a pre-estimated seed OD matrix, as well as both aggregate (loop sensor based) and disaggregated (from observed trajectories) data collected at for specific day d . The optimum sets of the microscopic simulation model parameters $[\alpha]_0$ are then used as base-parameters in an aggregate calibration process using the aggregated data available for each event observation i . After calibration, the optimum set of parameters for each event i , $[\alpha]_i$ is used to generate a set of (artificial) detailed traffic variables. Finally, this set of detailed traffic variables are then used jointly with the associated accident records to estimate the intended safety model (see Figure 3-6).

As previously mentioned, the artificial trajectories were obtained from a calibrated model for the specific traffic conditions observed during the event i . However, this does not mean that there is a direct association between the event i occurrence and the generated artificial specific trajectory itself. Also, it is typically expected that both the loop-based variables used for calibration and the accident occurrence reported variables are defined for a pre-defined time and spatial units. In some cases, such aggregated intervals may be too large to capture short-term variations; nevertheless several authors (Oh et al., 2001, Abdel-aty et al., 2005) have successfully used aggregated periods (up to 5 min intervals) to perform accident occurrence probability analyses. With the absence of true trajectory variables for each observed event (n, t) , the characterization of the detailed traffic variables for a specific accident occurrence must be linked by means of spatial and temporal aggregation. Additionally, it is well known that safety records have time and spatial errors (Mak and Fan, 2006). When refining time occurrence estimates, real aggregated traffic counts and speeds variations are typically used to infer on the true

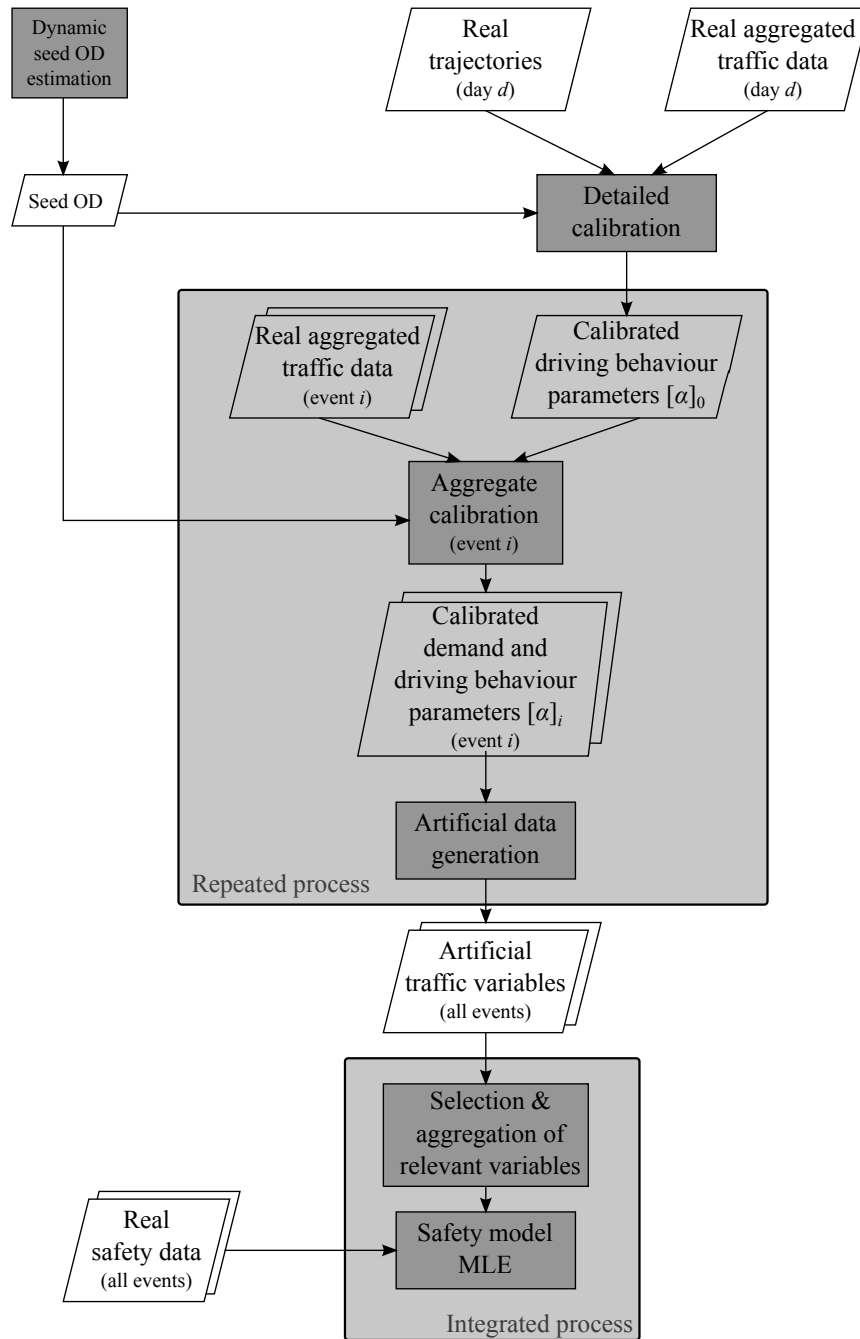


Figure 3-6: Estimation framework

accident starting time. Yet, the modeller is always limited to the recorded aggregated traffic variables time unit. Similarly, when detailing the analysis of the accident report forms and sketches, each occurrence event is always specified as belonging to a spatial interval and a time period by the police and road concessionaire officers. Therefore, one needs to aggregate all vehicle state outcome probabilities $\Pr_{n,t}(k)$ by standardized intervals of space, s , and time periods, p :

$$\Pr_{s,p}(k) = \frac{1}{N} \sum_N \Pr_{n,t}(k) \quad (3.29)$$

where $\Pr_{n,t}(k)$ is the probability of occurrence k for any relevant observation of vehicle n at time t , traveling in spatial interval s during time period p and defined by the proposed nested logit model; $\Pr_{s,p}(k)$ is the probability of occurrence k for a specific spatial interval s and time period p . N is the total number of observations for all vehicles that circulated in the spatial interval s during time period p . It is important to point out that, following this formulation, the model is based on mean values and not on extreme values. This follows the traffic micro-simulation specification philosophy, where the replication of averaged variables is expected. However, one may want to push the use of extreme formulations of equation 3.29 and then rely on detailed calibration methods of extreme values, or by extending the specification of the driver behaviour to better model such scenarios. For example, one may consider an aggregated probability based on an "at least one occurrence" formulation:

$$\Pr_{s,p}(k, k \in m_2) = 1 - \prod_{n,t} \left[\sum_{\forall r \neq k} \Pr_{n,t}(r) \right] \quad (3.30)$$

$$\Pr_{s,p}(k, k \in m_1) = \prod_{n,t} \left[\Pr_{n,t}(k) \right] \quad (3.31)$$

where, m_1 is the non-accident occurrence set and m_2 is the accident occurrences set; for any accident type ($k \in m_2$) to occur in spatial interval s during time period p , at least one accident observation k should occur for the set of relevant observations n, t on spatial interval s during period p . Thus, the probability of $\Pr_{s,p}(k)$ for each accident occurrence ($k \in m_2$) would be computed using the product of all non k events for all vehicle n observations for the pair segment-period s, p (equation 3.29). As mentioned in the previous Chapter, such extreme formulations for microscopic accident probability estimation are still in the early stage of research (Songchitruksa and Tarko, 2006) and,

although they form a very promising approach, their integration with traffic simulation tools needs further research and was not considered in the current dissertation.

With the aggregation formulation from equation 3.29, the maximum likelihood estimation can now be used to obtain consistent estimates of the safety model parameters. However, if one considers a large observation period, typically needed to have enough accident occurrences, it is expected that the loop sensors will fail for some instances. Furthermore, the computational memory and processing resources needed to generate and use the simulated trajectory data is impractical. For this purpose and to avoid using all no-accident occurrences, a outcome(choice)-based sampling was assumed. First, loop sensor failures are assumed to be independent of incident occurrence and the independent variables. Then, to account for this biased sampling process the weighted exogenous sample maximum likelihood function (WESML) proposed by Manski and Lerman (1977) is used, where each observation used in the log-likelihood function is weighted by its sampling ratio w_g :

$$w_g = W_g/H_g \quad (3.32)$$

where W_g and H_g are the fraction of the population and the sample of members in sampling stratum g , respectively.

Equation 3.33 is the final log-likelihood function to be maximized for the consistent estimation on the model parameters, where k are all possible outcomes considered for the proposed model (see Figure 3-1), $\text{Pr}_{s,p}(k)$ is the probability of outcome k for spatial interval s and time period p (given by equations 3.30 and 3.31), w_k is the outcome k -specific sampling ratio, $y_{k,s,p}$ is 1 if k is the observed outcome for the observation pair s, p and 0 otherwise:

$$\mathcal{L} = \sum_s \sum_p \sum_k y_{k,s,p} w_k \ln [\text{Pr}_{s,p}(k)] \quad (3.33)$$

3.5 Model limitations and possible enhancements

Following the description of the safety modelling framework assumptions, a few comments must be added to provide some insight on the limitations and potential for improvement of the proposed approach.

- A simple formulation of the systematic component was proposed. This specification was conditioned by both the simplified representation of the traffic system in the

microsimulation application, and by the focus on a less complex model for fast computation when integrated in the simulation platform. It is clear that as more driving task details will be represented by the microscopic simulation tool, more components may be directly included in the systematic component specification (e.g.: lateral movement, further tire/road surface interaction phenomenon, wind) and indirectly influence the output probability (e.g.: advanced driver assistance systems, ITS or even visibility aspects such as individual sight distance or lighting conditions);

- A limited disaggregation of just three accident types was considered. One may wish to distinguish between different LC (to the left lane or the right lane) or different types of ROR (to the outside or to the inside of curves) as these may represent different accident phenomena. However, further disaggregation typically depends on the availability of more detailed data, such as mechanical and geometric characteristics of the vehicle and roadway;
- The correlation between independent variables must also be monitored. In fact, it is expected that some simulated detailed traffic output will have some correlation between them, as they may be computed by the same microscopic behavior sub-models. For example, it is expected that in car-following state the speed and the headway are correlated. Therefore, correlation tests are advised and variable transformations may be needed (Camminatiello and Lucadamo, 2008);
- As stated earlier, key aspects of the accident phenomenon are related to driver attributes. Unfortunately, simulation tools limit these variables to the reaction time, the thresholds for the car-following model, the safety headways, the critical gap for the gap acceptance model, etc. At this point, the formulation relied only on observable variables. However, the formulation can be extended to account for latent variables;
- Correlation among observations of the same driver and vehicle can also be considered by including a driver specific error distribution v_n . This modelling feature was successfully applied in previous driver behaviour modelling efforts (Toledo, 2003) and may account, for example, for the influence of vehicle specific friction coefficients;
- It is also important to acknowledge that the influence of variables affecting accident

occurrence probabilities may vary across roadway segments. This is an important consideration because, due to variations in non-modelled explanatory variables (e.g.: roadside characteristics, road signs, enforcement) it may be unrealistic to assume that the effects of the modelled variables are the same across all roadway segments. In this case, the mixed logit formulation proposed by (McFadden and Train, 2000) may be used to explicitly account for these variations on accident occurrence probabilities;

- A well accepted speed-accident functional form of the probability relationship, as regards to ROR events, is still not clearly defined in the literature. In the current formulation, a linear form of the systematic component is proposed but one may also wish to use a quadratic function following the well known "U-shape curve" observed by Solomon (1964) and others. To this aim, statistical test of nonlinear specifications may be used (Ben-Akiva and Lerman, 1985);
- Traffic interactions were considered in the computation of the individual probability of accident occurrence. However, it was ignored that a second vehicle might be involved in the event outcome. In RE events, the interactions were formulated in terms of subject vehicle and its leading vehicle, avoiding the influence of joint probabilities. However, in the LC events, if both vehicles are willing to switch to the same lane or to swap lanes and are, therefore, the conflicting vehicle of each other, the probability of a LC accident will be considered twice; yet, in this case just one outcome is possible. To account for such dependencies, the model formulation becomes more complex. A different model formulation considering each interaction $\{n_1, n_2, t_1\}$ (instead of a vehicle state $\{n, t\}$) as observation needs to be specified if these situations are frequent, such as near congestion traffic conditions;
- As per findings of previous studies (Yamamoto et al., 2008), less severe accidents are more likely to be under-reported and the under-reporting rate tends to decrease with the increase in severity level. However, in the pilot study presented in the next chapter, all incidents were supervised by the road concessionaire patrols, and the expected under-reporting rate is much lower than for previous studies found in the literature. Thus, in the current estimation, it was assumed that all accidents were reported. If one wants to consider under-reporting rates, the likelihood function could be easily adapted to account for such sampling bias, by incorporating the

rates of each accident type in their respective weights. This aspect is another key advantage in using an unordered multinomial structure and the WESML estimator, when compared to the traditional ordered models which are unable to provide unbiased direct estimates in the presence of under reporting (Xu et al., 2013a).

Chapter 4

The Case Study

As it was shown in Chapter two and three, the estimation and calibration processes of microsimulation models require detailed traffic data. Furthermore, incident data is required to estimate the proposed safety model. In this Chapter, the steps needed for the appropriate application of simulation models for detailed analysis are discussed and the extensive traffic and safety data collection campaign for safety analysis is presented. Detailed vehicle trajectories were also collected, but as this task required the development of several methodological and theoretical contributions to the current state-of-the art it is presented in a dedicated section (Chapter 5).

4.1 General description of the pilot site

Located in the South bank of the Douro river, the A44 motorway is one of the main south entrances of the city of Porto, Portugal. Heavy good vehicles travelling to Douro's North bank, mainly to the international port of Leixões, and commuters traveling everyday from the south region of greater Porto to the city center and to industrial and service areas in the North, contribute significantly to the dense traffic on this short urban motorway. The road was initially designed as a single carriage way, the EN109, and the current layout still has several inadequate geometric attributes when compared to the actual motorway standards, such as (dedicated) bus lanes and stops, short acceleration and deceleration lanes and steep grades.

Currently, the A44 motorway is a dual carriageway two-lane urban motorway with a total length of 3940m divided in 4 short stretches (less than 1.5km) with a total of 5

main interchanges (see Figure 4-1). A New-Jersey like precast concrete safety barrier was installed between carriageways. Overall, each carriageway has two 3.50m width lanes, and 2m and 0.5m width right and left shoulders, respectively. Stretch B has three lanes in the north-south direction in almost all of its length and a bus stop with a 100m dedicated lane separated from the main lanes by a concrete barrier; and stretch C has additional lateral dedicated carriageways with one unique lane in both directions. The main interchanges at each end of the A44 road are a cloverleaf interchange with A1, in the North; and a trumpet interchange with A29 motorway in the South end. The other three main interchanges between A44 and other local roads are two diamond interchanges with a roundabout overpass and a partial cloverleaf interchange. The main section has acceleration and deceleration lanes in all interchanges, although in several cases as short as 130m. In and out-ramps are connected to local roads, generally with tight curves, intersections or pedestrian crossings, which tend to significantly reduce exiting vehicle speeds.

Regarding the horizontal alignment, the A44 does not have any significantly tight curves. The vertical alignment is characterised by an average 1,5% descending grade for stretches 1 to 3, and an ascending 2,4% grade slope in stretch 4 (Southbound direction as reference).

In 2009, the Portuguese road concessionaire Ascendi S.A. was still having several concerns with the A44 urban motorway operation: recurrent traffic perturbations, higher level of accident records as compared to other national motorways, diversity in the nature of the detected safety records and a need for assessment of any potential investment in ITS. Thus, this motorway has the main attributes for testing the real potential of simulation tools in detailed safety assessment: complex design and traffic characteristics that tend to weaken generic simulation outputs and atypical safety records. It is worth pointing out that by the end of 2010, a toll system was installed on the A29 (further south in Interchange 5). Due to this event, a share of the traffic was diverted to V. N. Gaia city streets, partially transferring traffic and safety problems to other parts of the road network.

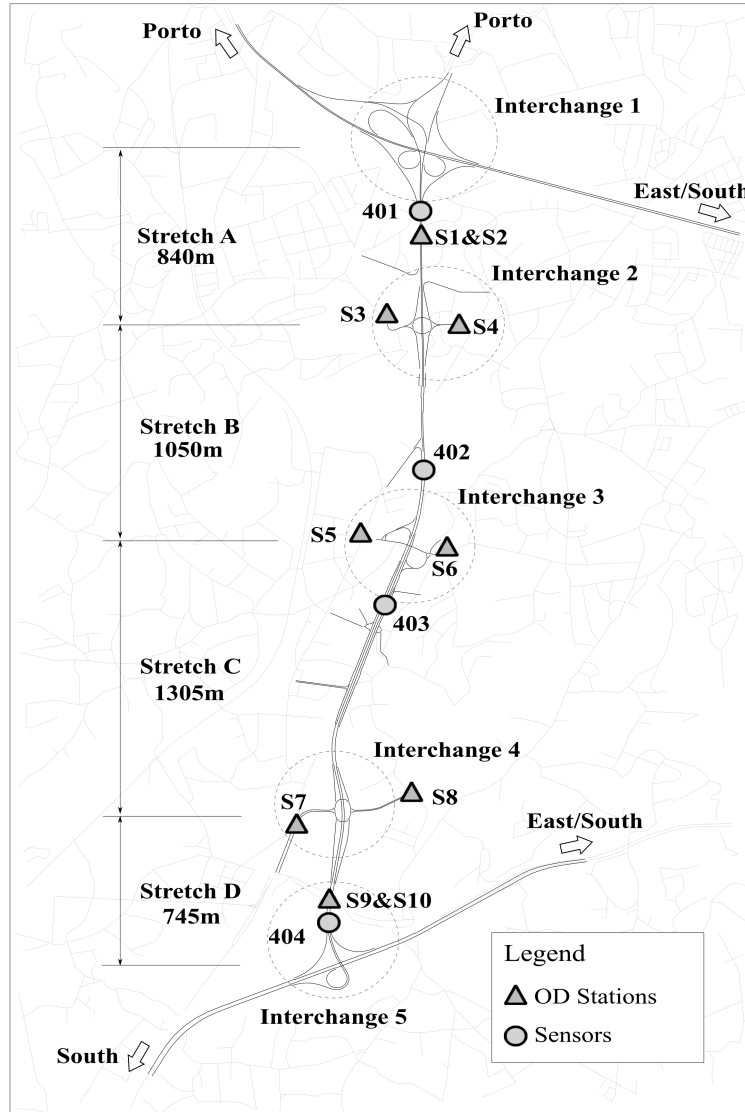


Figure 4-1: A44 network and data collection stations.

4.2 Sensor Data

The A44 road is equipped with an automatic traffic counting station (ATCS) on each stretch (see 4-1), located at kilometers 3.7, 2.4, 1.75 and 0.05. The eight (four per traffic direction) Marksman 660 HPLD loop sensors are able to count, classify and measure speed's vehicle in real time. The road concessionaire's data center keeps record of ATCS outputs in a simplified data format and aggregated by periods of five minutes:

- time stamp (date and time);
- traffic volume for each vehicle category (for all lanes);
- number of vehicles by speed bins (10km/h intervals) for each vehicle category;

- total occupancy for each vehicle category (%).

A total of 13 axle-distance based categories were used by the road concessionaire system for vehicle classification. These categories were aggregated into light, heavy good vehicles (HGV) and buses for simulation purposes (see Chapter 6).

Traffic data for a period of three years, from 2007 to 2009, was provided by the road concessionaire resulting in a total of 315,360 observations for each station. Although this data is processed and periodically checked by the road concessionaire by means of video based manual processing, a complementary verification and correction procedure was necessary to allow its use in the calibration and modelling tasks. For this purpose a two phase error detection procedure was adopted, resulting in the identification of two main types of errors:

Individual errors detection: A significant number of records had individual errors mainly due to isolated component's failure during the real time registration process. These errors are briefly described in Table 4.1. Errors R_1 to R_3 were corrected directly during the detection step. For R_2 and R_3 , the corrected number of vehicles detected for the speed bin $[0, 30]$ km/h (and for each of the erroneous vehicle types separately) was obtained by the difference between the total volume and the sum of vehicle counts for all the other speed bins.

Table 4.1: Errors in the speed database

Errors	Description	Likely Cause	[%]
R_1	Occupancy format error	Floating point location	<0.01
R_2	Speed bin $[0, 30]$ error (#10)	Vehicle misclassification	0.09
R_3	Speed bin $[0, 30]$ error (#3)	Vehicle misclassification	0.21
R_4	Uniform speed distribution	Stuck on	0.02

Error R_4 could not be corrected due to lack of information. In fact, for some observations the number of vehicles for all speed bins was the same and their sum not equal to the total volume registered. These observations were detected by filtering inappropriate regions in the fundamental diagram of traffic flow, and tagged for exclusion in the calibration process.

Time-series based Detection: For the detection of further system failures the daily statistics algorithm (DSA) proposed by Chen et al. (2003) was used. This algorithm uses

Table 4.2: Time-series errors

Errors	Description	Likely Cause	[%]
S_1	Occupancy and flow are equal to zero	Suck off	6.66
S_2	Non-zero occupancy and zero flow	Hanging on	<0.01
S_3	High occupancy	Hanging on	0.02
S_4	Constant occupancy	Stuck on or off	<0.01

the time series of flow and occupancy measurements to detect abnormal values, instead of signaling data problems just based on an individual observation. It is based on the empirical observation that good and bad detectors behave very differently over time. It assumes that, at any given instant, the flow and occupancy at a detector location may have a wide range of values, and one cannot exclude most of them. However, most detectors show a similar flow and occupancy pattern over a day and abnormal patterns may be detected when analysing the full day range of observations (Chen et al., 2003). The DSA was developed to recognize four types of errors (see Table 4.2). It is important to point out that the fraction of errors of type S_1 in Table 4.2 reaches 24.8% when the days without any record are also considered. In fact, in the provided database some days weren't registered at all, resulting in seriously high failure rates on the final database. This is probably due to the off-line extraction of data as the road concessionaire is contractually bound to much lower failure rates. Unfortunately, no database improvement procedure descriptions were provided by the concessionaire.

The original algorithm proposed by Chen et al. (2003) is based on 30s measurements of flow $q(d, t)$ and occupancy $k(d, t)$, where d is the index of the day and t the index of the 30s period. For our specific case study, the algorithm was adapted to the 5min measurements of the Marksman 660 HPLD, resulting in different thresholds and algorithm settings. The output is the diagnosis $\Delta(d)$ for the d^{th} day: $\Delta(d) = 0$ if the loop is good and $\Delta(d) = 1$ if the loop is malfunctioning. In contrast to existing algorithms that operate on each sample, DSA produces one diagnosis for all the samples of a loop on each day.

For each of the errors in Table 4.2, Chen et al. (2003) proposed the computation of a statistic which summarises the specific errors for the daily time series. Their formulation is given by equation 4.1, where $S_j(i, d)$ is the j^{th} statistic computed for the i^{th} loop on the d^{th} day. The decision Δ becomes a function of these four variables. For the i^{th} loop and d^{th} day, the decision whether the loop is bad or good is determined according to the

following rule:

$$\Delta_i(d) = \begin{cases} 1 & \text{if } \begin{aligned} &S_1(i, d) = \sum_{a \leq t \leq b} 1(k_i(d, t) = 0) > s_1^* \text{ or} \\ &S_2(i, d) = \sum_{a \leq t \leq b} 1(k_i(d, t) > 0) \cdot 1(q_i(d, t) = 0) > s_2^* \text{ or} \\ &S_3(i, d) = \sum_{a \leq t \leq b} 1(k_i(d, t) > k^*) > s_3^* \text{ or} \\ &S_4(i, d) = (-1) \sum_{x: p(x) > 0} \hat{p}(x) \log(\hat{p}(x)) < s_4^* \text{ with} \\ &\quad \hat{p}(x) = \sum_{a \leq t \leq b} 1(k_i(d, t) = x) / \sum_{a \leq t \leq b} 1 \end{aligned} \\ 0 & \text{otherwise} \end{cases} \quad (4.1)$$

where a and b are the first and last periods considered for day d .

The default thresholds s_j^* are given in Table 4.3. The specification of the statistics S_1 to S_3 in equation 4.1 is straightforward; S_4 computes the entropy of the occupancy samples, a well-known measure of the “randomness” of a variable. If $k_i(d, t)$ is constant in t , for example, its entropy is zero.

Table 4.3: DSA parameters

Parameter	Value
k^*	0.35
s_1^*	200
s_2^*	1
s_3^*	20
s_4^*	4

Because the ground truth about which detectors are actually bad is not available, the performance of this algorithm was verified visually. In Figure 4-2 the speed-occupancy-flow relationships are presented for sensors 401-2, 402-2, 403-2 and 404-2, all in the South-North Direction, for the year 2007. In blue are the 5 min observations for days with a malfunctioning sensor ($\Delta_i(d) = 1$) and in green are the R_4 errors. It is worth pointing out the high number of observations with $[flow, occupancy, speed] = [0, 0, 0]$.

A few authors have developed spatial and temporal methods to predict missing/erroneous data measurements: auto-regressive moving average (Nihan, 1997), linear regression (Chen et al., 2003), Kalman filter (Dailey, 1993), Kriging regression (Zou et al., 2012) or PCA (Qu et al., 2009). In the current case study, the errors do not occur randomly but may persist for several hours and days. Also, 95% of the missing data occurred for the same days for all sensors in the A44 motorway. Neighbour loop information from other roads is

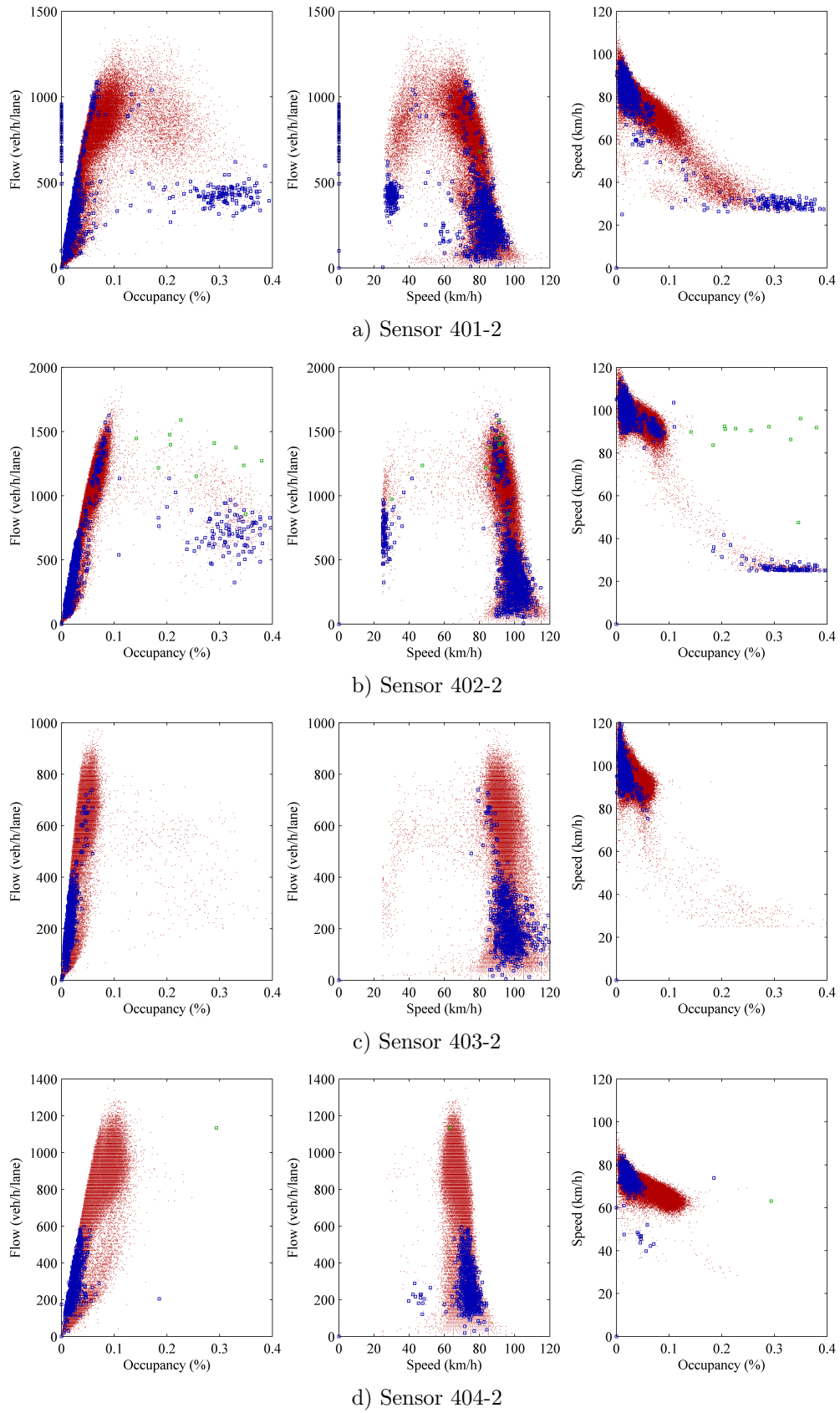


Figure 4-2: Five minutes loop sensor data for 2007.

also not available, resulting in poor or even impossible estimations using any alternative spatial imputation algorithms. Thus, all tagged erroneous observations were not corrected directly, but excluded from the calibration procedure.

The days with a detected malfunctioning sensor were tagged to avoid its use in a generic calibration process, which would generate to incorrect simulated outputs. Similarly, the few observations detected with R_4 errors were also tagged for its exclusion from any measure of performance in the calibration step.

A few comments on the layout of the sensor data are also relevant:

- It is clear that, for all sensors except 401-2 (in the South-North direction) and 404-1 (in the North-South direction, not shown in Figure 4-2), almost all observations are in the non-congested state. For those two stations, the influence of the weaving sections near the interchanges with, respectively, A1 and A29 motorways is clear;
- The use of an estimated average speed, based on mid-value of speed bins, instead of the full observations array, may lead to a higher dispersion on the flow-speed relationship, especially for low volumes. This data limitation is also evidenced by the absence of speed observations bellow 25km/h;
- Weather, road works and incidents may also affect road capacity, resulting in a higher dispersion in the flow-occupancy-speed relationships when compared to a theoretical fundamental diagram;
- The dispersion in the flow-occupancy graph may also be affected by individual lane-loop failures within a station. These errors were not considered in the present analysis, but a local spatial correction method based on the valid lane-loop records for the specific station and neighbour stations would be a solution for implementation. The detection procedure is however complex, especially in low-traffic conditions, as observation points with and without lane-loop failures will typically fall in the same region of the fundamental diagram.

4.3 Demand Data

Travel demand in microscopic applications is traditionally defined in the form of time-dependant origin-destination (OD) flows. Despite the small size of the case study network, the information regarding specific OD paths is essential, due to configuration of the

edging interchanges and the complex nature of the traffic, often leading to congested situations. No historical estimates of the A44 motorway OD existed in the road concessionaire database.

Seed Origin-Destination Matrix

In the past 30 years many methods to obtain OD trip tables based on link counts have been developed (for detailed reviews please refer to Ashok (1996) and Cascetta (2009)). These classic methods for static OD estimation have been extended and several new methods have been developed, for the specific problem of dynamic¹ OD estimation (and prediction): maximum likelihood (ML) and generalised least square (GLS) estimators (Cascetta et al., 1993, Cascetta, 2009), Bayesian estimators (Zijpp et al., 1997), Kalman filtering (Ashok and Ben-Akiva, 2002) and artificial neural networks (Yang et al., 1992).

All these methods traditionally aim at combining existing information on OD flows, also known as *direct measurements*, with traffic counts, or *indirect measurements*. For the present case study, an on-site data collection campaign was carried out in the first week of May 2011, with the specific purpose of collecting OD related data. The methodology used in this campaign was affected by the limited human resources and available equipment. The GLS simultaneous method presented by Cascetta et al. (1993) was then used for OD flows estimation by combining link counts and a sampled of identified vehicle paths.

Collected Data

Samples of OD paths were collected for several periods of the day, through audio recordings of license plate numbers collected at A44 main entry sections. Simultaneously, a sample of video recordings during specific time periods was also collected for the same sites. Loop counts aggregated by periods of 5 minutes from automatic detectors on the A44 main sections were provided by the road concessionaire for the entire collection campaign week. These three data-sets were combined in the dynamic estimation of a generic weekday OD matrix.

Direct measurements

During the OD data collection campaign a team of six available experienced officers (from the Department of Transportation of the National Laboratory of Civil Engineering-

¹Time-varying.

LNEC) collected plate numbers at ten stations on the connections of the A44 road (see S1 to S10 in Figure 4-1). These ten stations were chosen to cover the two main edging sections and the three mid interchanges of the studied road: interchange 2 (Madalena), 3 (Valadares) and 4 (EN 109). Station pairs S3 - S4, S5 - S6, and S7 - S8 covered respectively the west and east connections on interchange 2 (Madalena), 3 (Valadares) and 4 (EN 109). Stations S9 and S10 covered the southern edge of the A44 road, on the north-south and south-north directions respectively. Similarly, Stations S1 and S2 covered the northern edge of the A44 road. Five local connections and the split movements at the two bordering interchanges (1 and 5) were not covered by the audio recording campaign (see Figure 4-1), but were monitored using indirect video measurements (see the next section for further details).

Plate numbers were recorded in audio format by periods of 30 minutes from 7:30 am to 7:30 pm with a digital audio recorder during the first five week-days of May 2011. The general procedure followed the existing recommendations on manual plate number matching (Turner et al., 1998 and Fricker and Guy, 2005). The digital recorder clocks were synchronised at the beginning of the collection period for travel time estimation. The observers also classified the surveyed vehicles as light, heavy vehicles or buses. Recording locations were strategically and previously chosen on the side of the right shoulder or on overpass bridges, optimizing the field of view. Spelling alphabets are usually used when post-processing voice recognition softwares are available. In the current data collection campaign, Portuguese phonemes and manual processing was adopted to maximise the number of plate numbers recorded. At multi-lane stations, (random) sampling of all through-lanes movements was carried out. Finally, a full license plate number reading was chosen to avoid spurious matches.

By turns, six stations were monitored each day covering from 12 to 18 different OD pairs of the entire OD matrix (see Table 4.4). Only the afternoon and morning periods were monitored respectively for the first (Day 1) and last (Day 5) weekdays of the data collection week. With this procedure, all 56 main OD pairs of the A44 road were covered.

Each audio recording was then processed manually to form a data set of time records and plate numbers. A total of 136 377 well identified license plates were record during the five days. An average of 735 licence plates/hour were collected for the entire period,

Table 4.4: Map of OD stations coverage for plate number collection

Agent	Day 1	Day 2	Day 3	Day 4	Day 5
A	S3	S9	S1	S8	S5
B	S4	S10	S2	S7	S6
C	S5	S1	S3	S9	S7
D	S6	S2	S4	S10	S8
E	S7	S4	S9	S1	S3
F	S8	S6	S10	S2	S4

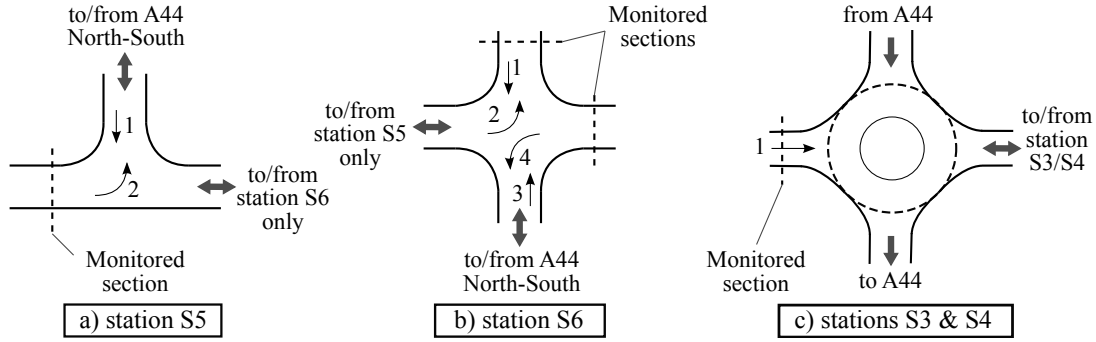


Figure 4-3: Monitored sections for stopping time measurements

with a maximum of 1780 license plates/hour for one of the officers².

An algorithm for matching the license plate numbers on different observation stations was developed for this specific data-set. Visual and auditive errors such as reading 'O' instead of 'Q' or processing 'M' instead of 'N' were considered, and a minimum of 4 out of 6 ordered characters were considered as a matched license plate. Each matched OD pair record was then filtered based on travel times. A first filter was used considering both minimum and maximum travel times based on the average speeds of 20km/h and 170km/h respectively. Additionally, if the considered path had intersections an additional maximum stopping time value was considered. These intersections are mainly located at the edge of A44 entry and exit ramps, namely those with two roundabouts (at stations S3 and S4, and at stations S7 and S8) and two non-signalised intersections at stations S5 and S6 (see Figure 4-3). The additional travel time values for intersection were separately estimated for each intersection movement, based on the 90th percentile of the observed stopping times collected by the video recording sample (see Figure 4-4).

This procedure resulted in a total of 20 776 journeys (or 41 552 matched license plate readings) covering the 56 OD pairs. The developed algorithm also recorded the number

²The maximum number of recorded license plates for the six agents reached the highest standards of the reported values in the literature (Martin and Bell, 1993, Fricker and Guy, 2005).

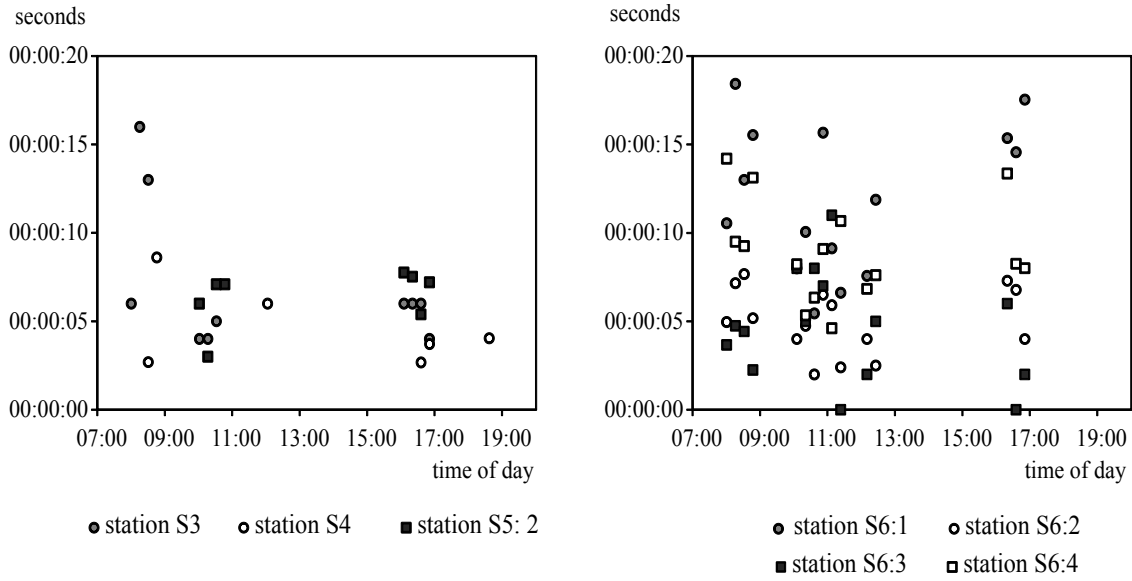


Figure 4-4: Average stopping times at different intersections

of successive trips in the network by the same vehicle. This allowed us to evaluate the commuter traffic share estimates on the network.

The matched records were distributed over the network OD pairs and aggregated by periods of 30 minutes (departure time). Thus, for each of the five monitored days, a list of 18 (time period based) OD matrices for matched vehicles were constructed. Similar lists were constructed with the average and the standard deviation of the observed travel times for matched vehicles. One should note that, following Table 4.4, several OD pairs were monitored more than once (for example, S3 was monitored on days 1, 3 and 5). The list of OD matrices was used in the generic OD matrix estimation process described in section 4.3.

Indirect measurements

Video recordings were also carried out during the license plate recognition campaign. These allowed for the collection of traffic counts through manual processing at the same entry and exit stations of the license plate sample collection. This data was used in the estimation procedure of the seed OD matrix presented in the next section. Furthermore, video recordings were used in the collection of disaggregated counts at the edging interchanges of the A44 (recordings on Station S1/S2 and S9/S10), allowing for the estimation of split shares for S1, S2, S9 and S10, which will be used in the calibration of lane-changes in these weaving sections. The related split shares were assumed to be independent of the OD path in the A44. Finally, the loop count records on each stretch of the A44 road

were made available by the road concessionaire for the entire week, following the format specified in section 4.2.

Seed OD Estimation

Following the specification in Cascetta (2009) for dynamic estimation of OD matrices, the flow on link l in period j can be expressed as:

$$f_l[j] = \sum_{t=1}^j \sum_{od} m_{lj}^{od,t} d_{od}[t] = \sum_{t=1}^j M[t, j] d[t] \quad (4.2)$$

where $d_{od}[t]$ is the vector of true demand flows on each OD pair at time t and $m_{lj}^{od,t}$ is the fraction of OD flow $d_{od}[t]$ contributing to the flow $f_l[j]$ on link l . The second equality expresses the same variables in the matrix form, using the $(n_l \times n_{od})$ dynamic assignment fraction matrices $M[t, j]$.

In the special case of the A44 network, the framework presented in Cascetta (2009) can be simplified in several ways. Traditional formulation assumes multiple possible paths for the same OD pair. However, in the present case study there is only a unique (logic) path for each OD pair (od), resulting in assignment fractions $m_{lj}^{od,t}$ independent of path choice. Furthermore, the demand flows $d_{od}[t]$ are assumed to be uniformly distributed between the leader and the last follower over a time span $[j]$. Thus, the assignment fractions $m_{lj}^{od,t}$ may take any value in the interval $[0, 1]$. This assumption was relaxed in Ashok and Ben-Akiva (2002), however it is still acceptable for the estimation process in this case study.

The assignment fractions $m_{lj}^{od,t}$ are usually obtained through the collection of link performances or using a dynamic traffic assignment model (path choice model). In the A44 case study, assignment fractions can be directly estimated from the license plate data collection campaign and the dynamic assignment may be computed directly from travel time records.

The general OD count based estimation problem may then be formulated as a constrained optimisation problem to minimise the deviations between observed and estimated variables:

$$d^* = \underset{\{x \geq 0\}}{argmin} \left[f_1(x, \hat{d}) + f_2(v(x), \hat{f}) \right] \quad (4.3)$$

where x is the unknown demand vector, which is a sample estimate of the demand.

The two functions $f_1(x, \hat{d})$ and $f_2(v(x), \hat{f})$ depend on the estimation framework used. These functions can be considered as two "distance" measures: f_1 is the "distance" of the unknown demand x from the apriori estimate \hat{d} and f_2 is the "distance" of the flows $v(x)$ obtained by assigning x to the network from the observed traffic counts \hat{f} . This general specification for dynamic OD matrices has been extended to the case where the a priori estimate \hat{d} is based on a sample of identified vehicles on the network (Zijpp et al., 1997, Asakura et al., 2000, Ashok and Ben-Akiva, 2002, Dixon and Rilett, 2002, Antoniou et al., 2004, Zhou and Mahmassani, 2006, Barceló et al., 2010).

In the current case study, the GLS estimator proposed by Cascetta et al. (1993) was used to solve the equation 4.3 optimisation problem. When choosing the GLS estimator, two alternative solution approaches are possible: the simultaneous approach where the OD for all periods are estimated together in a single step; and the sequential optimisation approach, which involves multiple steps by calculating iteratively the demand matrix for one period $[j]$ only at each step, using traffic counts for that period and the previous one (Cascetta et al., 1993). The GLS simultaneous estimator was chosen due to its computational efficiency and its very satisfactory results when applied to small networks (Cascetta, 2009). For the GLS simultaneous estimation, the two functions f_1 and f_2 in equation 4.3 take the matrix form:

$$f_1 = \sum_{j=1}^n \left[\left(\hat{d}[j] - x[j] \right)^T Z^{-1}[j] \left(\hat{d}[j] - x[j] \right) \right] \quad (4.4)$$

$$f_2 = \sum_{j=1}^n \left[\left(\hat{f}[j] - \sum_{t=1}^j \hat{M}[t, j] x[t] \right)^T W^{-1}[j] \left(\hat{f}[j] - \sum_{t=1}^j \hat{M}[t, j] x[t] \right) \right] \quad (4.5)$$

where Z is the variance-covariance matrix of the sampling errors (η) between the true unknown demand x and the sample estimates, $\hat{M}[t, j]$ is the estimated dynamic assignment matrix, and W is the variance-covariance matrix of the measurement errors (ε^{OBS}) and:

$$\hat{d}[j] = x[j] + \eta \quad (4.6)$$

$$\hat{f}[j] = f[j] + \varepsilon^{OBS} \quad (4.7)$$

Following this approach the estimated OD matrix d^* for this case study is composed by all 30 min interval OD matrices that form a half-day OD pattern ($d[1], \dots, d[n]$). The

half-day disaggregation was considered for data fitting and computation efficiency. Some additional assumptions were also considered in the estimation process:

- As we are estimating a generic weekday seed OD, the traffic demand was considered the same throughout the entire week. In fact, the collected loop sensor data showed insignificant variations between these five days. However, the assignment matrix \hat{M} was separately computed for each of the five weekdays. This assumption has been already proposed previously by Zhou et al. (2003) for combining loop counts and sampled paths data;
- For the computation of the dynamic assignment matrix $\hat{M}[t, j]$ it was assumed that travel times follow a left-truncated normal distribution. The mean and standard deviation of the travel-time for a specific OD path in period $[j]$ was directly computed from the license plate matching process. The observed travel times showed a maximum lagging of just one period. All vehicles departing at period $[t]$ reached their destination by the end of period $[t + 1]$. Again, it was also assumed that the demand flows $d_{od}[t]$ are uniformly distributed between the leader and the last follower over a span of time $[j]$;
- As only 12 to 18 of the 56 total paths were monitored each day, travel-time measurements were not available for all paths at time period $[j]$. When these specific measurements were not available, the average travel-time measured in period j on the other monitored days was adopted;
- The computation of \hat{d} requires the estimation of sampling rates. In fact, the collection campaign only allowed for a direct measurement of a subset of the total OD demand (d'). It was assumed that the licence plate readings were randomly sampled. This assumption is acceptable considering the method used in the matching process;
- Sampling rates in audio recording methods mainly depend on the total traffic flow, vehicle speeds and observers' visibility at each location (Fricker and Guy, 2005). In this case study, sampling rates at edging stations (S1, S2, S9 and S10) were computed directly, as loop counts were available for all periods in those locations;
- For the remaining stations (S3, S4, S5, S6, S7 and S8), a sample of video based counts were collected by all officers, for multiple periods and for at least 3 different stations.

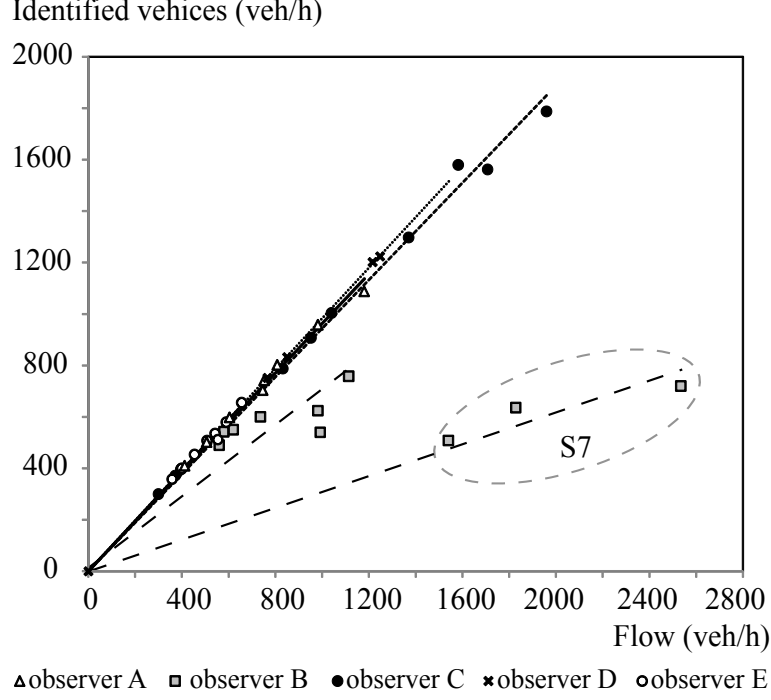


Figure 4-5: Sampling at entry and exit stations

Vehicle speeds were generally very low as all of these sections were located near intersections. Local visibility was assumed to be adequate, as 50m of non-obstructed view (both-ways) were assured for all counting stations. A simple analysis was then carried out to test sampling rate variability. Although non-linear relationships between the number of readings and the traffic flow were reported in the literature (Fricker and Guy, 2005), the collection campaign on the A44 road was characterised by a linear relationship with a very efficient sampling factor for 5 out of 6 officers (see Figure 4-5). Sampling rates between 0.945 and 0.985 were observed for these officers ($R^2 > 0.995$). For officer B two distinct sampling factors were calculated: one for station S7 where very low sampling rates were observed (0.311); and another for the remaining stations (0.706). The estimated OD path flow \hat{d} is a function of the OD counts d' and the sampling rates of agent k at each specific station at the vehicles' path origin (o) and destination (d):

$$\hat{d}_{od}[j] = \frac{1}{s_{dk_1}[j]} \cdot \frac{1}{s_{ok_2}[j]} \cdot d'_{od}[j] \quad (4.8)$$

- For computing convenience, matrices Z and W were assumed to be diagonal, ignoring the covariances between both error components η and ε^{OBS} (Cascetta, 2009).

Under the above mentioned simplifying assumptions, equation 4.3 may be re-written as:

$$d^* = \underset{\{x \geq 0\}}{\operatorname{argmin}} \left[\sum_j \frac{(\hat{d}_{od}[j] - x_{od}[j])^2}{\operatorname{Var}[\eta_{od}[j]]} + \sum_j \sum_l \frac{\left(\hat{f}_l[j] - \sum_{od} \left(\sum_{t=1}^j (\hat{m}_{l,j}^{od,t} x_{od}[t]) \right) \right)^2}{\operatorname{Var}[\varepsilon_l[j]]} \right] \quad (4.9)$$

The final estimated demand \hat{d} is a vector of 9×56 parameters (half-day periods \times OD paths), each of them representing an estimate of the true demand flow $x_{od}[t]$; also, $\hat{m}_{l,j}^{od,t}$ is an estimate of the fraction of OD flow $x_{od}[t]$ contributing to the flow $f_l[j]$.

Several algorithms may be used to solve this constrained optimisation problem. The non-linear conjugate gradient method was adopted and the estimation was carried under R (R Development Core Team, 2011) using the 'Rcgmin' package (Nash, 2011). This package implements a non-linear conjugate gradient algorithm allowing for box constraints, i.e. restricting estimates of $x_{od}[t]$ to non-negative values. The gradient function was computed manually and used as input in the optimisation algorithm. Under the above mentioned assumptions the gradient component $Gr_{od}[j]$ can be express as:

$$Gr_{od}[j] = 2 \left[\frac{(x_{od}[j] - \hat{d}_{od}[j])}{\operatorname{Var}[\eta_{od}[j]]} + \sum_{t=1}^j \sum_l \frac{\hat{m}_{l,j}^{od,t} \left(\sum_{od} \left(\sum_{t=1}^j \hat{m}_{l,j}^{od,t} x_{od}[t] \right) - \hat{f}_l[j] \right)}{\operatorname{Var}[\varepsilon_l[j]]} \right] \quad (4.10)$$

The general results of the optimisation process are presented in Table 4.5. The reduction of d^* reported in this Table illustrates the benefit of considering a *dynamic* OD compared to a *static* one. Different initial estimates were also tested for different trials of the estimation method. The values of the objective function for the uniform initial matrix, $d^*(uniform)$, of 200 vehicles/hour (20 for heavy good vehicles and 2 for buses) are also shown.

The simple GLS estimator presented in equation 4.3 and 4.9 also allow for different 'variances' of the available values used in the estimation process (Cascetta et al., 1993). Different weights for the f_1 and f_2 components of the objective function were also tested.

$$d^* = \underset{\{x \geq 0\}}{\operatorname{argmin}} \left[p \cdot f_1(x, \hat{d}) + q \cdot f_2(v(x), \hat{f}) \right] \quad (4.11)$$

Table 4.5: Main statistics for the Seed OD optimisation

Half-day	a.m.			p.m.		
Vehicle type	Light veh.	HGV	Bus	Light veh.	HGV	Bus
$d^*(uniform)$	83502786	838862	27502	88107095	882853	28697
$d^*(static)$	1492932	48008	477	2730429	59334	391
$d^*(final)$	1345800	45755	436	2555494	57499	367
Reduction of d^*	9.85%	4.69%	8.60%	6.41%	3.12%	6.14%

In Table 4.6 the main statistics of these tests and its comparison with the simple least square estimator statistics ($p = q = 1$) for light vehicles during the a.m. period are presented. The root mean square error (RMSE) and the root mean square percentage error (RMSPE) were used as measures of performance (MoP).

Table 4.6: Weighting of the objective function (light vehicles, a.m. period)

p	q	d^*	RMSPE	RMSE
1.50	0.50	1542257	0.111	0.300
1.20	0.80	1450742	0.038	0.103
1.10	0.90	1414826	0.018	0.052
0.90	1.10	1285179	0.017	0.048
0.80	1.20	1220292	0.033	0.091
0.50	1.50	1004852	0.078	0.219

The estimated dynamic seed OD estimate for light vehicles is represented in Figure 4-6. One may see the traffic increase during the morning peak hour, between 8:00 and 9:30, with higher entry and exit flows at the edging interchanges (S1, S2, S9 and S10). However, full network traffic volume remains at high values during all working hours. It is also interesting to note that the local traffic increases lightly at lunch time, from noon to two in the afternoon. This may indicate the presence of road users both living and working in this area. A similar representation of the HGV matrix, showed a clear domination of the non-local traffic of this type of vehicles on the A44 road. In fact, the main flow of HGV journeys is between the edges of the motorway, with only residual distribution flows from/to a few existing factories in the area (namely at S3 and S8).

The final estimated Seed OD was then expanded to fit the exact same origin and destination nodes as the ones represented in MITSIMLab. This expansion focused on the edging stations of the A44 (namely S1, S2, S9 and S10) where the video count samples collected allowed for the inference on split shares at the bordering interchanges 1 and 5.

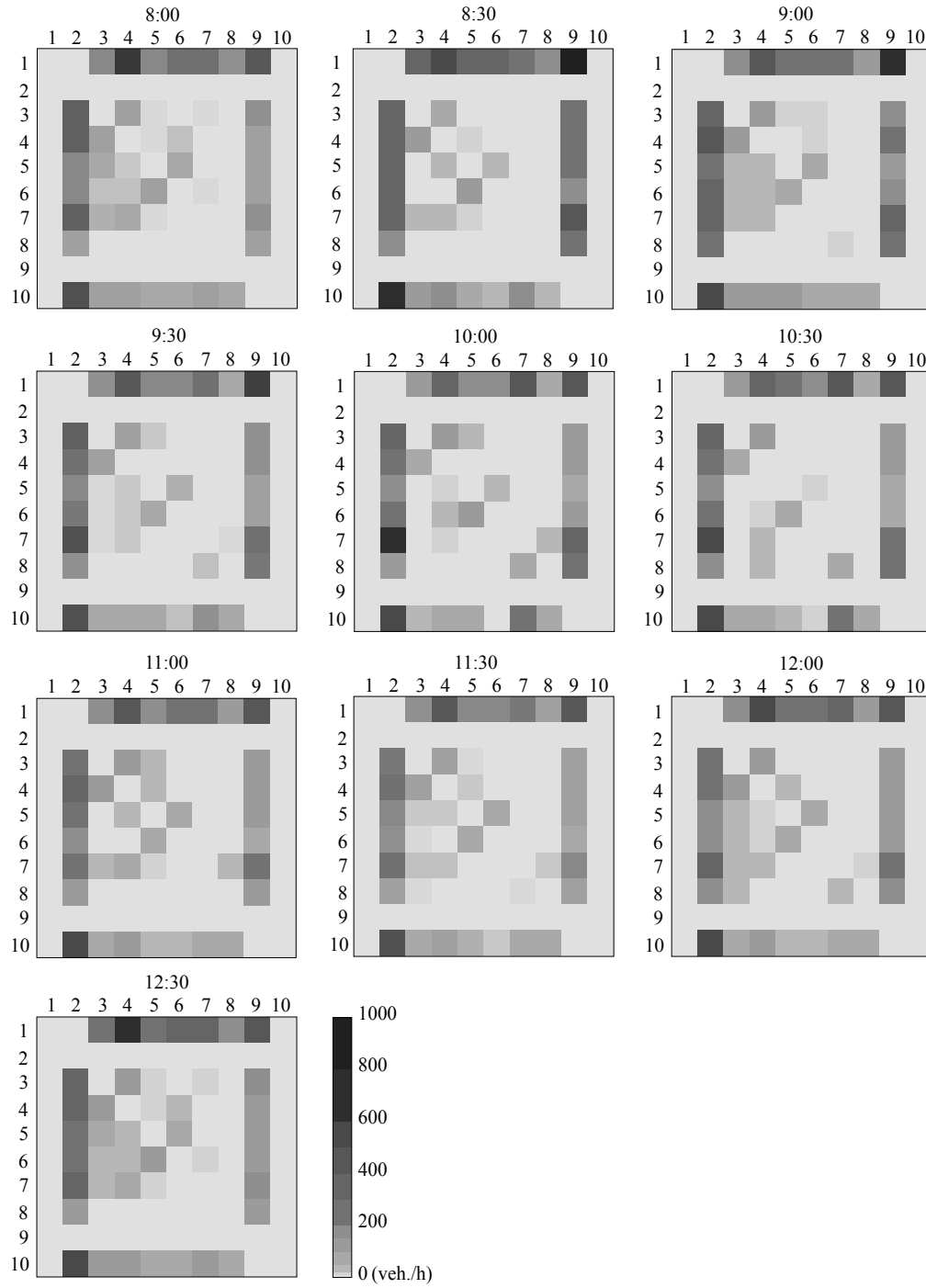


Figure 4-6: Seed OD dynamic matrix for light vehicles (am period)

Again, these shares were assumed to be independent of the upstream/downstream OD path in the A44 sub-network. Furthermore, a few of these sampled counts were also used to estimate flow factors for local entries and exits (a variable (hourly) multiplying factor of the main carriageway flow).

4.4 Incident Data


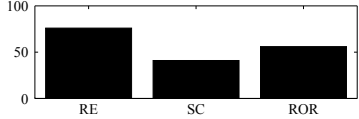
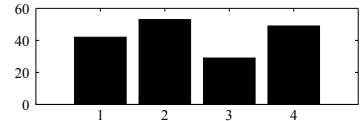
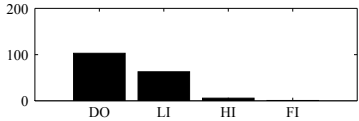
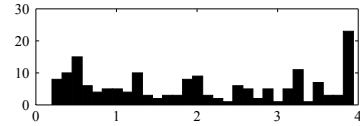
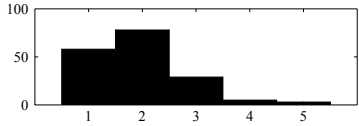
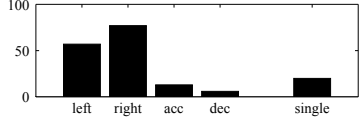
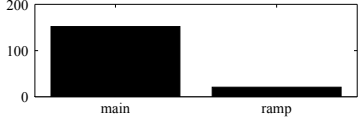
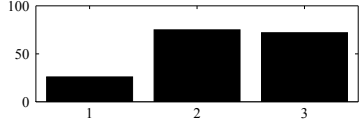
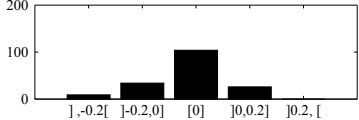
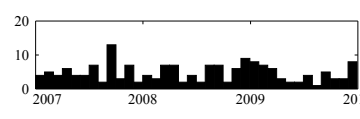
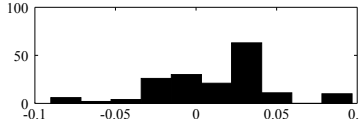
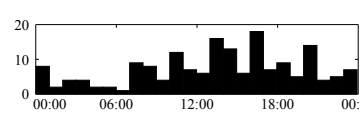
In Portugal, only accidents with injuries or fatalities are reported to road enforcement agencies and centrally recorded by the national road safety authority (ANSR). Different police departments, depending on the accident location, keep record of damage-only accidents for which they were alerted. Finally, some damage-only accidents are only recorded by the insurance companies, in some cases when a friendly agreement is reached between the drivers. According to Portuguese insurance companies, only one in ten accident claims is reported to the police (Quintero, 2010). This non-centralized nature of accident data along with small progress in the collection and registration methods have been the bigger obstacle in developing a comprehensive national analysis of road safety and, unfortunately, very small steps have been made to improve these issues. In most road concessions however, comprehensive safety records are usually also stored, albeit in a non standardized manner. Using the concessionaire emergency communication channels, real-time traffic monitoring systems and patrolling teams, the road concessionaire is typically alerted to any incident on the network. An internal report is then made by each road concessionaire and a record is kept in their own database. The A44 concessionaire only keeps a sketchy report for non-accident incidents.

The A44 incidents database for the 2007-2009 period was provided by Ascendi S.A., with a total of 749 occurrences. The range of its records vary from simple mechanical breakdowns to fatal accidents. A total of 173 side-collisions, rear-end collisions and run-off-road accidents were filtered out from the database and related further information was requested to the road concessionaire. In Table 4.7 the distribution of the collected variables are presented. During the period of analysis one fatality, seven serious injuries and 98 slight injuries were registered in the concessioned area.

From Table 4.7 a few particular observations may be already pointed out:

- From variable 3 (location of occurrence, expressed in km), it is clear that the edging

Table 4.7: Accident database description

Variable	Histogram	Variable	Histogram
1. direction X_{way}		8. type X_{type}	
2. stretch X_{str}		9. victims X_{vict}	
3. location x_{dist}		10. vehicles number X_{numv}	
4. lane X_{lane}		11. ramp X_{sec}	
5. lanes number X_{numl}		12. bulge X_{bulg}	
6. date X_{day}		13. grade (m/m) X_{grad}	
7. time X_{time}			

interchanges and its adjacent sections have a big share of the accident records. This is due to the motorway layout in these specific areas, with frequent lane changes and speed variations due to the appropriate route choice manoeuvres.

- From variable 8 (type of accident), 44% of the accidents are rear-end-collisions (RE), 32% are run-of-road (ROR) and 24% are side collisions (SC). Variable 10, the number of vehicles involved in the accident, also indicates that vehicle interactions have a clear impact in the A44 safety records.
- Variable 9 (victims) represents the consequences of the occurrence, with 'DO' as damage-only accidents, 'LI', 'HI' and 'FI' as, respectively, light injury, severe injury and fatality.
- From variable 11 (ramp, type of section), only 12% of the accidents occurred in entry or exit links.
- Variable 12 (bulge) is defined as the tangent of 1/4 of the included angle of the arc between the curve vertex edges. A negative bulge value indicates that the arc goes clockwise from the selected vertex to the next vertex. A bulge of 0 indicates a straight segment. This value is directly linked to the curve radius and a proxy of spiral curves. This measure is commonly used in simulation software and was kept as such for simulation modelling. The road curvature affects accident frequency, but the impact of this variable is significantly smaller under denser traffic conditions such as the generic A44 daylight traffic scenario. This partially explains the lower share of run-of-road accidents, when compared with the average percentage of run-of-road accidents on dual carriageway roads (typically around 50%, Roque and Cardoso (2011)).
- Variable 13 (grade) had a specific impact in the A44 motorway, namely the steep grade at the North-South direction when reaching Interchange 5 (A44/A29) slows down all vehicles considerably, especially the HGV, resulting in located congestion and higher rear-end collision rates.

These last two variables (bulge and grade) were obtained after a manual georeferencing of the road accidents by 50m segments. Each record on the concessionaire database had a field with the description of each occurrence by the patrolling agent. In case of an injury occurrence, the observation is typically a copy of the police report accident description

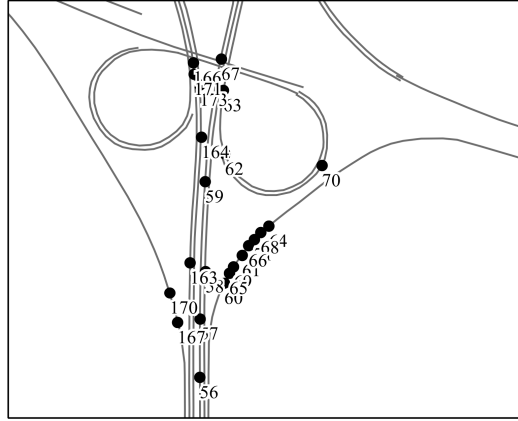


Figure 4-7: Sample of the GIS accident database

statement. For the manual georeferenciation, this description was of particular interest as it allowed to correctly locate each accident in an appropriate coordinate system (see Figure 4-7).

As no road design drawings nor listings were provided by A44 road concessionaire, road curvature was extracted from digital maps and road grade was extracted from a 3D terrain model with a 1.0m resolution obtained from aerial imagery (see Chapter 5).

4.5 Other Data

Weather data and other incident related data were also collected for the A44. Generally, weather parameters are direct inputs in the simulation application. The traffic demand and driving behaviour parameters can be calibrated for traffic under adverse weather conditions. This is typically carried out by selecting the appropriate days in the definition of the measures of performance, in the calibration step. Nevertheless, daily precipitation data for the 2007-2009 period were collect from the *Instituto Português do Mar e da Atmosfera*, Portugal, for monitoring purposes.

Similarly, other occurrences in the road system that might cause a significant change in the demand or supply are typically modelled by configuring the simulation layout appropriately or by calibrating the parameters of interest. Nevertheless, occurrences such as road works, mechanical failures an other lane interferences were supervised during subsequent analysis.

4.6 Comments

In this Chapter the case study for simulation analysis was presented. The available data for model calibration and estimation in detailed simulation applications was discussed. The case study is of particular interest for several reasons: atypical design layout due to its numerous interventions over the years, heterogeneous traffic with morning and afternoon congestion, a relatively high percentage of heavy goods vehicles and particular safety characteristics. State-of-the art methods to process input traffic data for simulation applications were presented with a focus on demand and safety data.

Along with the data set presented in the next chapter, this data set is particularly useful for estimation and calibration of driving behavior models, not only for comparison with foreign estimations, but also because of the particular characteristics of the site, generating high driver interaction frequencies and numerous lane and speed changing manoeuvres as well as short-term planning and anticipatory decisions. Finally, the limitations of existing national databases were exposed, revealing major constraints in current data sets for detailed safety analysis using simulation applications.

Chapter 5

Trajectory Extraction

The availability of detailed traffic data in the fine calibration of traffic microscopic simulation models is essential. In this Chapter, the work carried out for the collection of vehicle trajectories for the specific case study discussed in the last Chapter is presented. First, state-of-the-art trajectory extraction methods and algorithms are briefly reviewed. The proposed method for the vehicle detection and trajectory extraction is presented from section 5.3 to 5.5. Finally, the results of this collection campaign are discussed in the last section.

5.1 General Aspects

The study of detailed driving behaviour heavily depends on data availability. The estimation and calibration of driving behaviour models requires both detailed and comprehensive traffic data: detailed data is needed because these models attempt to represent sub-second vehicle-by-vehicle decisions; because they are applied to large networks, a great deal of coverage is also required (Hranac et al., 2004b). In the last couple of decades safety and behaviour modelling research has devoted efforts to collect and analyse detailed traffic data. This data may be categorized considering the type of the collection procedure used:

- **Vehicle-based methods.** Vehicles equipped with multiple sensors that travel in the traffic stream can collect time series information on the behaviour of a test driver and/or adjacent vehicles. Also known as probe vehicles, these can record driver performance and how the motion of the vehicle relates to the surrounding environment. They have been widely used in behaviour analysis for specific psycho-

logical, environmental, safety and vehicle performance studies, and several of this specific applications may be easily found in the literature. For the purpose of driving behaviour modelling, instrumented vehicles may register trajectories with several manoeuvring parameters of interest, including lane changes and car-following time based distances. However, these studies provided limited trajectory data, including trajectories of a small number of instrumented vehicles and only snapshot trajectories of adjacent vehicles. Until recently, the necessary sensor technology was too expensive and not available on a large scale, eventually affecting the consistency and replication of the estimated models. However, the well know "100-Car Naturalistic Driving Study" carried out by the Virginia Polytechnic Institute and State University (Virginia Tech) showed the enormous potential of such data. Driving activities of 100 drivers were monitored during one year (2001-2002) with the primary goal of providing vital exposure and pre-crash data necessary for understanding crashes (Neale et al., 2005). Since then, the cost of the technology used in these approaches has dropped considerably and collective efforts have recently been established to proceed with very large scale naturalistic studies. Under the Naturalistic Driving study of the Strategic Highway Research Program (SHRP 2), three thousand vehicles are being monitored for the period of two years (Antin et al., 2011). Similarly, first steps for a large scale naturalistic study have been achieved in Europe with the project PROLOGUE (Van Schagen et al., 2011), where small scale pilots have been carried out in five different countries, and more recently, with the first full scale study, under the UDrive program (SWOV, 2013);

- **Site-based methods.** Sensor technologies may be also installed in delimited areas for detailed trajectories collection. A wide range of video-based methods are generally preferred for such purposes (see 5.2 for a more detailed review) but other sensor technologies, such as RADAR, or infra-red may also be found in the literature (Aoude et al., 2011, Bhattacharya et al., 2011). A wide range of video post-processing algorithms have been and are still being developed by many computer vision research groups worldwide. These methods tend to differ on the systems' configuration, namely, on the number and the position of the sensor(s). Sensors may be placed either on poles, cables and high-rise buildings (static sensoring) or airborne vehicles such helicopters, aircraft drones and satellites (dynamic sensor-

ing). The main advantage of site-based methods is the potentially large sample of road users that may be monitored when data is collected for significant periods. Furthermore, road users usually ignore that they are being monitored, avoiding any induced change of behaviour. The main drawback of past site-based trajectory data collection is that the observation has been relatively short in time and restricted in space such that the consistency of drivers in maintaining their following and lane changing behaviour cannot be evaluated. From a practical point of view, it is often difficult to find suitable elevated points for positioning the camera (Hranac et al., 2004b, Antoniou et al., 2011a). These trajectory data can also be used in the estimation of macroscopic data, such as OD matrices, route choice or travel times. More recently, the use of smart phones has also been reported for the collection of trajectories (Schlaich et al., 2010). The degree of detail depends, of course, on the technical characteristics and penetration rate of the mobile equipment. Yet, with the increased hardware resources available in each new generation of handsets, this technology will soon represent an opportunity for the collection of large detailed positions data sets;

- **Mixed methods.** Recently, the first steps on data fusion and estimation of models with trajectory data from different sources have been tested (Chan and Bougler, 2005, Christoph et al., 2010). With the continuous development of new and accessible sensors and its integration in the telecommunication and vehicle technologies market, it is expected that the collection of behavioural data will be even more efficiently achieved through vehicle and site-based data fusion. A wide field of research opportunities in this specific area is foreseeable in the near future.

Besides all these observational methods, it is worth pointing out the existence of several experiments using driving simulators for the collection of trajectory data for the estimation of generic driving behavior models (Farah and Toledo, 2010). However, its use for the detailed calibration of specific real scenarios is of hard implementation and, therefore, out of the focus of this Chapter.

5.2 Image-based Trajectory Extraction Methods

Object tracking from photo and video cameras has been the main technique in site-based trajectories extraction in the last fifty years (Kometani and Sasaki, 1959, Treiterer and Myers, 1974, Smith, 1985). As mentioned in the previous section, the developed methods can be classified depending on the type of observation, as either static or dynamic.

5.2.1 Static observations

Since the early 1960s fixed video-based methods have been used for traffic data collection, and in the majority of the methods proposed in the last decades, traffic data extraction is based on vehicle detection and tracking techniques. Similarly to the dynamic methods, the static video-based methods include a 'moving object' detection algorithm, a vehicle identification algorithm and, more recently, a shadow detection and removal algorithm. This follows the pattern recognition reasoning where more accurate and computationally intensive operations are applied on a subset of the entire search space (Ismail, 2010).

The first spreading development of video-based computer vision in traffic analysis was based on the concept of virtual loop detectors (Michalopoulos, 1991). In the virtual loop approach, a manually defined area in the image window is automatically monitored for changes in colour or intensity, detecting any changes of the monitored road surface area when a vehicle passes. A wide range of commercial products developed in the last decade use this virtual loop approach. Nowadays, these systems use various algorithms, such as feature tracking, shape models, data association, Markov chain, Monte Carlo simulation, wire-frame models and line segment matching (Laureshyn, 2010, Wang et al., 2008).

The potential of video-based processing technology in vehicle trajectory extraction was soon identified and the first semi-automatic applications were soon developed for this specific purpose. At TU Delft, in the Netherlands, the semi-automatic application VIDARTS was used for the extraction of vehicle trajectories at intersections for safety surrogate measures analysis (van der Horst, 1990). Similarly, the ViVa-Traffic (Rudolph, 1996) developed at the University of Karlsruhe, provided a user-friendly interface for navigation through a video file frame by frame, and the possibility to manually mark vehicles' positions at each frame. Additional traffic parameters such as speed, headways and acceleration were computed directly by the software. The application was successfully

used in several applications including microscopic driving behaviour modelling (Hasan et al., 1998). Similarly to the Dutch research, studies carried out at the KTH Royal Institute of Technology in Sweden used a semi-automatic video analysis (SAVA) tool for safety analysis using the Traffic Conflicts Technique (TCT) (Archer, 2005a). These software applications are mainly focused on mapping screen coordinates to real world coordinates, sometimes predicting the position of vehicles in the next frame and computing several indicators such as speeds or headways. However, these semi-automatic methods tend to be very slow and expensive in human resources.

In the last two decades, several developments were made in image processing seeking for fully automatic vehicle tracking. One of the most important efforts, the Next Generation Simulation (NGSIM) program, was initiated by the Federal Highway Administration (FHWA) in the early 2000's. Having in mind the development of new microscopic driving behaviour models, trajectory data was collected at three different locations in California and one in Atlanta, Georgia, using an automated video analysis tool (Zhang et al., 2007). Several cameras were mounted on top of high-rise building and images at a rate of 10Hz were collected for different periods of the day. This effort resulted in the first extended and detailed trajectory data set and was used in several driving behaviour research studies. However, no reliability value was given for the automated procedure and several research studies have already found inconsistencies in the data set (Punzo et al., 2011). Since then, automatic image processing has been the main tool for trajectory extraction in naturalistic studies (Christoph et al., 2010), safety studies (Saunier and Sayed, 2008, Zheng et al., 2010), traffic flow theory (Laval and Leclercq, 2010, Cassidy et al., 2011), traffic management and surveillance (Collins et al., 2000) or driving behaviour modelling (Hidas and Wagner, 2004, Chen et al., 2012) in many different traffic scenarios.

5.2.2 Dynamic observations

Aerial imagery has been used in transportation research studies for more than eighty years (Johnson, 1929). However, it was in the mid 1980s, when the FHWA collected 13 hour-long trajectory data sets with an aircraft, that the first significant trajectory data set was collected for studying driving behaviour research (Smith, 1985). A regular camera was mounted on the side of an aircraft and pictures were taken every second. These pictures were then transcribed using a manual process. However, similarly to the

static observation studies, it was only in the past twenty years that, with enhancements in automatic image processing, trajectory extraction through airborne platforms has been increasingly adopted.

In Angel et al. (2003) a digital video camera was mounted vertically on a helicopter skid, and the flight altitude and position were recorded using a Global Positioning System (GPS) receiver. Given the focal length of the camera, flying at an altitude of 300 m above ground produced a field of view of approximately 300 m and a scale of 3 to 4 pixels/m. Similarly, Hoogendoorn et al. (2003) collected gray-scale images for trajectory extraction also using a helicopter. Flying at a low height, the authors collected images with high spatial and time resolution (5 pixels/m and 8.6 Hz respectively). However, they focused on a short (210 m) merging area of a motorway and the maximum duration of the usable image sequences was only 35 s. Despite the apparent limitation of this data set, it allowed for several developments on traffic flow theory and driving behaviour analysis for the observed scenarios (Ossen et al., 2006, Ossen and Hoogendoorn, 2008, Knoop et al., 2009, Hoogendoorn et al., 2011). A similar helicopter-based approach using colored video recording was used in (Rosten et al., 2009), where the probability distribution of velocities at every pixel in the image was calculated for speed profiles computation.

Lenhart et al. (2008) presented a system for automatic extraction of vehicle trajectories that is designed for commercial medium format cameras with a resolution of 25–40 cm and a rather low frame rate of only 1–3 Hz. The car detection process is divided into two stages. In the first step, vehicles with significant color features are extracted by a channel differencing approach. The second step is devoted to detecting the remaining gray-scaled vehicles and applies dynamic threshold constraints to blob-like structures. To this end, an adaptive shape-based matching algorithm is employed including internal evaluation and consistency checks. Recently, the authors expanded their research to the trajectory extraction through satellite imagery (Leitloff et al., 2010).

Further, potentially valuable sources of vehicle trajectories such as the DRIVE C2X project (Drive-C2X, 2012) are still under development and the transportation research community has been very active in enlarging the available data sets.

5.2.3 Image processing algorithms for vehicle tracking

Typical static and dynamic observations rely on the same image processing algorithms. Generally, these algorithms comprise two main tasks: identification of moving objects and filtering and classification of the road users of interest. The border between these two tasks is not always explicit but, in this section, we present the general aspects of each of the main algorithms found in the literature. This short description was based on the reviews presented in Kastrinaki et al. (2003), Yilmaz et al. (2006), Saunier and Sayed (2006), Wang et al. (2008), Morris and Trivedi (2008), Buch et al. (2011) and the reader should also refer to these references for additional details.

Background Subtraction: Background subtraction technique is one of the most common methods for detection of motion in many vehicle detection and tracking applications. Typically, each image frame is compared against a static background image, using a pixel-by-pixel value subtraction. To build the background image, several methods have been developed, including the frame average method, maximum/minimum intensity value method (Cho and Rice, 2004), median (and approximate median) value method (Remagnino et al., 1997, Hoogendoorn et al., 2003), Gaussian and mixture of Gaussian methods (Stauffer and Grimson, 1999, Magee, 2004) and Kalman filtering techniques (Cheung and Kamath, 2004). Background subtraction provides the most complete feature information and a high detection-rate, but the disadvantage of all these techniques is that they are extremely sensitive to dynamic scene changes due to lighting and extraneous events and, sometimes, computationally demanding. Knoop et al. (2009), for example, when focusing in car-following trajectory extraction on freeways, selected and processed just one line of pixels along each lane center-line, thus shortening processing time.

Feature-based tracking: Feature-based tracking is based on tracking points which have a particular texture in their respective image positions. These interest points have been long used in the context of motion, stereo, and tracking problems. A desirable quality of an interest point is its invariance to changes in illumination and camera viewpoint. These points (features) are then grouped considering spatial proximity or similar motion patterns along relevant multiple image frames. These algorithms have distinct advantages over other methods: they are robust to partial occlusions, they don't require

any initialization, and can adapt successfully and rapidly to variable lighting conditions, allowing real-time processing and tracking of multiple objects (Saunier and Sayed, 2006, Laureshyn, 2010). However, special requirements have to be met as regards to camera calibration and similar motion vectors of distinct objects (Ismail, 2010).

Segmentation (region-based tracking): The aim of image segmentation algorithms is to partition the image into perceptually similar regions (blobs). Most commonly, blobs identified in each frame are assigned to motion tracks using Kalman filters (Veeraraghavan et al., 2003). Region-based tracking is computationally efficient and works well in free-flowing traffic. However, under congested traffic conditions, vehicles partially occlude one another and shadows may influence the segmentation process, making individual blob identification much more difficult.

Contour-based tracking: Contour-based approaches rely on detecting and tracking a model of the object contour and motion. The vehicle contour is dynamically updated in order to fit the observed vehicle outline. Contour tracking is computationally more efficient than vehicle tracking techniques previously described by virtue of the simplicity of describing contour models. Other advantages of using contours are related to their flexibility to handle a large variety of object shapes and the detection of object merge and split. Silhouettes can be represented in numerous ways. Several successful applications of contour-based tracking may be found in the literature (Fan et al., 2002, Yilmaz et al., 2006), but when dealing with very similarly shaped objects, the contour-based tracking advantages might lose its significance.

Supervised learning: Object detection can be performed by learning different object views automatically from a set of examples by means of a supervised learning mechanism. Given a set of learning examples, supervised learning methods generate a function that maps inputs to desired outputs. These learning approaches include neural networks (Goerick et al., 1996), adaptive boosting (Viola et al., 2003) and support vector machines (Papageorgiou and Poggio, 2000).

Objects filtering: After the moving objects have been identified in all frames, road users are generally selected by knowledge-based or motion-based criteria. Knowledge

based methods employ a prior knowledge to decide whether the identified object is a road user of interest. Features like symmetry, color, shadow, vertical/horizontal edge, texture descriptors (such as wavelets) and 3D vehicle model are used as classification criterion (Bhattacharya et al., 2011). Motion-based methods use optical flow, a dense field of displacement vectors, defining the translation of each pixel in a region, which is computed using the brightness constraint, assuming brightness constancy of corresponding pixels in consecutive frames (Haag and Nagel, 1999).

Much of current image processing state-of-the-art research aims at improving the detection and tracking efficiency, classifying object motion patterns and also predicting objects trajectories (Morris and Trivedi, 2008, Zhou et al., 2011).

5.3 Data Collection System

Dynamic observation was carried out over the A44 road to collect aerial images for trajectory extraction. A Cessna T210L Centurion II with photographic equipment fixed to a gyro-stabilizing platform GSM3000 assuring the registration of all aircraft rotations (roll, pitch, yaw) was used in the image collection. The choice of such method (instead of static observation or more advanced dynamic ones) relied on both fulfilling budget limitations and its ability to collect partial trajectories over the entire length of the pilot study area.

A Digicam-H/39 (Digicam) camera with a RGB sensor of 7216x5412 pixels and a 80mm Hasselblad lens was placed in the aircraft gyro-stabilizing platform. The Digicam allowed for a very high resolution image collection, directly connected to a high precision positioning system through differential GPS and an inertial unit formed by optical fiber gyroscopes. Photos were collected at an average rate of 0.5Hz, triggered by a fixed image overlapping rate of 90% (the systems' maximum). The focal distance, shutter speed and aperture were fixed during the entire flight over the study site (A44 motorway).

On the morning of the 11th of October 2011, the aircraft overflew the A44 twelve times, between 7:45 and 12:00 am, six times in each road traffic direction. The average speed and altitude were 220km/h and 2800m respectively. These flight characteristics were selected considering the atmospheric conditions and an optimized resolution/coverage of the images, allowing for an average ground sample distance of 23 cm.

The orthorectification of the Digicam images was carried out by InfoPortugal S.A.,



Figure 5-1: Sample of a part of an aerial image taken by the Digicam camera

modelling the terrain in 3D and applying the needed transformations. This process accounted for the typical camera calibration task for perspective projection of real-world points onto the image plane representation.

5.4 Image Processing

The image processing procedure is composed of many sub-tasks that in some cases may be integrated in a single algorithm, depending on the chosen approach (see section 5.2). In this specific case study, a background subtraction approach was used in the detection of moving vehicles. To achieve this task, the following steps were carried out:

- local image rectification to account for terrain model and main orthorectification errors;
- detection of moving objects;
- filtering vehicles from other objects.

All image processing tasks were carried out at the *printart server* owned by the Institute for Systems and Robotics of IST-Lisbon. The server holds 48Gb of RAM memory and 16

Intel® Xeon® E620 quad-core processors at 2.4 GHz, allowing for a faster computation during the intensive image processing. The code was built in **MATLAB**. It is worth mentioning that the library **OpenCV** is, along with **MATLAB**, one of the most commonly used platforms for image processing. Although this **C/C++** based library might have several advantages, **MATLAB**'s Image Processing Toolbox easy use, interface and memory management were the reasons to opt for this offline application.

Local orthorectification

To minimize the errors of each image main orthorectification and 3D terrain model, an automatic local rectification process was used. Each image was divided into grids, scaled and referenced automatically using the SIFT (Scale Invariant Feature Transform) method (Lowe, 2004). In the SIFT method, a scale-space is constructed by convolving the image with Gaussian filters at different scales. In the space-scale framework each image is represented as a one-parameter family of smoothed images, parametrized by the size of the smoothing kernel used for suppressing fine-scale structures. Convolved images are then used to generate difference-of-Gaussians images. Candidate interest points are then selected from the minima and maxima of the difference-of-Gaussians images across scales. The next step updates the location of each candidate by interpolating the color values using neighboring pixels. Then, low contrast candidates as well as the candidates along the edges are eliminated. Finally, remaining interest points are assigned orientations based on the peaks in the histograms of gradient directions in a small neighborhood around a candidate point. For each image grid, matching points between Digicam grid images were then used to fit a projective transformation using the RANSAC (random sample consensus) algorithm (Fischler and Bolles, 1981). RANSAC is as simple algorithm for robust fitting of models in the presence of many data outliers. Unlike conventional sampling techniques that use as much of the data as possible to obtain an initial solution and then eliminate outliers, RANSAC uses the smallest set possible and proceeds to enlarge this set with consistent data points. The reader may refer to both (Lowe, 2004) and (Fischler and Bolles, 1981) for details on these two image processing algorithms.

Background subtraction

For each flight over the A44 a background was constructed using the median filter. The colored background was computed by taking the 1-D median (in the temporal direction) and computed on all three channels (**R**ed, **G**reen and **B**lue) separately. For each image, the color similarity metric (Cutler and Davis, 1998) was then used for the background subtraction and extract foregrounds pixels $F(x, y)$:

$$F(x, y) = \sum_{C \in \{R, G, B\}} |I_c(x, y) - B_c(x, y)| \quad (5.1)$$

where $I_c(x, y)$ is the value of the pixel (x, y) for color channel C of the image I , $B_c(x, y)$ is the color value for the same pixel in the background image and $\{R, G, B\}$ are the three color channels. For early flights, when congestion was observed, the background computed for later flights was used for smoothing the background pixel values, as slow/stopped vehicles would bias the median value. Foreground pixels $F(x, y)$ in each grid image were then marked considering an uni-modal threshold automatically computed for each image using the maximum deviation algorithm proposed by Rosin (2001). This algorithm is specially suitable to images where a much larger proportion of just one class of pixels (e.g. the background) dominates the foreground histogram. A straight line is drawn from the peak (dominant) to the high end of the histogram. More specifically, the line starts at the largest bin and finishes at the first empty bin of the histogram following the last filled bin. The threshold point is selected as the histogram index bin that maximizes the perpendicular distance between the line and the point on the histogram curve (see Figure 5-2).

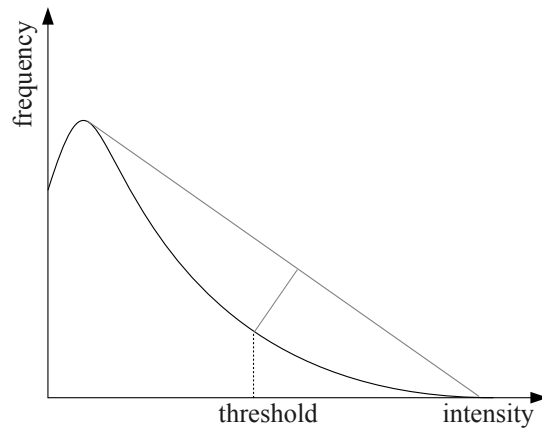


Figure 5-2: Rosin's Uni-modal Threshold (adapted from Rosin (2001))

Vehicles Filtering

After marking all foreground pixels (moving objects), pixels belonging to moving shadows must be filtered out to minimize the errors of the automatic positioning of vehicles. As colored images were used, this issue was solved using the spectral rationing technique, successfully applied to traffic scenes (Tsai, 2006). First, foreground and background images were transformed into the invariant colored model YCbCr, and the spectral ratio measure was calculated for each pixel:

$$S(x, y) = \frac{I_{Cr}^{scaled}(x, y) + 1}{I_Y^{scaled}(x, y) + 1} \quad (5.2)$$

where $S(x, y)$ is the value of spectral ratio at the pixel (x, y) , $I_{Y \text{ or } Cr}(x, y)$ is the value of the pixel intensity for the invariant color Y or Cr scaled to $[0, 1]$. Shadowed regions, having higher ratio values, were marked into a logical shadow mask. The Otsu's method (Otsu, 1979) was used to automatically determine the threshold for segmenting shadow regions in each image grid. Finally, simple morphological operations such as removing isolated pixels and erosion followed by dilation were used for the shadow mask enhancement.

After filtering the foreground for non-shadow pixels, a region-based analysis is performed to extract blobs out of connected pixels in the foreground image. Each blob i is then filtered based on its specific geometric features: minimum and maximum projected area (A), minimum and maximum projected width and length (l^{min} , l^{max}), and specific shape based relationships:

$$i \in S \equiv \left\{ \begin{array}{l} 1.25m^2 < A_i < 90.0m^2 \\ l_i^{min} > 1.00m \\ l_i^{max} < 10.00m \\ \frac{l_i^{max}}{l_i^{min}} < 4.15 \\ \frac{A_i}{(l_i^{max} \times l_i^{min})} > 0.55 \end{array} \right. \quad (5.3)$$

where S is the final set of vehicle candidates. With such method, vehicle-like shape blobs and their characteristics were extracted (see Figure 5.3.e). It is worth mentioning that the thresholds referred in equation 5.3 do not represent typical vehicle geometric features, but the way they are interpreted during the image processing. As an example, the $1.25m^2$

used for the minimum projected area accounts for the possibility of detection of just the car hood in the foreground, due to windshield color properties in aerial images. The final values shown in equation 5.3 were manually tuned for a sample of images.

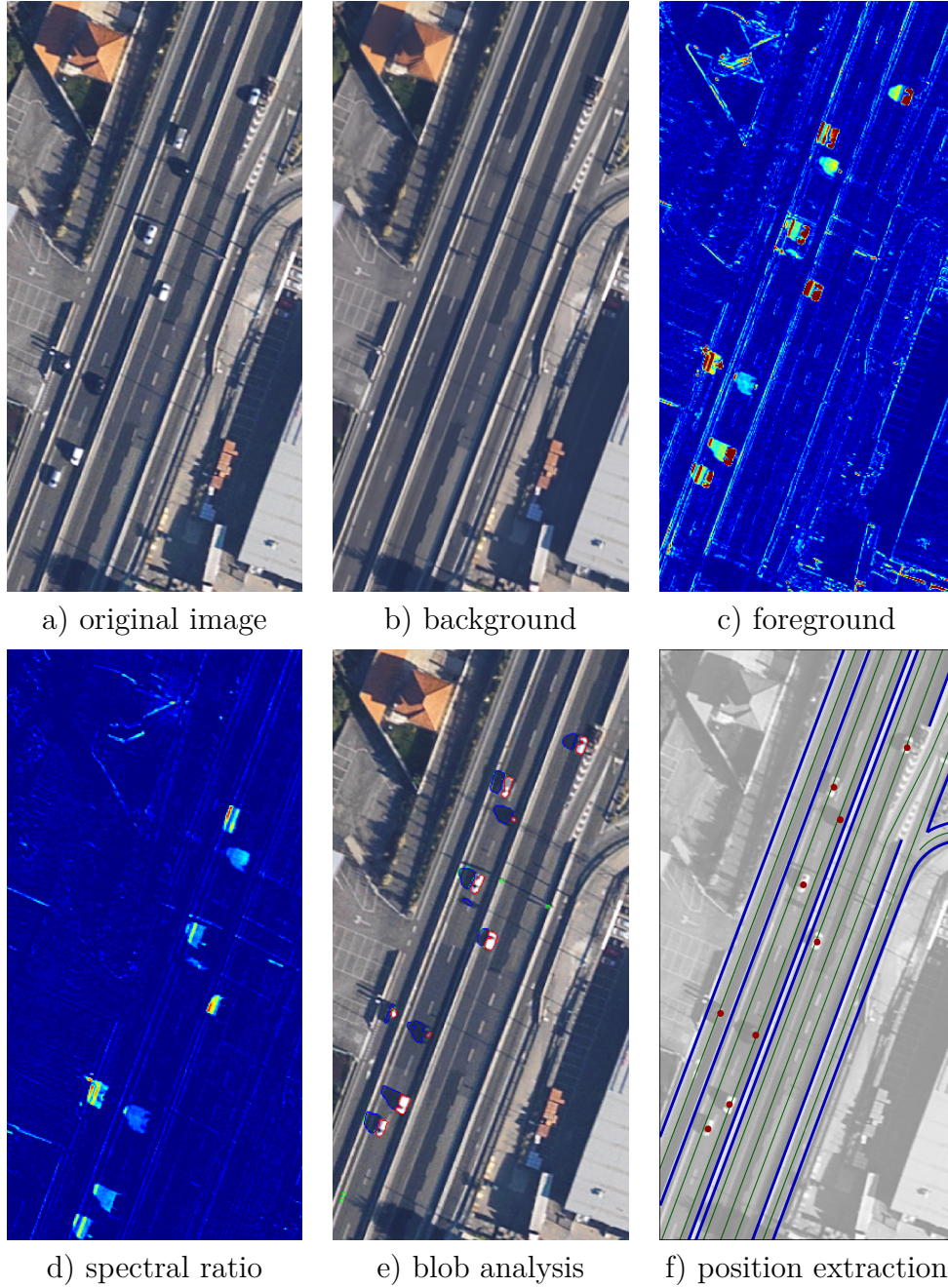


Figure 5-3: Image processing steps

5.5 Vehicle Tracking

After achieving the time-independent detection of vehicles, the second step consists in modeling motions to link identified candidate positions into the most likely trajectories.

Several methods may be found in computer vision literature, with a greater prevalence of different Kalman filtering applications, particle filtering, dynamic programming and hybrid approaches, where detections are first connected into short tracks, which are then linked together using a higher-level method. However, each of these methods has its own weaknesses, such as frequent identity switches or non-simple tuning of its model parameters. For a more detailed review, the reader may refer to Buch et al. (2011).

Along with these generic methods, graph theory has been recently applied to the vehicle tracking problem with success. Typically, every region in a frame is represented by a node in a graph. A link between each region in two consecutive frames is generated and labeled with a discrete variable representing the number of objects moving from linked nodes. Trajectories are then extracted using global optimization using a min-cost flow algorithm. Linear Programming can be used to link multiple detections over time, and therefore solve the graph problem (Song and Nevatia, 2007). However, the computational complexity of the dynamic programming approach can be prohibitive when the frame or/and vehicle number is high.

Recently Berclaz et al. (2011) reformulated the Linear Programming (LP) problem as a *k-shortest disjoint paths* problem on a directed acyclic graph. In their study, the area of interest in the image sequence and the time recording interval were discretized and linked by possible object motions, resulting in a directed acyclic graph. Two additional nodes (*source* and *sink*) were added to account for a consistent flow of vehicles in the data set (see Figure 5-4). These two nodes are linked to all the nodes representing positions through which objects can respectively enter or exit the area, such as occlusions or the camera field of view, and to all nodes in first (*source*) and last image (*sink*). Any path between the *source* and *sink* nodes represent the flow of a single object in the original problem along the edges of the path, hence a vehicle trajectory. The node-disjointness constraint is needed to assure that no location can be shared by two paths.

The optimization function depends on the marginal posterior probability of the presence of an object in each image, which was obtained previously during the object detection task. In our current application the information obtained from the segmentation analysis in the vehicle detection task, such as blob area or average blob color, is error prone due to the small ground sample distance and varying lighting conditions. The use of such features as main tracking function is not suitable under these conditions.

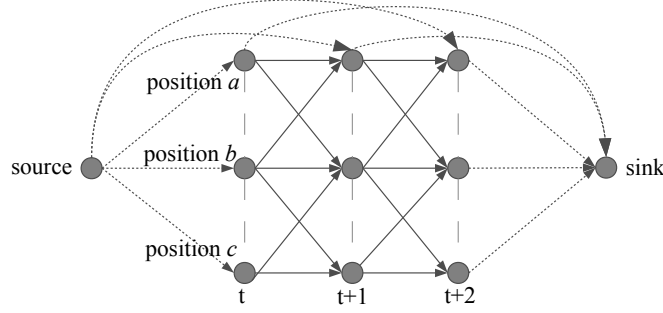


Figure 5-4: Generic multiple object tracking (adapted from Berclaz et al. (2011))

To overcome these limitation an alternative approach was adopted: using vehicle motion parameters as an optimizing function. It was assumed that the set of motion parameters is limited, setting bounding limits for speed, acceleration and deceleration. Then it was also assumed that any driver has a motion-based optimizing function, i.e., that any trajectory is subject to a set of motion-based objectives of the driver. Ideally, complex microscopic driving behaviour models and Kalman-filter models may be used in this process using large number of variables and parameters to reconstruct trajectories along with the k -shortest disjoint path algorithm. Due to the specific nature of the current application a simpler approach was considered. In free-flow conditions, it is known that a driver tends to reach and maintain its target speed. When relaxing the free-flow constrain, one may assume that the driver tends to minimize changes in acceleration. These changes are even smaller if observations are more frequent. Regarding lateral movement, a similar approach can be formulated with the inclusion of lane change tags: when the lateral acceleration is constant and different from zero for a longer period of time, a lane change might be tagged for that trajectory.

5.5.1 Graph construction

Similarly to the approach proposed by Berclaz et al. (2011), our optimization problem in matching vehicle positions into trajectories was expressed as a graph problem. Instead of discretisizing the area of interest into possible locations, the graph was built from the candidate positions already detected in the previous task (see section 5.4).

Primal Graph

Each detected vehicle position candidate $k_i^t \in K^t$, where $t \in T$ is the image shooting instant, represents a node in primal graph the A . For any location k_i^t , let $N(k_i^t) \subset K^{t+1}$ denote the possible positions of k_i^t at the next observation time $t + 1$. To model vehicle positions over time, let us consider a labeled directed graph with $\sum_t K^t$ nodes, which represents every position candidate at every instant. Its edges correspond to admissible vehicle motions between successive image shots. For k_i^t and k_j^{t+1} (denoted as i and j for simplicity) to be connected with an edge e_{ij} , its computed speed should satisfy equation 5.4 and lane connectivity assured.

$$0 \leq V_{ij}^l = \frac{X_j^l - X_i^l}{\Delta t_{ij}} \leq V_{max}^l, \quad (5.4)$$

where X^l is the longitudinal (l) vehicle position along the lane center line. Equation 5.4 is also used to compute edge costs $c_{ij}^l = V_{ij}^l$, where V_{ij}^l represents the longitudinal speed from two consecutive positions i and j . A lane change tag $c_{ij}^l = \{0, 1\}$ equal to 1 if $lane_i = lane_j$ and 0 otherwise can also be computed for each edge e_{ij} .

Dual Graphs

After constructing the primal graph, accelerations might be computed from adjacent edge combinations. Such combination produce a weight for each pair of adjacent edges in the graph, similar to turn costs in route planing graphs. These weights cannot be stored easily with the edges or nodes in the primal graph A , but they can be attached to a linear dual graph. The basic idea is to replace edges in the original graph by nodes, and pairs of consecutive edges by edges using a linear dual graph (Winter et al., 2002).

Given a primal directed weighted graph $A(N, E)$, the graph $B(N', E')$ with the following properties is called its complete linear dual graph:

- For each edge e_{ij} in A there is a node $n'_{ij} = d(e_{ij})$ in B . d is an objective function so that $d^{-1}(n'_{ij}) = e_{ij}$;
- For each pair of consecutive edges (e_{ij}, e_{jk}) in A , there is an edge e' in B between the corresponding nodes $n'_{ij} = d(e_{ij})$ and $n'_{jk} = d(e_{jk})$;
- A cost function $f_{c'} : E' \rightarrow \mathbb{R}$.

The number of nodes in B equals the number of edges in A and the number of edges in B equals the number of connected edge pairs in A . A first dual graph representing the accelerations, called \dot{B} , may be obtained by performing the above procedure once. A second dual graph representing variation of accelerations, called \ddot{B} , is obtained by performing a second iteration:

1. Acceleration Dual Graph \dot{B}

$$\begin{aligned}\dot{c}_{ijk}^l &= a_{ijk}^l = \frac{V_{jk}^l - V_{ij}^l}{\Delta t_{jk} + \Delta t_{ij}} \\ \dot{c}_{ijk}^{lc} &= c_{ij}^{lc} \times c_{jk}^{lc}\end{aligned}\tag{5.5}$$

2. Acceleration Variation Dual Graph \ddot{B}

$$\begin{aligned}\ddot{c}_{ijkl}^l &= \Delta a_{ijkl}^l = a_{jkl}^l - a_{ijk}^l \\ \ddot{c}_{ijkl}^{lc} &= c_{ijk}^{lc} \times c_{jkl}^{lc}\end{aligned}\tag{5.6}$$

where, i, j, k and l are the node indexes in the primal graph A . These transformations are represented in Figure 5-5, where the primal graph A is represented in continuous grey lines, the dual graph \dot{B} by dashed grey lines and the final dual graph \ddot{B} by bold dark nodes and edges.

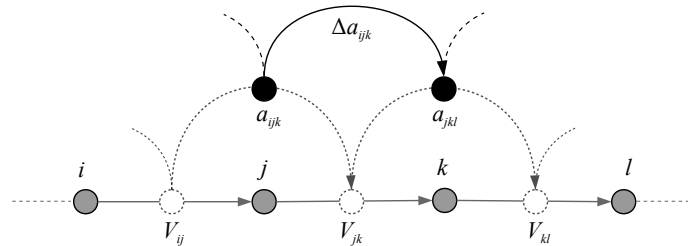


Figure 5-5: Dual graph construction

Additional acceleration-based criteria were used to filter out edges in the acceleration dual graph \dot{B} . Using minimum and maximum longitudinal and lateral accelerations, all edges not satisfying equation 5.7 were eliminated from \dot{B} .

$$a_{min}^l \leq a_{ijk}^l \leq a_{max}^l,\tag{5.7}$$

The majority of shortest path algorithms take as input a unique edge cost value.

To avoid the use of multi-criteria shortest path optimization, a cost function to integrate longitudinal and lateral vehicle movements must be specified. In our application, a simple linear optimizing function was considered. For any edge $a = i, j, k, l$ in the final dual graph \ddot{B} , the cost \bar{c}_a was computed as:

$$\bar{c}_a = \omega_l \bar{c}_a^l + \omega_{lc} \bar{c}_a^{lc} \quad (5.8)$$

where \bar{c}_a^l is the value of \check{c}_a^l normalized to $[0, 1]$ and \bar{c}_a^{lc} is equal to $(1 - \check{c}_a^{lc})$. ω_l and ω_{lc} represent therefore weights of the longitudinal acceleration variation and a lane change factor. It is worth mention that this simplified approach is acceptable for non-saturated motorway traffic, but does not however, represent a drivers' trajectory optimizing function valid for all traffic conditions. The lane change factor, for example, considers that a driver tends to stay in the same lane, underestimating the effect of strategical lane change in drivers' trajectory optimizing function. Different combinations of weight pairs were tested against a manually constructed trajectory set with dense traffic situations (see Table 5.1). A set of specific MoP were computed for both a manually extracted trajectories and those reconstructed by the proposed algorithm: mean (μ), standard deviation (σ), skewness (γ) and inter-quantile range (iqr) for speed, acceleration, headways, time-to-collision, lane gaps, etc. A few examples of the obtained root mean square percentage error (RMSPE) of a set of MoP are presented in Table 5.1.

Table 5.1: RMSPE (%) for different weights combination and MoP

ω_l	N° paths	Speed				Headway			Acceleration		
		μ	σ	γ	iqr	μ	σ	γ	μ	σ	γ
0.500	116	0.32	6.95	38.4	7.55	0.42	0.37	27.9	5.37	8.33	11.2
0.750	53.8	0.16	3.68	68.8	2.46	0.21	0.52	1.93	2.68	6.37	3.47
0.800	38.2	0.15	3.26	77.1	2.53	0.19	0.42	1.98	2.77	7.02	3.80
0.850	25.3	0.15	2.88	12.4	2.50	0.16	0.01	0.10	2.07	5.96	3.20
0.900	14.0	0.15	2.68	10.5	2.70	0.14	0.01	0.08	1.85	4.68	1.46
0.925	6.99	0.15	2.65	10.7	2.45	0.13	0.02	0.08	1.90	4.82	2.17
0.940	0.54	0.15	2.02	10.7	1.67	0.11	0.03	0.05	1.34	4.42	4.24
0.950	6.45	0.25	1.18	3.99	0.6	0.45	0.22	30.5	1.78	1.85	2.30
0.960	12.4	0.22	1.18	4.11	0.77	0.42	0.50	30.5	1.55	1.46	2.37
0.975	22.6	0.26	2.00	4.40	1.33	0.45	0.27	29.9	2.07	4.00	4.25

From the results presented in Table 5.1 it is clear that the proposed method achieves very good results for higher weights of the longitudinal acceleration. However, the lane

change also brings a non-negligible enhancement to the estimates of the mean (μ), standard deviation (σ), skewness (γ) and inter-quantile range (iqr) of longitudinal motion-based variables. ω_l and ω_{lc} ($= 1 - \omega_l$) were respectively set to 0.94 and 0.06 for the vehicle tracking in all flight runs.

5.5.2 The k -shortest disjoint paths algorithm

An extension of the k -shortest disjoint paths algorithm proposed by Suurballe (1974) was used to compute the best set of trajectories for each flight. Suurballe's algorithm relies on the iterative *augmentation* of signed paths and on any general shortest path algorithm on a modified costs graph. In this section we present a short description of this implementation proposed by Berclaz et al. (2011), and one should refer to both articles for further details.

Interlacing path and Augmentation

A signed path is a sequence of sign-labeled edges connecting them in order to form a path in a directed graph G , where each edge is assigned with a positive label \oplus or a negative label \ominus . An *interlacing path* s , is a special type of signed path linked to a path set P_l , which satisfies the following two conditions:

1. An edge is common to both s and P_l if and only if it has a negative label;
2. A node is common to both s and P_l if and only if it is on an edge with negative label.

Both conditions are essential to achieve both edge and node-disjointness needed in the current application. The *augmentation* of P_l and s may be viewed as the addition and subtraction of labelled paths, where adding positive labeled edges of s to P_l and removing negative labeled edges of s from P_l . The *augmentation* process is illustrated in Figure 5-6 for a simple graph. The path set obtained in b) composed by a single path $\{i, j, k, l\}$ is augmented by the path $\{i, k, j, l\}$ showed in e), resulting in the disjoint paths set $[\{i, k, l\}, \{i, j, l\}]$.

Graph Transformation

To account for signed paths and *augmentation* in the original graph G , Suurballe (1974) proposed two transformations to allow the use of *interlacing paths*:

- Node splitting: the node-disjointness criteria is relaxed to an arc-disjointness by node splitting: for each node i , an auxiliary node i' is created, reassigning all outputs on i as outputs on i' , leaving all arc lengths unchanged and connecting i and i' with an auxiliary link $e_{ii'}$ with cost $c_{ii'} = 0$ (see Figure 5-6);
- Path inversion: to account for signed labelling, the direction and algebraic sign of the cost of each arc in p is inverted; this transformation represents a transformation from signed paths to directed unsigned paths.

The two step transformation is illustrated in Figure 5-6 for a simple path. In c), nodes j and k in path $\{i, j, k, l\}$ are split into j, j' and k, k' respectively. Finally, in d), *source* and *sink* nodes were not split to allow multiple flows (paths) from these two nodes. All edges direction in path $\{i, j, k, l\}$ were reverted and its cost signs inverted.

Suurballe's algorithm

The Suurballe's algorithm performs the following steps:

1. Find the shortest path p_1 from *source* to *sink* in G using a generic shortest path algorithm (Figure 5-6 b.);
2. Split every node i in p_1 and reverse the direction and algebraic sign of all edges in P_1 , according to the previous section, resulting in the transformed graph G_E (Figure 5-6 c. and d.);
3. Find the shortest path p_2 in the transformed graph G_E using a generic shortest path algorithm (Figure 5-6 e.);
4. Discard the reversed edges of p_2 from both p_1 and p_2 . The remaining edges of p_1 and p_2 form a sub-graph with two edge-disjoint paths from *source* to *sink* (Figure 5-6 f.).

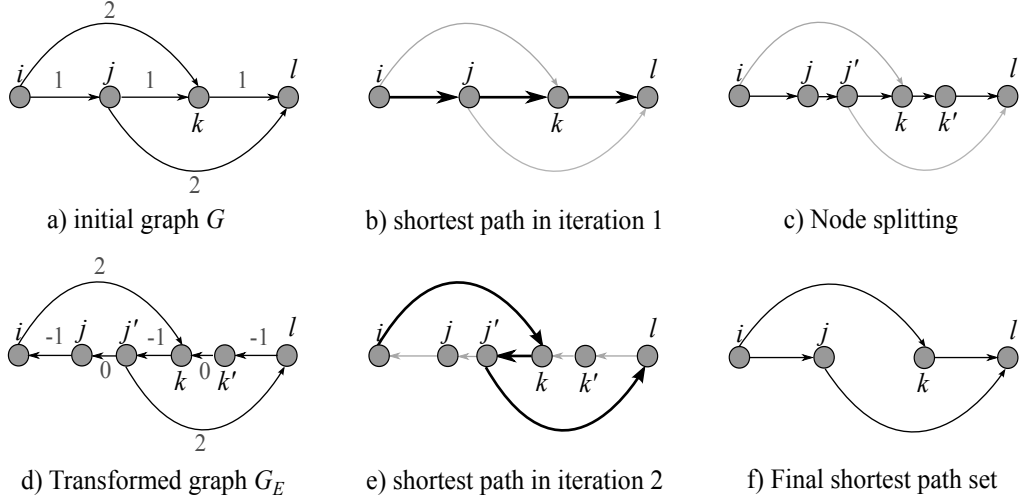


Figure 5-6: Suurballe General Framework

Cost Transformation

As the number of vehicles passing in the observed area is unknown, one also needs to optimize the number of paths k . Berclaz et al. (2011) formulated the general optimizing problem by establishing an equivalence to the linear programming (LP) formulation. As discussed in their paper, the equivalence of the LP and the k -shortest paths formulation by Suurballe results from assuming a convex function of the path set total cost with respect to k . In fact, when assuming that path costs are monotonically increasing $p_n \leq p_{n+1}$ at each iteration n , being p_n the shortest path computed at the n^{th} iteration of the algorithm, the total cost function $cost(P_n)$ is convex with respect to n , where $cost(P_n) = \sum_{i=1}^n (cost(p_i))$. Therefore, the global minimum is reached when $cost(p_n)$ changes sign and becomes non-negative.

In our case study a transformation of the already combined acceleration variations and lane changes was used to allow a similar approach:

$$cost_a = \log \left(\frac{\bar{c}_a}{1 - \bar{c}_a} \right) \quad (5.9)$$

where \bar{c}_a is defined by equation 5.8. Doing so, the $cost(P_n)$ is convex with respect to n , and the stopping criterion of the algorithm to obtain the best k^* trajectories is defined as:

$$cost(P_{k^*-1}) \geq cost(P_{k^*}) \leq cost(P_{k^*+1}) \quad (5.10)$$

General Framework

The general algorithm for vehicle tracking and trajectory extraction from the processed images may be summarized as follows:

1. Construct primal position graph (A)
2. Compute dual acceleration and lane change graphs (\dot{B}_a, \dot{B}_{lc})
3. Compute dual acceleration variation and lane change graphs ($\ddot{B}_a, \ddot{B}_{lc}$)
4. Compute the transformed combined cost graph (B^T)
5. Iteration 1: Compute the shortest path p_1 on B^T using the Bellman-Ford algorithm (Bellman, 1958, Ford and Lester, 1956)
6. Iteration n :
 - (a) if $cost(P_{n-1}) \geq cost(P_n)$, then
 return P_{n-1}
 end
 - (b) Compute the transformed graph B_E^T using Suurballe's transformation steps
 - (c) Compute the shortest path p_n on B_E^T using the Bellman-Ford algorithm
 - (d) Compute the *interlacing* path s_n from p_n
 - (e) Compute P_n by *augmentation* of s_n on P_{n-1}

5.6 Results

The method presented in this section successfully collected a total of 1855 trajectories from all twelve flights. During the first three flight runs over the A44, congestion was observed in the South-North direction, near the weaving area of Interchange 1. Levels of service E and F were observed for this subset, which correspond to the 7:45-8:30 AM period. The distribution of key traffic variables were extracted for each flight run for assessment. The selection process of these variables relies in the calibration of traffic simulators and is discussed in the next section. In Figure 5-7, the empirical CDF for some of these variables are presented. As expected, speed and headway have a (truncated) normal distribution. It is worth noting that low values for speed and headway were still collected in some sections

of the A44, resulting in a bimodal nature of their distribution (see Figure 5-7 a) and b)). Acceleration and deceleration follow a half-normal distribution with the typical upper and lower range values for non aggressive manoeuvres. This driving behaviour during the collection period is also noticeable when looking at the TTC and DRAC distributions. High TTC values and low DRAC correspond to typical safe scenarios, with $TTC > 1.5s$ and $DRAC < 1m/s^2$ (Cunto, 2008). There are few observed unsafe records and negative values for both left and right gaps, which are mainly due to errors in the position and vehicle length estimates in stop and go scenarios.

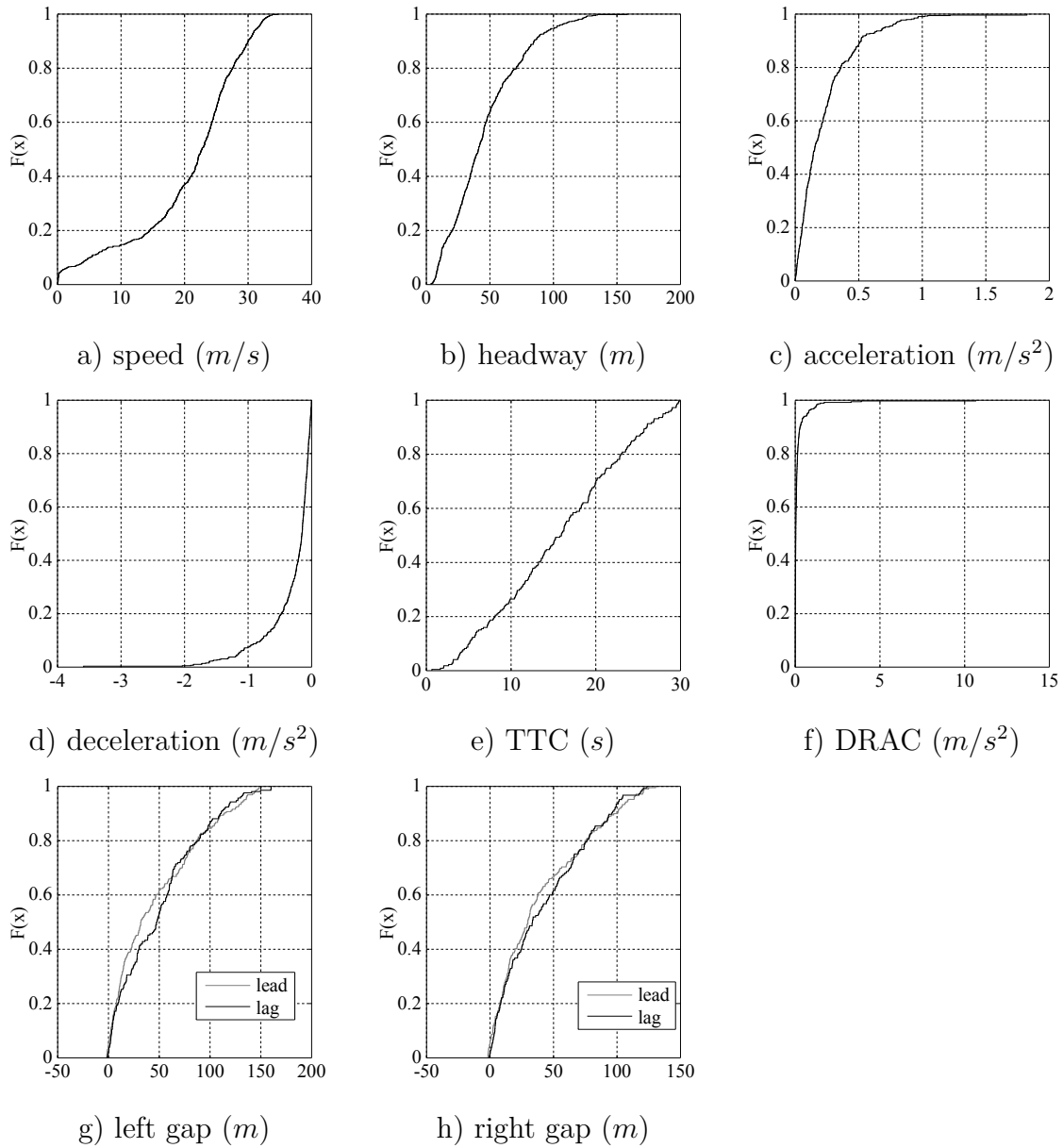


Figure 5-7: Empirical CDF of traffic variables

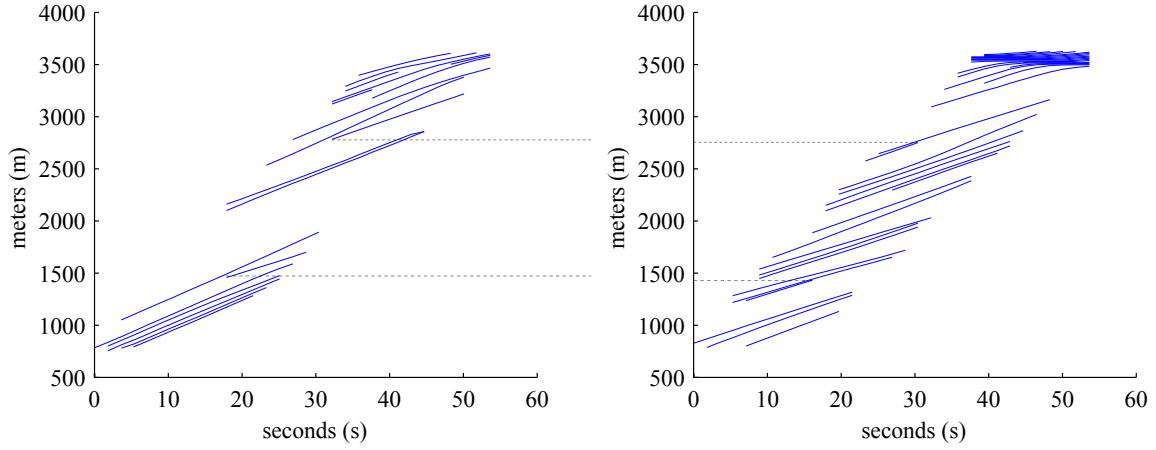
In Figure 5-8 and 5-9, a set of trajectories in both main lanes in the South-North

direction of the A44 motorway extracted from an early flight are analysed. Again, the congestion at the end of lane 2 is evident throughout all graphs. Different lane changes may result in different graph changes as shown by the following two examples: a heavy vehicle switches from lane 2 to lane 1 near km 3,000, increasing the headway in lane 2 and decreasing the speed on lane 1; a car near km 1,500 on lane 1 accelerates to overpass the preceding vehicle, decreasing the TTC in lane 1 and the speed in lane 2, before and after the lane change, respectively.

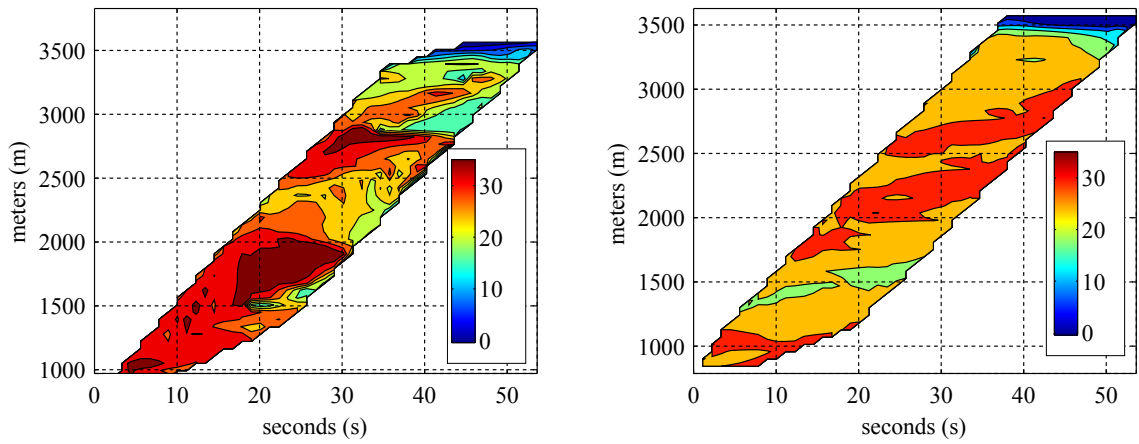
5.7 Discussion

In this Chapter a description of the method used for automatic extraction of vehicle trajectories is presented, in order to collect detailed traffic variables required for microscopic simulation modelling and calibration. A large set of successfully extracted motion parameters allowed for the characterization of driving behaviour, even under limited resources in the collection procedure. Despite the successful results, three main sources of limitations must be considered in future applications:

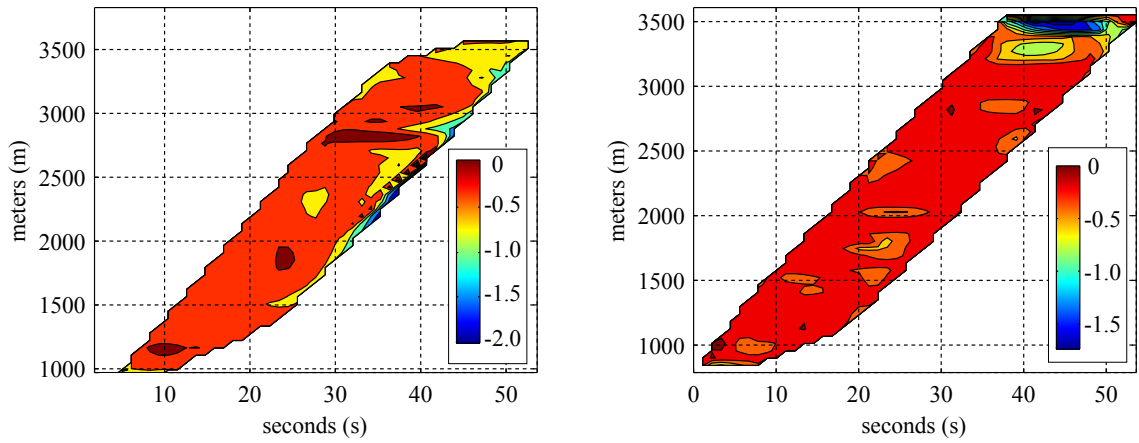
1. The results of this method might improve significantly with lower ground sample distance (resolution) and higher photo shooting rates or video. Inevitably, when opting for traditional and less expensive aircraft instead of helicopters, only partial trajectories are collected due to the dynamic nature of the observation point. Unmanned Aerial Vehicles (UAV) may bring a much higher flexibility to this process, specially for small study areas;
2. The available computational resources allowed for the use of simple and robust foreground detection such as the median filter. However, the high ground sampling distance affected the region segmentation and the accuracy of vehicle features extraction. Shadows are always a serious problem during the analysis of many outdoor image sets. Although the advanced spectral filter limited errors in the position extraction, it originated false negatives. Dynamic shadow models and 3D vehicle models may be found in the literature to minimize these issues. Also, the use of stereo imagery would contribute to avoid these modelling burdens, albeit at a higher cost;
3. Finally, the original specification of the Suurballe algorithm applied to dual graphs



a) time-space trajectories



b) speed (m/s)



c) deceleration (m/s^2)

Figure 5-8: Tracking results for lane 1 (left) and 2 (right) in the S-N direction

may not converge to the true optimal solution. This allows for node-joint paths in the final solution of the algorithm. In fact, there are dependencies between different nodes in the dual graphs \dot{B} and \ddot{B} that are derived from the transformations of

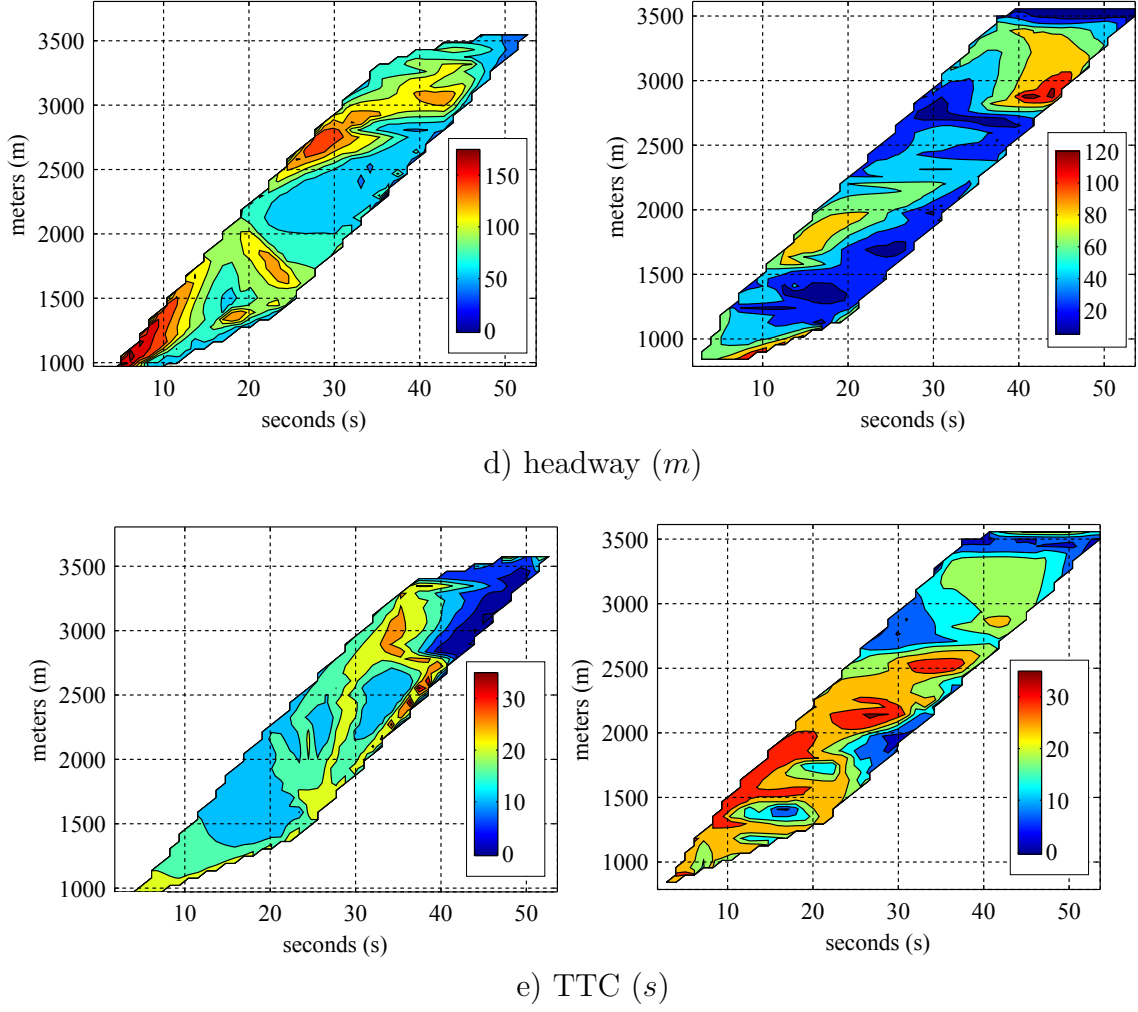


Figure 5-9: Tracking results for lane 1 (left) and 2 (right) in the S-N direction

edges sharing the same nodes in A . When ignoring these dependencies, node-joint paths in A may be verified in final solution of the algorithm, resulting in overlapping trajectories. A possible solution is to use a Integer Programming (IP) formulation, as proposed by (Berclaz et al., 2011), instead of the graph-oriented formulation. This problem can be solved by a generic LP solver. However, due to the very large size of the vehicle and image set, specially under dense traffic scenarios, this solution would require much higher computer processing time. The usual workaround is to relax the integer assumption and solve a continuous Linear Programming (LP) instead, always assuring that the constraint matrix exhibits a property known as total unimodularity, for the needed convergence of the LP.

Chapter 6

Microsimulation Application

In this Chapter the steps for the appropriate use of an advanced microscopic simulation tool for detailed traffic and safety assessment are discussed. Advanced methods for the global calibration of simulation applications are proposed and applied to the case study presented in Chapter 4. As discussed in section 2.2 of Chapter 2, driving behaviour may be specified by many different model formulations. Furthermore, the intrinsic heterogeneous nature of human-based decisions forces all these formulations to include an important stochastic component. The model formulation and its stochastic nature affect the choice, setup, calibration, validation and the final application of a simulation tool. In the first section, a specific advanced microscopic simulation tool is presented and its selection for the application in the presented case study is discussed. Then, a new sensitivity analysis-based method to simultaneously assess the influence and estimate the appropriate value of all sub-models parameters is proposed, and the replication of observed variables is validated. Finally, an advanced calibration algorithm is demonstrated through the simultaneous demand-supply calibration of the microsimulation tool with the purpose of generating artificial data for the related simulated scenarios.

6.1 MITSIMLab

MITSIMLab is a microscopic traffic simulation application developed to evaluate Advanced Traffic Management Systems (ATMS) and Advanced Traveler Information Systems (ATIS) at the operational level, by the Massachusetts Institute of Technology, USA. MITSIMLab can represent a wide range of traffic management systems and model the response of

drivers to real-time traffic information and control. This enables **MITSIMLab** to simulate the dynamic interactions between traffic management systems, vehicle motions, and driver's decisions. **MITSIMLab** consists of three main modules:

- Microscopic Traffic Simulator (**MITSIM**);
- Traffic Management Simulator (**TMS**);
- Graphical User Interface (**GUI**).

In **MITSIMLab**, like in almost all micro-simulation applications, the road network is represented by nodes, links, segments (links are divided into segments with uniform geometric characteristics) and lanes. Traffic control and surveillance devices are represented at the microscopic level. Travel demand is input in the form of time-dependent OD flows, from which individual vehicles wishing to enter the network are generated. A probabilistic model is used to capture drivers' route choice decisions and driving behavior parameters and vehicle characteristics are randomly assigned to each driver-vehicle unit. **MITSIM** moves vehicles according to route choice, acceleration and lane changing models. The acceleration model captures drivers' response to neighbouring conditions as a function of surrounding vehicles motion parameters. The lane changing model integrates mandatory and discretionary lane-changes in a single model. Merging, drivers' responses to traffic signals, speed limits, incidents, and tollbooths are also captured. The driving behavior models implemented in **MITSIM** are those estimated by Yang (1997), Ahmed (1999) and Toledo et al. (2007), and described in detail in Appendix A. The **MITSIM** lane changing model was later enhanced by Choudhury (2007), for the specific purpose of integrating latent plans in the lane selection process, namely in urban arterials and in freeways with a large number of lanes. This model was however not used in this Chapter, due to the nature of the case study presented in Chapter 4, but its effects on replicating detailed traffic and safety variables should be tested in future research. **TMS** mimics the traffic control system in the network under consideration. A wide range of traffic control and route guidance systems can be simulated. These include intersection controls, ramp control, freeway mainline control, lane control signs, variable speed limit signs, portal signals, variable message signs and in-vehicle route guidance. **TMS** can represent different designs of such systems with logic at varying levels of sophistication (pre-timed, actuated or adaptive). In the present Chapter this module will not be used, as we focus our attention on

the driving behaviour calibration. Finally, the **GUI** module allows the visualization of all simulated elements in run-time.

MITSIMLab is an open-source application, its core models being written in **C++** and fully available. It has been successfully applied in several traffic studies in the USA, the UK, Sweden, Italy, Switzerland, Japan, Korea and Malaysia. Some of its features represent modelling advantages regarding other available platforms, namely the integrated lane selection model, an extensive probabilistic nature (instead of rule-based) for several of its sub-models, the unique target gap acceleration model, courtesy merging features and a high level of tunable stochasticity and driving behaviour parameters. Furthermore, all models and the data used for its estimation are well documented. These attributes make **MITSIMLab** a tool suitable for a flexible and comprehensive analysis of our case study and for the replication of detailed traffic variables as accurately as possible.

For the setup of the simulated road network presented in Chapter 4 a Geographic Information System (GIS) was used. A **Python** tool was then developed to transform the previously formatted shapefiles into the specific **MITSIMLab** road network input file format (.txt). This tool has proved to be very useful as the majority of road network data is kept in geo-coded format and has already been used in other research projects (Basak et al., 2013). The seed OD matrix estimated in Chapter 4 were also formatted following **MITSIMLab** input file specifications. Finally, all driving behaviour sub-model formulations and its code were carefully analysed for a comprehensive understanding of the interactions at stake. This demanding task revealed to be a key step in the present analysis as several changes to the **C++** code of **MITSIM** were mandatory to minimize gridlock occurrence in the short segments existing in the case study network (see Appendix C). A detailed description of all **MITSIM** driving behaviour models and parameters is presented in Appendix A.

6.2 Sensitivity Analysis¹

6.2.1 Sensitivity analysis in traffic micro-simulation studies

As mentioned in Chapter 2, traffic micro-simulation tools have been developed based on a high level of modelling complexity. It is becoming increasingly recognized the crucial importance of analysing these models, understanding how they work and, in particular, what influences their capability to reproduce the physical phenomena they are intended to simulate (Ciuffo et al., 2012). Global sensitivity analysis (SA) is the family of tools to be used with this aim. Together with uncertainty analysis, SA studies how the uncertainties in model inputs affect the model response. In this picture, uncertainty analysis quantifies the output variability while SA describes the relative importance of each input in determining this variability (Saltelli et al., 2008). These analysis are of high importance in reducing the number of parameters to calibrate and minimising the weight of non-influential parameters in the optimization process (Punzo and Ciuffo, 2009).

Generally, previous SA on micro-simulation models refer to applications to a sub-model with few parameters. When dealing with complex traffic simulation models, it is common practice to make a selection of the parameters to involve in the sensitivity analysis. Traditionally, this selection is based on prior knowledge of the model, on developers advice and on common sense.

On top of this, the *one-at-time* (OAT) approach remains the most adopted method when dealing with microscopic simulation models. OAT measures are based on the estimation of partial derivatives, and assess how uncertainty in one factor affects the model output keeping the other factors fixed to a nominal value. The main drawback of this approach is that interactions among factors cannot be assessed, since they require the inputs to be changed simultaneously (Campolongo et al., 2001). In addition, this approach pertains to a family of SA techniques usually referred to as “local sensitivity analysis”, used to derive information on the behaviour of the model around a certain point rather than for exploring its input space. However, its simplicity and parsimony makes it the preferred choice for practitioners. The OAT approach has been applied to traffic microscopic simulation models by Nicholas E. Lownes (2006) and Mathew and Radhakrishnan

¹The work presented in this Chapter was developed under the activities of the Cost Action TU0903 - Multitude: Methods and tools for supporting the use calibration and validation of traffic simulation models, in close collaboration with Dr. Biagio Ciuffo from EU’s Joint Research Center.

(2010) in order, respectively, to prioritize model parameters in terms of their effects on model outputs, and to select the parameters to be calibrated. In Kesting and Treiber (2008) the same approach is followed in order to get additional insight on the meaning of parameter values resulting from the calibration of two car-following models.

A more advanced method also referenced in the literature is the *analysis of variance* (ANOVA). Multi-factor ANOVA studies the effect of two or more parameters on a response variable and it is used to determine both the first-order and the interaction effect between parameters and a response variable. For further details on experimental design techniques and ANOVA, one may refer to technical books such as Law and Kelton (1999). In the traffic microscopic simulation research, ANOVA has been used in Bartin et al. (2005) and Li et al. (2009) to draw inference about the first order effect of a set of **PARAMICS** parameters. Interaction effects were not captured since a two level full factorial design was adopted in both studies. A three level factorial design was used in Beegala et al. (2005), Ciuffo et al. (2007) and in Punzo et al. (2011) for the **AIMSUN** model. However, second order interactions effects of parameters could be evaluated only in the last two studies where a full factorial design was adopted who adopted a fractional design. In Park and Qi (2005) five levels per parameter were taken into account and a Latin hypercube sampling algorithm was used to define the experimental design of an ANOVA. However, even in this case, the interaction effect of the parameters was not evaluated.

Further to using the standard definition of ANOVA, a more efficient method based on variance decomposition can be used for model SA. This method consists in evaluating two types of sensitivity indices (that will be detailed in section 6.2.3) and represents the most advanced and conceptually sound way of performing model SA. With respect to the experimental design used in ANOVA, the Monte Carlo approach ensures a more thorough exploration of the model inputs space. In traffic modeling, this approach was used by Punzo and Ciuffo (2009) for the SA of two car-following models.

All the mentioned works refer to applications on models with either few parameters or considering just a sub-set of them. In particular, when dealing with complex traffic simulation models it is common practice to make a selection of a sub set of parameters to involve in the analysis. The selection is based on prior knowledge of the model, on developers advice and informed judgement. This, however, is a fairly dangerous practice, as many interactions among groups of parameters may remain hidden even to the most

expert model users and different simulated scenarios may led to different parameters sub sets. The problem is that complex traffic simulation models involve dozens of parameters and a SA would require too many model evaluations (e.g: for a 20 parameter sub set an ANOVA based on a two levels full factorial design would require more than 10^6 model evaluations for evaluating just the first order effect of each parameter). In fact, the access to both new advanced modelling techniques and detailed traffic and behavioural data, is increasing the level of detail of new and updated traffic simulation models, such as HUTSIM (Koskinen et al., 2009), SimMobility-ST (Basak et al., 2013) or MATSim (Balmer et al., 2006). Furthermore, traffic simulators are increasingly being applied in many different traffic situations and consistency with the available data needs to be assured. These challenges have been linked to the need for a consistent understanding of the simulators performance, along with appropriate calibration and validation procedures. As already pointed out, the generic calibration of traffic models relies directly on the choice of the subset of parameters to calibrate. Although the importance of the accurate identification of this subset of parameters is well reported (Hollander and Liu, 2008), only a few number of recent studies focus on the systematization of such procedures (Punzo and Ciuffo, 2009).

Regarding MITSIM calibration, almost all previous efforts considered just a small subset of (driving behaviour) parameters. These subsets were typically defined based on the purpose of each calibration and without any prior statistical analysis. Sterzin (2004) used an iterated OAT to test the sensitivity of a set of parameters from four specific models: the car-following and free-flow acceleration models, the gap acceptance model and the lane utility model. The main purpose if this task was to identify the parameters to be calibrated for the analysis of weather factors, using an older version of MITSIM in a freeway corridor in Virginia, USA. The constant parameters of the former car-following model (noted as α_{cf}^{acc} and α_{cf}^{dec} in Appendix A), the desired speed constant parameter of the free-flow acceleration (β_{ff}) and the gap acceptance constant parameter (α^{lead} and α^{lag}) were found to be significant as regards as sensor data. Kurian (2000) used experimental design techniques to test the sensibility of eight parameters of MITSIM car-following model towards speed, counts and density sensor measurements in a short congested corridor in California, USA. He identified as sensitive only three parameters of the car-following deceleration (h_{cf}^{lb} , α_{cf}^{dec} and γ_{cf}^{dec}). Although these results were obtained using older versions

of the simulation tool and limited methods of SA, they form an interesting baseline for comparison of new results as MITSIM has maintained its basic structure throughout all enhancements.

6.2.2 A multi-step global sensitivity analysis

To overcome the above mentioned limitations of generic calibration approaches and test simulator capabilities to replicate detailed data in safety assessment, a multi-step approach for model SA of traffic simulation models is proposed.

In a first step, parameters are grouped with respect to the sub-models they belong to, and a SA is carried out considering the different groups rather than the different parameters. Then, the most influential groups (sub-models) on the model outputs are singled out and a new SA on the parameters of the sub-models identified is carried out. Again, if still too many parameters are considered, an additional group analysis may be applied to further reduce their number. In these intermediate steps simplified SA approaches can be adopted, but advanced variance-based approaches are always preferred. Finally, a last SA identifies the subset of model inputs to be estimated with particular care (see Figure 6-1).

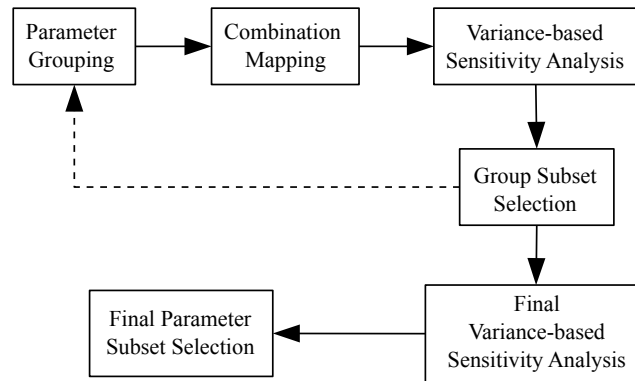


Figure 6-1: Multi-step Sensitivity Analysis Framework

The proposed approach applies to any type of traffic simulation model and, in general, to any modelling framework composed of different independent sub-models interacting with each other. This approach is thought for models in which the total number of parameters makes the direct application of the selected SA technique unfeasible.

As shown in Figure 6-1, the SA step is based on the computation of first order and total order sensitivity indices with a variance-based approach (Saltelli et al., 2008). In

the next section, the mathematical details of the variance-based method on the Sobol decomposition of variance is presented, and its benefits are discussed. Following this approach, the model has to be evaluated $N \times (k + 2)$ times, where k is the number of model parameters and N is the dimension of the Monte Carlo experiment (ranging from few hundreds to many thousands). The methodology proposed for global SA of the microscopic simulation tool is composed by the following steps:

1. Group model parameters on the basis of their similarities (e.g. parameters pertaining to the same sub-model or having the same physical interpretation);
2. Create a map between a number in the range $[0, 1]$ (the value assigned to the group) and a combination of values for the parameters within the same group;
3. Apply variance-based SA to the groups to identify those accounting for the highest share of model variance;
4. Select the parameters in the influential groups:
 - (a) If the number is sufficiently small, apply variance-based techniques to the new set of parameters;
 - (b) If the number is still too high, go to step 1.
5. Define the set of parameters to include in the subsequent analyses.

Step 2 is a key task in this methodology. The map between a number in the range $[0, 1]$ and a combination of parameters' values determine the quality of the sensitivity indices. In general, it is necessary to have a sufficient exploration of the parameters space. In order to do so, for the presented case study, different combination sizes N using Sobol's quasi-random sequences (Sobol, 1976) were identified, depending on the number of the parameters at each step of the above mentioned procedure. In case that the variability in this first set of combinations is too high, a new set should be identified. Then, at each step, the sequence define k numbers in the range $[0, 1]$ in order to guarantee the best coverage of the parameters space. Then the value to be assigned to each parameter is extracted from the uniform distribution defined by the thresholds reported in Table B.1 of Appendix B. Once the N combinations have been defined, the map between a number in the $[0, 1]$ range is simply created assigning to each of the combinations the

same probability equal to $1/N$. In the next section, the variance-based method for SA is described.

6.2.3 Variance-based methods on the Sobol decomposition of variance

The variance-based method based on the Sobol decomposition of variance is one of the most recent and effective global SA techniques. The original formulation of the method is due to Sobol (1976) where he provided the analytical derivation and the Monte Carlo-based implementation of the concept. The latest setting for its practical implementation, however, is due to Saltelli et al. (2008).

Given a model in the form $Y = f(Z_1, Z_2, \dots, Z_r)$, two factors are said to interact when their effect on Y cannot be expressed as a sum of their single effects. Interactions represent important features of traffic models, and are more difficult to detect than first-order effects. For example, by using regression analysis tools it is fairly easy to estimate first-order indices, but not interactions. With Y a scalar, a variance based first order effect for a generic factor Z_i can be written as:

$$V_i = V_{Z_i} [E_{Z_{\sim i}} (Y | Z_i)] \quad (6.1)$$

where Z_i is the i^{th} factor and $Z_{\sim i}$ is the matrix of all factors but Z_i . Furthermore it is known that the unconditional variance can be decomposed into main effect and residual:

$$V(Y) = V_{Z_i} [E_{Z_{\sim i}} (Y | Z_i)] + E_{Z_i} (V_{Z_{\sim i}} [Y | Z_i]) \quad (6.2)$$

Equation 6.2 shows that for Z_i to be an important factor $E_{Z_i} (V_{Z_{\sim i}} [Y | Z_i])$ needs to be small; that is to say that the closer $V_{Z_i} [E_{Z_{\sim i}} (Y | Z_i)]$ is to the unconditional variance $V(Y)$ the higher the influence of Z_i . Thus we may define our first order sensitivity index of Z_i with respect to Y as:

$$S_i = \frac{V_{Z_i} [E_{Z_{\sim i}} (Y | Z_i)]}{V(Y)} \quad (6.3)$$

Sensitivity indices as in equation 6.3 can be calculated per each factor and per each factors combination. This, however, would need a huge amount of model evaluations. In order to reduce the efforts required, a synthetic indicator to be coupled with the first

order sensitivity index is the total effects index, defined as follows (Saltelli et al., 2008):

$$S_{T_i} = 1 - \frac{V_{Z_{\sim i}}[E_{Z_i}(Y | Z_{\sim i})]}{V(Y)} = \frac{E_{Z_{\sim i}}[V_{Z_i}(Y | Z_{\sim i})]}{V(Y)} \quad (6.4)$$

Total effects index of the input factor i provides the sum of first and higher order effects (interactions) of factor Z_i . When the total index is $S_{T_i} = 0$ the i^{th} factor can be fixed without affecting the outputs' variance. Since the analytical feasibility of traffic flow models limits the use of the calculation of the variances reported in equation 6.2, the application of this method can be effectively performed in a Monte Carlo setting. The calculation, in a Monte Carlo framework, of the variance-based sensitivity indices presented in equations 6.3 and 6.4 has been object of research in the last decades. Different approaches and strategies may provide results with different accuracy and efficiency.

The approach adopted in the present work has been specified in Saltelli et al. (2008) and applied to car-following models by Punzo et al. (2011) as a way to avoid brute-force computation of the multidimensional integrals in the input factors space, and can be summarized in the following points:

- Generate a $(N, 2k)$ matrix of random numbers (k is the number of inputs and N is the experiment size or base sample) and define two matrices of data (A and B), each containing half of the sample, using sequences of quasi-random numbers (Sobol, 1976):

$$A = \begin{bmatrix} z_1^{(1)} & z_2^{(1)} & \dots & z_r^{(1)} \\ z_1^{(2)} & z_2^{(2)} & \dots & z_r^{(2)} \\ \vdots & \vdots & \ddots & \vdots \\ z_1^{(N)} & z_2^{(N)} & \dots & z_r^{(N)} \end{bmatrix} \quad B = \begin{bmatrix} z_{r+1}^{(1)} & z_{2+2}^{(1)} & \dots & z_{2r}^{(1)} \\ z_{r+1}^{(2)} & z_{2+2}^{(2)} & \dots & z_{2r}^{(2)} \\ \vdots & \vdots & \ddots & \vdots \\ z_{r+1}^{(N)} & z_{r+2}^{(N)} & \dots & z_{2r}^{(N)} \end{bmatrix} \quad (6.5)$$

- Define a matrix C_i formed by all columns of A except the i^{th} column, which is taken from B , (with i varying from 1 to r) :

$$C = \begin{bmatrix} z_1^{(1)} & z_2^{(1)} & \dots & z_{r+i}^{(1)} & \dots & z_{2r}^{(1)} \\ z_1^{(2)} & z_2^{(2)} & \dots & z_{r+i}^{(2)} & \dots & z_{2r}^{(2)} \\ \vdots & \vdots & \vdots & \vdots & \ddots & \vdots \\ z_1^{(N)} & z_2^{(N)} & \dots & z_{r+i}^{(N)} & \dots & z_{2r}^{(N)} \end{bmatrix}, \text{ for } i = 1, \dots, r \quad (6.6)$$

- Evaluate the model for all the $[N \times (r + 2)]$ combinations of input variables as given by matrices A , B and C and generate the $(N \times 1)$ vectors of outputs $y_A = f(A)$, $y_B = f(B)$ and $y_{C_i} = f(C_i)$ for $i = 1, \dots, r$. These vectors are sufficient for the evaluation of all the first order S_i and total effects S_{T_i} indices. This is the reason why, the application of this technique for variance-based methods requires just $[N \times (r + 2)]$ combinations. Because there are k factors, the cost of this approach is $N + N$ runs of the model for matrices A , B , plus k times N to estimate k times the output vector corresponding to matrix C_i . The total cost is hence $N(k + 2)$, much lower than the N^2 runs of the brute-force method. Since N is usually not lower than a few hundreds, the number of evaluations required by this efficient approach is not, in any case, negligible, especially for complex and expensive models. Nevertheless, in the common practice, the approach presented in this section can be considered relevant.

The sensitivity indices can be then evaluated using the following formulations (Saltelli et al., 2008):

$$S_i = \frac{\frac{1}{N} \sum_{j=1}^N [y_B^{(j)} (y_{C_i}^{(j)} - y_A^{(j)})]}{\frac{1}{2N} \sum_{j=1}^N [(y_{A+B}^{(j)})^2] - \left(\frac{1}{2N} \sum_{j=1}^N [y_{A+B}^{(j)}] \right)^2} \quad (6.7)$$

$$S_{T_i} = \frac{\frac{1}{2N} \sum_{j=1}^N [(y_A^{(j)} - y_{C_i}^{(j)})^2]}{\frac{1}{2N} \sum_{j=1}^N [(y_{A+B}^{(j)})^2] - \left(\frac{1}{2N} \sum_{j=1}^N [y_{A+B}^{(j)}] \right)^2} \quad (6.8)$$

In the scalar product $y_A \cdot y_{C_i}$ values of Y computed from A are multiplied by values of Y for which all factors but Z_i are re-sampled while the values of Z_i remain fixed. If Z_i is non-influential, then high and low values of y_A and y_{C_i} are randomly associated. If Z_i is influential, then high (or low) values of y_A will be preferentially multiplied by high (or low) values of y_{C_i} increasing the value of the resulting scalar product. The reader should refer to Saltelli et al. (2008) for a detailed explanation of equations 6.7 and 6.8.

The choice of N is the last point to be discussed in this section. There are no universal recipes: N can vary from few hundreds to several thousands. In order to assess if the indices calculated for a given N are sufficiently stable, it is worth calculating their confidence interval. This can be easily carried out via a parametric bootstrapping. In practice, in order to calculate sensitivity indices with equations 6.7 and 6.8, per each step of the process in the range $[1, N]$, the term in the summation at the numerator of both

equations needs to be available. Performing a parametric bootstrapping of the indices means sampling N' combinations of these terms of the same size N with replacement. Then the confidence interval will be created given the distribution of the N' indices. If the confidence interval will result sufficiently small, then the number of model evaluations can be considered sufficient. For the present study, the results of the SA will be presented in the graphical form.

6.2.4 Sensitivity analysis using aggregated data

In this section, the proposed methodology is applied to the identification of the parameters to be considered in an aggregated-data based calibration of MITSIM for the A44 case study. The estimated seed OD and 5 min aggregated daily loop counts described in Chapter 4 were used in the OD estimation, using the already presented GLS simultaneous method (see Chapter 4). A simulation scenario of the morning period (7:30AM to 12:00AM) of a specific day was set up in MITSIMLab, adopting a warming period of 30min. Since possible model outputs account for time series of counts and speed at the existing 8 different detectors a strategy to aggregate them in a single measure needs to be put in place. Willing to assess spatial influence on the SA results, 22 distinct MoP were computed for different output locations: 16 on each single detector (8×2 , for counts and speeds), 4 for each road direction (2×2) and 2 for the entire network. To compare real and simulated MoP, three different Goodness of Fit (GoF) measures were computed in order to assess the dependence on the GoF statistic itself, namely, the root mean squared error ($RMSE$), the root mean squared normalized error ($RMSNE$), and the Theil inequality coefficient U (one may refer to Hollander and Liu (2008) for a detailed discussion on alternative GoF measures):

$$RMSE = \sqrt{\frac{1}{I} \sum_{i=1}^I (x_i - y_i)^2} \quad (6.9)$$

$$RMSNE = \sqrt{\frac{1}{I} \sum_{i=1}^I \left(\frac{x_i - y_i}{y_i} \right)^2} \quad (6.10)$$

$$U = \frac{\sqrt{\frac{1}{I} \sum_{i=1}^I (x_i - y_i)^2}}{\sqrt{\frac{1}{I} \sum_{i=1}^I x_i^2} + \sqrt{\frac{1}{I} \sum_{i=1}^I y_i^2}} \quad (6.11)$$

where x_i are the simulated values, y_i are the observed values and I is the total number of observations. Regarding the Theil's inequality coefficient values, $U = 0$ indicates a

perfect fit, $U = 1$ indicates the worst fit. For readability reasons, only the U statistic is presented in the current Chapter as this statistic is sensitive to variance and covariance (Hollander and Liu, 2008). Any raucous finding regarding $RMSE$ and $RMSNE$ results will also be pointed out. In total, SA of 66 different model outputs were performed.

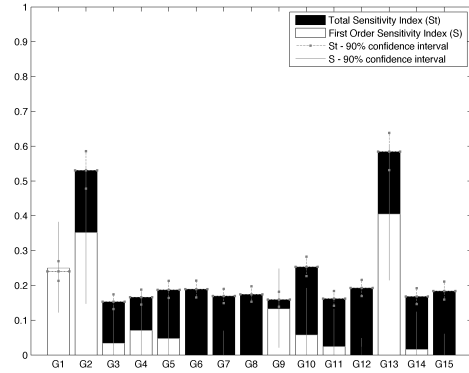
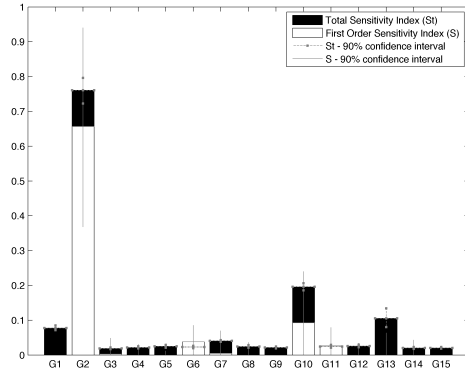
Finally, for the carrying out this computationally demanding task, MITSIMLab was installed under Scientific Linux in a cluster with 80 cores with 1GB of RAM memory, thanks to the support of the Portuguese National Grid Initiative (INGRID). This resource allowed for the fast processing of the required high number of simulations.

First step: Group sensitivity analysis

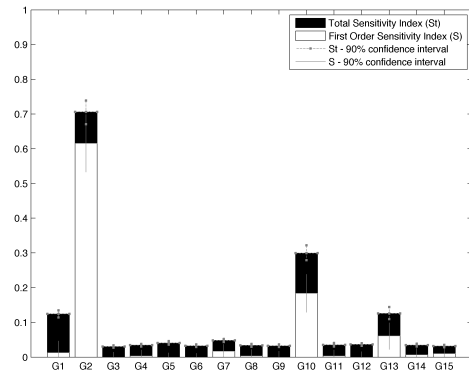
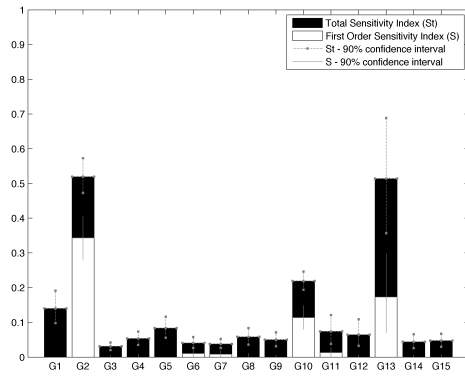
In what concerns the group analysis, groups were identified on the different sub-models of MITSIM as defined in the Appendix A. Lower and upper bounds used in mapping the Sobol quasi-random sequences were based on previous estimations of each sub-model (Yang, 1997, Ahmed, 1999, Toledo et al., 2007) and are presented in Table B.1 of the Appendix B. The correspondence of the group numbers are detailed in Table B.1 of Appendix B and in the numbering of the list presented in Appendix A. A total of 34,816 non-replicated simulations (assuming $N = 2048$ for the Monte Carlo experiment) were carried out on the cluster to compute the group sensitivity indices.

In Figure 6-2, results of model SA considering the Theil inequality coefficient GoF measures calculated on counts and speed are reported. It is clear that, from first order indices (white bar) count profiles are mainly driven by the parameters combinations of Group 2 (Car Following Model), and 13 (Lane Utility Model), while speed profiles are also influenced by Group 10 (Driver Heterogeneity Model) and also (but less) by Group 1 (Reaction Time Model).

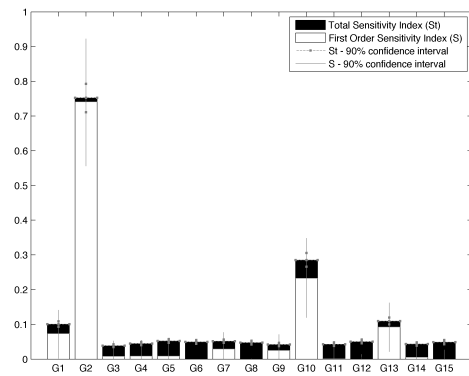
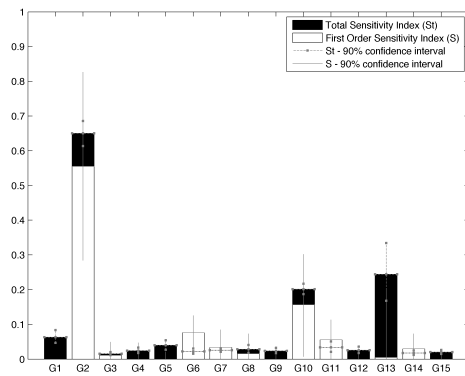
The model stochasticity accounts for almost 20-25% of variance with counts and 10-15% with speed. In fact, just a few groups are influencing model outputs with their main effect or/and their interactions: for example, Group 2 and 10 account for 80% of the output variance of the count data in the Northbound direction. The higher impact of model stochasticity using counts than speed suggests the use of speed in the driving behavior model calibration. Different directions (diverse traffic conditions) showed different sensitive parameters, e.g.: the lane-change related models (merging - Group 5, yielding - Group 9 and target gap acceleration - Group 11) had less significance in the non-congested



a) South-North direction



d) North-South direction



c) all sensors

Figure 6-2: Group analysis bar plots of first (white) and total (black) order sensitivity indices based on the Theil coefficient, using counts (left) and speed (right) profiles

(North-South) direction. In addition groups interactions happen to be non-negligible in the congested South-North direction. This was as expected, as lane-change models are typically strongly linked to several other sub-models (gap acceptance, gap choice...) which brings more complexity to the calibration procedure.

Final step: Final variance-based sensitivity analysis

The most influential groups on the model outputs were identified with the previous group analysis. The four selected groups are those influencing most the speed profiles, therefore: Groups 1 (Reaction Time model), 2 (Car Following Model), 10 (Driver Heterogeneity Model) and 13 (Lane Utility Model). These groups account for 41 parameters in total, with a consequent reduction of almost 2/3 in the number of parameters to analyze. This number might still be considered quite high for a comprehensive variance-based analysis, suggesting further group analysis. However, we considered the possibility of performing the variance-based SA evaluating only the total order sensitivity indices. In fact, as clearly pointed out in Saltelli et al. (2008), total order indices reach stability much sooner than first order ones, thus requiring less model evaluations. We therefore tried using a size of the Monte Carlo experiment of $N = 512$, thus with 22,016 model evaluations. Three replications of each combination were considered for the analysis, and the other parameters values were set to the values obtained from the group analysis. The identification of each parameter number is detailed in Table B.2 of Appendix B.

In Figure 6-3, the relatively narrow confidence intervals show the good quality of the estimated indices. It is possible to ascertain that there are six parameters outperforming all the others in accounting for the output's variance: μ_{RT} (1), α_{cf}^{dec} (12), γ_{cf}^{dec} (13), ρ_{cf}^{dec} (14), μ_{DS} (23) and μ_{dv}^h (19) (from Groups 1, 2 and 10) both in counts and speed. In addition, five other parameters account for a non-negligible share of the total outputs' variance: α^{CL} (25), $\beta_{nlc,1}$ (36), θ_{MLC} (41) (Group 13), α_{cf}^{acc} (7) and β_{cf}^{acc} (8) (Group 2). Together with their interactions, these parameters are able to account for a high share of the outputs' variance (estimated to be 89%), thus sufficient to provide, once correctly estimated, a correct representation of traffic dynamics with just around 11% of uncertainty:

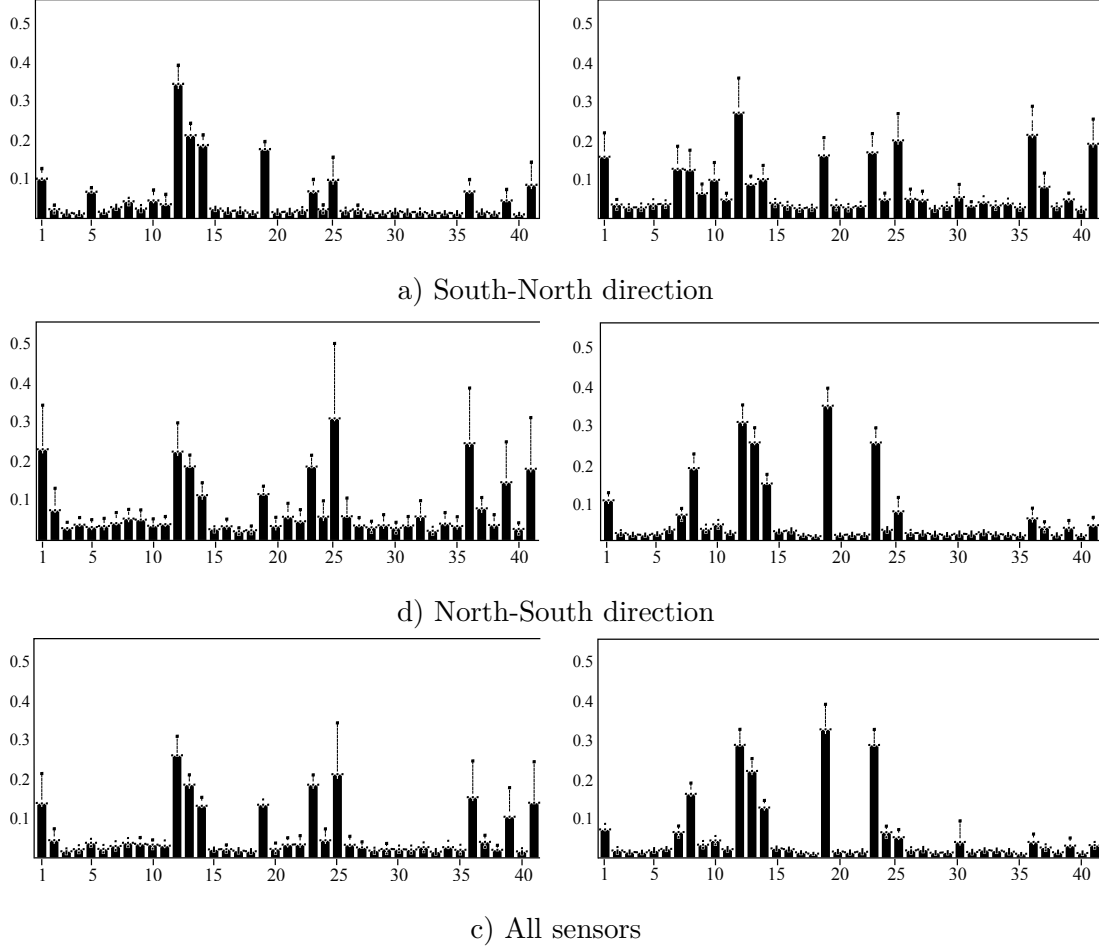


Figure 6-3: Final analysis bar plots of total order sensitivity indices on the Theil coefficient, using counts (left) and speed (right) profiles

- μ_{RT} (1) and $\mu_{dw}^h(19)$ are the mean of the reaction time and headway threshold distributions respectively. μ_{DS} (23) is the distribution mean of the desired speed factor. These are known to be important parameters, especially when analysing individual models separately. As expected, their share in the outputs variance is evident when analysing the total sensitivity index of the group analysis, as both of them are directly integrated in other sub-models;
- α_{cf}^{acc} (7) and α_{cf}^{dec} (12) are the constant parameters of the car-following acceleration and deceleration models. They both are typical parameters considered for any calibration, and their contribution is once again evidenced in this analysis;
- β_{cf}^{acc} (8) is the speed parameter in the car-following acceleration model, and it emerged as sensitive mostly when analysing non-congested speed GoF;
- γ_{cf}^{dec} (13) and ρ_{cf}^{dec} (14) are the gap and speed difference between the subject and

the leader vehicles of the car-following deceleration model. Although the γ_{cf}^{dec} was already found as significant in previous SA, it is clear that it is closely linked to the speed difference and both parameters should be taken jointly into account;

- $\alpha^{CL}(25)$, $\beta_{nlc,1}$ (36) and θ_{MLC} (41) are parameters of the lane changing model. The two lane carriageway layout of the A44 motorway clearly conditioned this outcome, as the network configuration almost only requires for one mandatory lane-change throughout its entire extension.

General remarks

The results sustained the relevance of the deceleration car-following model parameters already stated in previous studies. However, other parameters usually excluded from calibration procedures appear to be quite relevant as well. The description of parameters, such as the reaction time and headway threshold distributions or even the main constant parameter of the lane utility model, augured their importance even at the aggregate calibration and its total sensitivity indices proved as such. Another important conclusion is the importance of SA itself. The identification of parameters to be calibrated is very sensitive to the particular case study configuration and the observed traffic conditions. Figure 6-4, shows a clear difference between GoF for a dense traffic scenario (b) and for the non-congested one (a). Similar conclusions were obtained for MoP differentiated by loop sensors, where sensors near ramps revealed lane-change and merging models parameters to be much more relevant for a calibration process. Figure 6-4 also show that while the model is almost able to nullify the distance between real and simulated counts, this is not the case for the average speed. This is due to the prior GLS estimation of the OD matrix presented in Chapter 4.

The sizes of both Monte Carlo experiments were found to be sufficient as all of the GoF for the group and individual parameters analysis converged. Finally, the above presented results were, in general, the same for the *RMSNE* GoF. However, a clear slower convergence of the Monte Carlo results was obtained for the *RMSE*.

The group analysis has allowed to single out the four most important sub-models, namely the reaction time model, car-following model, the lane utility model and the drivers' heterogeneity model. In addition it has allowed choosing among different possible measures of goodness of fit and traffic measures those able to better depict traffic

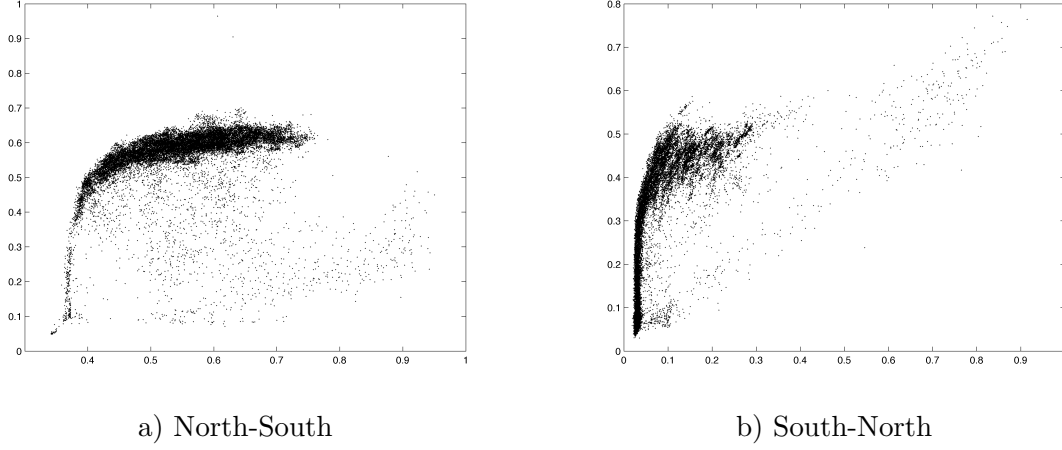


Figure 6-4: Counts vs. speed Theil inequality coefficient

dynamics. The final SA was then performed with the last 41 model parameters and a group of 11 parameters (out of 102) was identified, which accounts for almost the 90% of the output's variance, with a consequent significant simplification of the subsequent model calibration/estimation phases. In addition, the methodology required 56,832 model evaluations instead of the 212,992 (-73%) otherwise required for applying variance based techniques to the whole set of parameters with $N = 2048$ and without replications for direct stochasticity control.

6.2.5 Sensitivity analysis using detailed trajectory data

When detailed trajectory data is available for model calibration, four different approaches may be considered:

- Re-estimation, where the model is re-estimated using either traditional maximum-likelihood or Bayesian approaches based on the new set of trajectory data;
- Conditional estimation, in which the model is estimated with a traditional Bayesian approach using the new trajectory data set as main data, but introducing prior knowledge on the parameters values based on the previous estimations;
- Disaggregate calibration method, where each real trajectory point observation (X, Y, t) is compared with simulated values, and the parameters are calibrated using a numerical optimization algorithm accordingly;
- Aggregate calibration method, where a set of aggregate statistics of the real trajectories are pre-defined and compared against the simulated statistics, also using an

optimization method.

The first two approaches are probably the ones that should result in better parameter estimates as they typically do not depend on the performance of an optimization function. However, in complex modelling frameworks (such as **MITSIMLab**) the likelihood function is a complex equation and the estimation procedure a demanding process that might not be suitable for fast application. The disaggregate calibration method requires a predefined configuration of input files (namely, the network configuration and the initial network state) to allow the specification of the exact same starting conditions (such as vehicle positions) of observed trajectories. Many microscopic simulation tools might not include this feature. The last method, the aggregate calibration method, has several advantages: use of aggregate calibration methods, the choice and use of the statistics of interest and a smaller computational and mathematical burden. In Jie et al. (2013), for example, this method was used for the calibration of five **VISSIM** driving behaviour parameters and the desired speed and acceleration distributions using real trajectories collected by image processing at an intersection in Rotterdam, the Netherlands.

Similarly to section 6.2.4, the aggregate calibration methodology proposed in section 6.2.2 is now applied to the identification of sensitive parameters regarding detailed trajectory statistics. This time, a set of statistics for the simulated vehicle's trajectories were extracted and compared against true trajectories collected on-site through aerial remote sensing (see Chapter 5). Aiming at replicating as close as possible the main variables specified by the model components presented in Chapter 3, a set of 11 MoPs were selected for describing the trajectory data:

1. Speed;
2. Acceleration;
3. Deceleration;
4. Headway;
5. Time-to-collision (TTC);
6. Deceleration rate to avoid crash (DRAC);
7. Number of lane-changes (NLC);
8. Left lead gap;

9. Left lag gap;
10. Right lead gap;
11. Right lag gap.

For each of these variables (except for the number of lane-changes) 11 statistics were considered to characterise their distribution and computed separately for each of the flight runs: the minimum value, nine percentiles (10^{th} , 20^{th} , 30^{th} , 40^{th} , 50^{th} , 60^{th} , 70^{th} , 80^{th} and 90^{th}) and the maximum value of the distribution. Each observation i used in the computation of the GoF presented in equations 6.9, 6.10 and 6.11 is now a one of these statistics for the respective variable distribution and for a specific flight run (time of day). Also, in order to assess the dependence from the GoF measure selected, the *RMSE*, *RMSNE* and *U* were computed. For the group analysis, parameters were grouped considering the different sub-models of MITSIM, likewise the grouping for the calibration using aggregate data (see Appendix A). Lower and upper bounds used in mapping the Sobol quasi-random sequences were the same as those used in the previous analysis.

The simulation period was configured to match the trajectory extraction period, from 7:30AM to 12:00AM, adopting the first 30 min as warming period. The OD for the morning of the 11th October 2011 (the day of the trajectory data collection) was again estimated using the GLS simultaneous estimation method (Cascetta et al., 1993). MITSIMLab allows for the extraction of position, speed and acceleration of each vehicle; C++ code was added to the MITSIMLab core code (see Appendix C) and a post-processing tool was developed in MATLAB for the computation of the other mentioned variables. Finally, the INGRID computational resources were, once again, used for this task.

First step: Group sensitivity analysis

A total of 34,816 non-replicated simulations (assuming $N = 2048$ for the Monte Carlo experiment) were carried out to compute the group sensitivity indices. In Figures 6-5 and 6-6, results of model SA considering the Theil's inequality coefficient calculated for all 11 GoF measures are reported. The correspondence of the group numbers are detailed in Table B.1 of Appendix B and in the numbering of the list presente in Appendix A.

A few comments may be pointed out regarding these results:

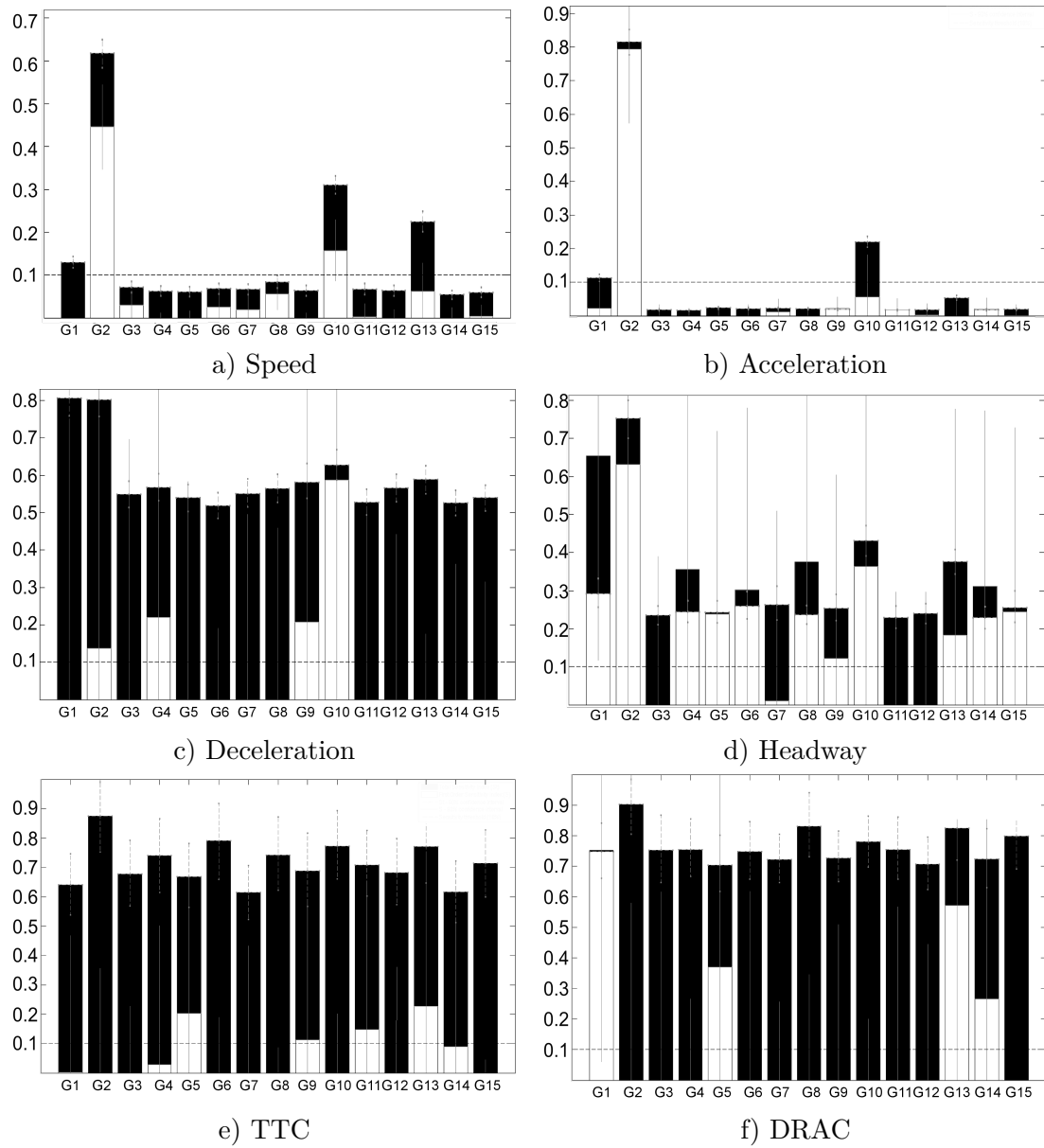


Figure 6-5: Group analysis bar plots of first (white) and total (black) order sensitivity indices on the Theil coefficient of trajectory based MoP (1)

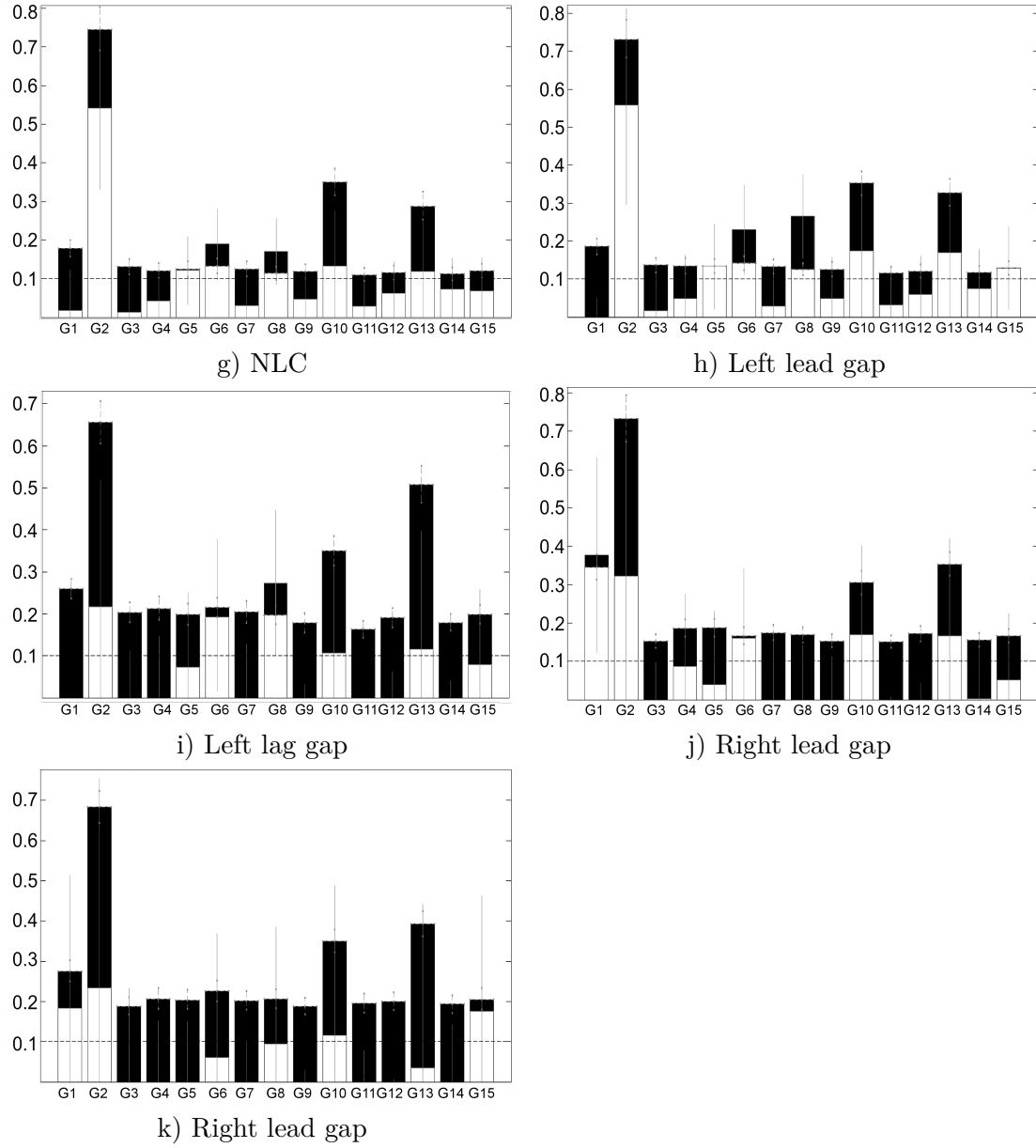


Figure 6-6: Group analysis bar plots of first (white) and total (black) order sensitivity indices on the Theil coefficient of trajectory based MoP (2). Grey lines are the 90% confidence intervals.

- The most sensitive groups for the speed GoF were those already identified for the SA with aggregated data from the previous section. However, Group 10 (Driver Heterogeneity Model) showed higher first and total indices. Forced merging models (Yielding probabilities - Group 6, Nosing rules - Group 7 and Nosing model - Group 8) showed some increased indices when compared to the previous analysis. This is explained with the monitoring of speeds in the entire section of the motorway rather than just the loop sensors sections;
- The headway GoF showed a much more distributed sensitivity. The Reaction time model (Group 1) and the Car-following model (Group 2) accounted for the largest share of uncertainty, especially due to the dense nature of the traffic in the A44 motorway;
- Similarly, the acceleration and deceleration GoFs were especially affected by the Car-following model (Group 2). The first order sensitivity indices of the deceleration GoF, however, showed a strong contribution of the Merging model (Group 4), the Courtesy Yielding Probabilities (Group 9) and the Driver Heterogeneity Model (Group 10). The first two models are strongly related to the weaving and merging areas, which in the A44 motorway are the locations with congested traffic and, therefore, frequent accelerations and decelerations. Furthermore, the total sensitivity indices show that the interactions between all groups contribute significantly to the deceleration outputs of MITSIM. This may be explained by the intrinsic formulation of MITSIM, in which the deceleration is chosen as the lowest from a subset of computed decelerations from different models (car-following deceleration, emergency deceleration, target gap deceleration, yielding deceleration, etc);
- The TTC and DRAC are both function of speed, headway and acceleration variables. Thus, it is expected that the impact of interactions between parameters for these two MoP will be larger than for other measures. The first order sensitivity index clearly indicates four main sensitive groups for the DRAC: the Reaction Time model (Group 1), the Mandatory Lane-change model (Group 5), the Lane Utility model (Group 13) and Target Gap model (Group 14). For the TTC first order sensitivity index, the Courtesy Yielding Probabilities (Group 9) and the Target Gap Acceleration model (Group 11) are also relevant;
- As expected, the number of lane changes GoF is directly linked to the four gap

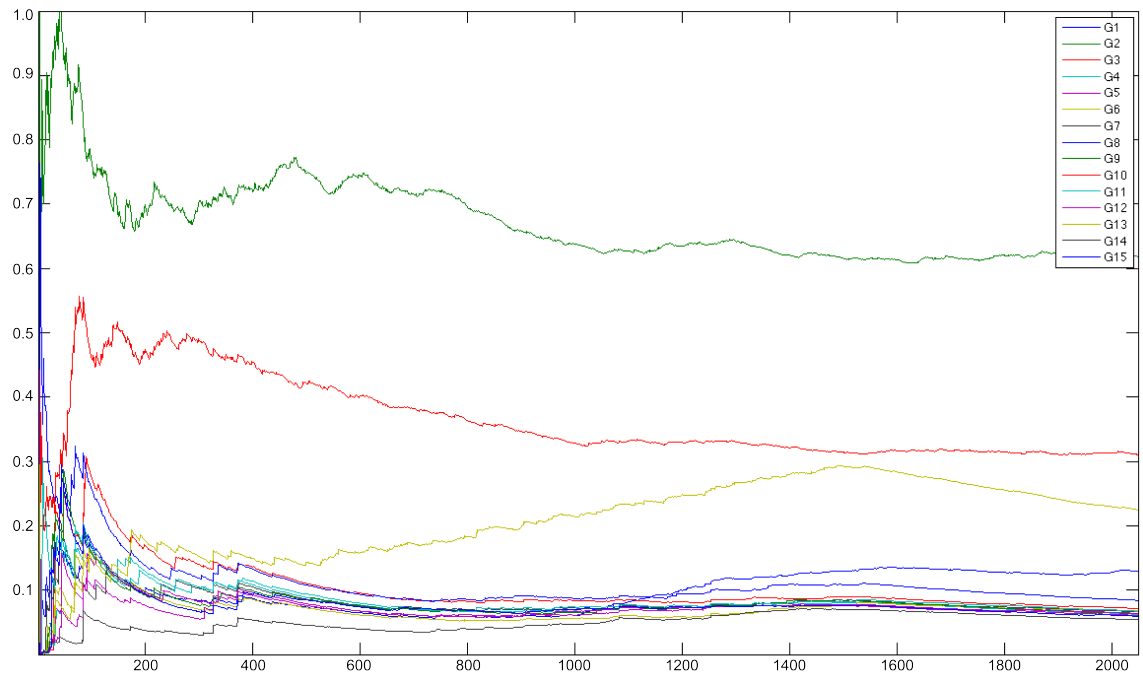
related GoF computed (Left lead gap, Left lag gap, Right lead gap and Right lag Gap). Here, the Driver Heterogeneity Model (Group 10) as well as almost all models related to lane-change tactics show up as sensitive, namely: Mandatory Lane-change model (Group 5), Yielding Probabilities (Group 6), Nosing model (Group 8), Lane Utility model (Group 13) and Target Gap model (Group 14). The Car-following model (Group 2) is the most sensitive sub-model. However, this is mainly due to the continuous computation of lateral gaps, rather than a conditioned computation on the intention of a lane-change.

Some fundamental groups are the same for both the detailed trajectory data and the aggregated data SA. However, important interaction components and the consideration of relative spacing MoPs revealed the relevance of several lane-changing models that were not detected in the aggregated data SA, especially those related to (forced) merging and weaving. This is obviously linked to the case study network layout but the influence of these models should be always supervised in detailed calibrations of congested networks, especially at the vicinity of interchanges and on sections with high volume-capacity ratios.

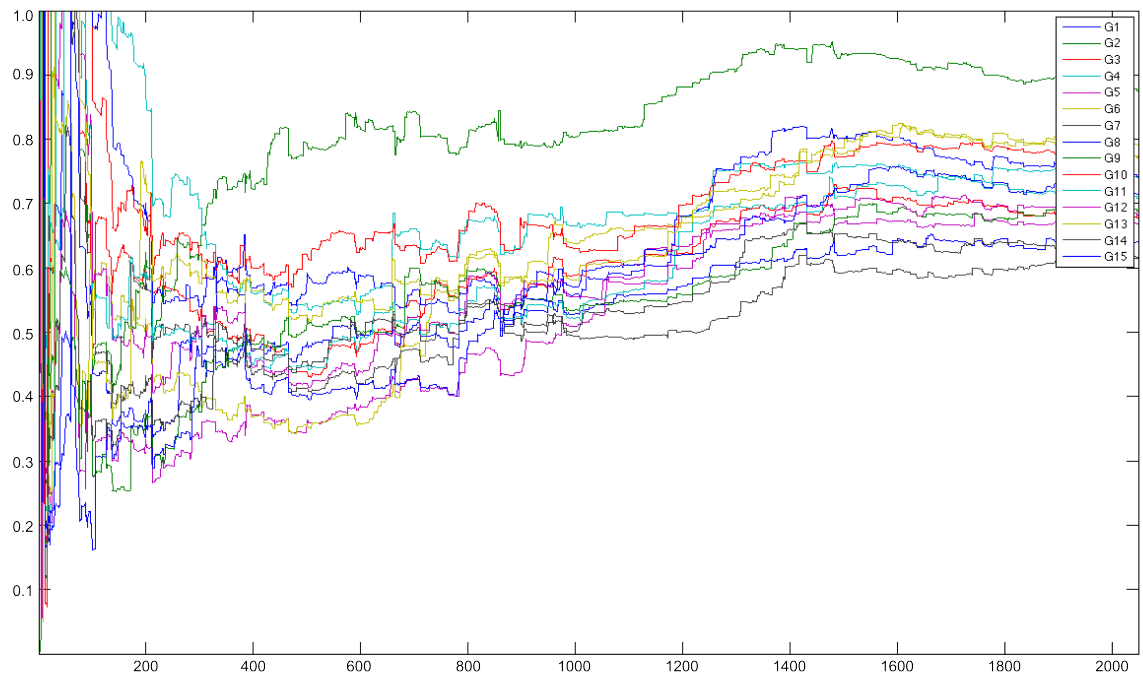
It is worth noting that not all GoF converged perfectly for the size of the Monte Carlo experiment. In fact, the deceleration, DRAC and TTC GoFs total order sensitivity indices slower convergence in Figure 6-5 may be related to this. In Figure 6-7, the Speed and TTC GoF are presented. Although more simulations could be carried out to reach a perfect convergence of the Monte Carlo experiment, the results from these 34,816 simulations are sufficient for a robust definition of the next parameter of interest subset. Groups 1 (Reaction Time Model), 2 (Car Following Model), 10 (Driver Heterogeneity Model) and 13 (Lane Utility Model), 8 (Nosing Model), 5 (Mandatory lane-change rules) and 9 (Courtesy yielding) were selected for further analysis. These 7 Groups represent a total of 56 parameters.

Second step: quasi-Optimized Trajectories Elementary Effects

The number of parameters in the selected sensitive Groups (56) is substantially higher than in the previous aggregated data based SA (41). Furthermore, the size of the Monte Carlo experiment may reach a significant number, due to the multiple nature of the MoP considered for the trajectory-based SA. As the sub-models of MITSIM have a consistent structure, a different grouping design needed for an additional group SA might be counter-



a) Speed



c) TTC

Figure 6-7: Convergence of total order sensitivity indices on the Theil coefficient of speed and TTC trajectory based MoP

intuitive. Instead, a screening method was tested to further identify most influential inputs. Screening methods are of special interest in computationally intensive models or in models with a large number of inputs, where the computational cost of other variance-based measures is not affordable.

The Elementary Effects method (EE) is one of the most common screening approaches when dealing with complex models (Morris, 1991). Consider a model Y with k input parameters that, for any possible value of these k parameters in the input space, i.e. $X = [X_1, \dots, X_k]$, the corresponding model output $Y(X)$ is formulated as $Y(X_1, \dots, X_k)$. If only the i^{th} parameter is changed by a certain value Δ , new the output will consequently be $Y(X_1, \dots, X_i + \Delta, \dots, X_k)$. The Elementary Effect of the i^{th} parameter, EE_i , is defined as:

$$EE_i = \frac{Y(X_1, \dots, X_i + \Delta, \dots, X_k) - Y(X_1, \dots, X_i, \dots, X_k)}{\Delta} \quad (6.12)$$

Through randomly generating a number m of X points from the input space, and each time Y is computed changing the i^{th} parameter by Δ , the m EEs for the i^{th} parameter can be derived according to equation 6.12. The mean μ_{EE_i} , the standard deviation σ_{EE_i} , and the absolute mean $\mu_{EE_i}^*$ of these m EEs can accordingly be used to infer on the sensitivity of the i^{th} parameter as follows (Morris, 1991, Campolongo et al., 2007):

- If $\mu_{EE_i}^*$ is low, then i is a negligible parameter;
- If $\mu_{EE_i}^*$ is high and σ_{EE_i} is low, i has linear and additive effects but no interactions with others;
- If $\mu_{EE_i}^*$ and σ_{EE_i} are both high, i has non-linear effects and/or strong interactions with others;
- If μ_{EE_i} is low but $\mu_{EE_i}^*$ is high, i will have oscillating effects depending on the value assumed by other parameters.

As the model needs to be evaluated twice for calculating each EE, the computational cost of the basic EE method is $2mk$. However, some of these evaluations may be used for the computation of different EE_i . By sampling the parameter input space using trajectories, a lower experiment size of $m(k+1)$ can be achieved (see Morris (1991) for further details). An improved sampling method was proposed by Campolongo et al. (2007), called the

Sampling with Optimized Trajectories (OTEE). Following this approach, when deriving the EEs, only a limited number of the most "spread" trajectories are considered instead of taking all above mentioned m random trajectories. The concept "spread" is defined based on the Euclidean distance between any two trajectories T_x and T_y :

$$d_{xy} = \begin{cases} \sum_{p=0}^k \sum_{q=0}^k \sqrt{\sum_{r=1}^k [X_r^p(x) - X_r^q(y)]^2} & x \neq y \\ 0 & otherwise \end{cases} \quad (6.13)$$

where k is the number of parameters, $X_r^p(x)$ is the r^{th} coordinate of the p^{th} point in T_x .

By enumerating all possible sets that contain n trajectories from the randomly generated set of m trajectories, the set with the largest distance can be found. The advantage of using OTEE is that with a smaller number of trajectories, it covers better the parameter space than any grid like or random set. Hence it facilitates a better scanning of the input space without increasing the number of model runs. However, one needs to find the optimized set of n trajectories out of the original m trajectories. In this optimization process the total number of possible n trajectory combinations is very large ($m! / [n! \times (m - n)!]$).

Very recently, Qiao and Menendez (2013) proposed the quasi-Optimized Trajectories EE (quasi-OTEE) approach and applied it to the sensitivity analysis of VISSIM parameters. Instead of a prior selection of the n optimized trajectories directly from the original m trajectories set (named S_0), the set (named S_1) of $m - 1$ trajectories that have the largest Euclidean distance within S_0 are selected; then, the set of $m - 2$ trajectories with the maximum dispersion based on S_1 is selected (named S_2), and so on. The size of the chosen trajectory set is decreased by one in each step, and finally a set (named S_{m-n}) with only n trajectories will be selected. These n trajectories are not necessarily the same ones found by the OTEE approach, thus called quasi-OTEE. The total number of trajectory combinations considered in this approach for finding the set S_{m-n} will be $(m - n + 1) \times (m + n) / 2$.

For the present case study a set of $m = 500$ trajectories and $n = 100$ quasi-OTEE were selected. 56,000 simulations would be necessary for the basic EE method (assuming the total number of parameters as $k = 56$), whereas 5,700 are needed for the quasi-OTEE method. The $\mu_{EE_i}^*$ and σ_{EE_i} values of EE_i of speed, headway, TTC and DRAC are plotted in Figure 6-8 as an example of the output layout. The other 46 parameters values were set to the combination with the best combined GoF (Euclidean distance to the origin of the

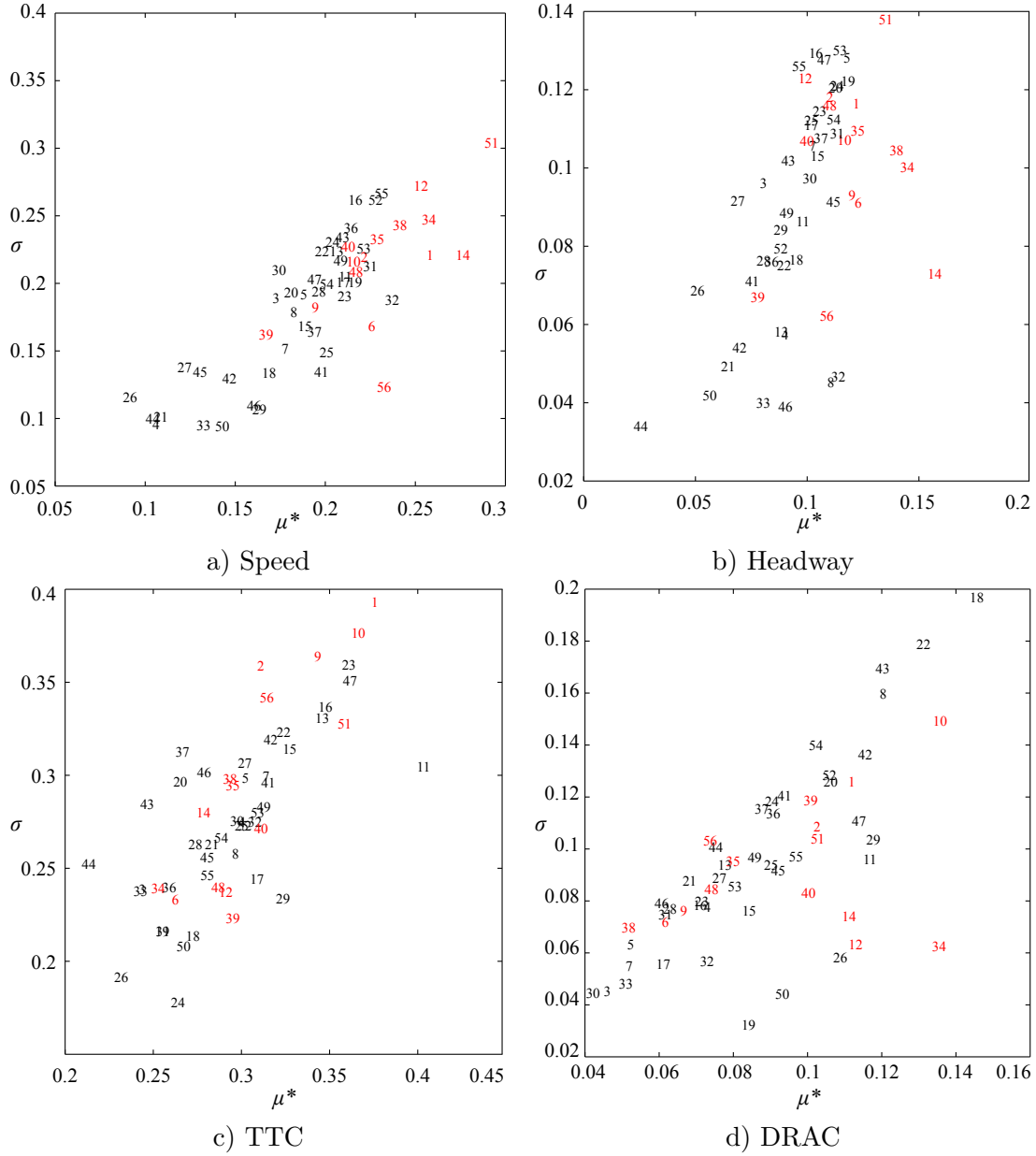


Figure 6-8: Absolute mean $\mu_{EE_i}^*$ vs. standard deviation σ_{EE_i} example

space) based on the first seven MoP (hereafter called overall GoF) for the group analysis. The identification of each parameter number is detailed in Table B.3 of Appendix B.

In Figure 6-9 the ranking based on the mean of the distribution of the absolute values μ_{EE}^* is presented. This ranking is sufficient to provide a reliable ranking of the input factors (Campolongo et al., 2007). Darker cells are those corresponding to higher μ_{EE}^* values.

The selection of a parameter subset for finer calibration has to consider the different nature of the MoPs at stake. In fact, depending on the calibration aim, one may either choose a subset that is more influenced by a specific MoP analysis, or consider an overall

		56	55	56	51	56	56	54	54	55	45	47
		40	44	42	39	31	47	40	42	43	32	23
		12	9	1	4	3	3	7	7	7	5	6
		4	4	8	9	6	11	3	3	5	6	5
5	—	29	39	16	47	36	8	36	39	45	35	42
		34	48	52	50	12	15	47	49	50	46	51
		15	26	24	23	38	10	21	22	14	25	24
		37	31	39	28	25	52	39	45	39	15	34
10	—	27	42	33	49	50	17	45	41	48	51	45
		39	43	30	38	54	49	48	48	42	37	35
		41	21	41	26	55	53	29	23	31	31	28
		55	56	54	42	34	43	37	34	34	49	49
		50	52	55	24	43	37	35	31	29	38	48
		53	54	50	55	27	32	55	55	54	55	55
15	—	38	49	53	40	40	39	46	38	35	48	31
		47	41	23	36	47	28	43	44	41	44	41
		25	18	38	21	28	14	15	15	28	28	25
		7	15	3	7	8	16	8	9	6	12	12
		21	33	6	20	4	5	20	25	18	11	14
20	—	17	27	31	27	19	35	32	32	24	29	33
		3	6	35	11	20	13	9	8	17	9	15
		18	23	11	25	49	41	30	33	38	20	19
		36	35	34	22	52	23	33	35	33	24	36
		31	19	18	33	21	44	44	46	36	30	37
25	—	16	32	22	19	32	27	13	12	10	13	22
		1	3	7	2	1	9	2	2	1	2	1
		6	5	26	10	30	20	16	16	15	17	8
		26	10	40	15	16	21	18	20	27	21	18
		9	28	10	12	26	50	12	10	9	16	11
30	—	8	7	2	5	7	1	4	4	3	7	4
		30	36	21	46	15	18	38	37	44	47	46
		33	38	19	37	44	22	26	29	11	40	38
		5	8	4	6	5	2	5	5	4	3	3
35	—	52	53	51	53	11	46	53	53	52	53	53
		43	37	45	52	22	24	42	43	49	52	54
		28	20	12	13	9	12	10	11	12	26	13
		20	40	32	30	18	19	31	30	25	33	20
		54	50	49	56	23	7	56	56	56	56	56
		22	14	36	32	42	51	49	47	32	43	29
40	—	48	34	14	41	45	40	52	52	53	50	50
		24	16	43	14	39	33	14	19	22	18	21
		14	11	15	17	41	54	25	26	23	39	27
		42	13	46	31	10	30	41	40	47	19	26
		2	1	5	1	2	4	1	1	2	1	2
45	—	13	17	9	34	17	34	23	17	19	8	9
		11	12	28	8	13	6	11	13	8	10	10
		19	30	44	45	51	42	28	27	21	41	40
		44	46	48	44	35	26	34	36	40	36	43
		35	25	20	16	37	36	19	14	26	22	30
50	—	10	2	27	3	14	38	6	6	16	4	7
		51	51	47	54	53	55	51	51	51	54	52
		49	29	37	18	29	48	22	21	20	23	17
		32	47	17	48	48	29	24	28	30	34	39
		23	24	13	29	33	31	27	24	13	14	16
55	—	46	22	29	35	24	45	17	18	37	27	32
		45	45	25	43	46	25	50	50	46	42	44
		1	2	3	4	5	6	7	8	9	10	11

Figure 6-9: Ranking of the 56 parameter subset based on the μ_{EE}^* value for all 11 computed GoF

indicator. Like in other SA methods, there is no fixed rule for the parameter selection. In the current study, parameters with absolute mean values μ_{EE}^* greater than the 75th percentile for at least 75% of the computed GoF for different MoP were selected. Parameters with atypical values in the $\mu_{EE_i}^*-\sigma_{EE_i}$ graphs illustrated in Figure 6-8 were also considered. Following this criteria, there are 15 parameters outperforming all the others:

- μ_{RT} (1) and σ_{RT} (2) are the mean and standard deviation of the reaction time distribution. As expected, the reaction time mean value, is one of the most important parameters. The σ_{RT} is not typically considered in calibration procedures, and was not identified as relevant in the SA using loop-based data. However, its effects in all parameters, especially for the deceleration and DRAC GoFs are evident;
- Similar conclusions may be pointed out for the μ_{dv}^h (34) and σ_{dv}^h (35) parameters. These are, respectively, the mean and standard deviation of the headway threshold distribution. $\mu_{EE_i}^*$ and σ_{EE_i} are both high for the headway standard deviation parameter, reflecting its possible strong interaction with the mean headway distribution parameter;
- μ_{DS} (38) and σ_{DS} (39) are the mean and standard deviation of the desired speed distribution. The first is typically selected for calibration and was already proved as a sensitive parameter regarding loop sensor data. The later however, revealed to be an important factor regarding the DRAC and side gaps GoF;
- h_{cf}^{lb} (6) is the headway threshold lower bound for the car-following model, a sensitive parameter regarding acceleration, deceleration, and headway and side gaps GoF;
- γ_{cf}^{acc} (9) and ρ_{cf}^{acc} (10) are the gap and speed difference between the subject and the leader vehicles of the car-following acceleration model. These two parameters do not present the highest ranking values for any specific GoF, but have an overall importance. Due to their intrinsic nature, their sensitivity is expected to increase for congested situations, but their contribution should be further assessed in the next step;
- α_{cf}^{dec} (12) and ρ_{cf}^{dec} (14) are the gap and speed difference between the subject and the leader vehicles of the car-following deceleration model. Although the γ_{cf}^{dec} (13) was found to be a significant parameter in the previous SA, it only affects speed and acceleration related GoF, and thus, not fulfilling the criteria used for selection;

- $\alpha^{CL}(40)$, $\beta_{tail}^{TL}(48)$, $\beta_{nlc,1}(51)$ and $\theta_{MLC}(56)$ are parameters of the lane changing model. The high rank values for these parameters show the importance of the lane selection model in MITSIM, especially regarding headway and side gaps GoF. Again, the characteristics of the A44 motorway clearly conditioned this outcome, as the network configuration almost only allows for one lane-change throughout its entire extension.

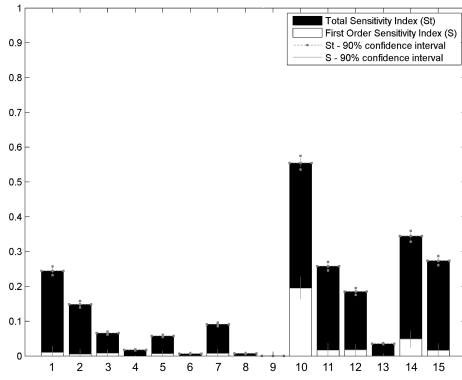
These set of 15 parameters were marked in red in Figures 6-8 and 6-9, and were selected for a final variance-based SA test and the computation of final uncertainty control values.

Final step: Final variance-based sensitivity analysis

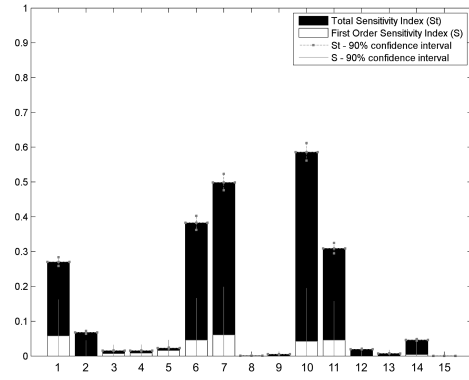
The quasi-OTEE screening method allowed to quickly identify the most sensitive parameters but, however, without providing a quantification of the related uncertainty. With the reduced number of parameters (15 instead of 56), a variance-based SA is now computationally feasible. We therefore started with a smaller size for the Monte Carlo experiment of $N = 256$, thus with 4,352 model evaluations. If convergence is not achieved, a additional simulations are necessary. The other 41 parameters values were set to the values of the best overall GoF combination of the quasi-OTEE analysis. As we are collecting individual vehicle observations no replications of each combination were performed at this point as the stochasticity was assumed to be captured by the large number of vehicle position observations computed. The identification of each parameter number is detailed in Table B.3 of Appendix B. The results of the first and total order sensitivity indices are presented in Figures 6-10 and 6-11.

Together with their interactions, only a small set of nine parameters have a total sensitivity index higher than 0.1 for more than 25% of the outputs. Considering that the values of all other 93 parameters were adjusted during the previous steps, it is expected that a fine calibration of these nine parameters should be sufficient to reach a robust replication of the trajectories:

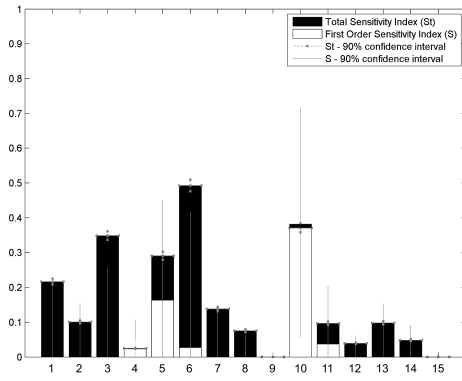
- μ_{RT} (1) and σ_{RT} (2) are the mean and standard deviation of the reaction time distribution;
- μ_{DS} (10) and σ_{DS} (11) are the mean and standard deviation of the alternative desired speed distribution;



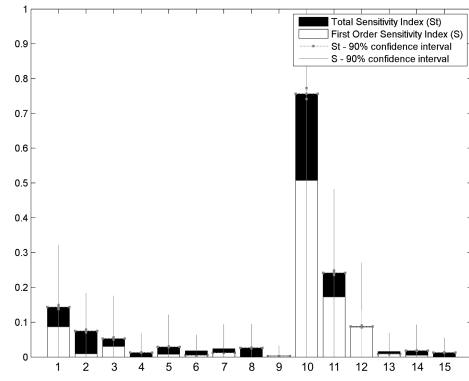
a) Speed



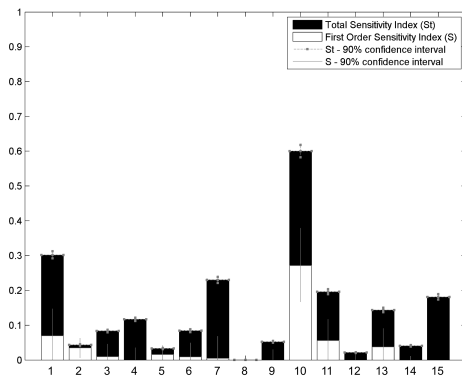
b) Acceleration



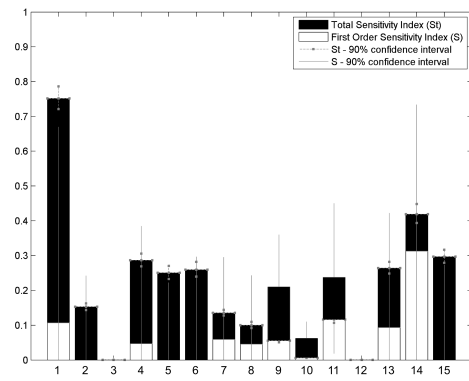
c) Deceleration



d) Headway

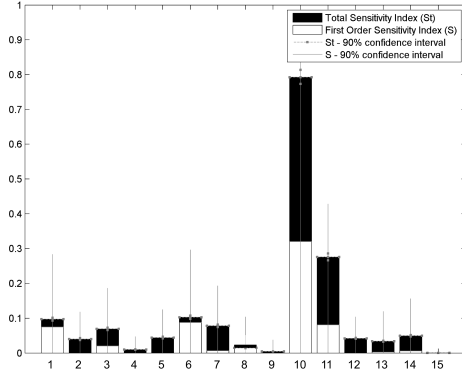


e) TTC

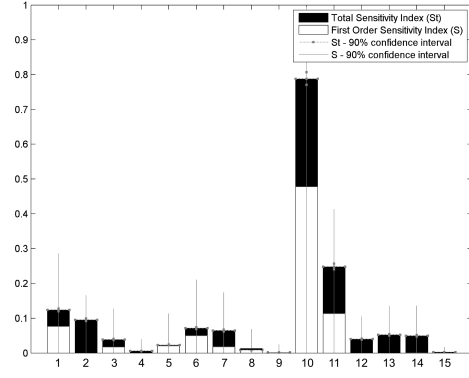


f) DRAC

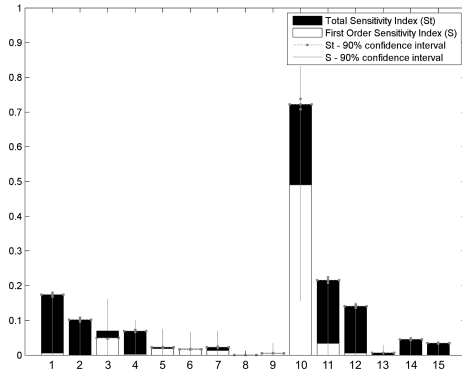
Figure 6-10: Final analysis bar plots of first (white) and total (black) order sensitivity indices on the Theil coefficient of trajectory based MoP (1)



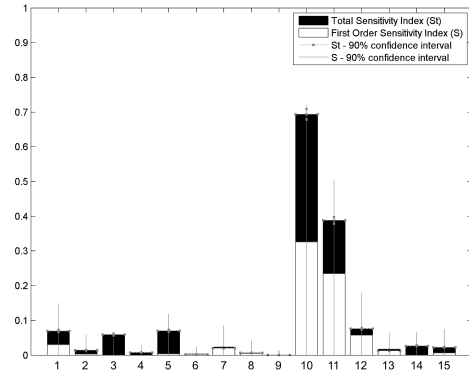
g) NLC



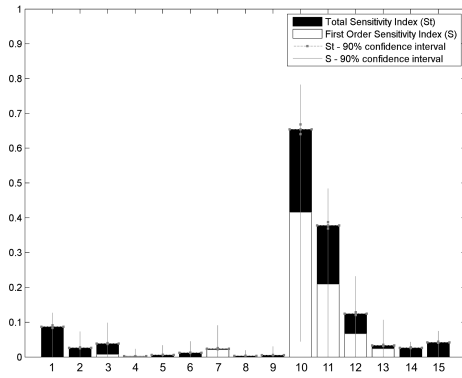
h) Left lead gap



i) Left lag gap



j) Right lead gap



k) Right lead gap

Figure 6-11: Final analysis bar plots of first (white) and total (black) order sensitivity indices on the Theil coefficient of trajectory based MoP (2)

- α_{cf}^{dec} (6) and ρ_{cf}^{dec} (7) are the gap and speed difference between the subject and the leader vehicles of the car-following deceleration model;
- β_{tail}^{TL} (13), $\beta_{nlc,1}$ (14) and θ_{MLC} (15) are the tailgating, one lane-change required to stay in path, and the distance to exit parameters of the lane selection model.

General remarks

As expected, the proposed global SA framework using the distributions of trajectory statistics resulted in a more complex procedure than using data from a small set of loop sensors. To avoid grouping parameters from different sub-models, a screening SA method was tested with the framework presented in Figure 6-1 instead of a variance-based group analysis. At each step of the analysis, the parameters left out were fixed using the best combination regarding the overall GoF. This means that at each step, these parameters were calibrated for the current case study, and did not need further fine tuning. However, this does not mean that these parameters are not relevant.

The use of an overall GoF is expected to result in the best possible trajectory statistics replication, but not in the best individual performances regarding each individual MoP measure. However, if one aims at only replicating the statistics of a particular MoP, the selection procedure may be adjusted accordingly.

The majority of the relevant parameters from the SA with loop-based data was still detected as sensitive in the last steps of the current SA. This vouches the consistency of both the proposed global SA and the MITSIM driving behaviour model itself. Reaction time, desired speed, deceleration constant and density parameters, and lane selection (utility) model were again revealed as fundamental models. However, some other parameters are also important in the replication of trajectory statistics for urban motorways: standard deviations of relevant driving behaviour heterogeneity modelling, namely the reaction time (σ_{RT}) and desired speed (σ_{DS}); interaction parameters (speed difference and density) of the car-following acceleration; or even parameters from the nosing and courtesy yielding models. The identification of calibration parameters is very sensitive to each case study configuration and observed traffic conditions, and these two models were, in fact, expected to result as important models in the busy A44 case study.

It is important to point out that the low value for the Monte Carlo Experiment ($N = 256$) in the final variance-based SA still resulted in good statistics, mainly thanks to the

appropriate control of the uncertainty in the two previous steps. The different sizes of both Monte Carlo experiments were found to be sufficient as all of the GoF for the group and individual parameters analysis converged. As in previous steps, the above presented results were, in general, the same for the *RMSNE* and *RMSE* GoF.

The last nine model parameters (out of 102) accounted for, at least, 50% of the output's variance of each computed GoF (first order indices). The interaction component however, is still very important for all trajectory-based MoP and is responsible for a higher share in the out-put variance for the selected nine parameters. In addition, with this methodology 44,868 model evaluations were performed instead of the 212,992 (-79%) required for applying variance based techniques to the whole set of parameters.

6.3 Calibration of Sensitive Parameters

The calibration task of many microsimulation studies is typically based on aggregated data: local counts, speeds, occupancies or, eventually, path travel times. When dealing with a large set of MoP, GoF measures, replications and parameter sets the simulations to be performed may reach an unfeasible number. This figure represents the major obstacle in the calibration task of traffic micro-simulation applications.

In recent years it was demonstrated that the use of meta-models may significantly reduce the computational burden of the calibration and validation task of traffic simulation models (Toledo and Koutsopoulos (2004), Ciuffo et al. (2011)). By definition, a metamodel is an approximation of the input to output function that is defined by the simulation model. This approach has been widely used in general simulation and optimization fields, and is particularly well suited for the purpose of our statistical validation. Thus, per each MoP/GoF combination, an analytical function which has the same mathematical features as the simulation model, both locally and globally, may be computed and used for parameter calibration.

In this section, both the sensitivity analysis results from the previous section and a Kriging metamodel approach are used for the calibration of the microscopic simulation tool. The parameters found as most sensitive in the previous section are integrated in a final Kriging calibration, while the other parameter values are set considering the best parameter combination at each time step of the SA.

6.3.1 A Kriging metamodel approach

Kriging models have been applied in many research fields and several application studies may be easily found in the literature. They were recently applied with success in the evaluation of different calibration algorithms of the AIMSUN micro-simulation application (Ciuffo et al., 2011). The Kriging model was originally developed in the geostatistics field, by Daniel Krieg and formulated mathematically by Matheron (1963), and may be viewed as an estimator based on the value of neighboring points. The basics of the (ordinary) Kriging model are presented in the next paragraphs but the reader may refer to Matheron (1963) and Kleijnen (2007) for further details.

The Kriging model assumes that the output $w(d)$ of a simulation model is given by:

$$w(d) = \mu + \delta(d) \quad (6.14)$$

where d is the vector of model variables; μ the simulation output averaged over the experimental area; $\delta(d)$ a zero mean stationary covariance process. The Kriging model uses the following linear predictor $y(d)$ of the output of a simulation model for a variable combination d :

$$y(d) = \lambda(d, D)^T w(D) \quad (6.15)$$

where D is the input variables design matrix of the simulation experiment for which the simulation output is known/simulated; and $\lambda(d, D)$ is a matrix of weights between the new variables specific combination d to be used as input in the metamodel and the points in D . $\lambda(d, D)$ values are not constant but decrease as the distance between d and D increases. To select the optimal values λ^* for the weights $\lambda(d, D)$ one may use the Best Linear Unbiased Predictor which minimizes the Mean Squared Error of the predictor in equation 6.14 (see Kleijnen (2007) for mathematical proof):

$$\lambda^* = \Gamma^{-1} \left[\gamma + \mathbf{1} \frac{\mathbf{1}^T \Gamma^{-1} \gamma}{\mathbf{1}^T \Gamma^{-1} \mathbf{1}} \right] \quad (6.16)$$

where $\mathbf{1}$ is the n -dimensional identical vector (n is the number of the experiment variable combinations in D); $\Gamma = \text{cov}(w_i, w_j)$ with $i, j = 1, \dots, n$ is the $n \times n$ symmetric and positive semi-definite matrix with the covariances of the simulated outputs $w(D)$; and $\gamma = \text{cov}(w_i, w_k)$ the n -dimensional vector with the covariances between the n simulated

outputs i and the output for the variables' combination to be predicted by the metamodel, w_K . In simulation applications, the elements of γ and Γ are estimated using a correlation function which is the product of k one-dimensional functions (being k the number of variables or parameters of the simulation model) and assuming that these correlations are determined by the distance between the inputs of the specific outputs considered:

$$\text{cov}(w_i, w_j) = \prod_{g=1}^k \text{cov}(d_{i,g}, d_{j,g}) \quad (6.17)$$

where $g = 1, \dots, n$. Furthermore the Kriging metamodel assumes a stationary covariance process, which implies that the covariances depend only on $|d_{i,g} - d_{j,g}|$. A popular function is the Gaussian correlation function Kleijnen (2007):

$$\text{cov}(w_i, w_j) = \prod_{g=1}^k \exp \left[- \left(\frac{|d_{i,g} - d_{j,g}|}{\theta_g} \right)^2 \right] \quad (6.18)$$

in which θ_g is a parameter of the correlation function for the variable g , denoting the importance of the variable itself (the higher θ_g is, the less effect the variable g has). In order to find the best Kriging metamodel for a simulation model, it is therefore only necessary to estimate the k -dimensional vector of θ_g , using a Maximum Likelihood Estimator. This problem was solved using the MATLAB toolbox dedicated to Kriging analysis DACE (Lophaven et al., 2002).

6.3.2 Testing the calibration using aggregated data

In this section we test if the Kriging calibration based on loop data results in appropriate estimates of both the aggregated data and the detailed traffic variables typically used in driving behaviour and safety studies. MITSIM was calibrated using the loop-based aggregate data for the specific day of the vehicle trajectory collection campaign (see Chapter 5). For the Kriging calibration experiment design, a set of 13,312 combinations ($1024 \times (11 + 2)$) were computed, each with 10 replications. The (11) parameters considered for calibrations were the ones detected as sensitive in section 6.2.4: $\mu_{RT}, \alpha_{cf}^{acc}, \beta_{cf}^{acc}, \alpha_{cf}^{dec}, \gamma_{cf}^{dec}, \rho_{cf}^{dec}, \mu_{dv}^h, \mu_{DS}, \alpha^{CL}, \beta_{next}$ and θ_{MLC} ; while the other parameters were fixed following the optimum value of the previous global SA.

Figure 6-12 shows the global convergence of Kriging speed and count results towards

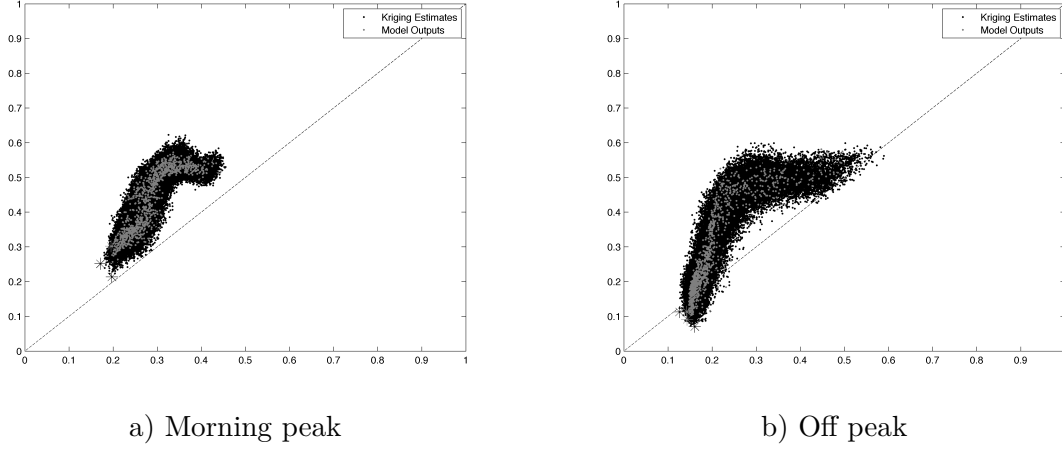


Figure 6-12: Counts vs. speed Theil inequality coefficient values for the simulated and Kriging estimates

a parameter combination which gives small GoF values. The cloud of Kriging points is regular and well shaped and embodies the real data. However, setting a single best solution is not advisable for several reasons: the Kriging approximation might not capture small changes existing in the true model; a single best option may easily change, depending on the daily traffic data; and the best solution for speed related GoF is not the best for count related GoF. For these reasons the thirty² best set of parameters combinations with comparable performances were kept for the validation testing.

Comparison with Aggregated Data from Loop Sensors

The thirty best combinations managed to replicate appropriately the observed loop sensor counts and speeds. Total loop sensor counts and average speeds in the entire network showed a good and stable fit along the daily variations (Figures 6-13 and 6-14), with an average and a best Theil's coefficient of 0.129 and 0.064 (for speeds) for a generic calibration of a full day using all sensor data. However, the selection of the best set for different time periods or sensor group has a significant impact on the calibration results.

As expected, local calibration resulted in better local fitting results ($U=0.061$, for the calibration of the SN direction in AM-peak period and $U=0.056$ for the calibration of the NS direction in off-peak period), but failed to capture traffic characteristics for non-calibrated scenarios. In Figure 6-13 b. and 6-14, for example, the best combinations for different MoP are presented. Simulated data from sensor 401-1 (located in the SN

²This number was selected by rounding the number of combination with a speed-based GoF measure lower than a user defined threshold ($U=0.085$).

direction) using a full network MoP calibration (6-13 b.) and MoPs based on just the sensors in either directions (Figure 6-14) show very different results.

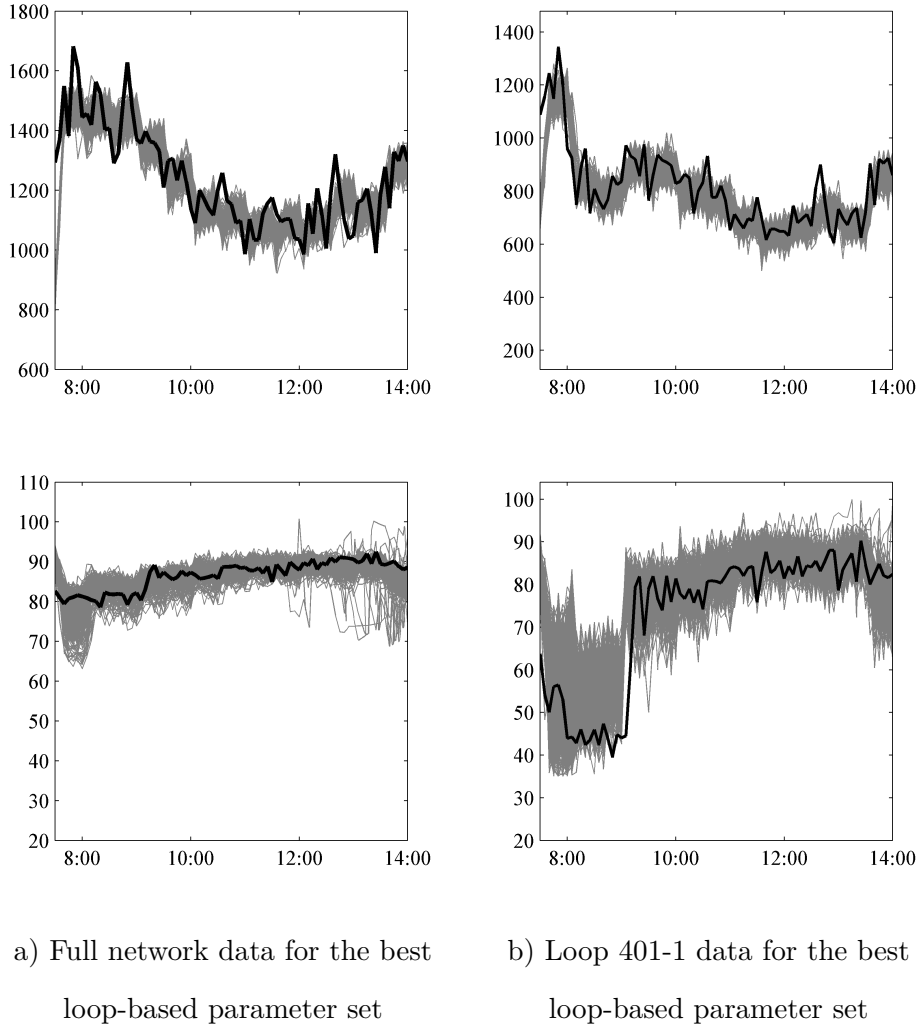


Figure 6-13: Simulated (grey) vs. true (black) counts (top) and average speed (bottom) (1)

Comparison with Detailed Data from Trajectories

It is common practice by practitioners and even researchers to use simulators calibrated with aggregated data to extract further traffic information from the transportation system under analysis. This practice is generally wrong, especially when the detailed variables or driving behaviors being scrutinized are considerable different from the ones specified in the original model or used during the calibration process. It might be the case where the appropriate conditions are met, but one should always compare these simulation outputs with its real counterparts. To this aim, simulated trajectories obtained using the previous

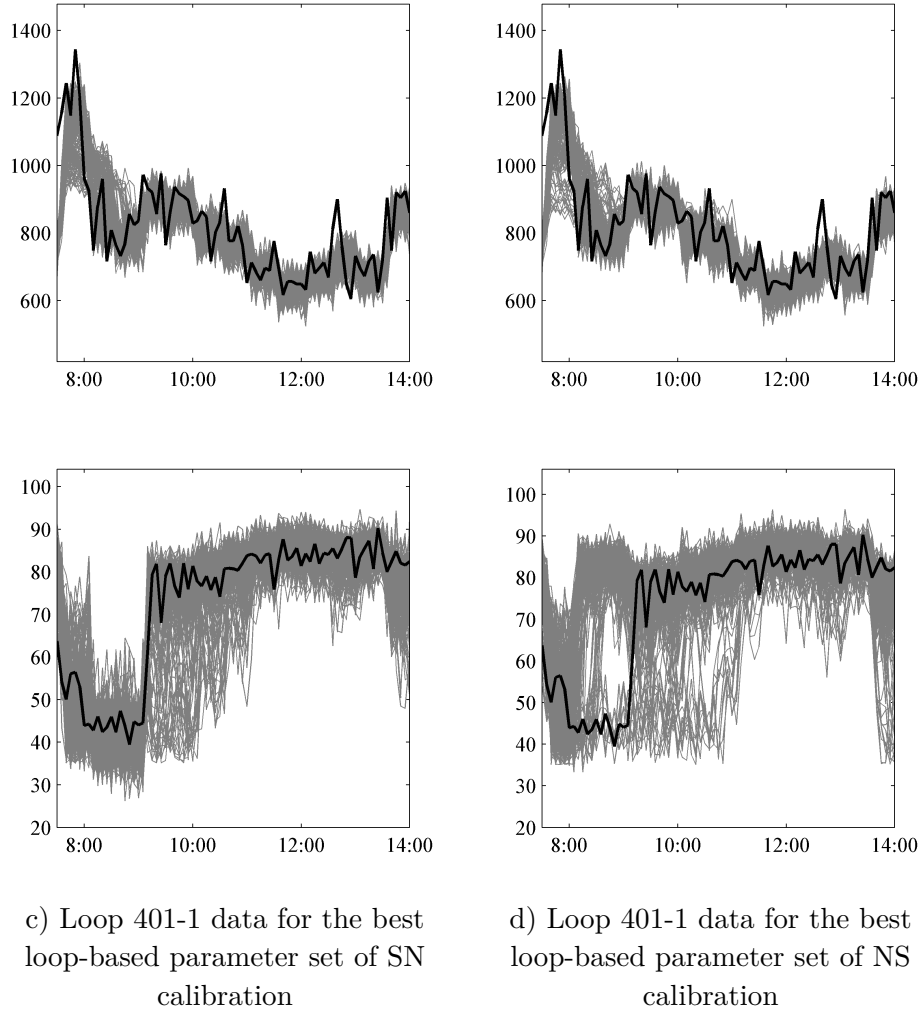


Figure 6-14: Simulated (grey) vs. true (black) counts (top) and average speed (bottom) for the loop-based calibration

thirty best parameter combinations were compared with real trajectories collected on-site through aerial remote sensing (see Chapter 5). CDF of a set of six detailed variables were extracted: speed, headway, acceleration, deceleration, and two safety related surrogate measures: the TTC and the DRAC (see Figure 6-15).

For the entire A44 motorway, including its entry and exit links, it is clear that some of the detailed variables could not be simulated appropriately. Although loop sensor speeds were used for aggregate calibration, speed and especially other detailed variables are far from being well replicated. It is worth mentioning that a general recommendation concerning the selection of sites for loop installation states that sections with stable traffic characteristics are preferable.

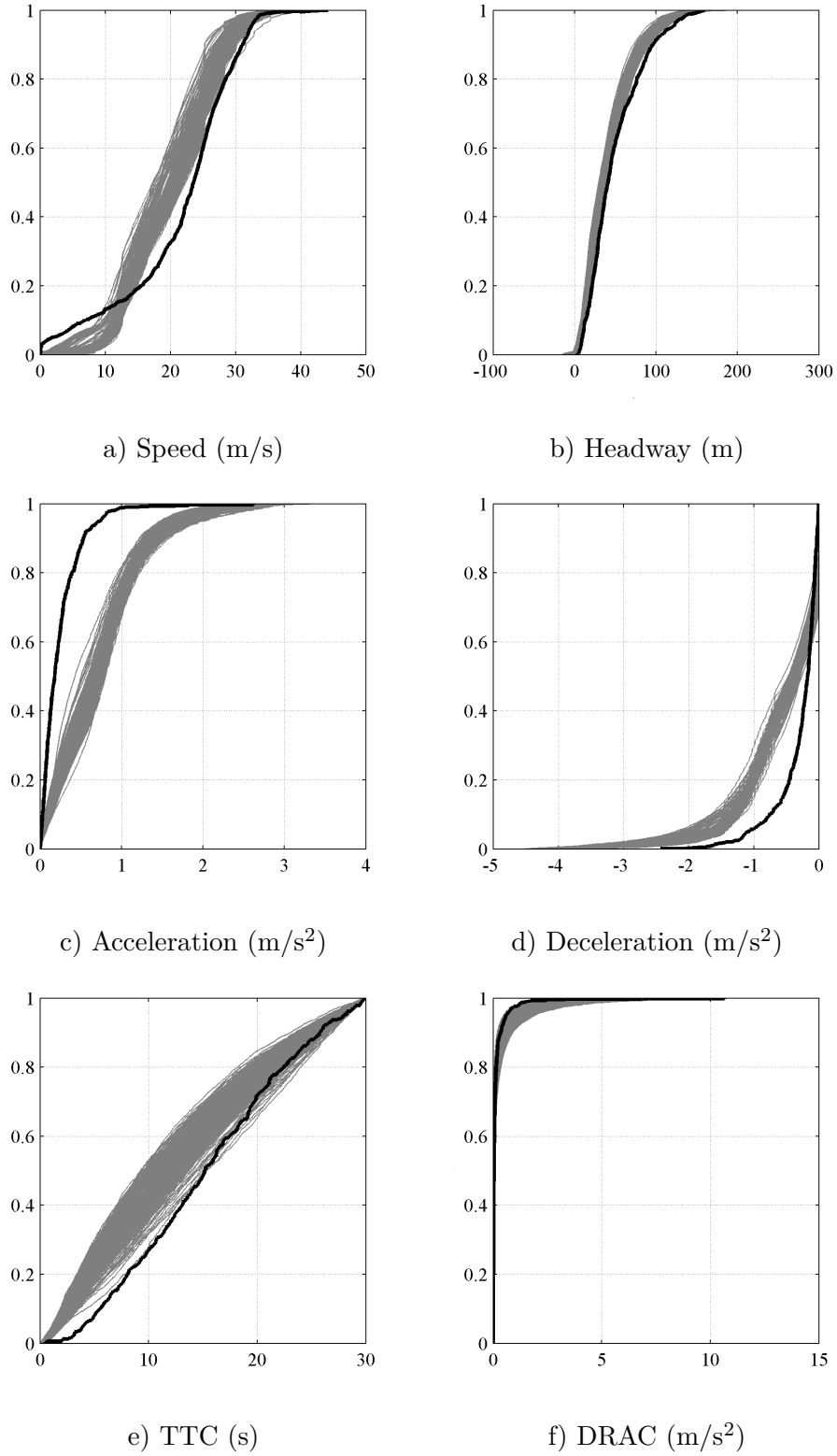


Figure 6-15: CDF for different detailed traffic variables for the 30 best combinations of the loop-based calibration (grey) and real data (black)

In Figure, for example, 6-17 it is clear that both TTC and deceleration rate for specific road sections were considerably under estimated by the model. On the other hand, Figure

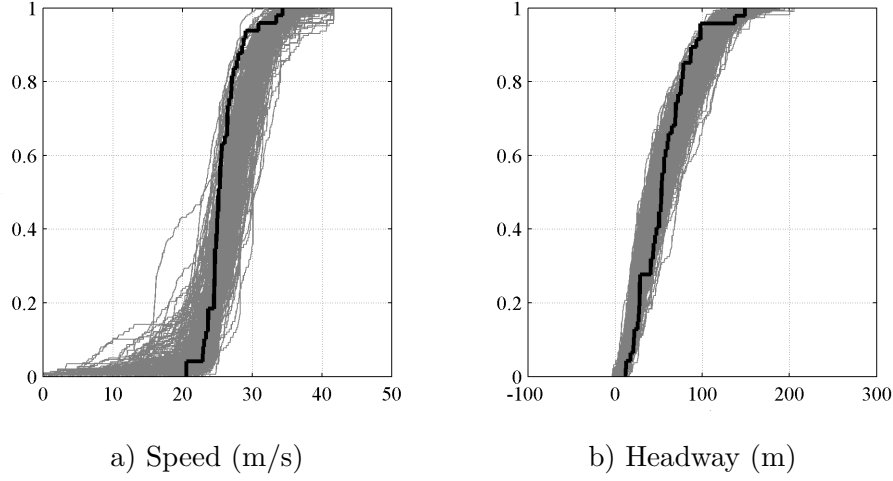


Figure 6-16: CDF in the right lane of two-lane sections, grade between 0 and +2%, speed-limit over 100 km/h and light traffic for the 30 best combinations of the loop-based calibration (grey) and real data (black)

6-16 shows a very good fit of simulated speeds and headways in another specific road section group. In fact, 37% of the loop sensors observations belong to similar apticular groups, resulting in a much better fitting. Thus, simulated accelerations and safety related surrogate measures cannot be used without their appropriate calibration using their on-site counterparts.

6.3.3 Testing the calibration using trajectory data

Similarly to the previous analysis, we now test if a Kriging calibration using the trajectory data results in much better traffic estimates. For this purpose, our MITSIM model is now calibrated using vehicle trajectory data (see Chapter 5), and the simulated traffic statistics are compared with the observed ones.

For the experiment design, a set of 11,264 combinations ($1024 \times (9 + 2)$) with 10 replications each were computed. The (nine) parameters considered in the calibration were the ones detected as sensitive in section 6.2.5: μ_{RT} , σ_{RT} , μ_{DS} , σ_{DS} , α_{cf}^{dec} , ρ_{cf}^{dec} , β_{tail}^{TL} , $\beta_{nlc,1}$, θ_{MLC} ; while the remainder parameters were fixed following the optimum value of the previous global SA steps (using the Euclidean distance to the origin of the space of the first seven GoF).

Similarly to the previous section, plots of all pairs of different output GoF were produced to check for the Kriging coverage of the output space. As an example, Figure 6-18 shows four of them. Assuming the robustness of MITSIM, it is expected that the values

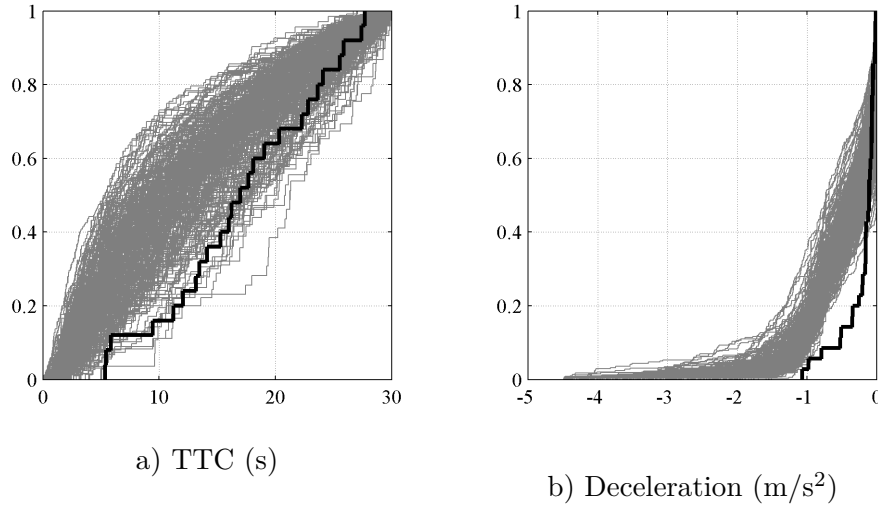
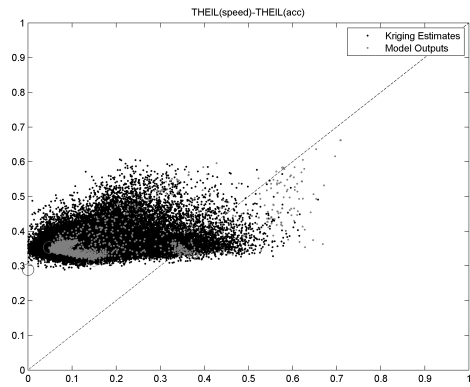


Figure 6-17: CDF in the left lane of two-lane sections (w/ acc. lane), grade lower than -2%, speed-limit over 100 km/h and low traffic for the 30 best combinations of the loop-based calibration (grey) and real data (black)

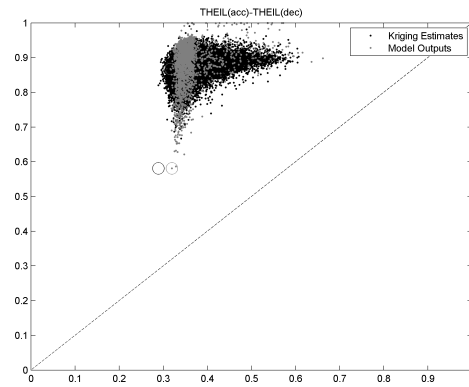
of the GoF measures will be greater than those using just 8 loop sensors, due to a higher level of detail and the heterogeneous nature of the multiple MoP used for calibration. The fact that during the SA presented in section 6.2.5, the parameters were always set to an overall best GoF combination, it is expected that it will hardly reach an individual GoF optimum for a specific MoP. If one had focused on just calibrating the parameters regarding, for example headway, all these plots would have a very different layout. It is clear that the convergence of Kriging outputs depends directly on the SA results, and that the method was not successful in capturing the entire variability regarding the deceleration, the DRAC and the TTC. However, the achieved GoF improvements justified its inclusion in the selection criteria of the best set of combinations. As in the previous section, for the validation of results, the thirty best overall set of parameters combinations were used.

Comparison with Aggregated Data from Loop Sensors

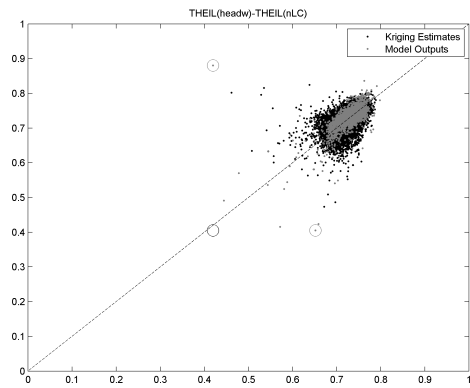
The thirty best combinations managed to replicate appropriately the observed loop sensor counts and speeds, even though no loop-based calibration process was directly implemented. It is worth remembering that a previously estimated seed OD using the observed counts was used for simulation, a procedure that contributed significantly to favorable count GoF results. Total loop sensor counts and average speeds in the entire network showed a good and stable fit along the daily variations (Figure 6-19), with a speed-based Theil's coefficient of as low as 0,083 (and an average $U=0.106$ for the 30 best combina-



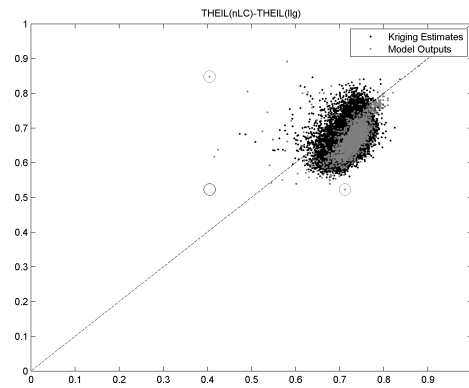
a) speed (x) vs. acceleration (y)



b) acceleration (x) vs. deceleration (y)



c) headway (x) vs. NLC (y)



d) NLC (x) vs. left lag gap (y)

Figure 6-18: Theil inequality coefficient values for the simulated and Kriging estimates for different output pairs

tions). From Figure 6-19 it is clear that a replication of loop sensors counts as good as the loop-based calibration was achieved. However, the 30 best combination speed outputs at loop stations showed a much higher variability. These results are mainly due to two distinct factors: the use of the overall GoF, where the speed is not the only detailed variable being optimized; the driving behaviour model as formulated in MITSIM may not be able to fully capture the variability among different simulated scenarios; and some of the best parameter combinations optimized using a general overall GoF do not replicate some of the loop sensor local conditions properly.

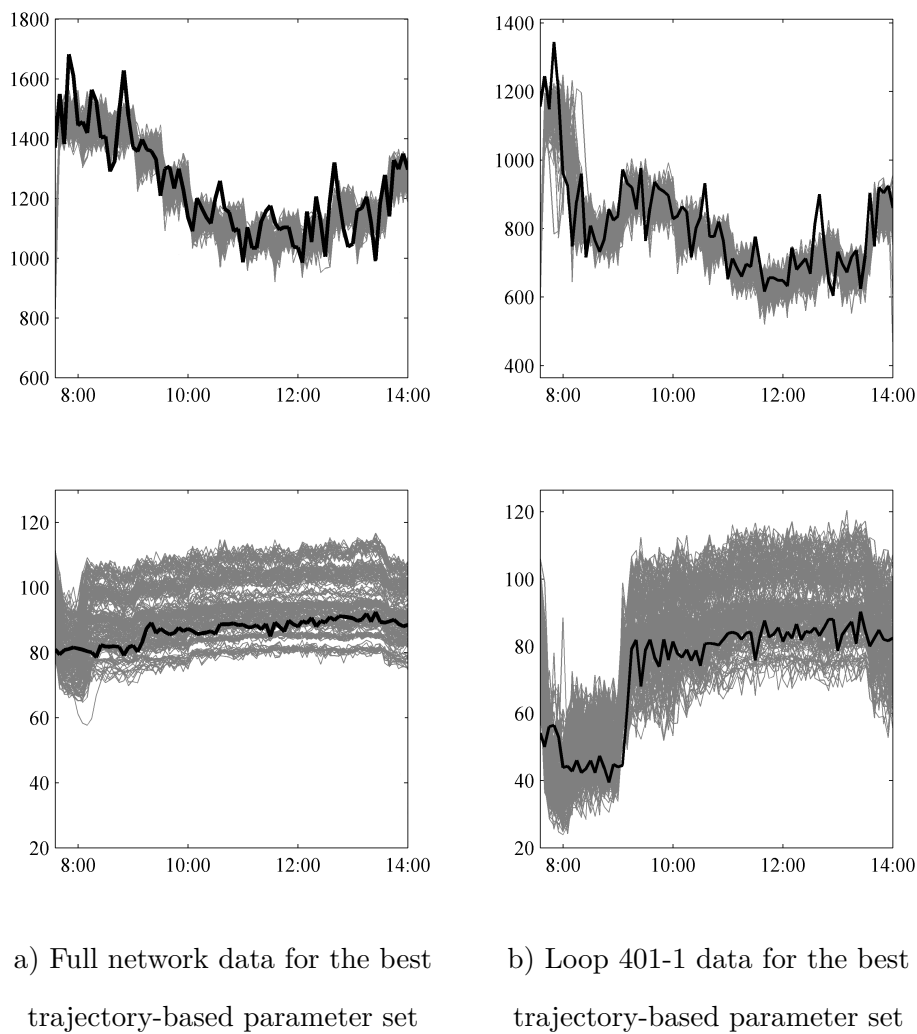


Figure 6-19: Simulated (grey) vs. true (dark) counts (top) and average speed (bottom) for the 30 best combinations of the trajectory-based calibration (grey) and real data (black)

Comparison with Detailed Data from Trajectories

It is now expected that the simulated trajectory statistics will fit better the observed ones. To evaluate this, simulated trajectories obtained using the above thirty best parameter combinations were compared with real trajectories collected on-site through aerial remote sensing (see Chapter 5) and CDF of the same set of six detailed variables were plotted (see Figure 6-20).

When comparing these plots with the ones presented in Figure 6-15, a clear improvement in the overall variables distributions is observed. However, perfect fit of specific MoP is not reached due to the limited calibration iterations, the intrinsic modelling errors and the overall MoP chosen as optimizing function. At the local and variable specific level, two main considerations may be pointed out:

- Both trajectory data and loop data based calibrations allowed for a good replication of the detailed variables for some of the simulated sections (see example in Figure 6-21 vs. Figure 6-16). However, a significant improvement regarding the trajectory based calibration was observed for some sections where the aggregate calibration did not manage to perform well (see example in Figure 6-22 vs Figure 6-17);
- The slight biased estimation of some of the overall safety related variables (lower TTC, higher accelerations and lower decelerations rates) might generate a bias in the estimation of the true parameters of any safety model. The resulting parameter values may be slightly different from their true values but they are still much closer than the estimated using just an aggregated-data based calibration.

Finally, in Table 6.1 the best values of the Theil's inequality coefficient regarding different MoP and for both SA-based calibrations using sensor data and trajectory data are presented. It is important to remember that the analysis of the best set of combinations (instead of a single combination) is more appropriate. The analysis of Table 6.1 is limited to a single combination results (and therefore, does not capture the model variability appropriately).

From all the previous analysis, the following general conclusions may be pointed out:

- As an overall assessment and considering the large number of parameters, **MITSIMLab** is a stable simulation tool, where the variability of all outputs is low when the full set of driving behaviour parameters is well controlled. However, the global SA

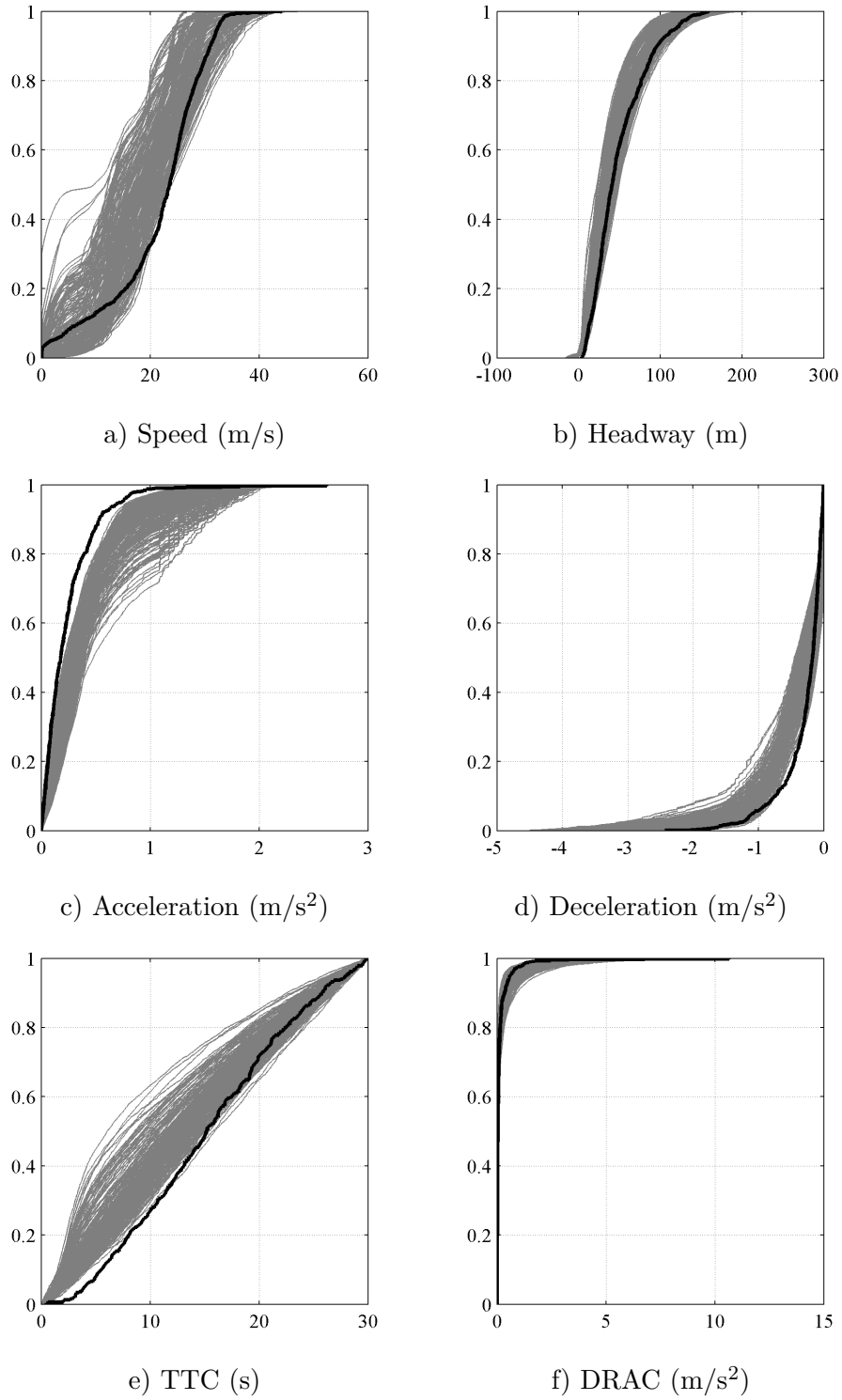


Figure 6-20: CDF for different detailed traffics variables for the 30 best combinations of the trajectory-based calibration (grey) and real data (black)

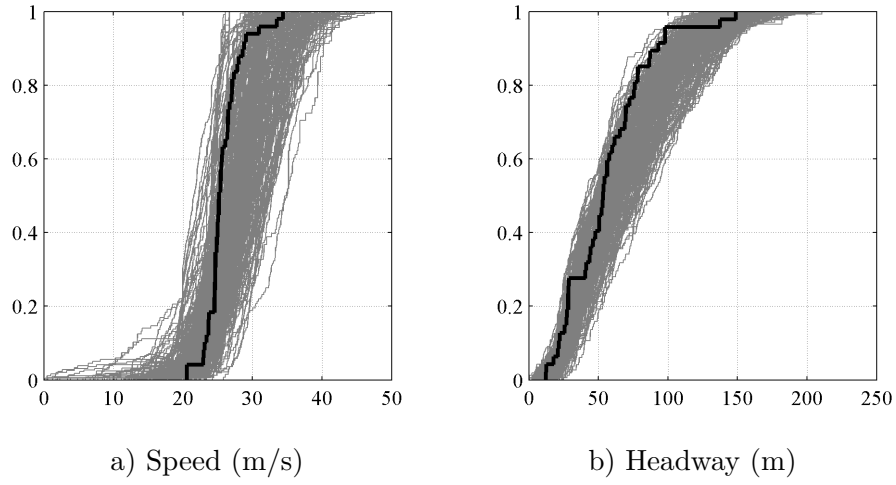


Figure 6-21: CDF in the right lane of two-lane sections, grade between 0 and +2%, speed-limit over 100 km/h and light traffic for the 30 best combinations of the trajectory-based calibration (grey) and real data (black)

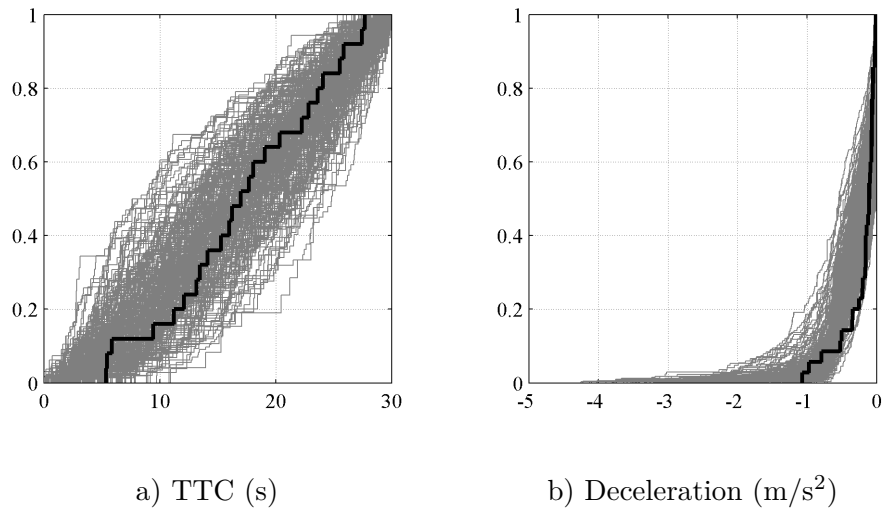


Figure 6-22: CDF in the left lane of two-lane sections (w/ acc. lane), grade lower than -2%, speed-limit over 100 km/h and low traffic conditions for the 30 best combinations of the trajectory-based calibration (grey) and real data (black)

calibration and the use of multiple types of data were key contributing factors to reach these controlled circumstances;

- No improvement regarding the loop sensor data was achieved when using a trajectory-based calibration. This is an important aspect to consider when a calibration process aims at reaching a model capable of well replicating aggregated network efficiency measurements. However, it is foreseen that travel times calibration, typically an essential step for efficiency assessment, should rely on the parameter sub-set identified as sensitive using the trajectory-based data;
- A significant improvement was observed regarding the replication of all detailed variables when calibrating using trajectory-based data. This is a very important aspect when the aim of the calibration is to replicate these variables. Their computation using just aggregated data calibration may easily result in significantly biased values;
- The values of the calibrated parameters are heavily dependent on the chosen MoP (both for aggregated-data and trajectory-data calibration).

The final parameter values for the best combination of both the loop-based and the trajectory-based calibrations are presented in Appendix B.

Table 6.1: Best Theil’s Inequality Coefficient values for both trajectory-based and sensor-based calibrations

MoP	Loop sensor based calibration	Trajectory based calibration
Average loop sensor counts	0.129	0.136
Average loop sensor speeds	0.064	0.083
Full network speed distribution	0.082	0.048
Full network acceleration distribution	0.292	0.197
Full network deceleration distribution	0.247	0.188
Full network headway distribution	0.172	0.100
Full network TTC distribution	0.123	0.118
Full network DRAC distribution	0.325	0.231
Total number of lane changes	0.521	0.337

A final comment on the number of replications used at each step of all the above experiments deserves to be added. As mentioned earlier, due to the existing stochasticity

in the formulation of traffic microscopic simulators, several replications are needed. The number of replications is typically defined by a sequential process, where after each (or a set of) additional replications, equation 6.19 is used to assess output variability for a level of confidence α and a desired accuracy ε :

$$N = \left(\frac{s \cdot t_{\alpha/2}}{\bar{x} \cdot \varepsilon} \right)^2 \quad (6.19)$$

where N is the required number of model runs; s is the standard deviation of the examined traffic measure; \bar{x} is the mean of the traffic measure; ε is the required accuracy, specified as a fraction of x ; $t_{\alpha/2}$ is the critical value of Student's t-test for the confidence level α . For the group SA and the quasi-OTEE trajectory-based screening method, the number of replications was defined by the limited computational and time resources. For the remainder experiments, the numbers of replications were sufficient to reach an $\varepsilon = 0.05$ and a confidence level of 0.975.

6.4 Event-specific Calibration

In the previous sections, the most sensitive parameters for both aggregate and disaggregated data were well identified and their influence in the variability of MoP was assessed. Furthermore, the full set of MITSIM's driving behaviour parameters were calibrated using a multi-step procedure that accounted for parameter interaction. In this section the focus is on the calibration of MITSIM to replicate detailed variables for a large set of scenarios of specific time periods and network locations. As it was concluded from the previous sections, the selection of a set of "best" combinations and a high number of replications is always preferable when dealing with stochastic simulation applications such as traffic microscopic simulation tools. This however, may cause a significant increase in the size of the simulation scenarios set. For each simulation scenario, the simplest metamodel may need thousands of replications for the selection of its best set of combinations. In the current study, we aimed at calibrating MITSIM and replicating the traffic conditions for each event of our safety database. For this purpose a very recent simultaneous demand-supply calibration method called the Weighted-Simultaneous Perturbation Stochastic Approximation (WSPSA) was used for the event-specific calibration (Lu et al., 2013). This type of simultaneous demand-supply method views the calibration process as an optimization

problem reaching a unique solution, rather than controlling data variability using multiple combinations.

6.4.1 Weighted-Simultaneous Perturbation Stochastic Approximation

The generic simultaneous demand-supply calibration of a dynamic traffic simulation application may be formulated as:

$$\text{Minimize } z(\theta) = k_1 \|F^m - F^s\| + k_2 \|\theta - \theta^a\| \quad (6.20)$$

subject to:

$$\begin{cases} F^s = f(\theta, R) \\ l_b \leq \theta \leq u_b \end{cases} \quad (6.21)$$

where F^m and F^s are vectors of time-dependent observed traffic measurements and corresponding simulated traffic measurements (in our case, sensor count and speed measurements), θ^a are prior values of the parameters to be calibrated, R is a vector of the road network characteristics (and other fixed simulation parameters), f is the traffic simulation model that generates simulated measurements, l_b and u_b are vectors of lower bounds and upper bounds for θ , respectively, and k_1 and k_2 are weights depending on the relative confidence on observed measurements and different sets of prior parameter values. The parameter bounds may be determined based on physical constraints or prior experience.

This optimization problem is highly non-linear when dealing with complex traffic models due to the absence of an analytic formulation for f (Antoniou et al., 2011b). Simultaneous perturbation stochastic approximation (SPSA) is an iterative gradient-free optimization algorithm designed for stochastic problems. It was initially proposed by Spall (1992) and successfully applied to the optimization of a variety of systems. SPSA efficiently approximates the gradient with only two successive measurements of the objective function (independently of the number of parameters) and therefore significantly saves computational time for large-scale problems over traditional gradient methods such as the finite-differences stochastic approximation. The general stochastic approximation algorithm starts from an initial estimation of the parameter vector and iteratively traces a

sequence of parameter estimates that converge to zero of the objective function's gradient.

$$\hat{\theta}_{k+1} = \hat{\theta}_k - a_k \hat{g}_k(\hat{\theta}_k) \quad (6.22)$$

where $\hat{\theta}_k$ is the estimate of the decision vector in the k^{th} iteration of the algorithm, \hat{g}_k is the estimated gradient, and a_k is an algorithm parameter that gets smaller as k becomes larger:

$$a_k = \frac{a}{(A + k + 1)^\alpha} \quad (6.23)$$

where a , A and α are constant parameters.

In SPSA the approximation of the gradient \hat{g}_k depends on two evaluations functions from a simultaneous perturbation of the parameters:

$$\hat{g}_{ki}(\hat{\theta}_k) = \frac{z(\hat{\theta}_k + c_k \otimes \Delta_k) - z(\hat{\theta}_k - c_k \otimes \Delta_k)}{2c_{ki}\Delta_{ki}} \quad (6.24)$$

where z is defined in equation 6.20, $\hat{g}_{ki}(\hat{\theta}_k)$ is the i^{th} element of the gradient vector, Δ_k is a random perturbation vector, generated through a Bernoulli process with values of +1 and -1 with equal probabilities, \otimes is the component-wise multiplication operator, and c_k is an algorithm parameter that determines the amplitude of the perturbation:

$$c_{ki} = \frac{c_i}{(k + 1)^\gamma} \quad (6.25)$$

where c_i is the i^{th} element in an algorithm constant parameter vector and γ is a constant parameter.

The characteristics of SPSA make it a suitable solution algorithm for the calibration of traffic simulation models (Balakrishna et al., 2007). Very recently Lu et al. (2013) extended the general SPSA framework, by incorporating known spatial and temporal correlation between parameters and measurements to minimize the noise generated by uncorrelated measurements, improving significantly its performance. SPSA only uses the aggregated error between model output and observed measurements, $z(\theta)$, ignoring a considerable amount of information: the location and time interval of different measurements and therefore, the correlation between θ and F^m . Furthermore, approximating the gradient for each parameter using the aggregate error in the whole network across the entire simulation period introduces noise from uncorrelated measurements. In the pro-

posed weighted simultaneous perturbation stochastic approximation (WSPSA), Lu et al. (2013) introduced a matrix W in the minimizing problem formulated by equation 6.20 to account for both spatial and temporal correlations between each parameter and the traffic measurements. W is called the weight matrix and is formed by two components: :

$$W = [W^e W^h] \quad (6.26)$$

$$W^e = \left\{ W_{p_{h_1}, m_{h_2}}^e \right\} = \begin{bmatrix} w_{1,1,1} & w_{1,1,2} & \dots & w_{1,1,M_1} & \dots & w_{1,1,M_H} \\ w_{2,1,1} & w_{2,1,2} & \dots & w_{2,1,M_1} & \dots & w_{2,1,M_H} \\ \vdots & \vdots & & \vdots & & \vdots \\ w_{P_1,1,1} & w_{P_1,1,2} & \dots & w_{P_1,1,M_1} & \dots & w_{P_1,1,M_H} \\ \vdots & \vdots & & \vdots & & \vdots \\ w_{P_H,1,1} & w_{P_H,1,2} & \dots & w_{P_H,1,M_1} & \dots & w_{P_H,1,M_H} \end{bmatrix} \quad (6.27)$$

where $W_{p_{h_1}, m_{h_2}}^e$ is the relative correlation between the p^{th} model parameter in interval h_1 and the m^{th} measurement in interval h_2 , assuming that the time period of interests can be divided into intervals $h = 1, 2 \dots H$; $p = 1, 2, \dots, P$ are the set of model parameters and $m = 1, 2, \dots, M$ is the set of measurements within each interval.

The second component accounts for the correlation of historical parameter values, as formulated in equation 6.20. If the confidence on each historical value is the same, it can be considered as the identity matrix:

$$W^h = I \quad (6.28)$$

Incorporating the weight matrix in the estimation of the gradient can reduce the algorithm noise significantly. Instead of calculating the i^{th} element in the gradient vector $\hat{g}_{ki}(\hat{\theta}_k)$ using the objective function value as in equation 6.20, a weighted sum of the measurement error changes related to the i^{th} parameter is used:

$$z(\theta) = \begin{bmatrix} k_1 (F^m - F^s) (F^m - F^s)^T \\ k_2 (\theta - \theta^a) (\theta - \theta^a)^T \end{bmatrix} \quad (6.29)$$

Thus the i^{th} element in the estimated gradient vector is:

$$\hat{g}_{ki}(\hat{\theta}_k) = \frac{z(\hat{\theta}_k + c_k \otimes \Delta_k) - z(\hat{\theta}_k - c_k \otimes \Delta_k)}{2c_{ki}\Delta_{ki}} W_i \quad (6.30)$$

where W_i is the i^{th} line in the weight matrix W . The output of the evaluation function z results now in a vector with length equal to the number of parameters to be calibrated, rather than a scalar. For further details on the WSPSA and SPSA approaches, the reader should refer to Lu et al. (2013), Spall (1992).

The way to calculate weight matrices for WSPSA depends on the configuration of the case study, the parameters considered and the measurements available. Considering that parameter p in period h_1 influences measurement m in period h_2 by $d_{p_{h_1}, m_{h_2}}$, the corresponding weight may be defined as:

$$w_{p_{h_1}, m_{h_2}} = \frac{d_{p_{h_1}, m_{h_2}}}{\sum_{i=1}^M \sum_{j=1}^H p_{h_1, i_j}} \quad (6.31)$$

Several spatial and temporal considerations may be assumed when computing the weight matrix (Lu et al., 2013), but no further applications of the WSPSA were found in the literature for its assessment.

6.4.2 WSPSA test

When applying the above method to the A44 case study, the demand-supply calibration parameter set is composed by the dynamic OD pairs of interest (depending on the simulation period) and the selected 11 most sensitive driving behaviour parameters for aggregated data (see section 6.2.4) as the only available data for event-specific calibration is the loop-based data. The seed OD estimation has a total of 100 OD paths per each 30 min period in a generic weekday (see Chapter 4 for further details). As no significant intra-variability was found in almost all intervals, a total of 100 demand parameters may be considered for each 30 min period. For each of the demand parameters, a weight $w_{p_{h_1}, m_{h_2}}$ in equation 6.31 can be defined as the relative correlation between the flow of OD pair p in period h_1 and the count of sensor m in period h_2 . Due to the small size of our case study, these correlations were calculated using simple static assignment proportions directly computed from the network configuration. A more complex approach would con-

sider dynamic assignment proportions. If no prior travel time information was available, assignment proportions may be computed using a path choice model and simulated travel times. As all vehicles departing at time t reach their destination at $t + 1$ at most, the static simplification is acceptable.

Regarding the driving behaviour parameters, the 11 most sensitive parameters from the loop-based SA presented in section 6.2.4 were selected for calibration. The rest of the parameters were set to their best values for the trajectory-based calibration (see section 6.3.3 for the details on the calibration method and Appendix B for each parameter final value). Driving behaviour parameter weights were set to 1 as no distinction was made between individual effect on different loop sensor output. In a more complex approach, SA results may be used to compute different driving behaviour parameter weights as distinct driving behaviour sub-model parameters may affect each sensor differently. The generic equation 6.20 may now be written as:

$$z(\theta) = \begin{bmatrix} k_1^{speeds} (F_{speeds}^m - F_{speeds}^s) (F_{speeds}^m - F_{speeds}^s)^T \\ k_1^{counts} (F_{counts}^m - F_{counts}^s) (F_{counts}^m - F_{counts}^s)^T \\ k_2 (\theta - \theta^a) (\theta - \theta^a)^T \end{bmatrix} \quad (6.32)$$

where $F_{speeds/counts}^{m/s}$ are vectors of 5 min observed (m) and simulated (s) loop-based measurements of *speed* and *counts*, θ^a are all seed OD dynamic (30 min based) entries and prior values of the 11 driving behaviour parameters, and k are the different weights of a combined optimizing function. While the SPSA has a single scalar as objective function, a vector forms the objective function in WSPSA. A comparison between their performance can be made based on a single and unique measure of effectiveness (MOE) applied to the exact same measurements.

As example of this specific WSPSA application, the results for the calibration of the 30 min periods before and after a specific rear-end accident that occurred at 8:30, km 3,300 in the SN direction of the A44 motorway are here presented. A warming period of 30 min was used for simulation stabilization. The total F^m observations relied in count and speed measurements from the eight loop sensors, resulting in a total of 192 observations for the single hour of effective simulation period (Table 6.2). The assumed weights of the optimizing function (equation 6.32) are $k_1^{counts} = 0.3$, $k_1^{speeds} = 0.5$ and $k_2 = 0.2$. These values were defined previously, based on the contribution of each information on

the calibration process. As we focus on detailed traffic statistics a higher contribution was given to speed related data. A sensitivity analysis on these weight values may, however, enhance the calibration final results. One should also note that the calibration results at each iteration are stochastic due to the inherent stochasticity of several **MITSIM** sub-models and to the random perturbation generated during the WSPSA algorithm. Hence, three replications were performed at each algorithm iteration in order to obtain a stable calibration. Finally, the constant parameters of the WSPSA algorithm (A , a , α , γ and c) were set to previously estimated values for a generic SPSA application to **MITSIM** calibration (Vaze et al., 2009). The number of iterations used in SPSA is typically large, but in the WSPSA framework much fewer iterations are required to reach satisfactory values (Lu et al., 2013). As we aim at reducing this number as much as possible, the stopping criteria was a threshold of relative improvement between consecutive iterations of 5% in both count and speeds *RMSNE* (see equation 6.10).

Table 6.2: Test calibration setup

WSPSA parameter	Value
Number of OD parameters	200
Number of driving behaviour parameters	11
Number of count measurements	192
Number of speed measurements	192
Number of replications	3
Number of iterations	30

The WSPSA algorithm was implemented in **MATLAB** and the **INGRID** computational resources were, once again, used for this task.

After just 30 iterations, the WSPSA converged and the *RMSNE* improved by 80.1% for speed observations, reaching the value of 0.19, and by 77% for counts, with a final value of 0.22 (see Figure 6-23)

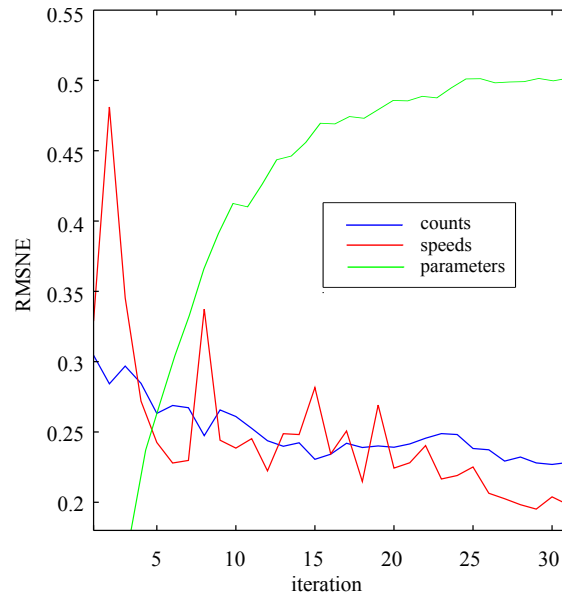


Figure 6-23: WSPSA test performance for a specific event calibration

As a result of the good GoF, this advanced calibrated method achieved a very good fit of individual loop-based measurements (see Figure 6-24 a. and b.). In Figure 6-24 c. and d., the final calibrated demand parameters (OD pairs) and driving behaviour parameters are plotted against their initial values: the GLS estimated seed OD and the trajectory-based best parameter combination.

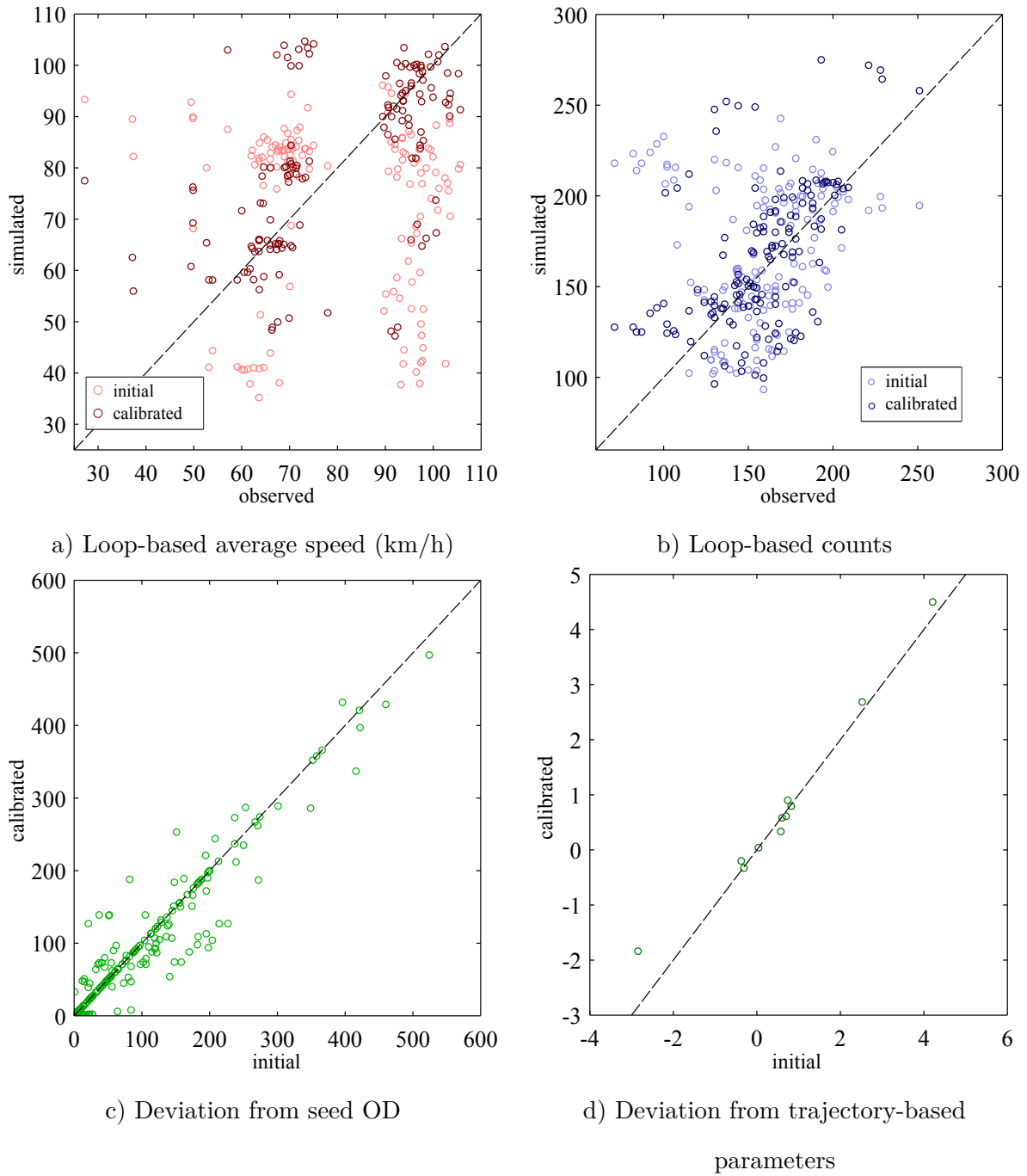


Figure 6-24: WSPSA test performance for a specific event calibration

The presented WSPSA method and configuration was used in the event-based calibration of all occurrences used in the safety estimation framework. The variability of both the calibrated parameters set and the generated output for all events considered are analysed in the next Chapter.

6.5 Concluding remarks

With the increasing complexity of simulation tools it is becoming of crucial importance analysing them, understanding how they work and, in particular, what influences their capability to reproduce physical phenomena. Global SA is the family of tools to be used with this aim. The problem in using global SA is that, even with the most sophisticated sampling strategies, the exploration of the input space requires many model runs to be performed. When the model is computationally intensive, which is fairly common in transportation modelling, SA becomes almost unfeasible. This is highly inefficient, especially when the number of model parameters is quite high. To deal with this issue, practitioners usually perform SA on a subset of model parameters chosen on the basis of their experience and use simplified SA methods that, for example, ignore uncertainty linked to parameters interactions. Additionally, the common approach usually adopted for calibrating a microscopic traffic simulator involves an optimization problem in which the distance between some traffic variable measurements and its simulated counterpart is minimized by changing the value of its parameters. This approach does not take into account the high level of uncertainty of traffic scenarios, namely in the traffic demand (both day-to-day and within-day uncertainties) and in the model parameters (especially in what concerns their distribution among the vehicles of the simulated scenario). In addition, the entire problem is made more complex as the value obtained in a measurement is just one of the possible traffic realizations due to the same demand, supply and composition of the population (e.g. due to differences in departing times, etc.).

In sections 6-1 to 6.3, the entire problem of calibration is treated under the light of uncertainty management, by performing a number of preliminary analyses by grouping model parameters on the basis of their possible common features and, then, by using SA to discover which groups of parameters accounts for the highest share of the outputs' variance. At the end of these preliminary steps a final SA on the parameters pertaining to the most influential groups can be performed to individuate the most important among them. The proposed methodology was applied to the high-dimension **MITSIM** model (102 model parameters), uncovering the role played by the different parameters and by the model stochasticity with 70% fewer model evaluations. Then, to better catch the model variability, rather than finding the parameter combination which best reproduces the real measures, one should look at a set of combinations for which the model behaves relatively

well and analyse the model stochasticity in the form of distributions of model outputs. In this framework, the validation of the model should be carried out by checking whether or not the individuated uncertainty is sufficient to account for the uncertainty of the real system. Despite the successful results, the proposed global SA was only tested for a particular urban motorway scenario and a specific microscopic simulation tool. In the future, the efficiency of the proposed method should also be tested in different freeway scenarios as well as in the assessment of different driving behaviour model structures.

A typical aggregated calibration formulation was successfully applied to the calibration of MITSIM using vehicle trajectory data, avoiding the modelling complexity of classical estimation methods and the arduous configuration set ups needed in detailed disaggregated calibration. When a detailed description of the traffic phenomenon is desired the availability of detailed data is a fundamental factor in the replication effectiveness by such complex models. Furthermore, it was shown that the choice of the MoP and GoF plays a major role in the values of the calibrated parameters for both the loop data and trajectory data based calibrations. To fully assess the efficiency of the aggregated calibration logic to disaggregated data, a comparison with the other three estimation frameworks described in section 6.2.5 must be carried out.

Finally, in the last two sections a very recent simultaneous demand-supply calibration method was successfully applied to MITSIM. The traditional SPSA was already successfully applied for a single calibration case study, but the enhancements existing in the WSPSA formulation, allowed for an extremely fast convergence. Such fast method is extremely useful when a high number of calibration tasks is at stake, especially if an overall detailed calibration has already been made. The simplifying assumptions made regarding the weight matrix and the combined optimizing function for the A44 case study allowed for a very fast and effective convergence. The relaxation effects of such assumptions in other traffic simulation studies should however be assessed in future work.

Chapter 7

Safety Modelling Results

In this Chapter, estimation results of the probabilistic safety model using the artificial data generated by MITSIMLab are described. A detailed description of the data used for estimation is first presented. Statistical assessment and physical interpretation of the estimation results are then discussed. The model was estimated using the maximum likelihood estimation framework presented in Chapter 3.

7.1 Data for estimation

7.1.1 Accident event starting times

The available accident records report an estimate of the time of occurrence by either the road concessionaire or the police forces. However, it is well known that these records are typically biased due to delays in the emergency call or to wrong human time estimates. It is important to correctly estimate the time of crash occurrence, as the detailed artificial data generated by the simulation will directly depend on it. Thus, the registered accident occurrence time was validated by detecting reductions in the traffic flow and average speed of 25% or more, at the closest downstream loop sensor (see Figure 7-1). Shock-wave speeds were ignored as the traffic data was aggregated by 5 min and the loop sensors are relatively close to each other. The accident occurrence time at very low traffic conditions (e.g.: night time) and those under the influence of traffic disturbances were not identifiable by this process. 67% of the accident records were corrected, resulting in an average and standard deviation delay times of 17 and 11.5 min, respectively (see Figure 7-2).

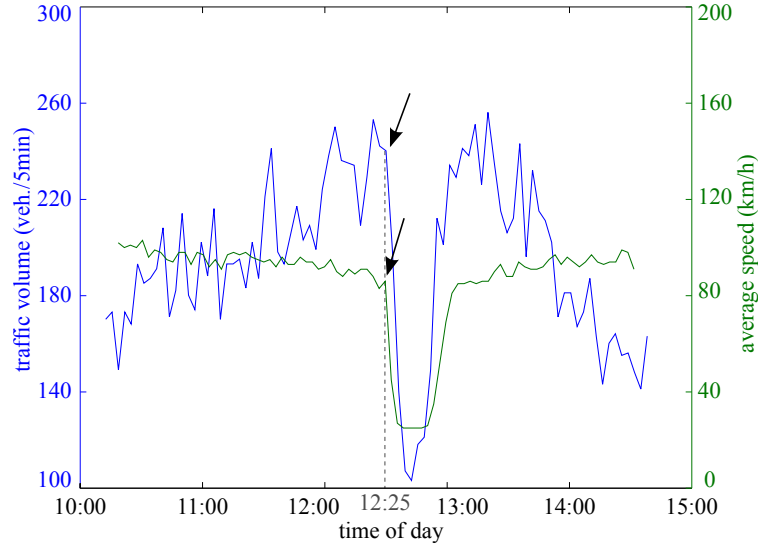


Figure 7-1: Accident occurrence detection example

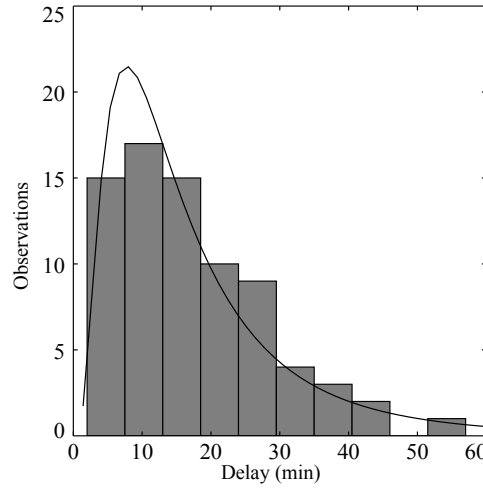


Figure 7-2: Histogram of accident time record delays and log-normal fit

7.1.2 Sampling

As described in Chapter 4, the data available for estimation was collected for the period of 2007 to 2009. Along with the 5 min temporal units for traffic data, the nature of the accident location record required a spatial observation unit of 50 m. These units are the ones to be considered for the aggregation of individual probabilities (vehicle n at time t) defined by equations 3.30 and 3.31.

During the three years in analysis, 173 accidents were recorded. As expected, a very large number of non-accident events were observed during this three years period. With the above spatial and temporal units, 710 segments of 50 m and 257,184 time periods of 5 min (excluding the periods with bad loop sensor data, see section 4.2) were obtained,

resulting in a total of more than 180×10^6 events to be considered for simulation. This number is not only impractical due to infeasible computational times at the simulation level, but also at the safety estimation level, where huge input trajectory files would rapidly fill up current computer memories. To deal with these issues, outcome(choice)-based sampling was introduced in Chapter 3 and the estimation framework was directly formulated to consider this sampling technique by incorporating sampling weights in the WESML likelihood formula:

$$w_g = W_g/H_g. \quad (3.32)$$

where W_g and H_g are the fraction of the population and the sample of members in sampling stratum g , respectively.

As stated, the loop sensor failures also affect the events sampling. These failures were assumed to be independent from any event occurrence and from the explanatory variables considered in the safety model formulation. For accident events, all available accidents with good traffic data were considered. A total of 144 from the 173 accidents ($w_{RE} = 0.803$, $w_{LC} = 0.902$, $w_{ROR} = 0.821$, for rear-end - RE, lane change conflicts - LC and run-off-road - ROR events, respectively) were used for the estimation. As regards the non-accident events (NA), the days with bad sensor data were removed from the available observations set and a random sampling technique was assumed. Due to computational limitations, a weight $w_{NA} = 3.5 \times 10^{-5}$ was selected, such that the simulation time to generate artificial trajectories and the computer memory needed to store them during the model estimation phase would remained tractable. These sampling rates, resulted in a total of 6,544 events to be simulated in MITSIMLab (Table 7.1).

Table 7.1: Events sampling

Events	Total	Sample
Accidents	173	144
No-accidents	182,600,467	6,400
Total	182,600,640	6,544

7.1.3 Simulation parameter values

To better replicate the traffic conditions for each event, a specific calibration based on the existing aggregated traffic data must be carried out (the grey box “Aggregate calibration

for event i'' in the estimation framework Figure 3-6). with this aim, the WSPSA algorithm presented in Chapter 6 was used for the calibration of the 11 most sensitive parameters of MITSIMLab driving behaviour model of each event in the sample considered in Table 7.1. The calibration was based on the traffic conditions for the 30 min periods before the occurrence and on the full parameters set calibrated for the on-site trajectories as starting point. In Figure 7-3, the distribution of the performance of the WSPSA calibration is presented in terms of RMSNE reduction for counts and speeds. Using just 30 iterations of the WSPSA algorithm, the reductions rates are quite satisfactory; yet, for a non-negligible fraction of the events, the reduction rates remained below 10%. These low performances mainly affected events where the starting value of the objective function was already low. Further iterations in a dedicated processing would be necessary to improve these calibrations.

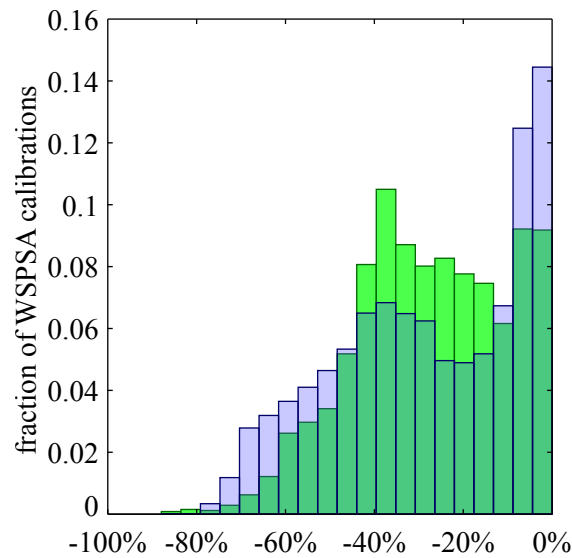


Figure 7-3: Distribution of the RMSNE reduction rates for counts (green) and average speed (blue) during the events calibration

In Figure 7-4 the probability density estimate of the calibrated 11 parameters for accident (red) and non-accident (grey) events is presented. The estimate is based on a normal kernel function, using a window parameter based on 100 equally spaced points that cover the range of each parameter. In blue and green are marked the default parameters estimated by Ahmed (1999) and Toledo (2003), respectively. It is worth remembering that Ahmed (1999) estimated an independent formulation of the lane-changing and acceleration models. Also, it is crucial to understand that there are interactions between these parameters and the analysis of the variability of a single parameter should be carefully

done.

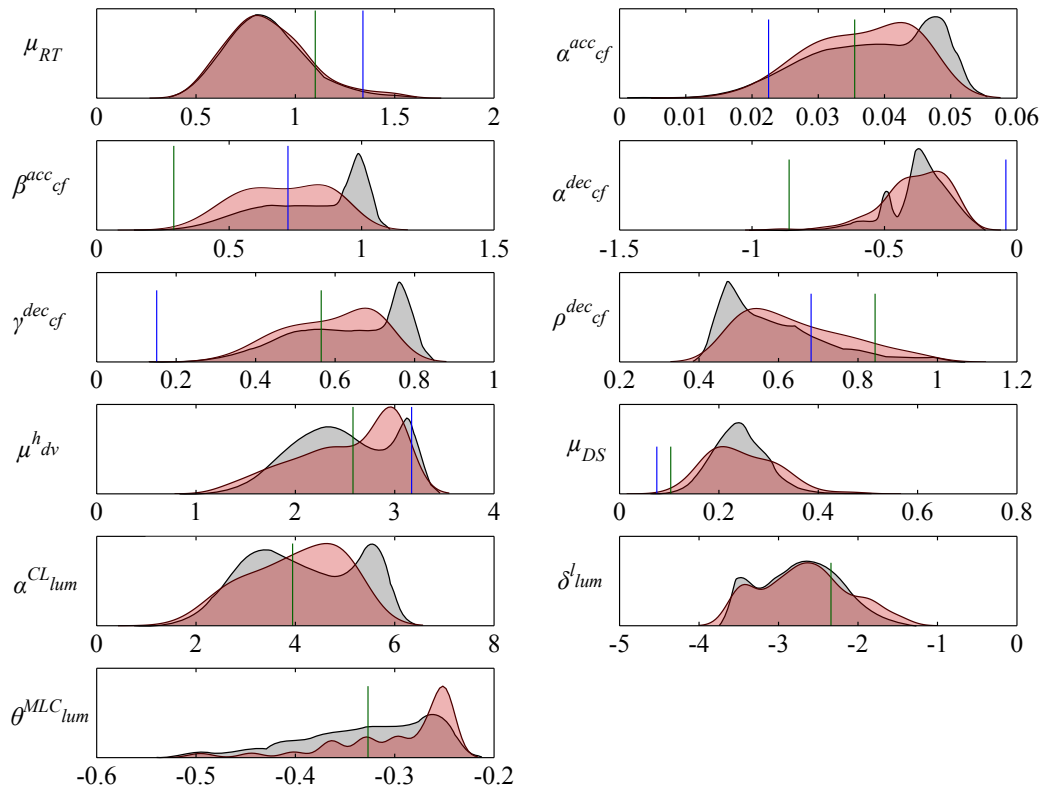


Figure 7-4: Distribution of calibrated parameters for accident (red) and non-accident (grey) events

It is clear from Figure 7-4 that the distribution of μ_{RT} , μ_{DS} , ρ_{cf}^{dec} and θ_{lum}^{MLC} show substantial differences from past estimates. The estimated average reaction time (μ_{RT}) for both calibrated accident and non-accident events remained close to the value estimated using the trajectory data set from Chapter 5 and to typical low safety thresholds values found in the literature. Also, the estimated desired speed add-on (regarding the speed limit) parameter, μ_{DS} , will obviously result in higher free flow speed values.

No significant differences in the distribution of μ_{RT} and μ_{DS} were observed between accident and no-accident calibrations. Lower values for α_{cf}^{acc} and β_{cf}^{acc} were observed for the calibrated accident events, generally resulting in lower car-following (CF) acceleration rates under the same conditions. The lower γ_{cf}^{dec} and higher ρ_{cf}^{dec} for calibrated accident events, result in higher deceleration rates for these conditions: a lower γ_{cf}^{dec} parameter, the headway parameter for the CF model, results in deceleration rates more sensitive to the headway distance to the front vehicle; ρ_{cf}^{dec} is the speed difference deceleration parameter for the CF model and its higher value results in deceleration rates more sensitive to the speed difference between the follower and the leader vehicles. The higher headway

threshold mean μ_{dv}^h for accident events represents a broader control of CF model over the free flow acceleration model, i.e. a vehicle is under the influence of a front vehicle stimulus for larger headways. Finally, the θ_{lum}^{MLC} distribution shows the importance of the distance to the desired exit in the lane change decision. For calibrated accident events, higher parameter values result in an expected higher number of lane changes for shorter distances to exit.

Even if the estimates of straightforward safety influencing parameters such as the reaction time or the desired speed do not have significant differences for both accident and non-accident sample, their combination with other parameters may still be related with unsafer events. The desired speed parameter (as it is specified in MITSIMLab, i.e. only for free flow conditions) for example is not, in fact, a primal factor in the occurrence of the rear-end collisions or side collisions under dense traffic scenarios as observed in the A44. The complexity of the underlying mechanisms of the relationship between the chosen driving behaviour model and unsafe events is thus exposed.

7.1.4 Artificial Data generation

The artificial vehicle trajectory data simulated for the location and time of each occurrence will be used to generate the required variables for the safety assessment model. For the accident occurrences, the 144 simulations resulted in an average of about $1,5 \times 10^5$ observations of vehicle motion variables at a frequency of 1Hz. These observations were recorded for the 50 m section upstream the accident location, and within the 5 min period before its occurrence. The 6,400 no-accident events resulted in an average of about $4,5 \times 10^6$ observations for the same spatial and temporal units. As mentioned in Chapter 6, a high number of replications is always desirable when working with simulated data. However, when dealing with the above mentioned number of observations per simulated scenario, the total number of trajectory records for multiple replications quickly becomes unmanageable during the estimation phase. Thus, due to computational limitations, only three replications of each event were performed. Table 7.2 and 7.3 summarize statistics of several variables for both accident and non-accident events, respectively. The distributions of speed, acceleration, headway are also shown in Figure 7-5.

A few differences between the variables statistics for accident and non-accident may be pointed out:

Table 7.2: Statistics of variables related to artificial trajectories for the 5 min before accident occurrences

Variable	Mean	Std	Median
Speed (m/s)	12.51	10.00	12.19
Acceleration (m/s ²)			
Positive	1.17	0.89	0.93
Negative	-1.10	0.92	-0.87
Headway (m)	21.83	29.87	6.80
Front relative speed (m/s)	0.10	2.33	0.11
Lane change attempts	2.18	1.28	2
Lead Gap (m)	4.49	6.95	1.90
Lag Gap (m)	3.68	5.37	1.87
Lead relative speed (m/s)	3.76	5.84	2.04
Lag relative speed (m/s)	0.33	2.35	0.04

Table 7.3: Statistics of variables related to artificial trajectories for the 5 min before non-accident occurrences

Variable	Mean	Std	Median
Speed (m/s)	18.97	8.78	19.50
Acceleration (m/s ²)			
Positive	0.79	0.61	0.71
Negative	-0.92	0.86	-0.72
Headway (m)	38.23	34.57	29.50
Front relative speed (m/s)	0.27	2.64	0.17
Lane change attempts	2.45	1.35	2
Lead Gap (m)	9.68	10.91	4.5
Lag Gap (m)	10.19	8.71	8.56
Lead relative speed (m/s)	10.14	8.73	8.59
Lag relative speed (m/s)	0.53	1.80	0.55

- The average speed is lower for the accident events sample than for the non-accident events. This suggests that some accidents took place at lower speed sections (such as entry and exit ramps) or under more dense traffic scenarios. However, this lower average speed does not means that the drivers have made adequate speed choices. The speed standard deviation, often used as a surrogate indicator for two-vehicle crashes, is higher. It is also worth pointing out the more closer values of the observed speed statistics extracted from the real trajectories (see for example the mean $22.5m/s$ from Figure 5-7) to the simulated speed statistics of the non-accident events;

- Both acceleration mean and standard deviations are significantly higher for simulated accidents than for non-accident events. Similarly, deceleration values are much more conservative for non-accident events. A possible explanation for these values, is the presence of denser traffic conditions for the simulated accident events. The values simulated by MITSIMLab are far from the thresholds identified in the real trajectories, but still in the range of previously reported trajectory data sets (Toledo, 2003, Choudhury, 2007);
- Front relative speeds are defined as the speed of the front vehicle minus the speed of the subject vehicle, under car-following situations. Their distributions do not differ much for both samples, with a very small mean value and a higher standard deviation. However, the headway values for the accident events are much smaller than for the non-accident;
- The relations between the subject and the lead and lag vehicles affect the gap acceptance and gap choice behaviors and, therefore, lane change conflicts. The statistics of the lead and lag gaps (for both left and right lanes) and relative speeds were only computed when a driver wished to switch lanes. The average values for both lead and lag gaps for accident events are much smaller than the non-accident ones and than those found in previous studies (Toledo, 2003, Choudhury, 2007).

7.1.5 Modelling assumptions

For the computation of the RE (rear-end) and ROR (run-of-road) model components, both $\mu_{long}(n, t)$ in equation 3.10 and $\mu_{lat}(n, t)$ in equation 3.21 must be specified. For the current case study, the following formulation for the friction coefficient was adopted:

$$\mu_g(n, t) = f_g(v(n, t), \alpha^{type}, \alpha^{wet}) \quad (7.1)$$

where μ_g is the longitudinal (*long*) or lateral (*lat*) friction coefficient, which is dependent on the speed of the vehicle $v(n, t)$, with α^{type} and α^{wet} as constant parameters.

Unfortunately, measured values on-site for μ_g are not available. Hence, generic $\mu_g^0(n, t)$ values were adopted based on measurements from other urban freeways found in the literature (Inoue and Hioki, 1993): a direct variation from 0.85 at 0 km/h to 0.75 at 130 km/h for dry pavements and from 0.70 at 0 km/h to 0.20 at 130 km/h for wet pavements

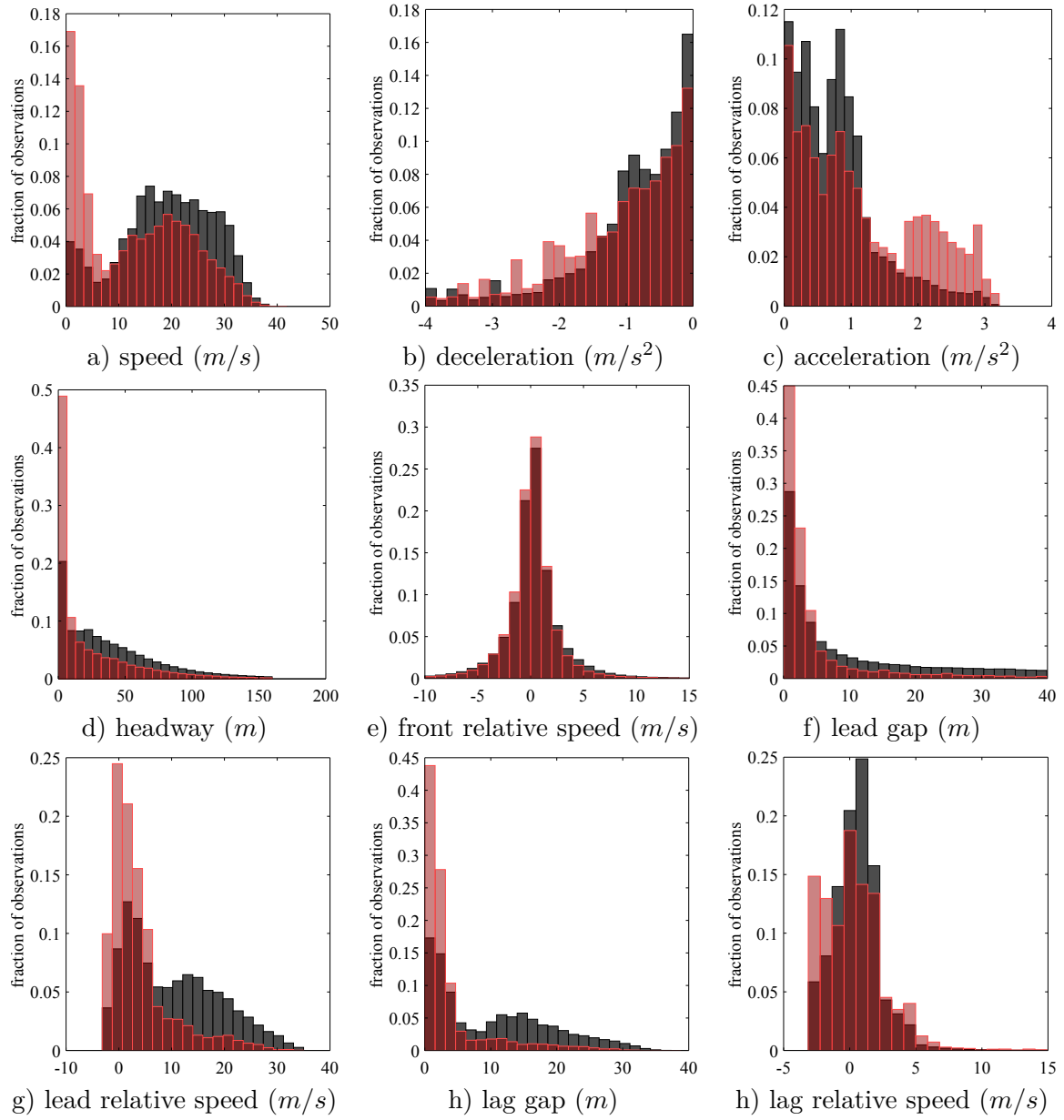


Figure 7-5: Distribution of simulated variables for accident (red) and non-accident (grey) occurrences

for the μ_{long} . An increase factor of 1.10 was considered for the lateral coefficient μ_{lat} . Furthermore, both μ_{long} and μ_{lat} were decreased by a factor of 0.70 for heavy vehicles in dry conditions.

As the road super-elevation e needed for the computation of the ROR (run-of-road) probability (see equation 3.19) is not available, values were estimated using the Portuguese national design standards for dual-carriageway roads.

It is worth pointing out that, estimation accuracy would benefit from field measurements of all these constant parameters. Alternatively, the effect of pre-defined values for these constant parameters may be assessed by means of sensitivity analysis.

The availability of each occurrence alternative was included in the specification of the likelihood function in equation 3.33. A lane change conflict event, for example, is not possible in single lane sections and therefore should not be considered as an available occurrence alternative during the modeling stage. Thus, for each observation of vehicle n at time t :

- a rear-end conflict was considered as possible whenever the subject vehicle n is in a car-following state;
- a lane change conflict was considered as possible if the road carriageway has two or more lanes and if the subject vehicle n wants to perform a lane change;
- a run-of-road event was considered as possible if the road section is a curve or if the subject vehicle n is performing a lane-change.

Finally, another interesting estimation challenge is how to deal with multiple replications. Ideally, multiple replications should be used directly in the estimation phase within a Monte Carlo process, similar to a panel data estimation. In such approach, several observations (replications) for the same event are available and directly included in the safety score function with an additional event specific component (typically, an independent and identically distributed error term). The main burden in such an approach is the computer memory and processing resources needed during the estimation phase. With the above mentioned number of observations per replication, the memory and the processing time required for simulation and estimation quickly reaches unpractical magnitudes. In the current study, the estimation process was carried out by using the multiple replications as independent observations: probabilities are first calculated at the model formulation unit

$\{n, t\}$, aggregated over $\{s, p\}$ and included as r observations in the likelihood function (and therefore, ignoring the existing correlation).

7.2 Results

In this section the results of the safety model estimation are presented. Each considered event may be specified with the generic safety score function:

$$V_k(n, t) = \beta_0^k + \sum_i \beta_i^k X_i^k(n, t) \quad (7.2)$$

where $V_k(n, t)$ is the safety score of event k , β are the model parameters to be estimated and $X_i^k(n, t)$ are the event specific explanatory i variables for an observation of vehicle n at time t . The no-accident event (NA) is used as reference, with $\beta_0^{NA} = 0$. The maximum likelihood estimates of the model parameters are found by maximizing this function:

$$\mathcal{L} = \sum_s \sum_p \sum_k y_{k,s,p} w_k \ln \left[\Pr_{s,p}(k) \right]. \quad (3.33)$$

where k are all possible outcomes considered for the proposed model (see Figure 3-1), $\Pr_{s,p}(k)$ is the probability of outcome k for spatial interval s and time period p (given by equation 3.29), w_k is the outcome k -specific sampling ratio, $y_{k,s,p}$ is 1 if k is the observed outcome for the observation pair s, p and 0 otherwise. In this study, the **PythonBIOGEME** open source freeware, designed for the estimation of discrete choice models, was used (Bierlaire, 2003). **PythonBIOGEME** is a version of **BIOGEME** based on the **Python** language which allows the user to write explicitly the model and the likelihood function.

In this section two different model formulations are presented, discussed and compared:

1. The Aggregate Model (AM), where all observations of each variable collected for each vehicle are aggregated by road segment s (by 50 m long) and event simulation period p (5min) to match the accident data units. The safety score functions, although keeping the same structure and independent variables, are defined for the unit (s, p) :

$$V_k(s, p) = \beta_0^k + \sum_i \beta_i^k X_i^k(s, p) \quad (7.3)$$

where $V_k(s, p)$ is the safety score of event k and, for a road segment s and a period p , β

are the model parameters to be estimated and $X_i^k(s, p)$ are the event specific explanatory variables as specified by equations 3.11, 3.16 and 3.22 but using the variables computed for a unit segment-period (s, p) instead of vehicle-time step (n, t) . This computation of $X_i^k(s, p)$ considered in this model was the average:

$$X_i^k(s, p) = \frac{1}{N} \sum_{n, t} X_i^k(n, t) \quad (7.4)$$

where N is the number of observations of variable X_i^k for all vehicles circulating in segment s during period p . This approach is similar to the real-time accident probability models using simulation found in the literature (see Chapter 2), where simulated traffic statistics for road segments are used in the estimation of the accident probability at a predefined road segment during a standardized time period.

2. The Disaggregate Model (DM) as specified in Chapter 3, equations 3.11, 3.16 and 3.22.

7.2.1 The Aggregated Model (AM)

Estimation results of the AM model are presented in Table 7.4.

The statistic ρ^2 is a transformation of the log-likelihood statistic and is intended to mimic the R^2 metric of linear regression for logistic regressions. $\rho^2 = 1 - \ln(\mathcal{L}_{final}) / \ln(\mathcal{L}_0)$, where \mathcal{L}_0 is the value of the likelihood function for a model with no predictors and \mathcal{L}_{final} the likelihood for the model being estimated; ρ^2 is always between 0 and 1, the greater corresponding to a better fit. $\bar{\rho}^2 = 1 - \ln(\mathcal{L}_{final} - k) / \ln(\mathcal{L}_0)$, with k as the number of parameters being estimated. For numerical reasons, it is good practice to scale the data so that the absolute values of the parameters are between zero and 1 (except the event specific constant parameters β_0 which will be affected by the sampling weights); thus, all relative gap variation variables were divided by 10 and the lateral acceleration difference specified in $0.1m/s^2$.

From Table 7.4, some variables were found to be statistically significant:

- Both the positive and the negative needed relative decelerations ratios (β_1^{RE} and β_2^{RE}) in the RE safety score. The RE event is considered only for car-following states with conflicting trajectories, i.e. only when there is a vehicle in front of the subject vehicle with a $TTC > 0$. When the positive RA^{need} component is close to

Table 7.4: Estimation results for the AM Model

Parameter	value	st. dev.	t-stat.	p-val.
RE constant β_0^{RE}	-14.4*	0.201	-21.88	<0.01
Positive relative needed dec. ratio β_1^{RE}	0.103	0.0352	2.93	0.01
Negative relative needed dec. ratio β_2^{RE}	-0.239	0.112	-2.13	0.03
Max. available dec. ratio β_3^{RE}	-0.102	0.0544	-1.87	0.06
LC constant β_0^{LC}	-14.6*	0.342	-12.96	<0.01
Positive relative lag gap variation β_1^{LC}	-0.0502	0.0727	-0.69	0.49
Negative relative lag gap variation β_2^{LC}	0.0137	0.0529	0.26	0.80
Positive relative lead gap variation β_3^{LC}	-0.063	0.0652	-0.97	0.18
Negative relative lead gap variation β_4^{LC}	-0.115	0.0541	-2.12	0.03
ROR constant β_0^{ROR}	-14.6*	0.281	-15.89	<0.01
Positive lateral acc. difference β_1^{ROR}	1.1	0.437	2.53	0.02
Negative lateral acc. difference β_2^{ROR}	0.376	0.322	1.17	0.26
Scale parameter for the accident nest μ^{m_2}	1.22	0.396	3.09	0.01

N° of parameters: 13 (* parameter affected by weights)
 Sample size: 18969 (3 replications)
 Initial log-likelihood: -13506.281
 Final log-likelihood: -2297.499
 ρ^2 : 0.829
 $\bar{\rho}^2$: 0.828
 Iterations (run-time): 76 (2:08)

zero, the relative deceleration is close to the *DRAC* and thus closer to a safe situation (see equation 3.7). When the averaged positive component RA_+^{need} increases the probability for a RE accident is higher, as the averaged distance between the vehicles relative deceleration rates and their *DRAC* gets higher. Regarding the negative component, i.e. when the follower has already adjusted its acceleration, lower relatives decelerations rates (safer situation) and lower *TTC* (less safer situations) will decrease the averaged RA_-^{need} value. In fact, understanding the sign and magnitude of this parameter is not straightforward. From the estimation, the parameter β_2^{RE} is negative corresponding to an increased RE probability for lower RA_-^{need} values, possibly due to lower *TTC*. Yet, one would expect a higher absolute magnitude for β_1^{RE} .

- The negative component of the lead gap variation during LC events, β_4^{LC} . This parameter is associated with $RG_-^{lead}(n, t)$ defined in equation 3.15. Largest abso-

lute values represent significantly shrinking lead gaps. As $\beta_4^{LC} < 0$, any negative component $RG_-^{lead}(n, t)$ will increase the probability of a LC accident event. The fact that this relative gap variation came out as the most statistically significant of all four components is not surprising, considering the much smaller lead gaps not only when compared to lag gaps but also when comparing accident events with no-accidents (see Figure 7-5).

- The positive lateral acceleration difference for the ROR events, β_1^{ROR} . As mentioned in Chapter 3, the safety score of a ROR event is assumed to be linked to $\Delta a^{lat}(n, t)$, the difference between the current lateral acceleration of a vehicle n and a site specific critical lateral acceleration. When $\Delta a^{lat}(n, t)$ is positive, the lateral acceleration computed by the simulator is higher than the critical lateral acceleration and the vehicle is under unsafe conditions. Under these conditions, the $\beta_1^{ROR} > 0$ will lead to an increased probability of ROR events.

The averaged maximum available deceleration ratio for RE events, β_3^{RE} , also had a satisfactory performance. This parameter accounts for consider heterogeneous safety conditions regarding different vehicle categories and different pavement conditions (e.g. dry/wet). A larger distance between the simulated *DRAC* and the maximum lateral acceleration (thus, a larger RA^{lim}) should result in a larger probability of RE collision. However, the negative sign of the estimated parameter reflects the opposite effect. As this variable is correlated with the relative needed decelerations ratios, due to the intrinsic nature of its calculation being based on the *DRAC*, further tests should be carried out before its consideration in a final aggregated model. Also, the nature of the RE accident occurrence in the A44 motorway might not depend on inappropriate adaptation to pavement surface conditions, but only in the vehicle interaction itself.

The estimated scale parameter of the accidents nest μ^{m_2} was 1.22, resulting in a relatively small effect of shared unobserved attributes between the different types of accident, and therefore still close to a simpler non-nested formulation.

In general, the results are consistent with previous accident probability models based on detailed loop sensor data where the upstream occupancy (and occupancy variance) and speed variance were found to be significantly correlated with the likelihood of accidents (Xu et al., 2013a). The less significant parameters might still have higher statistical importance when using a larger sample during the estimation, as the tests carried out

with smaller samples resulted in higher standard deviation parameters.

7.2.2 The Disaggregated Model (DM)

Estimation results of the DM model are presented in Table 7.5.

Table 7.5: Estimation results for the DM Model

Parameter	value	st. dev.	t-stat.	p-val.
RE constant β_0^{RE}	-13.09*	0.608	-5.08	<0.01
Positive relative needed dec. ratio β_1^{RE}	2.917	0.917	3.18	0.01
Negative relative needed dec. ratio β_2^{RE}	-1.92	0.784	-2.45	0.03
Max. available dec. ratio β_3^{RE}	2.03	1.034	1.96	0.07
LC constant β_0^{LC}	-7.08*	0.457	6.32	<0.01
Positive relative lag gap variation β_1^{LC}	-0.011	0.012	-0.92	0.38
Negative relative lag gap variation β_2^{LC}	-0.568	0.338	-1.68	0.12
Positive relative lead gap variation β_3^{LC}	-0.311	0.255	-1.22	0.25
Negative relative lead gap variation β_4^{LC}	-0.628	0.315	-1.99	0.07
ROR constant β_0^{ROR}	-12.45*	0.367	-6.68	<0.01
Positive lateral acc. difference β_1^{ROR}	0.023	0.013	1.77	0.10
Negative lateral acc. difference β_2^{ROR}	1.775	0.965	1.84	0.09
Scale parameter for the accident nest μ^{m_2}	1.622	0.567	2.86	0.01

N° of parameters: 13 (* parameter affected by weights)
 Sample size: 10733084 (3 replications)
 Initial log-likelihood: -9636.49
 Final log-likelihood: -2047.53
 ρ^2 : 0.787
 $\bar{\rho}^2$: 0.786
 Iterations (run-time): 56 (6d 3h 4:26)

Similarly to the previous model, all relative gap variation variables were divided by 10 and the lateral acceleration difference specified in $0.1m/s^2$, for numerical reasons.

When comparing the estimation results with the previous specification, the statistical significance of some of the model parameters increased along with the magnitude of the estimates, due to the absence of an aggregation effect:

- Both the positive and the negative relative needed decelerations ratios (β_1^{RE} and β_2^{RE}) in the RE safety score. Similarly to the previous analysis, positive relative needed decelerations ratios close to zero represent safer situations. When the posi-

tive component RA_+^{need} increases the probability for a RE accident is higher. However, the much higher estimate for β_1^{RE} when compared to the AM model, will result in much higher probabilities for vehicles with extreme RA_+^{need} . Here, β_1^{RE} has a higher absolute magnitude thus penalizing much more any safety decay in the unsafe domain ($RA^{need} > 0$) rather than in the safe one ($RA^{need} < 0$). Again, lower RA_-^{need} will result in an increased RE probability due to lower TTC .

- The positive sign of β_3^{RE} and its statistical significance makes the consideration of different exogenous safety conditions non-negligible in a disaggregated formulation. It is worth pointing out that both the vehicle category and the pavement (wet/dry) conditions were considered.
- The negative components of the lead and lag gaps variation during LC events, β_2^{LC} and β_4^{LC} . Again, the fact that the lead relative gap variation came out as the most statistically significant and with higher magnitude is due to the much smaller simulated lead gaps during lane-change not only when compared to lag gaps but also when comparing accident events with no-accidents (see Figure 7-5). Although still having low performances, the statistical significance and the estimates signs and magnitudes of the other relative gap variations are now consistent with the model assumptions.
- Both the positive and negative lateral acceleration difference for the ROR events, β_1^{ROR} . As mentioned in Chapter 3, the safety score of a ROR event is assumed to be linked to $\Delta a^{lat}(n, t)$, i.e. the difference between the current lateral acceleration of a vehicle n and the site-specific critical lateral acceleration. When $\Delta a^{lat}(n, t)$ is positive, the lateral acceleration computed by the simulator is higher than the critical lateral acceleration and the vehicle is under unsafe conditions. Under these conditions, when $\beta_1^{ROR} > 0$ there is a higher probability of ROR events. Similarly, when $\Delta a^{lat}(n, t)$ is negative, larger absolute values are related to safer conditions, as the simulated lateral acceleration is much smaller than the critical one ($\beta_2^{ROR} < 0$). Yet, one would expect a higher absolute magnitude for β_1^{ROR} , but these results may be justified with the small number of observations with $\Delta a^{lat}(n, t) > 0$.

The smaller value of ρ^2 is due to the absence of the aggregation effect. Yet, the resulting final log-likelihood value is better than in the previous model. To statistically compare the

two models, the Akaike information criterion (AIC) can be used Akaike (1973). The AIC penalizes the maximum likelihood value of each model to account for model complexity:

$$AIC = -2\mathcal{LL}(\beta^*) + 2k \quad (7.5)$$

where $\mathcal{LL}(\beta^*)$ is the maximum log-likelihood value, k is the number of estimated parameters (ignoring the sample size correction, as both models have large samples). For the present case, the AIC criteria relies in the model with the smaller log-likelihood value, as the number of parameters is the same, thus recommending the DM model over the aggregated one.

The final model was re-estimated without the non-statistically significant variables. In summary, the safety model can be formulated by a nested structure for the available accidents with a scale parameter of 1.62 and the following safety scores:

$$V^{RE}(n, t) = -13.09 + 2.917 \times RA_+^{need}(n, t) - 1.921 \times RA_-^{need}(n, t) + 2.03 \times RA^{lim}(n, t) \quad (7.6)$$

$$V^{LC}(n, t) = -7.05 - 0.568 \times RG_-^{lag} - 0.628 \times RG_-^{lead} \quad (7.7)$$

$$V^{ROR}(n, t) = -12.45 + 0.023 \times \Delta a_+^{lat}(n, t) + 1.77 \times \Delta a_-^{lat}(n, t) \quad (7.8)$$

7.3 Validation

In this section, validation results of the probabilistic safety assessment model are reported and compared against the aggregate model. As no other accident data set was available, the validation was performed using a new set of artificial data, generated by **MITSIMLab** for the same sample of events. Two additional replications of the calibrated model of the A44 were carried out generating two new artificial data sets.

In Table 7.6 the ratio of the averaged probabilities between a specific type of accident and no-accident events are presented for the estimation and validation data sets.

The range of both input variables and estimated probabilities for the validation data set are similar to the estimation ones. Yet, significant differences are observed for the DM model, where much higher probabilities of each of the accident types considered are obtained. The trade-offs captured by the model are also visible, especially between the rear-end and lane-change conflicts.

Table 7.6: Probability ratios

Events		AM			DM		
		$Pr(RE)$	$Pr(LC)$	$Pr(ROR)$	$Pr(RE)$	$Pr(LC)$	$Pr(ROR)$
Estimation	RE	1.193	1.422	1.022	3.783	3.880	0.359
	LC	1.075	2.473	1.028	2.284	3.581	0.468
	ROR	0.935	0.703	1.361	1.755	0.499	1.241
Validation	RE	1.170	1.575	1.150	4.352	5.824	0.344
	LC	1.132	2.123	1.025	2.363	3.027	0.391
	ROR	0.872	0.697	1.373	1.306	0.277	1.299

It is worth pointing out that the DM may also be validated at the vehicle level, as its structure was formulated as such. In Table 7.7 the accuracy rates of the accident types considered in the DM framework are presented using the validation data set. In a previous model using real loop sensor data, Oh et al. (2001) estimated the prediction accuracy for accidents and non-accidents as 55.8% and 72.1%, and a false alarm rate of 27.9%. more recently, Xu et al. (2013a) estimated the same rates as 61.0%, 80.0% and 20.0%, respectively. The rates obtained with the proposed model with artificial data still remain bellow the values found in the literature for aggregated models using real data. The small sample used for estimation and the limited number of model formulations tested affected this number. Yet, the false alarm rate is considerably lower then values reported in other studies, indicating a high specificity of the proposed model. Also, the flexible nature of the model specification allows for an easy enhancement in future applications.

Table 7.7: Summary of predictive performance (%)

	DM
Accuracy of accidents	38.6%
Accuracy of NA	92.1%
False alarms	7.9%

7.4 General Comments

In this chapter, the modelling assumptions for the probabilistic safety assessment estimation were discussed. Estimation results for an aggregated model using averaged traffic

data statistics and the disaggregated model specification presented in Chapter 3 were presented and compared. Both estimations captured trade-offs between the different accident types, captured by the nested structure. However, the contribution of these shared unobserved effects was more significant in the disaggregated formulation, where individual driver interactions are modelled.

Not all variables considered for estimation resulted in statistically significant parameters. In the rear-end conflicts safety score, the importance of the needed deceleration ratios was evident. The benefits of extra deceleration rates in scenarios with conflicting trajectories where the driver has already adjusted his acceleration is lower than for those where he still hasn't. The maximum available deceleration ratio is also non-negligible for the disaggregated model, corroborating the importance of considering heterogeneous safety conditions, as already suggested in recent studies.

The lane-change conflict probability was found to be linked to shrinking lead gaps. This is compatible with the specification assumption and with the smaller lead gaps observed during lane-changes (when compared to the lag gaps). Yet, further validation with real individual data collected for accidents during lane change manoeuvres is needed.

Run-off-road events would be easier to model if no direct interaction between vehicles was considered. However, it is known that there are trade-offs between this type of accidents and rear-end and side conflicts. The nested structured allowed to capture these trade offs. Furthermore, these accidents are typically more data demanding in terms of detailed vehicle and road characteristics and the proposed safety score formulation can easily integrate such information.

Despite the successful estimation results, further enhancements of the model should be tested. While several variable transformations (e.g.: use of absolute values instead of ratios) were tested for the aggregated formulation, only simple variations of the proposed framework were tested in the disaggregated structure due to computational time limitations. The interaction between vehicle gaps and relative motions has been proved as a key factor for accident occurrence in previous safety related studies. Yet, no probabilistic formulation accommodating such interaction and integrated in traffic simulation models was found in the literature. In the presented estimation these factors came out as relevant.

The small sample size for all three types of accidents affected the statistical performance of the model. Also, only data from the A44 was available and the extension

of the modelling framework to different traffic scenarios will probably enhance the final performance.

Finally, it is important to point out that the integration of such safety model into simulation tools and its use for traffic management policy implementation requires further estimation and validation tasks, as only scant information was available for this study. Yet, the flexible structure and methodology demonstrated in this document allows for a valid and consistent assessment of accident occurrence for specific driving behaviour models. It is worth remembering that the modelling and estimation structures were formulated in terms of expected behavioural considerations but constrained by the driving behaviour simulation model limitations. In fact, when a safety assessment model (probabilistic or not) is integrated into a simulation tool, the safety formulation should also consider the modelling assumptions and limitations of the traffic simulator. The choice of **MITSIMLab** relied on its ability to outrun several other driving behaviour models in dense traffic motorway scenarios; the estimation results presented in this Chapter are closely linked to its structure, formulation and performance.

Chapter 8

Conclusions

This chapter summarizes the research presented in this dissertation and highlights the major contributions achieved. Directions for future research are suggested in the closing section.

8.1 Research Summary

Traffic microsimulation applications are currently becoming a common tool in both the transportation practitioners and researchers communities. The original purpose for developing such tools was network efficiency assessment; currently, numerous successful applications with this aim may be found in the literature. The need for simultaneously assessing other impacts of transportation systems soon arose and analytical extensions such as vehicular networks efficiency or fuel consumption and emissions models were quickly integrated in many microscopic tools. However, despite several enhancements at the driving behaviour modelling level, safety assessment has always been frequently neglected as a result of the limited model formulation of driver's perception, decision and error mechanisms that have an important share in accident genesis. In recent years, several efforts to enhance driving behaviour models have been made. Simultaneously, methods have also been proposed to extract safety measurements relevant for safety surrogate indicators calculation from the current state-of-the-art simulation tools.

The link between accident occurrence and simulated traffic variables has typically been achieved by fitting a regression model using linear and non-linear combinations of aggregated traffic variables or surrogate safety indicators. In such approaches, four main

problems may be mentioned: the absence of a causal relationship between different levels of vehicle interactions; the lack of discrimination between distinct cause-effect relationships for different types of accidents; the absence of a specific interaction between different types of conflicts; and statistical problems of aggregation due to the use of aggregate traffic data and count safety records.

The focus of this thesis is the development of a probabilistic safety assessment framework for traffic microscopic simulation tools. A generic framework for modelling cause-effect mechanisms between detailed traffic variables and the accident occurrence probability is proposed. The probability for a specific accident occurrence k is assumed to be estimable by an accident propensity function U_k , composed by a (deterministic) safety score (V_k) component and a random component (ε_k). The assumption of the deterministic safety score component agrees with recent research streams, where detailed interaction variables, road and environmental characteristics, and vehicle specific motion variables are assumed to directly affect the accident occurrence probability. The random component ε is assumed to represent the unobserved effects involved in the determination of the outcome, whether these are derived from a random process in the occurrence of a specific event outcome or caused by a lack of knowledge of this process. As the accident phenomenon is expected to differ for distinct types of accidents, the formulation of the safety score will depend on the type of outcome k . Lastly, as accidents may be triggered by evasive manoeuvres to avoid an accident of a different type, interactions between different types of accident are integrated directly in the model structure. This prevented the use of an ordered (hierarchical) structure for the generic event modelling.

The proposed generic event model is then specified for the case of urban motorways using a nested logit structure for no-accident events and three types of accidents: rear-end, lane-changing and run-of-road accidents. The rear-end safety score component is formulated in terms of needed additional deceleration to reach a safe state (specified in terms of the deceleration rate to avoid crash) and time-to-collision; the lane-changing safety score component is formulated in terms of relative available gap variations; and the run-of-road safety score is formulated in terms of the actual speed difference to a local-specific critical speed value. The model is specified in terms of event probabilities for any time t and for any vehicle n . However, as there is still no available large disaggregated data set linking trajectories to accident occurrence, a probability aggregation procedure

integrated in the estimation framework is required. Moreover, the weighted exogenous sample maximum likelihood is used for model estimation using different sampling rates for accident and no-accident events.

The final estimated safety model allowed for the identification and interpretation of several vehicle interactions at stake. Rear-end accident probability is linked to the needed deceleration ratios. The benefits of extra deceleration rates for scenarios with conflicting trajectories where the driver has already adjusted its acceleration is lower than for those where he still hasn't. The maximum available deceleration ratio is also non-negligible, corroborating the importance of the consideration of different exogenous safety conditions. The lane-change conflict probability is mainly connected with shrinking lead gaps; and run-off-road events to available lateral accelerations. The nested structure allowed to capture existing trade offs between these three types of accidents. The fact that these considerations were extracted from simulated analysis shows the real potential of traffic microscopic simulation regarding detailed safety assessments.

To deal with the lack of real trajectory data sets for different occurrence types, calibrated artificial trajectories from a microscopic simulation tool are used for the model estimation. The calibration task is therefore a key aspect, as it is assumed that the microsimulation model is able to appropriately replicate detailed statistics. Enhanced trajectory estimates are achieved through a comprehensive calibration effort: extracting trajectories for a specific scenario, calibrate the simulation tool for this specific scenario using trajectories, and re-calibrate the microsimulation model for each of the events aimed for replication, using aggregate data.

A method for automatic extraction of vehicle trajectories using aerial imagery was developed, in order to collect the needed detailed traffic variables. This method is based on colored high-resolution images and on the k-shortest disjoint paths algorithm adapted for a motion based optimization. With this method a large set of trajectories was successfully extracted, in spite of the limited resources available for data collection.

The entire problem of calibration is then treated under the light of uncertainty management. A global sensitivity analysis based calibration was developed, where a multi-step approach is formulated to identify and estimate a large set of parameters. At each step, the parameters are grouped on the basis of their possible common features. The groups that account for the highest share of the outputs' variance are selected for further analysis.

At the end, a final variance based sensitivity analysis on the parameters pertaining to the most influential groups can be performed to individuate the most important among them. Then, to better represent the model variability, rather than finding the parameter combination that best reproduces the real measures, a set of combinations for which the model behaves relatively well is analysed and the model stochasticity in the form of distributions of model outputs are monitored. Finally, a very recent simultaneous demand-supply calibration method, called the weighted simultaneous perturbation stochastic approximation (Lu et al., 2013), is tested and successfully used in the calibration of each occurrence event. Then, the artificial data for safety estimation is finally generated.

All the above models and algorithms were tested with data from the A44 motorway near Porto, Portugal, and using the microscopic traffic simulator **MITSIMLab**. The flexible structure and methodology proposed in this document allows for a valid and consistent assessment of accident occurrence under **MITSIMLab** specific driving behaviour models. It is worth remembering that the modelling formulation and estimation was formulated in terms of real behavioural considerations but constrained by the simulated driving behaviour model limitations. In fact, it is expected that when integrating a safety assessment model (probabilistic or not) into a simulation tool, the road safety formulation should consider the modelling assumptions and limitations of the traffic simulator.

8.2 Directions for Future Research

The development of safety assessment methods has been consistent and sustained by continuous improvements in data collection equipment, relevant statistical methods and computational performances. However, the largest efforts have been developed regarding the individual analysis of several key factors at stake: road geometry, driver attention, mechanical features. With the coming increased availability of new types of on-site and on-board large data sets it is expected that in the near future several field of potential research streams in safety modelling will be explored. Furthermore, the development of more advanced driving behaviour models has increased the potential use of microscopic traffic simulation tools. Yet, much more remains to be learned and tested; some the directions for further research derived from the present study are presented below:

- The availability of large detailed trajectory data sets, such as the SHRP2 in the

USA (Antin et al., 2011) and the U-Drive in Europe (SWOV, 2013), will be a key source for potential improvements in the development of probabilistic safety models. Conflict probabilities may, in fact, be directly computed from possible trajectories estimated at every time step against feasible evasive manoeuvres. This will avoid the use of aggregate safety data in the estimation process, and allow for the estimation of the probabilities based on both accident and near-accident trajectories, driving error models and safety thresholds.

- The most recent driving behaviour model formulations already allow for several improvements (especially regarding the car following behaviour model) such as decoupling the simulation step from reaction times, adding look-ahead abilities, making the estimation of the leader’s deceleration more flexible, accounting for anticipation and supporting multiple regime decisions. However, even considering that the number of sub-models and their parameters has grown significantly, results at the disaggregated level, such as detailed vehicle interactions, are not always well replicated. Furthermore, several conceptual perception and error modelling frameworks have not yet been tested under integrated traffic microscopic simulation tools. Implementing non-accident-free models relies in cognitive and driving error modelling structures that seem to be the coming step to improve results reliability and to provide a more general framework compatible with safety analysis.
- Several enhancements regarding the specific formulation of the proposed probabilistic safety model for urban motorways may be introduced, following on data availability and the development of novel driving behaviour modelling features: the inclusion of ignored components in the safety scoring function (e.g.: lateral movement), the formulation of non linear safety score functions, the specification of additional accident types, the addition of driver and segment specific error terms, and the definition of a more advanced modelling structure such as the mixed logit formulation.
- Traffic interactions were considered in the computation of the individual accident occurrence probability. However, it was disregarded that a second vehicle might be involved in the event outcome. In RE events, the interactions were formulated in terms of subject vehicle and its leading vehicle, ignoring the influence of joint probabilities. However, in the LC events, if both drivers want to switch to the

same lane or to swap lanes and are, therefore, the conflicting vehicle of each other, the probability of a LC accident will be considered twice; yet, in this case just one outcome is possible. To account for such dependencies, the model formulation will need to be more complex. A different model formulation, considering each interaction $\{n_1, n_2, t_1\}$ (instead of a vehicle state $\{n, t\}$) as an observation needs to be specified if these situations are frequent, such as near congestion traffic conditions.

- The proposed model still needs a validation using different accident data sets and motorway layouts. Performing this task depends, however, on the availability of such data. Similarly, assumptions made regarding the constant parameters (e.g.: friction coefficient, maximum lateral acceleration when performing a lane change...) would benefit from being estimated using field data. Although no significant differences are expected regarding the model coefficient magnitudes, a sensitivity analysis should still be performed to enhance the model robustness.
- Besides the validation using other sets of data and traffic scenarios, a benchmark against a few existing safety assessment tools using traffic microscopic simulation would be valuable. The first steps in the compatibility between the "state-of the-practice" Safety Assessment Model (SSAM) developed by the Federal Highway Administration (Gettman et al., 2008) and MITSIMLab have been established. SSAM examines one by one the paths of vehicles and identifies potential conflicts; it was described in more detail in Chapter 2. SSAM calculations are based in a specific (binary) trajectory format (.trj). Although other traffic microscopic simulation tools already have an SSAM specific export option, a Java tool was developed for transforming MITSIMLab trajectory output into the .trj file. A robust statistical benchmark between the proposed approach and the SSAM should be expected in the near future.
- The use of artificial data for model estimation is still not a widely used method. As mentioned in the previous Chapter, several estimation simplifications had to be assumed for the computational tractability of this complex problem, namely through a separate estimation for different replications of the simulated events. As a promising enhancement to the current estimation method, multiple replications may be used directly in the estimation phase within a Monte Carlo simulation process, similar to a panel data estimation. In such approach, several observations

(replications) for the same person (event) are available and directly included in the safety score function with an additional event specific component (typically, an independent and identically distributed error term).

Motion parameters successfully extracted from the vehicle tracking algorithm based on aerial remote sensing successfully allowed for the characterization of driving behaviour. However, this task also raised some challenging research questions deserving further study and experimentation.

- The influence of aerial remote sensing system parameters (such as flight and stabilizing platform motion parameters) and image conditions (such as shadows, different ground sampling distance and occlusions) different from those observed for the present case study were not evaluated. These and the possibility for different configurations of the image collection systems (Unmanned Aerial Vehicles, stereo imagery, etc) should be assessed as they may bring a much higher flexibility and efficiency to the process.
- The tracking algorithm was initially developed by Berclaz et al. (2011) for real-time operation. In the present case study, the motion based adaptation was implemented off-line. Extending the tracking algorithm for real-time applications will substantially increase the potential for its widespread and a much more straightforward trajectory extraction.
- Finally, the original specification of the Suurballe algorithm (Suurballe, 1974) applied to Dual graphs does not always converge to the true optimal solution, due to dependencies between different nodes in the dual graph. A possible solution to be tested is the use of an Integer Programming (IP) formulation, as proposed by (Berclaz et al., 2011), instead of the graph-oriented formulation.

Finally, the proposed sensitivity analysis based calibration resulted in successful fits for the present case study. Yet, a couple of future enhancements were detected during the development and application tasks:

- The proposed global sensitivity analysis was only tested for a particular urban motorway scenario and a specific microscopic simulation tool. In future applications, the efficiency of the proposed method should also be tested for different motorway scenarios, and different driving behaviour model structures should also be assessed;

- The adopted driving behaviour model calibration procedure using trajectory data was specified based on an aggregate formulation. Traditional complex methods generally estimate specific driving behaviour model parameters based on observations from scenarios where the driver tasks of interest are expected to be frequent, using maximum likelihood or Bayesian techniques directly on space-time observations, and outside of the simulation tool. Alternatively, one may want to specify a disaggregated calibration, where an optimizing function is specified in terms of space-time observations. The simulation tool must then be configured to match each real initial trajectory and the simulation positions be compared to the real ones. To fully assess the efficiency of the aggregated calibration logic using disaggregated data presented in this thesis, a comparison with these other estimation frameworks needs to be carried out.

Whereas the research innovations regarding trajectory extraction and the traffic simulation calibration presented in this thesis are ready for practitioners use, several new research questions arose during the safety modelling research. The results obtained in the presented case study are promising, especially when considering the flexible and innovative structure of the probabilistic assessment. Yet, despite the decades of separate developments, driving behaviour modelling and safety probabilistic modelling streams have only very recently merged as a single problem. At the same time, these models must cope with the constant integration of new elements into the transportation system, namely the developments made by the automotive and the transportation technologies industries. Based on the extension of the state-of-the-art on simulated safety modelling presented in this document, several challenging efforts to better model and predict accident occurrences with computational applications were proposed. These efforts relied on mandatory data and modelling requirements that have to be met for the successful application of probabilistic frameworks to simulated traffic environments. If such requirements are satisfied, microscopic traffic simulation tools can be used as a tool for comparative safety evaluation of traffic system's operation.

Bibliography

- Abdel-aty, M., Gayah, V., 2010. Real-Time Crash Risk Reduction on Freeways Using Coordinated and Uncoordinated Ramp Metering Approaches. *ASCE Journal of Transportation Engineering* 136 (5).
- Abdel-aty, M., Pande, A., Das, A., Knibbe, W. J., 2008. Assessing Safety on Dutch Freeways with Data from Infrastructure-Based Intelligent Transportation Systems. *Transportation Research Record: Journal of the Transportation Research Board* 2083, 153–161.
- Abdel-aty, M., Pande, A., Lee, C., Gayah, V., 2007. Crash Risk Assessment Using Intelligent Transportation Systems Data and Real-Time Intervention Strategies to Improve Safety. *Journal of Intelligent Transportation Systems* 11 (3), 107–120.
- Abdel-Aty, M., Pemmanaboina, R., 2006. Calibrating a Real-Time Traffic Crash-Prediction Model Using Archived Weather and ITS Traffic Data. *IEEE Transactions on Intelligent Transportation Systems* 7 (2), 167–174.
- Abdel-aty, M., Pemmanaboina, R., Hsia, L., 2006. Assessing crash occurrence on urban freeways by applying a system of interrelated equations. *Proceedings of the 85th Annual Meeting of the Transportation Research Board* (November 2005).
- Abdel-aty, M., Uddin, N., Pande, A., 2005. Split Models for Predicting Multivehicle Crashes During High-Speed and Low-Speed Operating Conditions on Freeways. *Transportation Research Record* (1908), 51–58.
- Abdel-Aty, M., Uddin, N., Pande, A., Abdalla, M. F., Hsia, L., Abdelwahab, H., Jan. 2004. Predicting Freeway Crashes from Loop Detector Data by Matched Case-Control Logistic Regression. *Transportation Research Record* 1897 (1), 88–95.
- Abdelwahab, H., Abdel-Aty, M., Jan. 2001. Development of Artificial Neural Network Models to Predict Driver Injury Severity in Traffic Accidents at Signalized Intersections. *Transportation Research Record* 1746 (1), 6–13.
- Abdelwahab, H., Abdel-Aty, M., Jan. 2002. Artificial Neural Networks and Logit Models for Traffic Safety Analysis of Toll Plazas. *Transportation Research Record* 1784 (1), 115–125.
- Absil, N., 2008. Driver Behaviour Model For the Multi-Agent Real-time Simulation. Msc, Delft University of Technology.
- Ahmed, K., 1999. Modeling Drivers' Acceleration and Lane Changing Behavior. Ph.D. thesis, Massachusetts Institute of Technology.
- Akaike, H., 1973. Information theory and an extension of the maximum likelihood principle. In: Csake, B. P., F. (Eds.), *Second International Symposium on Information Theory*. pp. 267–281.

- Allen, B., Shin, T., Cooper, P. J., 1978. Analysis of traffic conflicts and collisions. Transportation Research Record: Journal of the Transportation Research Board 667, 67–74.
- Angel, A., Hickman, M., Mirchandani, P., Chandnani, D., 2003. Methods of Analyzing Traffic Imagery Collected From Aerial Platforms. IEEE Transactions on intelligent transportation systems 4 (2), 99–107.
- ANSR, 2013. Sinistralidade Rodoviária para o ano de 2012. Tech. rep., Autoridade Nacional de Segurança Rodoviária, Lisbon, Portugal.
- Antin, J., Lee, S., Hankey, J., Dingus, T., 2011. Design of the In-Vehicle Driving Behavior and Crash Risk Study. SHRP 2 Report S2-S05-RR-1. Tech. rep., Transportation Research Board, Washington, D.C.
- Antoniou, C., Auberlet, J.-M., Lima Azevedo, C., Barceló, J., Bhaskar, A., Flötteröd, G., Buisson, C., Casas, J., Ciuffo, B., Daamen, W., Hoogendoorn, S. P., Knoop, V., Ou, Q., Kolehkina, T., Toledo, T., Koutsopoulos, H., Leonhardt, A., Liu, R., Punzo, V., Vortisch, P., Peter Wagner, 2011a. Review of traffic data collection and estimation techniques and review of methodologies for traffic estimation, calibration and validation. Draft version of the State-of-the-art report of the MULTITUDE COST Action (TU0903). Tech. rep., COST Action TU0903.
- Antoniou, C., Balakrishna, R., Koutsopoulos, H. N., Ben-Akiva, M. E., 2011b. Calibration methods for simulation-based dynamic traffic assignment systems. International Journal of Modelling and Simulation 31 (3).
- Antoniou, C., Ben-Akiva, M. E., Koutsopoulos, H. N., Jan. 2004. Incorporating Automated Vehicle Identification Data into Origin-Destination Estimation. Transportation Research Record: Journal of the Transportation Research Board 1882, 37–44.
- Aoude, G. S., Desaraju, V. R., Stephens, L. H., How, J. P., Jun. 2011. Behavior classification algorithms at intersections and validation using naturalistic data. In: 2011 IEEE Intelligent Vehicles Symposium (IV). IEEE, pp. 601–606.
- Archer, J., 2001. Developing micro-simulation for the assessment of safety in relation to intelligent speed adaptation. In: Conference presentation, article published in 8th World Congress on ITS. pp. 1–8.
- Archer, J., 2005a. Indicators for traffic safety assessment and prediction and their application in micro-simulation modelling : A study of urban and suburban intersections. Ph.D. thesis, KTH - Royal Institute of Technology.
- Archer, J., 2005b. Indicators for traffic safety assessment and prediction and their application in micro-simulation modelling : A study of urban and suburban intersections Doctoral Thesis Stockholm , Sweden 2005. Ph, KTH - Royal Institute of Technology, Stockholm, Sweden.
- Ariza, A., 2011. Validation of Road Safety Surrogate Measures as a Predictor of Crash Frequency Rates on a Large-Scale Microsimulation Network by Validation of Road Safety Surrogate Measures as a Predictor of Crash Frequency Rates on a Large-Scale Microsimulation Network. Msc, University of Toronto.
- Asakura, Y., Hato, E., Kashiwadani, M., 2000. Origin-destination matrices estimation model using automatic vehicle identification data and its application to the Han-Shin expressway network.

- Ashok, K., 1996. Estimation and Prediction of Time-Dependent Origin-Destination Flows. Phd thesis, Massachusetts Institute of Technology, Cambridge, USA.
- Ashok, K., Ben-Akiva, M. E., May 2002. Estimation and Prediction of Time-Dependent Origin-Destination Flows with a Stochastic Mapping to Path Flows and Link Flows. *Transportation Science* 36 (2), 184–198.
- Astarita, V., Guido, G., Vitale, A., Giofr , V., 2012. A new microsimulation model for the evaluation of traffic safety performances. *European Transport \ Trasporti Europei* (51).
- Azeredo Lopes, S. M., Cardoso, J. a. L., 2009. Accident prediction models for bidirectional data on portuguese motorway. Tech. rep., LNEC, National Laboratory of Civil Engineering, Lisbon, Portugal.
- Balakrishna, R., Antoniou, C., Ben-Akiva, M. E., Koutsopoulos, H., Wen, Y., Jan. 2007. Calibration of Microscopic Traffic Simulation Models: Methods and Application. *Transportation Research Record* 1999 (1), 198–207.
- Balmer, M., Axhausen, K., Nagel, K., Jan. 2006. Agent-Based Demand-Modeling Framework for Large-Scale Microsimulations. *Transportation Research Record* 1985 (1), 125–134.
- Bando, M., Hasebe, K., Nakayama, A., Shibata, A., Sugiyama, Y., 1995. Dynamical model of traffic congestion and numerical simulation. *Physical Review E* 51 (2), 1035–1042.
- Barcel , J., Sep. 2010. *Fundamentals of Traffic Simulation*, 1st Edition. Springer.
- Barcel , J., Casas, J., 2003. Dynamic network simulation with AIMSUN. In: *Proceedings of the International Symposium on Transport Simulation*. Yokohama, Japan, pp. 1–25.
- Barcel , J., Montero, L., Marqu s, L., Carmona, C., Jul. 2010. A Kalman-Filter Approach For Dynamic OD Estimation In Corridors Based On Bluetooth And Wifi Data Collection. In: *Proceedings of the 12th World Conference on Transport Research*. Lisbon, p. 29.
- Bartin, B., Ozbay, K., Yanmaz, O., Rath, N., Sep. 2005. Modeling and simulation of an unconventional traffic circle. pp. 384 – 389.
- Basak, K., Hetu, S., Li, Z., Lima Azevedo, C., Loganathan, H., Toledo, T., Xu, R., Xu, Y., Peh, L.-S., Ben-Akiva, M. E., 2013. Modeling reaction time within a traffic simulation model. In: *92nd Annual meeting of the Transportation Research Board*. Transportation Research Board, Washington D.C., USA, p. 19.
- Beegala, A., Hourdakis, J., Michalopoulos, P., Jan. 2005. Methodology for Performance Optimization of Ramp Control Strategies Through Microsimulation. *Transportation Research Record: Journal of the Transportation Research Board* 1925 (1), 87–98.
- Bellman, R., 1958. On a routing problem. *Quarterly of Applied Mathematics* 16, 87–90.
- Ben-Akiva, M. E., 1973. Structure of passenger travel demand models. Ph.D. thesis, Massachusetts Institute of Technology.
- Ben-Akiva, M. E., Lerman, S. R., 1985. *Discrete choice analysis: theory and application to travel demand*. MIT Press.
- Berclaz, J., Fleuret, F., Turetken, E., Fua, P., Sep. 2011. Multiple Object Tracking Using K-Shortest Paths Optimization. *IEEE Transactions on Pattern Analysis and Machine Intelligence* 33 (9), 1806 –1819.

- Bevrani, K., Chung, E., Dec. 2011. An Examination of the Microscopic Simulation Models to Identify Traffic Safety Indicators. *International Journal of Intelligent Transportation Systems Research* 10 (2), 66–81.
- Bhattacharya, S., Idrees, H., Saleemi, I., Ali, S., Shah, M., 2011. Moving Object Detection and Tracking in Forward Looking Infra-Red Aerial Imagery. In: McMillan, R. W. (Ed.), *Machine Vision Beyond Visible Spectrum (Augmented Vision and Reality)*. Springer, pp. 221–252.
- Bierlaire, M., 2003. BIOGEME: A free package for the estimation of discrete choice models. In: *Proceedings of the 3rd Swiss Transportation Research Conference*. Ascona, Switzerland.
- BMVBW, 1998. Systems for influencing traffic flow on German Motorways: State of the art and Future Perspectives. Tech. rep., Bundesministerium für Verkehr, Bau- und Wohnungswesen.
- Boer, E., Hildreth, E., Goodrich, M., 1998. A driver model of attention management and task scheduling: Satisficing decision making with dynamic mental models. In: *Proceedings of the XVIIth European Annual Conference on Human Decision Making and Manual Control*. Valenciennes, France.
- Boer, E., Hoedemaeker, M., 1998. Modeling driver behavior with different degrees of automation: A Hierarchical Decision Framework of Interacting Mental Models. In: *Proceedings of the XVIIth European Annual Conference on Human Decision Making and Manual Control*. Valenciennes, France.
- Bonsall, P., Liu, R., Young, W., 2005. Modelling safety-related driving behaviour: impact of parameter values. *Transportation Research Part A* 39, 425–444.
- Bortkiewicz, L., 1898. *Das Gesetz der kleinen Zahlen*.
- Brackstone, M., McDonald, M., Dec. 1999. Car-following: a historical review. *Transportation Research Part F: Traffic Psychology and Behaviour* 2 (4), 181–196.
- Breheret, L., Jan. 2003. Simulation microscopique du trafic routier. *Revue generale des routes* (813).
- Buch, N., Velastin, S. a., Orwell, J., Sep. 2011. A Review of Computer Vision Techniques for the Analysis of Urban Traffic. *IEEE Transactions on Intelligent Transportation Systems* 12 (3), 920–939.
- Camminatiello, I., Lucadamo, A., 2008. Estimating multinomial logit model with multicollinear data. In: *Methods, Models and Information Technologies for Decision Support Systems*. p. 4.
- Campolongo, F., Cariboni, J., Saltelli, A., 2001. From screening to quantitative sensitivity analysis: a unified approach. *Computer Physics Communications* 182, 978–988.
- Campolongo, F., Cariboni, J., Saltelli, A., 2007. An effective screening design for sensitivity analysis of large models. *Environmental Modelling and Software* 22 (10), 1509–1518.
- Cardoso, J. a. L., 1996. Estudo das relações entre as características da estrada, a velocidade e os acidentes rodoviários. Aplicação a estradas de duas vias e dois sentidos. Phd, Instituto Superior Tecnico.
- Cascetta, E., Sep. 2009. *Transportation Systems Analysis: Models and Applications*, 2nd Edition. Springer.

- Cascetta, E., Inaudi, D., Marquis, G., Nov. 1993. Dynamic Estimators of Origin-Destination Matrices Using Traffic Counts. *Transportation Science* 27 (4), 363–373.
- Cassidy, M. J., Bertini, R. L., Feb. 1999. Some traffic features at freeway bottlenecks. *Transportation Research Part B: Methodological* 33 (1), 25–42.
- Cassidy, M. J., Jang, K., Daganzo, C. F., 2011. Macroscopic Fundamental Diagrams for Freeway Networks: Theory and Observation. *Transportation Research Record: Journal of the Transportation Research Board* (2260), 8–15.
- CEMT/ITF, 2007. Congestion, a Global Challenge: The Extent of and Outlook for Congestion in Inland, Maritime and Air Transport. Tech. rep., European Conference of Ministers of Transport and the International Transport Forum.
- Champion, A., Espie, S., Auberlet, J.-M., 2001. Behavioral Road Traffic Simulation with ARCHISIM. In: *Proceedings of the Summer Computer Simulation Conference*. Orlando, Florida, USA.
- Chan, C. Y., Bougler, B., 2005. Evaluation of cooperative roadside and vehicle-based data collection for assessing intersection conflicts. In: *IEEE Proceedings. Intelligent Vehicles Symposium*, 2005. IEEE, pp. 165–170.
- Chang, L.-Y., Wang, H.-W., Sep. 2006. Analysis of traffic injury severity: an application of non-parametric classification tree techniques. *Accident Analysis and Prevention* 38 (5), 1019–27.
- Chen, C., Kwon, J., Rice, J., Skabardonis, A., Varaiya, P., Jan. 2003. Detecting Errors and Imputing Missing Data for Single-Loop Surveillance Systems. *Transportation Research Record* 1855 (1), 160–167.
- Chen, D., Laval, J., Zheng, Z., Ahn, S., Apr. 2012. A behavioral car-following model that captures traffic oscillations. *Transportation Research Part B: Methodological*.
- Chen, S., 1995. Car-Following measurements, simulations and a proposed procedure for evaluating safety. In: *IFAC/IFIP/IFORS/IEA Symposium: Analysis, design and evaluation of man-machine systems*. Pergamon, Oxford, England, Cambridge, Massachusetts, pp. 529–534.
- Cheung, S.-c. S., Kamath, C., 2004. Robust Background Subtraction With Foreground Validation For Urban Traffic Video. In: *IS&T/SPIE's Symposium on Electronic Imaging*. Vol. 2005. San Jose, CA, USA, pp. 2330–2340.
- Cho, Y., Rice, J., Dec. 2004. Estimating velocity fields on a freeway from low resolution video recordings. *IEEE Transactions on Intelligent Transportation Systems* 7 (4), 463–469.
- Choudhury, C. F., 2007. Modeling Driving Decisions with Latent Plans. Phd thesis, Massachusetts Institute of Technology.
- Chovan, J., Tijerina, L., Alexander, G., Hendricks, D., 1994. Examination of Lane Change Crashes and Potential IVHS Countermeasures. Tech. Rep. March, US Department of Transportation, NHTSA, Washington D.C., USA.
- Christoforou, Z., Cohen, S., Karlaftis, M. G., Nov. 2010. Vehicle occupant injury severity on highways: an empirical investigation. *Accident; analysis and prevention* 42 (6), 1606–20.

- Christoph, M., van Nes, N., Pauwelussen, J., Mansvelders, R., van der Horst, R., Hoedemaeker, M., 2010. In-vehicle and site-based observations of vehicles and cyclists A small-scale ND study in the Netherlands. PROLOGUE Deliverable D3.4. Tech. Rep. December 2010, TNO - Nederlandse Organisatie voor Toegepast Natuurwetenschappelijk Onderzoek, Soesterberg, The Netherlands.
- Ciuffo, B., Punzo, V., Montanino, M., 2012. The Calibration of Traffic Simulation Models Report on the assessment of different Goodness of Fit measures and Optimization Algorithms. Tech. rep., EU Joint Research Center.
- Ciuffo, B., Punzo, V., Quaglietta, E., 2011. Kriging Meta-Modelling to Verify Traffic Micro-Simulation Calibration Methods. In: TRB 90th Annual Meeting Compendium of Papers.
- Ciuffo, B., Punzo, V., Torrieri, V., 2007. A framework for calibrating a microscopic simulation model. In: Proceedings of the 86th Annual Meeting of the Transportation Research Board. Washington D.C., USA.
- Collins, R., Lipton, A., Kanade, T., Fujiyoshi, H., Duggins, D., Tsin, Y., Tolliver, D., Enomoto, N., Hasegawa, O., May 2000. A System for Video Surveillance and Monitoring. Tech. Rep. CMU-RI-TR-00-12, Robotics Institute, Carnegie Mellon University, Pittsburgh, PA.
- Conway, R. W., Maxwell, W. L., 1962. A queuing model with state dependent service rates. *Journal of Industrial Engineering* 12, 132–136.
- Cooper, D. F., Ferguson, N., 1976. Traffic studies at t-junctions - a conflict simulation model. *Traffic Engineering and Control* 17, 306–309.
- Cooper, P. J., 1983. Experience with traffic conflicts in Canada with emphasis on "post encroachment time techniques. In: Proceedings of the NATO Advanced Research Workshop on International Calibration Study of Traffic Conflict Technique. p. 15.
- Corby, M. J., Saccomanno, F., 1997. Analysis of Freeway Accident Detection. *Transportation Research Record: Journal of the Transportation Research Board* 1603, 80–89.
- CubeDynasim, 2013. <http://www.citilabs.com/new-dynasim-4>.
- Cunto, F., 2008. Assessing Safety Performance of Transportation Systems using Microscopic Simulation. Ph.D. thesis, University of Waterloo.
- Cutler, R., Davis, L., 1998. View-based detection and analysis of periodic motion. *Proceedings. Fourteenth International Conference on Pattern Recognition* 1, 495–500.
- Dailey, D. J., 1993. Improved error detection for inductive loop sensors. WA-RD 3001. Tech. rep., Washington State Department of Transportation, Olympia, USA.
- Das, S., Box, P. O., Bowles, B. A., Bowlesscdettindcom, B., 1999. Simulations of Highway Chaos Using Fuzzy Logic. In: Conference of the North American Fuzzy Information Processing Society. pp. 130–133.
- Davis, G., Davuluri, S., Pei, J., 2006. Speed as a Risk Factor in Serious Run-off-Road Crashes: Bayesian Case-Control Analysis with Case Speed Uncertainty. *Journal of Transportation and Statistics* 9 (1), 17–28.
- Delen, D., Sharda, R., Bessonov, M., May 2006. Identifying significant predictors of injury severity in traffic accidents using a series of artificial neural networks. *Accident; analysis and prevention* 38 (3), 434–44.

- Dijkster, T., 2012. FOSIM (Freeway Operations SIMulation) <http://www.fosim.nl>.
- Dijkstra, A., Marchesini, P., Bijleveld, F., Kars, V., Drolenga, H., Maarseveen, M. V., 2010. Do Calculated Conflicts in Microsimulation Model Predict Number of Crashes? *Transportation Research Record: Journal of the Transportation Research Board* 2147, 105–112.
- Dixon, M. P., Rilett, L. R., Jan. 2002. Real Time OD Estimation Using Automatic Vehicle Identification and Traffic Count Data. *Computer Aided Civil and Infrastructure Engineering* 17 (1), 7–21.
- Drive-C2X, W. P., 2012. <http://www.drive-c2x.eu/project>.
- Duncan, G., 2000. Paramics Technical Report: Car-Following, Lane-Changing and Junction Modelling. Tech. rep., Quadstone, Ltd., Edinburgh, Scotland.
- Duong, D., 2009. Calibration of microscopic traffic model for simulating safety performance. In: 89th Annual Meeting of the Transportation Research Board. Washington D.C., USA, p. 17.
- Duong, D., Hellenga, B., Saccomanno, F., 2010. A mechanistic approach for evaluating the safety impacts of left-turn lane offsets. In: 2010 Annual Conference of the Transportation Association of Canada. Halifax, Nova Scotia, Canada, pp. 1–18.
- El-Basyouny, K., Sayed, T., 2009. Accident prediction models with random corridor parameters. *Accident Analysis and Prevention* 41, 1118–1123.
- Eluru, N., Paleti, R., Pendyala, R., Bhat, C., 2010. Modeling multiple vehicle occupant injury severity: a copula-based multivariate approach. *Transportation Research Record: Journal of the Transportation Research Board* 2165, 1–11.
- Elvik, R., 2011. Assessing causality in multivariate accident models. *Accident Analysis & Prevention* 43 (1), 253–264.
- EUCommission, 2010. Towards a European road safety area: policy orientations on road safety 2011-2020. Tech. rep., European Commission, EU2010.
- Fan, Z., Zhou, J., Gao, D., Rong, G., 2002. Robust contour extraction for moving vehicle tracking. In: *Proceedings. International Conference on Image Processing*. Vol. 1. IEEE, pp. 625–628.
- Farah, H., Toledo, T., 2010. Passing behavior on two-lane highways. *Transportation Research Part F: Psychology and Behaviour* 13 (6), 355–364.
- Fernandes, R., D'Orey, P., Ferreira, M., 2010. DIVERT for realistic simulation of heterogeneous vehicular networks. pp. 721–726.
- Ferreira, S., Couto, A., Mar. 2013. Urban Road Network Safety Model at the Transportation Planning Process. *Journal of Transportation Safety & Security* 5 (1), 46–65.
- Fischler, M. A., Bolles, R. C., Jun. 1981. Random sample consensus: a paradigm for model fitting with applications to image analysis and automated cartography. *Commun. ACM* 24 (6), 381–395.
- Ford, J., Lester, R., 1956. *Network Flow Theory*, paper p-92 Edition. RAND Corporation, Santa Monica, California.

- Fricker, J. D., Guy, B., Dec. 2005. Guidelines for Data Collection Techniques and Methods for Roadside Station Origin-Destination Studies. Tech. rep., Federal Highway Administration, Washington D.C., USA.
- Fritzsche, H. T., May 1994. A model for traffic simulation. *Traffic Engineering & Control* 35 (5).
- Fuller, R., Nov. 1984. A conceptualization of driving behaviour as threat avoidance. *Ergonomics* 27 (11), 1139–55.
- Fuller, R., 2000. The task-capability interface model of the driving process. *Recherche - Transports - Sécurité* 66, 47–57.
- Gasser, I., Seidel, T., Siritto, G., Werner, B., 2007. Bifurcation analysis of a class of car following traffic models II: variable reaction times and aggressive drivers 2 (2), 587–607.
- Gazis, D. C., Herman, R., Rothery, R. W., 1961. Nonlinear Follow-The-Leader Models of Traffic Flow. *Operations Research* 9 (4), 545–567.
- Geraldes, R., Viegas, J. M., 2010. Methodology to estimate possible gains from real time changes in road network topology. In: *Proceedings of the 12th World Conference on Transport Research*. Lisbon, Portugal.
- Gettman, D., Head, L., Jan. 2003a. Surrogate Safety Measures from Traffic Simulation Models. *Transportation Research Record* 1840 (1), 104–115.
- Gettman, D., Head, L., 2003b. Surrogate Safety Measures From Traffic Simulation Models - Final Report. Tech. rep., Federal Highway Administration, McLean, Virginia, USA.
- Gettman, D., Sayed, T., Pu, L., Shelby, S., Jun. 2008. Surrogate Safety Assessment Model and Validation. Tech. Rep. June, Federal Highway Administration, McLean, Virginia, USA.
- Gipps, P., Apr. 1981. A behavioural car-following model for computer simulation. *Transportation Research Part B: Methodological* 15 (2), 105–111.
- Goerick, C., Noll, D., Werner, M., Apr. 1996. Artificial neural networks in real-time car detection and tracking applications. *Pattern Recognition Letters* 17 (4), 335–343.
- Golob, T. F., Recker, W. W., Alvarez, V. M., Nov. 2004. Freeway safety as a function of traffic flow. *Accident Analysis & Prevention* 36 (6), 933–946.
- Gomes, S. V., Geedipally, S. R., Lord, D., 2012. Estimating the safety performance of urban intersections in Lisbon, Portugal. *Safety Science* 50 (9), 1732–1739.
- Green, M., Sep. 2000. "How Long Does It Take to Stop?" Methodological Analysis of Driver Perception-Brake Times. *Transportation Human Factors* 2 (3), 195–216.
- Haag, M., Nagel, H.-H., 1999. Combination of Edge Element and Optical Flow Estimates for 3D-Model-Based Vehicle Tracking in Traffic Image Sequences. *International Journal of Computer Vision* 35 (3), 295–319.
- Habtemichael, F. G., Picado Santos, L., 2013a. Safety and operational benefits of VSL under different traffic conditions and driver compliance levels. In: *92nd Annual Meeting of the Transportation Research Board*. Washington D.C., USA, p. 18.

- Habtemichael, F. G., Picado Santos, L., 2013b. Sensitivity analysis of vissim driver behavior parameters on safety of simulated vehicles and their interaction with operations of simulated traffic. In: 92nd Annual Meeting of the Transportation Research Board. Washington D.C., USA, p. 17.
- Habtemichael, F. G., Picado Santos, L., Jun. 2013c. The impact of high-risk drivers and benefits of limiting their driving degree of freedom. Accident; analysis and prevention.
- Halati, A., Lieu, H., Walker, S., 1997. CORSIM: Corridor traffic simulation model. In: Proceedings of the Traffic Congestion and Traffic Safety in the 21st Century Conference. pp. 570–576.
- Hasan, M., Cuneo, D., Chachich, A., 1998. Analysis of traffic video to develop driver behaviour models for microscopic traffic simulation. Image Processing.
- Hassan, H., Abdel-Aty, M., 2013. Predicting reduced visibility related crashes on freeways using real-time traffic flow data. *Journal of Safety Research* 45 (0), 29–36.
- Hauer, E., Oct. 1982. Traffic conflicts and exposure. *Accident Analysis & Prevention* 14 (5), 359–364.
- Hauer, E., 2009. Speed and Safety. *Transportation Research Record: Journal of the Transportation Research Board* (2103), 10–17.
- Hayward, J., 1971. Near misses as a measure of safety at urban intersections. Ph.D. thesis, The Pensilvania State University.
- Helly, W., 1961. Simulation of bottlenecks in single-lane traffic flow. In: *Proceedings of the Theory of Traffic Flow Symposium*. Elsevier Publishing Company, pp. 207–238.
- Hemakom, A., Pan-ngum, S., Narupiti, S., 2008. Development of the Inner City Following-Lane Changing Model and Meandering Model of Motorcycles. In: *IEEE Intelligent Vehicles Symposium*. Eindhoven, The Netherlands, p. 6.
- Hidas, P., 1998. A car-following model for urban traffic simulation. *Traffic engineering & control* 39 (5), 300–305.
- Hidas, P., 2002. Modelling lane changing and merging in microscopic traffic simulation. *Transportation Research* 10, 351–371.
- Hidas, P., 2005a. Modelling Individual Behaviour In Microsimulation Models. In: *28th Australian Transport Research Forum (ATRF)*. Vol. 28. Sidney, New South Wales, Australia, p. 11.
- Hidas, P., 2005b. Modelling vehicle interactions in microscopic simulation of merging and weaving. *Transportation Research* 13, 37–62.
- Hidas, P., Wagner, P., Jan. 2004. Review of Data Collection Methods for Microscopic Traffic Simulation. In: *Proceedings of the World Conference on Transport Research (WCTR)*. Vol. 2. Istambul, Turkey, pp. 1–19.
- Higgs, B. J., Jan. 2012. Application of Naturalistic Truck Driving Data to Analyze and Improve Car Following Models.
- Hollander, Y., Liu, R., Jan. 2008. The principles of calibrating traffic microsimulation models. *Transportation* 35 (3), 347–362.

- Hoogendoorn, S. P., Hoogendoorn, R. G., Daamen, W., Dec. 2011. Wiedemann Revisited. *Transportation Research Record: Journal of the Transportation Research Board* 2260 (-1), 152–162.
- Hoogendoorn, S. P., Zuylen, H. J. V., Schreuder, M., Gorte, B., Vosselman, G., van Zuylen, H. J., 2003. Microscopic traffic data collection by remote sensing. *Transportation Research Record* (1855), 121–128.
- Hossain, M., Muromachi, Y., Mar. 2012. A Bayesian network based framework for real-time crash prediction on the basic freeway segments of urban expressways. *Accident; analysis and prevention* 45, 373–81.
- Hranac, R., Gettman, D., Toledo, T., Kovvali, V., Vassili Alexiadis, 2004a. NGSIM Task E.1-1: Core Algorithms Assessment. Tech. Rep. February, Federal Highway Administration.
- Hranac, R., Margiotta, R., Alexiadis, V., 2004b. NGSIM Task E.3: High-Level Data Plan. Publication No. FHWA-HOP-06-011. Tech. Rep. July, Cambridge Systematic, Inc., Cambridge MA, USA.
- Huang, F., Liu, P., Yu, H., Wang, W., Jan. 2013. Identifying if VISSIM simulation model and SSAM provide reasonable estimates for field measured traffic conflicts at signalized intersections. *Accident; analysis and prevention* 50, 1014–24.
- Hunt, J., Lyons, G., 1994. Modelling dual carriageway lane changing using neural networks. *Transportation Research Part C: Emerging Technologies* 2 (3), 231–245.
- Hydén, C., 1987. The development of a method for traffic safety evaluation: The Swedish Traffic Conflicts Technique. Tech. rep., Lund University, Lund, Sweden.
- Inoue, T., Hioki, Y., 1993. Skid resistance monitoring in Japan. *Roads* 280.
- Ismail, K. A., 2010. Application of computer vision techniques for automated road safety analysis and traffic data collection. Ph.D. thesis, University of British Columbia.
- Japan Society of Traffic Engineers, 2005. *Traffic Engineering Book*.
- Jie, L., Zuylen, H. V., Chen, Y., Viti, F., Wilmink, I., 2013. Calibration of a microscopic simulation model for emission calculation. *Transportation Research Part C: Emerging Technologies* 31 (0), 172–184.
- Johnson, A. N., 1929. Maryland aerial survey of highway traffic between Baltimore and Washington. *Highway Research Board Proceedings* 8, 106–11.
- Jones, E. R., Goolsby, M. E., 1970. The environmental influence of rain on freeway capacity. *Highway Research Record* (321), 74–82.
- Kastrinaki, V., Zervakis, M., Kalaitzakis, K., Apr. 2003. A survey of video processing techniques for traffic applications. *Image and Vision Computing* 21 (4), 359–381.
- Kesting, A., Treiber, M., Mar. 2008. Calibrating Car-Following Models using Trajectory Data: Methodological Study. *Transportation Research Record: Journal of the Transportation Research Board* 2088, 148–156.
- Kesting, A., Treiber, M., Helbing, D., 2007. General Lane-Changing Model MOBIL for Car-Following Models. *Transportation Research* 1999, 86–94.

- Kesting, A., Treiber, M., Helbing, D., 2010. Enhanced intelligent driver model to access the impact of driving strategies on traffic capacity. *Philosophical Transactions of the Royal Society Society A* 368, 4585–4605.
- Kikuchi, S., Chakroborty, P., 1992. Car-following model based on fuzzy inference system. *Transportation Research Record* (1365).
- Kita, H., Apr. 1999. A merging-giveway interaction model of cars in a merging section: a game theoretic analysis. *Transportation Research Part A: Policy and Practice* 33 (3-4), 305–312.
- Kleijnen, J. P. C., 2007. Kriging Metamodeling in Simulation: A Review. *European Journal of Operational Research* 192 (3), 707–716.
- Klunder, G., Abdoelbasier, A., Immers, B., 2006. Development of a micro-simulation model to predict road traffic safety on intersections. Tech. rep.
- Knoop, V. L., Van Zuylen, H. J., Hoogendoorn, S. P., 2009. Microscopic Traffic Behaviour near Incidents. In: *Proceedings of Second Sino-Dutch Joint Workshop in Transportation and Traffic Study*. No. 2007. Shanghai, China.
- Kometani, E., Sasaki, T., 1959. Dynamic behaviour of traffic with a non-linear spacing-speed relationship. In: *Proceedings of the Symposium on Theory of Traffic Flow*. Research Laboratories, General Motors, Elsevier, New York, USA, pp. 105–119.
- Koskinen, K., Kosonen, I., Luttinen, T., Schirokoff, A., Luoma, J., 2009. Development of a nanoscopic traffic simulation tool. *Advances in transportation Studies - an international Journal Section B* 17.
- Kosonen, I., 1999. HUTSIM - Urban Traffic Simulation and Control Model: Principles and Applications HUTSIM - Urban Traffic Simulation and Control Model: Principles and Applications. *Transportation Engineering*, 249.
- Krajzewicz, D., Hertkorn, G., Wagner, P., Rössel, C., 2002. SUMO (Simulation of Urban MObility): An open-source traffic simulation. In: *Proceedings of Simulation in Industry, 14th European Simulation Symposium*. Dresden, Germany, pp. 318–322.
- Kurian, M., 2000. Calibration of a Microscopic Traffic Simulator. Ph.D. thesis.
- Lambert, D., 1992. Zero-inflated Poisson regression, with an application to defects in manufacturing. *Technometrics* 34 (1), 1–14.
- Laureshyn, A., 2010. Application of automated video analysis to road user behaviour. Ph.D. thesis, Lund University.
- Laureshyn, A., Svensson, A. s., Hydén, C., 2010. Evaluation of traffic safety, based on micro-level behavioural data: Theoretical framework and first implementation. *Accident Analysis & Prevention* 42 (6), 1637–1646.
- Laval, J. A., Leclercq, L., Oct. 2010. A mechanism to describe the formation and propagation of stop-and-go waves in congested freeway traffic. *Philosophical transactions. Series A, Mathematical, physical, and engineering sciences* 368 (1928), 4519–41.
- Law, A., Kelton, W. D., Dec. 1999. *Simulation Modeling and Analysis*, 3rd Edition. McGraw-Hill.

- Lee, C., Abdel-aty, M., 2008. Two-Level Nested Logit Model to Identify Traffic Flow Parameters Affecting Crash Occurrence on Freeway Ramps. *Transportation Research Record* (2083), 145–152.
- Lee, C., Hellinga, B., Saccomanno, F., 2003. Real-Time Crash Prediction Model for Application to Crash Prevention in Freeway Traffic. *Transportation Research Record* 1840, 67–77.
- Lee, C., Hellinga, B., Saccomanno, F., Jun. 2006. Evaluation of variable speed limits to improve traffic safety. *Transportation Research Part C: Emerging Technologies* 14 (3), 213–228.
- Lee, C., Ph, D., 2009. Effects of Lane-Change and Car-Following-Related Traffic Flow Parameters on Crash Occurrence by Lane. In: *Proceedings of the 88th Annual Meeting of the Transportation Research Board*. No. 09. Washington D.C.
- Lee, C., Saccomanno, F., Hellinga, B., Jan. 2002. Analysis of Crash Precursors on Instrumented Freeways. *Transportation Research Record* 1784 (1), 1–8.
- Leitloff, J., Hinz, S., Stilla, U., 2010. Vehicle Detection in Very High Resolution Satellite Images of City Areas.
- Lenhart, D., Hinz, S., Leitloff, J., Stilla, U., Sep. 2008. Automatic traffic monitoring based on aerial image sequences. *Pattern Recognition and Image Analysis* 18 (3), 400–405.
- Li, X., Lord, D., Zhang, Y., Xie, Y., 2008. Predicting motor vehicle crashes using support vector machine models. *Accident Analysis and Prevention* 40 (4), 1611–1618.
- Li, Z., Liu, H., Zhang, K., Jul. 2009. Sensitivity Analysis of PARAMICS Based on 2K-P Fractional Factorial Design. *American Society of Civil Engineers*, pp. 3633–3638.
- Liu, Q., 2010. Development of a methodology to compare and select an appropriate crash surrogate for freeways safety analysis: a case study on truck lane restriction strategies. Phd, University of Virginia.
- Liu, R., Vliet, D. V., Watling, D., 1999. DRACULA: a microscopic , day-to-day dynamic framework for modelling traffic networks.
- Lophaven, S. N., Nielsen, H. B., Jacob, S., 2002. DACE: A Matlab Kriging Toolbox.
- Lord, D., 2006. Modeling motor vehicle crashes using Poisson-gamma models : Examining the effects of low sample mean values and small sample size on the estimation of the fixed dispersion parameter. *Accident Analysis and Prevention* 38, 751–766.
- Lord, D., Geedipally, S., Guikema, S., 2010a. Extension of the application of conway-maxwell-poisson models: analyzing traffic crash data exhibiting underdispersion. *Risk Analysis* 30 (8), 1268–1276.
- Lord, D., Mannering, F. L., Savolainen, P. T., Quddus, M. A., Jun. 2010b. The statistical analysis of crash-frequency data: A review and assessment of methodological alternatives. *Transportation Research Part A: Policy and Practice* 44 (5), 291–305.
- Lowe, D. G., Nov. 2004. Distinctive Image Features from Scale-Invariant Keypoints. *Int. J. Comput. Vision* 60 (2), 91–110.
- Lu, L., Yan, X., Antoniou, C., Ben-Akiva, M. E., 2013. W-SPSA: An Enhanced SPSA Algorithm for the Calibration of Dynamic Traffic Assignment Models.

- Lundy, R. A., Jul. 1964. Effect of Traffic Volumes and Number of Lanes On Freeway Accident Rates. Contract (2), 138–156.
- Ma, J., Kockelman, K. M., Damien, P., May 2008. A multivariate Poisson-lognormal regression model for prediction of crash counts by severity, using Bayesian methods. *Accident; analysis and prevention* 40 (3), 964–75.
- Madanat, S., Liu, P., 1995. A prototype system for real-time incident likelihood prediction - IDEA project final report. Tech. rep., Transportation Research Board, National Research Council, Washington, D.C., USA.
- Magee, D. R., Feb. 2004. Tracking multiple vehicles using foreground, background and motion models. *Image and Vision Computing* 22 (2), 143–155.
- Mak, C., Fan, H., 2006. Heavy SSow-based incident detection algorithm using information from two adjacent detector stations. *Journal of Intelligent Transportation Systems* 10 (1), 23–31.
- Malyshkina, N. V., Mannering, F. L., 2009. Markov switching multinomial logit model: An application to accident-injury severities. *Accident Analysis and Prevention* 41, 829–838.
- Manski, C. F., Lerman, S. R., 1977. The Estimation of Choice Probabilities from Choice Based Samples. *Econometrica* 45 (8), 1977–88.
- Markkula, G., Benderius, O., Wolff, K., Wahde, M., Jun. 2012. A Review of Near-Collision Driver Behavior Models. *Human Factors: The Journal of the Human Factors and Ergonomics Society* 54 (6), 1117–1143.
- Martin, P. T., Bell, M. C., 1993. Vehicle Tracking Through Unsampled Registration-Plate Observation. *Traffic Engineering and Control* 34 (1), 8–12.
- Matheron, G., 1963. Principles of geostatistics. *Economic Geology* 58, 1246–66.
- Mathew, T. V., Radhakrishnan, P., Mar. 2010. Calibration of Microsimulation Models for Nonlane-Based Heterogeneous Traffic at Signalized Intersections. *Journal of Urban Planning and Development* 136 (1), 59–66.
- McDonald, M., Wu, J., Brackstone, M., 1997. Development of a fuzzy logic based microscopic motorway simulation model. pp. 82–87.
- McDowell, M., Wennell, J., Storr, P., Darzentas, J., 1983. Gap acceptance and traffic conflict simulation as a measure of risk - Technical Report 776. Tech. rep., Transportation and Road Research Laboratory.
- McFadden, D., 1981. Chapter 5 - Econometric Models of Probabilistic Choice. In: MIT Press (Ed.), *Structural analysis of Discrete Data with Econometric Applications*. Cambridge, USA, Ch. 5, pp. 198–272.
- McFadden, D., Train, K., 2000. Mixed MNL models for discrete response. *Journal of Applied Econometrics* 15, 447–470.
- Mehmood, A., Easa, S. M., 2009. Modeling Reaction Time in Car-Following Behaviour Based on Human Factors. *Engineering and Technology* 3, 710–718.
- Michalopoulos, P. G., 1991. Vehicle detection video through image processing: the Autoscope system. *IEEE Transactions on Vehicular Technology* 40 (1), 21–29.

- Minderhoud, M. M., Bovy, P. H. L., 2001. Extended time-to-collision measures for road traffic safety assessment. *Accident Analysis & Prevention* 33 (1), 89–97.
- Morris, B. T. B., Trivedi, M. M. M., Aug. 2008. A Survey of Vision-Based Trajectory Learning and Analysis for Surveillance. *IEEE Transactions on Circuits and Systems for Video Technology* 18 (8), 1114–1127.
- Morris, M. D., 1991. Factorial sampling plans for preliminary computational experiments. *Technometrics* 33 (2), 161–174.
- Nagel, K., Schreckenberg, M., 1992. A cellular automaton model for freeway traffic. *Journal of Physics I*, 2221–2229.
- Nash, J. C., 2011. Rcgmin: Conjugate gradient minimization of nonlinear functions with box constraints. R package version.
- Neale, V. L., Dingus, T. A., Klauer, S. G., Sudweeks, J., Goodman, M., 2005. An overview of the 100-car naturalistic study and findings. In: *Proceedings - 19th International Technical Conference on the Enhanced Safety of Vehicles*. Washington, D.C., USA., pp. 1–10.
- Newell, G. F., 2002. A simplified car-following theory: a lower order model. *Transportation Research Part B: Methodological* 36 (3), 195–205.
- NHTSA, 2012. Traffic Safety Facts - Research Note: 2011 Motor vehicle crashes. DOTHS811701. Tech. Rep. December, National Highway Traffic Safety Administration, U.S. Department of Transportation.
- Nicholas E. Lownes, R. M., 2006. VISSIM: a multi-parameter sensitivity analysis. In: *Proceedings of the Winter Simulation Conference*. Monterey, USA, pp. 1406–1413.
- Nihan, N., 1997. Aid to Determining Freeway Metering Rates and Detecting Loop Errors. *Journal of Transportation Engineering* 123 (6), 454–458.
- NTIMC, 2006. Benefits of Traffic Incident Management. Tech. rep., National Traffic Incident Management Coalition.
- Oh, C., Oh, J.-S., Ritchie, S., Chang, M., Jan. 2001. Real-time estimation of freeway accident likelihood. In: *Proceedings of the 80th Annual Meeting of the Transportation Research Board*. Transportation Research Board, Washington D.C., p. 17.
- Oh, J., Washington, S. P., Nam, D., 2006. Accident prediction model for railway-highway interfaces. *Accident Analysis and Prevention* 38 (2), 346–356.
- Okamura, M., Corporation, A., Fukuda, A., Morita, H., Suzuki, H., Nakazawa, M., 2011. Impact evaluation of a driving support system on traffic flow by microscopic traffic simulation. In: *3rd International Conference on Road Safety and Simulation*. Indianapolis, USA, p. 18.
- Oketch, T., Jan. 2000. New Modeling Approach for Mixed-Traffic Streams with Nonmotorized Vehicles. *Transportation Research Record: Journal of the Transportation Research Board* (1705), 61–69.
- Ossen, S., Hoogendoorn, S. P., Dec. 2008. Validity of Trajectory-Based Calibration Approach of Car-Following Models in Presence of Measurement Errors. *Transportation Research Record: Journal of the Transportation Research Board* 2088, 117–125.

- Ossen, S., Hoogendoorn, S. P., Gorte, B. G., 2006. Interdriver differences in car-following: a vehicle trajectory based study. *Transportation Research Record: Journal of the Transportation Research Board* 5752 (1965), 121–129.
- Otsu, N., 1979. A threshold selection method from grey-level histograms. *IEEE Trans. Systems Man Cybern.* 9, 62–66.
- Ozaki, H., 1993. Reaction and anticipation in the car-following behavior. In: *12th International Symposium on the theory of traffic flow and transportation*. Berkeley, CA, USA, pp. 349–366.
- Ozbay, K., Yang, H., Bartin, B., Mudigonda, S., 2008. Derivation and Validation of a New Simulation-based Surrogate Safety Measure. *Transportation Research Record, Journal of Transportation Research Board*, 1–19.
- Pande, A., Abdel-aty, M., 2006. Assessment of freeway traffic parameters leading to lane-change related collisions. *Accident Analysis and Prevention* 38, 936–948.
- Panwai, S., Dia, H., 2005. Comparative evaluation of microscopic car-following behavior. *IEEE Transactions on Intelligent Transportation Systems* 6 (3), 314–325.
- Papageorgiou, C., Poggio, T., Jun. 2000. A Trainable System for Object Detection. *International Journal of Computer Vision* 38 (1), 15–33.
- Park, B., Qi, H., Jan. 2005. Development and Evaluation of a Procedure for the Calibration of Simulation Models. *Transportation Research Record* 1934 (1), 208–217.
- Patil, S., Geedipally, S. R., Lord, D., Mar. 2012. Analysis of crash severities using nested logit model - Accounting for the underreporting of crashes. *Accident Analysis & Prevention* 45, 646–653.
- Perkins, D., Harris, J., 1967. Criteria for traffic conflict characteristics - Report GMF 632. Tech. rep., General Motors Corporation, Warren, MI, USA.
- Persaud, B., Dzbik, L., 1993. Accident prediction models for freeways. *Transportation Research Record: Journal of the Transportation Research Board* (1401), 55–60.
- Pipes, L. A., 1953. An operational analysis of traffic dynamics. *Journal of applied Physics* 24 (3), 274–287.
- Pirdavani, A., Brijs, T., Bellemans, T., Wets, G., 2010. Evaluation of traffic safety at unsignalized intersections using microsimulation : a utilization of proximal safety indicators. *Transportation Research* 22, 43–50.
- Pólya, G., 1930. Sur quelques points de la théorie des probabilités. *Annales de l'I.H.P.* 2 (2), 117–161.
- PTV, 2009. VISSIM 5.20 User Manual. Tech. rep., Planung Transport Verkehr AG, Karlsruhe, Germany.
- Punzo, V., Ciuffo, B., 2009. How Parameters of Microscopic Traffic Flow Models Relate to Traffic Dynamics in Simulation. *Transportation Research Record* (2124), 249–256.
- Punzo, V., Ciuffo, B., August, S., Claudio, V., 2011. Sensitivity analysis of car-following models : methodology and application. In: *Transportation Research Board 90th Annual Meeting*. Transportation Research Board, Washington D.C., USA, pp. 1–18.

- Qiao, G., Menendez, M., 2013. An improved approach for the sensitivity analysis of computationally expensive microscopic traffic models: a case study of the Zurich network in VISSIM. In: 92nd Annual meeting of the Transportation Research Board Meeting.
- Qintero, A., 2010. Mesa redonda sobre segurança rodoviária - Melhorias nos últimos 20 anos e perspectivas futuras. In: 6.º Congresso Rodoviário Português.
- Qu, L., Li, L., Zhang, Y., Hu, J., 2009. PPCA-Based Missing Data Imputation for Traffic Flow Volume: A Systematical Approach. *IEEE Transactions on Intelligent Transportation Systems* 10 (3), 512–522.
- Quddus, M. A., Wang, C., Ison, S. G., May 2010. Road Traffic Congestion and Crash Severity: Econometric Analysis Using Ordered Response Models. *Journal of Transportation Engineering* 136 (5), 424–435.
- R Development Core Team, R., 2011. R: A Language and Environment for Statistical Computing.
- Rahman, M., Chowdhury, M., Xie, Y., He, Y., 2013. Review of Microscopic Lane-Changing Models and Future Research Opportunities. *IEEE Transactions on Intelligent Transportation Systems*, 1–15.
- Rakha, H., Zhang, Y., 2004. The INTEGRATION 2.30 Framework for Modeling Lane-Changing Behavior in Weaving Sections. *Transportation Research Record: Journal of the Transportation Research Board* 1883, 140–149.
- Remagnino, P., Baumberg, A., Grove, T., Hogg, D., Tan, T., Worrall, A., Baker, K., 1997. An Integrated Traffic and Pedestrian Model-Based Vision System. In: *Proceedings of the Eighth British Machine Vision Conference*. pp. 380–389.
- Reuschel, A., 1950. Vehicle movements in a platoon with uniform acceleration or deceleration of the lead vehicle. *Zeitschrift des Österreichischen Ingenieur und Architekten Vereines* 95, 59–62, 73–77.
- Rioux, T. W., 1977. The development of the Texas traffic and intersection simulation package. Phd thesis, University of Texas, Austin, Texas.
- Roque, C., Cardoso, J. a. L., 2011. Análise de Dados de Sinistralidade e Modelação de Despistes. Safeside: Sinistralidade Envolvendo a Área Adjacente à Faixa de Rodagem. Tech. rep., LNEC - Laboratório Nacional de Engenharia Civil, Lisbon, Portugal.
- Rosin, P. L., Nov. 2001. Unimodal thresholding. *Pattern Recognition* 34 (11), 2083–2096.
- Rosten, E., Loveland, R., Hickman, M., Dec. 2009. Automatic creation of urban velocity fields from aerial video. *Computing Research Repository*, 1–8.
- Rudolph, V., 1996. Das VideoVerkehrsAnalyse-System VIVAttraffic (in German) Video analysis system VIVAttraffic. In: Topp, H. H. (Ed.), *Traffic safety work with video processing*. Transportation Department, University Kaiserslautern, Kaiserslautern, Germany.
- Saltelli, A., Ratto, M., Andres, T., Campolongo, F., Cariboni, J., Gatelli, D., Saisana, M., Tarantola, S., Feb. 2008. *Global Sensitivity Analysis: The Primer*, 1st Edition. Wiley-Interscience.
- Salvucci, D., Jun. 2006. Modeling Driver Behavior in a Cognitive Architecture. *Human Factors: The Journal of the Human Factors and Ergonomics Society* 48 (2), 362–380.

- Samimi, A., Hellenga, B., Jan. 2012. Sensitivity of a real-time freeway crash prediction model to calibration optimality. *European Transport Research Review* 4 (3), 167–174.
- Saunier, N., Sayed, T., 2006. A feature-based tracking algorithm for vehicles in intersections. In: *The 3rd Canadian Conference on Computer and Robot Vision*. IEEE, Quebec, Canada.
- Saunier, N., Sayed, T., 2008. Probabilistic Framework for Automated Analysis of Exposure to Road Collisions. *Journal of the Transportation Research Board* (2083), 96–104.
- Savolainen, P. T., Mannering, F. L., Lord, D., Quddus, M. A., Sep. 2011. The statistical analysis of highway crash-injury severities: A review and assessment of methodological alternatives. *Accident Analysis & Prevention* 43 (5), 1666–1676.
- Schakel, W. J., Knoop, V. L., van Arem, B., 2012. Integrated Lane Change Model with Relaxation and Synchronization. *Traffic Flow Theory and Characteristics 2012, Driver Behavior; Pedestrian and Simulation Modeling* 2, 47–57.
- Schlaich, J., Otterstätter, T., Friedrich, M., 2010. Generating Trajectories from Mobile Phone Data. In: *Transportation Research Board 89th Annual Meeting*. Washington D.C., USA, p. 17.
- Schrank, D., Eisele, B., Lomax, T., 2012. Urban Mobility Report. Tech. Rep. December, Texas A&M Transport Institute.
- Shina, K., Washington, S. P., 2012. Empirical Bayes method in the study of traffic safety via heterogeneous negative multinomial model. *Transportmetrica* 8 (2), 131–147.
- Siuhi, S., Kaseko, M. S., 2010. Parametric Study of Stimulus-Response Behavior for Car-Following Models. In: *89th Annual Meeting of the Transportation Research Board*. Washington D.C, USA, p. 19.
- Smeed, R. J., 1949. Some Statistical Aspects of Road Safety Research. *Journal of the Royal Statistical Society. Series A (General)* 112 (1), 1–34.
- Smith, S. A., 1985. Freeway Data Collection for Studying Vehicle Interactions. Technical Report FHWA/RD-85/108. Tech. rep., Federal Highway Administration, US Department of Transportation, McLean VA, USA.
- Sobol, I., Jan. 1976. Uniformly distributed sequences with an additional uniform property. *USSR Computational Mathematics and Mathematical Physics* 16 (5), 236–242.
- Solomon, D., Jul. 1964. Accidents on main rural highways related to speed, driver and vehicle. Tech. rep., U.S. Department of Commerce, Washington D.C.
- Song, X., Nevatia, R., Feb. 2007. Detection and Tracking of Moving Vehicles in Crowded Scenes. p. 4.
- Songchitruksa, P., Tarko, A. P., 2006. The extreme value theory approach to safety estimation. *Accident Analysis and Prevention* 38 (4), 811–822.
- Spall, J. C., 1992. Multivariate Stochastic Approximation Using a Simultaneous Perturbation Gradient Approximation. *IEEE Transactions on Automatic Control* 37, 332–341.
- Sparmann, U., 1979. The Importance of Lane-Changing on Motorways. *Traffic Engineering and Control* 20 (6), 320–323.

- St. John, A. D., Harwood, D. W., 1998. TWOPAS User's Guide: A Microscopic Computer Simulation Model of Traffic on Two-Lane, Two-Way Highways. Report No. 7533-S(6). Tech. rep., Federal Highway Administration, Washington, D.C., USA.
- Stauffer, C., Grimson, W., 1999. Adaptive background mixture models for real-time tracking. In: Proceedings. 1999 IEEE Computer Society Conference on Computer Vision and Pattern Recognition (Cat. No PR00149). IEEE Comput. Soc, pp. 246–252.
- Sterzin, E., 2004. Modeling influencing factors in a microscopic traffic simulator. Msc thesis, Massachusetts Institute of Technology, Cambridge, MA.
- Suurballe, J. W., 1974. Disjoint paths in a network. *Networks* 4 (2), 125–145.
- SWOV, 2013. UDrive Project.
- Tarko, A. P., Davis, G., Saunier, N., Sayed, T., Washington, S. P., 2009. Surrogate Measures of Safety: A White Paper. Tech. Rep. 3, Transportation Research Board. ANB20 - Committee on Safety Data Evaluation and Analysis.
- Teixeira, P. J., 2010. Correlação de variáveis representativas de segurança rodoviária. Ph.D. thesis, Universidade de Aveiro.
- Toledo, T., 2003. Integrated Driving Behavior Modeling. Phd thesis, Massachusetts Institute of Technology.
- Toledo, T., Koutsopoulos, H., Ben-Akiva, M. E., 2007. Integrated driving behavior modeling. *Transportation Research* 15, 96–112.
- Toledo, T., Koutsopoulos, H. N., 2004. Statistical Validation of Traffic Simulation Models. *Transportation Research Record: Journal of the Transportation Research Board* (1876), 142–150.
- Tomar, R. S., Verma, S., Tomar, G. S., Nov. 2010. Prediction of Lane Change Trajectories through Neural Network. 2010 International Conference on Computational Intelligence and Communication Networks, 249–253.
- Torday, A., Baumann, D., Dumont, A.-G., Barceló, J., Montero, L., Perarnau, J., 2003. Safety indicators for microsimulation based assessments. In: 3rd Swiss Transport Research Conference. No. January. Ascona, Italia.
- Torday, A., Lavoc, E., Dumont, A.-g., Huguenin, F., 2005. Evaluation of traffic safety using microsimulation. In: 5th Swiss Transport Research Conference. Acona, Italia.
- Tordeux, A., Lassarre, S., Roussignol, M., 2010. An adaptive time gap car-following model. *Transportation Research Part B* 44 (8-9), 1115–1131.
- Treiber, M., Hennecke, A., Helbing, D., Aug. 2000. Congested traffic states in empirical observations and microscopic simulations. *Physical review E* 62 (2A), 1805–1824.
- Treiber, M., Kesting, A., Helbing, D., 2006. Delays , inaccuracies and anticipation in microscopic traffic models. *Physica A* 360 (May 2005), 71–88.
- Treiterer, J., Myers, J. A., 1974. The hysteresis phenomenon in traffic flow. In: Proceedings of the Sixth International Symposium on Transportation and Traffic Theory. Vol. 6. Elsevier Publishing Company, Incorporated, Sidney, pp. 13–38.

- Tsai, V., Jun. 2006. A comparative study on shadow compensation of color aerial images in invariant color models. *IEEE Transactions on Geoscience and Remote Sensing* 44 (6), 1661–1671.
- TU0903-Cost Action, 2012. <http://www.multitude-project.eu/>.
- Turner, S., Eisele, W., Benz, R., Holdener, D., Mar. 1998. Travel Time Data Collection Handbook. Tech. rep., Federal Highway Administration, Washington D.C., USA.
- Turner, S., Roozenburg, A., Smith, A., 2009. Roundabout crash prediction models: Report n 386. Tech. rep., New Zealand Agency Research.
- Van Aerde, M., Hellinga, B., Baker, M., Rakha, H., Aerde, M. V., 1992. INTEGRATION: Overview of Simulation Features. In: 75th Annual Meeting of the Transportation Research Board. Vol. 1802. Washington, D.C., USA.
- van der Horst, A., 1990. A time-based analysis of road user behaviour in normal and critical encounters. Ph.D. thesis, Delft University of Technology.
- Van Schagen, I., Welsh, R., Backer-Grøndhal, A., Hoedemaeker, M., Lotan, T., Morris, A., Sagberg, F., Winkelbauer, M., 2011. Towards a large-scale European Naturalistic Driving study : final report of PROLOGUE. Deliverable D4.2. Tech. Rep. July, SWOV Institute for Road Safety Research, Leidschendam, The Netherlands.
- van Winsum, W., de Waard, D., Brookhuis, K. A., 1999. Lane change manoeuvres and safety margins. *Transportation Research Part F: Traffic Psychology and Behaviour* 2 (3), 139–149.
- Vasconcelos, L., Silva, A. B., Seco, A., Rouxinol, G., 2012. Estimation of Critical Headways at Unsignalized Intersections: A Microscopic Approach. *Advances in Transportation Research*, 59–72.
- Vaze, V., Antoniou, C., Wen, Y., Ben-akiva, M. E., Dec. 2009. Calibration of Dynamic Traffic Assignment Models with Point-to-Point Traffic Surveillance. *Transportation Research Record* 2090 (-1), 1–9.
- Veeraraghavan, H., Masoud, O., Papanikolopoulos, N., Jun. 2003. Computer vision algorithms for intersection monitoring. *IEEE Transactions on Intelligent Transportation Systems* 4 (2), 78–89.
- Viegas, J. M., May 2007. The Intermittent Bus Lane System: Lisbon Demonstration Project. *Public Transport International* 56 (3), 40–43.
- Vilarinho, C., 2012. Traffic Model Calibration: A Sensitivity Analysis. In: *Proceedings of the 15th Edition of the Euro Working Group on Transportation*. Paris, France, p. 10.
- Viola, P., Jones, M. J., Snow, D., Oct. 2003. Detecting Pedestrians Using Patterns of Motion and Appearance. In: *IEEE International Conference on Computer Vision (ICCV)*, Vol. 2. pp. 734–741.
- Wang, G., Xiao, D., Gu, J., 2008. Review on Vehicle Detection Based on Video for Traffic Surveillance. In: *International Conference on Automation and Logistics*. No. September. Qingdao, China, pp. 2961–2966.
- Wang, W., Jiang, X., Xia, S., Cao, Q., 2010. Incident tree model and incident tree analysis method for quantified risk assessment: An in-depth accident study in traffic operation. *Safety Science* 48 (10), 1248–1262.

- Washington, S. P., Karlaftis, M., Mannering, F. L., 2010. Statistical and Econometric Methods for Transportation Data Analysis, second ed. Edition. Chapman Hall CRC, Boca Raton, Florida, USA.
- WHO, 2011. Global Plan for the Decade of Action for Road Safety 2011-2020. Tech. rep., World Health Organization.
- WHO, 2013. Global status report on road safety. Tech. rep., World Health Organization, WHO.
- Wickens, C. D., Hollands, J. G., Sep. 1999. Engineering Psychology and Human Performance, 3rd Edition. Prentice Hall.
- Wiedemann, R., 1974. Simulation des Straßenverkehrsflusses. Ph.D. thesis, University of Karlsruhe, Germany, Karlsruhe.
- Wiedemann, R., 1991. Modelling of RTI-elements on multi-lane roads. In: Drive Conference. Vol. II. Brussels, Belgium.
- Willman, G., 1978. Zustandsformen des Verkehr sablaufs auf Autobahnen. Tech. rep., Schriftenreihe des Instituts für Verkehrswesen, University Karlsruhe, Karlsruhe, Germany.
- Winter, S., Grünbacher, A., Winter S., 2002. Modeling Costs of Turns in Route Planning. Geoinformatica 6 (4), 345–361.
- Xie, Y., Lord, D., Zhang, Y., 2007. Predicting motor vehicle collisions using Bayesian neural networks: an empirical analysis. Accident Analysis and Prevention 38 (5), 922–933.
- Xie, Y., Zhang, Y., 2008. Crash frequency analysis with generalized additive models. Transportation Research Record: Journal of the Transportation Research Board 2061, 39–45.
- Xin, W., Hourdos, J., Michalopoulos, P., Davis, G., 2008. The Less-than-perfect Driver : A Model of Collision-inclusive Car-following Behavior. Strategy (January), 612–626.
- Xu, C., Tarko, A. P., Wang, W., Liu, P., Aug. 2013a. Predicting crash likelihood and severity on freeways with real-time loop detector data. Accident; analysis and prevention 57, 30–9.
- Xu, C., Wang, W., Liu, P., Jun. 2013b. A Genetic Programming Model for Real-Time Crash Prediction on Freeways. IEEE Transactions on Intelligent Transportation Systems 14 (2), 574–586.
- Yamamoto, T., Hashiji, J., Shankar, V., 2008. Underreporting in traffic accident data, bias in parameters and the structure of injury severity models. Accident Analysis & Prevention 40, 1320–1329.
- Yang, H., Akiyama, T., Sasaki, T., 1992. A neural network approach to the identification of real time origin-destination flows from traffic counts. In: Proceeding of the Internaitonal Conference on Artificial Intelligence Applications in Transportation Engineering San Buenaventura. San Buenaventura, California, USA, pp. 253–269.
- Yang, Q., 1997. A Simulation Laboratory for Evaluation of Dynamic Traffic Management Systems. Ph.D. thesis, Massachusetts Institute of Technology.
- Yang, Q., Kousopoulos, H., Ben-Akiva, M. E., 1999. A simulation laboratory for evaluating dynamic traffic management systems. Transportation Research Board 88th Annual Meetingsearch Record: Journal of the Transportation Research Board 1710 (2000), 122–130.

- Yasmin, S., Eluru, N., 2013. Evaluating alternate discrete outcome frameworks for modeling crash injury severity. *Accident Analysis & Prevention* 59, 506–521.
- Ye, F., Lord, D., 2010. Investigating the Effects of Underreporting of Crash Data on Three Commonly Used Traffic Crash Severity Models : Multinomial Logit , Ordered Probit and Mixed Logit Models. *Transportation Research Record: Journal of the Transportation Research Board*.
- Ye, F., Lord, D., Jan. 2014. Comparing three commonly used crash severity models on sample size requirements: Multinomial logit, ordered probit and mixed logit models. *Analytic Methods in Accident Research* 1, 72–85.
- Yilmaz, A., Javed, O., Shah, M., Dec. 2006. Object tracking. *ACM Computing Surveys* 38 (4), 13.
- Young, W., Sobhani, A., Lenné, M. G., Sarvi, M., Jan. 2014. Simulation of safety: A review of the state of the art in road safety simulation modelling. *Accident; analysis and prevention* 66C, 89–103.
- Zhang, L., Kovvali, V., Clark, N., Sallman, D., Alexiadis, V., 2007. NGSIM - VIDEO User ' s Manual. Publication No. FHWA-HOP-07-009. Tech. Rep. March, Department of Transportation, Federal Highway Administration, Washington D.C., USA.
- Zhang, Y., Owen, L., Clark, J., Jan. 1998. Multiregime Approach for Microscopic Traffic Simulation. *Transportation Research Record: Journal of the Transportation Research Board* 1644, 103–114.
- Zheng, L., Ismail, K., Meng, X., 2013. Freeway Safety Estimation using Extreme Value Theory Approaches: a comparative study. *Accident Analysis & Prevention*.
- Zheng, Z., Ahn, S., Monsere, C. M., 2010. Impact of traffic oscillations on freeway crash occurrences. *Accident analysis and prevention* 42 (2), 626–636.
- Zhou, K., Varadarajan, K. M., Vincze, M., Liu, F., Oct. 2011. Driving behavior inference from traffic surveillance data. 2011 14th International IEEE Conference on Intelligent Transportation Systems (ITSC), 600–605.
- Zhou, X., Mahmassani, H. S., Mar. 2006. Dynamic origin-destination demand estimation using automatic vehicle identification data. *Intelligent Transportation Systems, IEEE Transactions on* 7 (1), 105–114.
- Zhou, X., Qin, X., Mahmassani, H. S., 2003. Dynamic Origin-Destination Demand Estimation with Multiday Link Traffic Counts for Planning Applications. *Transportation Research Record* (1831), 30–38.
- Zijpp, N. V. D., Section, T. E., Van Der Zijpp, N., Jan. 1997. Dynamic OD Matrix Estimation from Traffic Counts and Automated Vehicle Identification Data. *Transportation Research Record: Journal of the Transportation Research Board* 1607, 1–18.
- Zou, H., Yue, Y., Li, Q., Yeh, A., 2012. An improved distance metric for the interpolation of link-based traffic data using kriging: a case study of a large-scale urban road network. *International Journal of Geographical Information Science* 26 (4), 667–689.

Glossary

AADT - Average Annual Daily Traffic
AAN - Artificial Neural Networks
AIC - Akaike Information Criterion
AM - Aggregated Model
ANOVA - Analysis of Variance
ANSR - Portuguese National Road Authority
ATCS - Automatic Traffic Counting Station
ATIS - Advanced Traveler Information Systems
ATMS - Advanced Traffic Management Systems
CDF - Cumulative Distribution Function
CF - Car-Following
CI - Crash Index
CPI - Crash Potential Index
DAG - Direct Acyclic Graph
DLC - Discretionary Lane-Changing
DM - Disaggregated Model
DRAC - Deceleration Rate to Avoid Crash
DSA - Daily Statistics Algorithm
DSS - Difference between Space distance and Stopping distance
DVU - Driver-Vehicle Unit
EE - Elementary Effects
ET - Encroachment Time
EV - Extreme Value
FM - Forced Merging
GEH - Geoffrey E. Havers statistic
GEV - Generalized Extreme Value
GIS - Geographic Information Systems

GLM - Generalized Linear Model

GLS - Generalized Least Squares

GoF - Goodness of Fit

GP - Genetic Programming

GT - Gap Time

HGV - Heavy Good Vehicles

HOV - High Occupancy Vehicles

IAPT - Initially Attempted Post-Encroachment Time

IDM - Intelligent Driver Model

IIA - Independence of Irrelevant Alternatives

IP - Integer Programing

ITS - Intelligent Transportation Systems

LC - Lane-Change conflict

LINEC - National Laboratory of Civil Engineering

LP - Linear Programing

MADR - Maximum Available Deceleration Rate

MAPE - Mean Absolute Percent Error

MCMC - Markov Chain Monte Carlo

ML - Maximum Likelihood

MLC - Mandatory Lane-Changing

MNL - Multinomial Logit Model

MoP - Measures of Performance

NA - No Accident events

NL - Nested Logit

NLC - Number of Lane Changes

OAT - One-At-Time

OD - Origin-Destination

OTEE - Optimized Trajectories Elementary Effects

PCA - Principal Component Analysis

PET - Post-Encroachment Time

PSD - Proportion of Stopping Distance

RE - Rear-End conflicts

RGB - Red Green Blue

RLC - Random Lane-Changing

RMSE - Root Mean Squared Error
RMSNE - Root Mean Squared Normalized Error
RMSPE - Root Mean Squared Percentage Error
ROR - Run-Off-Road events
SA - Sensitivity Analysis
SC - Side Collisions
SDK - Software Development Kit
SPSA - Simultaneous Perturbation Stochastic Approximation
SSAM - Surrogate Safety Assessment Model
TCT - Traffic Conflicts Technique
TET - Time Exposed Time-to-Collision
TIDSS - Time Integrated Difference between Space distance and Stopping distance
TIT - Time Integrated Time-to-Collision
TTC - Time-to-Collision
UD - Unsafety Density Parameter
UVA - Unmanned Aerial Vehicles
VSL - Variable Speed Limits
WESML - Weighted Exogenous Sample Maximum Likelihood
WSPSA - Weighted-Simultaneous Perturbation Stochastic Approximation

Appendix A

Integrated driving behaviour model

MITSIM integrated driver behaviour model integrates four levels of decision-making: target lane, gap acceptance, target gap and acceleration, in a latent decision framework based on the concepts of short-term goal and short-term plan (see Figure A-1).

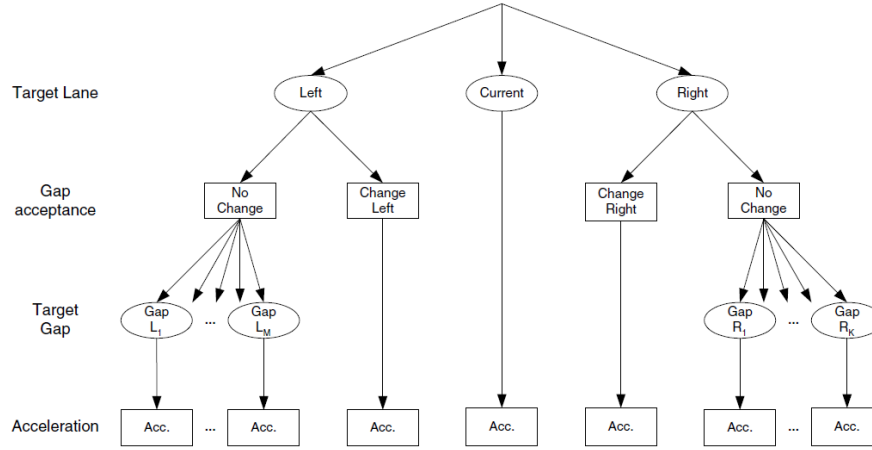


Figure A-1: Structure of the integrated driving behaviour model

In previous research, this model was integrated in the microscopic traffic simulator MITSIM and extended with other sub-components of the driver behaviour such as the reaction time model and the merging, nosing and yielding acceleration models. In this appendix, a brief review of the studied models is presented. The reader should however refer to (Yang (1997), Ahmed (1999), Toledo (2003)) for a full description. For consistency purposes, the notation used in this section follows the notation used by the authors in each of their publications. Thus, all the behavioral parameters considered for potential calibration were classified in 15 different groups:

1. When a new vehicle enters the network, it is randomly assigned an update step size which specifies the frequency with which drivers update their driving behaviour. This value is drawn from a truncated normal distribution with mean, standard deviation, lower and upper bounds $\mu_{RT}, \sigma_{RT}, lb_{RT}, ub_{RT}$ (named Group 1, with 4 parameters: $\mu_{RT}, \sigma_{RT}, lb_{RT}, ub_{RT}$).
2. Different models describe the acceleration behaviour under the various situations. The stimulus-sensitivity framework, which the GM model is based on Gazis et al. (1961), was adapted for all the acceleration models considered in MITSIM Yang (1997). The car-following model, for both the acceleration and deceleration ($g \in$

$\{acc, dec\}$), is given by equation:

$$a_{cf}^g(t) = \alpha_{cf}^g \left[V(t)^{\beta_{cf}^g} \Delta x(t)^{-\gamma_{cf}^g} \right] k(t)^{\delta_{cf}^g} \Delta V(t - \tau_{RT})^{\rho_{cf}^g} + \varepsilon_{cf}^g(t) \quad (A.1)$$

where, V is the speed of the subject vehicle; Δx and ΔV are the gap and speed difference between the lead and subject vehicles; k is the traffic density downstream of the subject vehicle; τ_{RT} its driver reaction time; and ε_{cf}^g the random error term. The car-following state depends on the headway between the subject and the front vehicle. In MITSIM each vehicle has its own headway threshold (see Group 10). However, general thresholds as the minimum response distance Δx_{cf}^{min} and the general headway lower bound h_{cf}^{lb} are also considered for this specific model (Group 2, with 11 parameters: Δx_{cf}^{min} , h_{cf}^{lb} , α_{cf}^{acc} , β_{cf}^{acc} , γ_{cf}^{acc} , δ_{cf}^{acc} , ρ_{cf}^{acc} , α_{cf}^{dec} , γ_{cf}^{dec} , δ_{cf}^{dec} , ρ_{cf}^{dec}).

3. When the headway between the subject and the lead vehicle is big enough the free-flow state is set and the vehicle acceleration is given by:

$$a_{ff} = \alpha_{ff} [V_{DS}(t - \tau_{RT}) - V(t - \tau_{RT})] + \varepsilon_{ff}(t) \quad (A.2)$$

$$V_{DS}(t) = \beta_{ff} + V_{lim} + \gamma_{ff} \delta_s^h + \delta_{ff}^k k(t) + \rho_{ff}^{V_f} V_f(t) \quad (A.3)$$

where, V is the speed of the subject vehicle; V_{DS} is its desired speed of the subject vehicle; V_{lim} is the local speed limit; δ_s^h is 1 if the subject vehicle is heavy and 0 otherwise; k is 1 if the traffic density downstream is equal or less than a threshold θ_{ff} and 0 otherwise; $V_f(t)$ is the front vehicle speed; τ_{RT} is the driver reaction time; and $\varepsilon_{ff}(t)$ the random error term (Group 3, with 6 parameters: α_{ff} , β_{ff} , γ_{ff} , δ_{ff}^k , $\rho_{ff}^{V_f}$, θ_{ff}).

4. When a vehicle has reached a lane dropping area, it may be tagged has a merging vehicle. In this situation, the acceleration is calculated relaxing the car-following gap limitation and restricting overtaking when using the dropping lane. Upstream (Δx_u) and downstream (Δx_d) lengths from the beginning section of dropping lane set the total area where a vehicle can be tagged with merging state. The probability of being tagged merging is given by the fixed parameter p_0 , and only if the number of merging vehicles in the merging area is less than n_{max} (Group 4, with 4 parameters: Δx_u , Δx_d , p_0 , n_{max}).

5. The mandatory lane change state (MLC) is derived from previous models of **MITSIM** (Ahmed (1999)). When the general lane changing model proposed by Toledo (Toledo (2003)) cannot be applied due to the lack of acceptable gaps (dense traffic conditions), a MLC may be initiated, limiting the lane alternatives in the lane choice and gap acceptance models. Additionally, a vehicle may switch to the MLC state only if its current lane is ending or does not connect to the next link in its path. The probability of initiation of such state is derived from the following equation when the distance to the downstream node is less than Δx_{min} .

$$P^{MLC} = \exp \left(- \frac{(\Delta x)^2}{\left(\alpha_0^{MLC} + \alpha_{n_{lc}}^{MLC} n_{lc}(t) + \alpha_k^{MLC} k(t) \right)^2} \right) \quad (A.4)$$

where, Δx is the distance to the downstream node limited by the lower bound Δx_{lb} ; n_{lc} is the number of lane changes required to reach the target lane; and k is the lane density. Δt_{min} is an additional parameter setting the minimum time in lane when tagged for MLC (Group 5, with 5 parameters: Δx_{lb} , α_0^{MLC} , α_1^{MLC} , α_k^{MLC} , Δt_{min}).

6. When a vehicle is in nosing state, the lag vehicle is set to yielding with probability p_{no} if it wasn't previously yielding and p_{yes} otherwise (Group 6, 2 parameters: p_{no}, p_{yes}).
7. When a vehicle has decided to change lanes and is in MLC state, a merging model that captures merging by gap creation, either through courtesy yielding of the lag vehicle or nosing of the subject vehicle, may be applied. The probability of a subject vehicle being set to the nosing state is given by:

$$P^{nos} = \frac{1}{1 + \exp \left(\alpha^{nos} + \beta_{\Delta V_-}^{nos} \Delta V(t) + \beta_{I_{\Delta x}}^{nos} I_{\Delta x}(t) + \beta_{l_{gap}}^{nos} l_{gap}(t) + \beta_{n_{lc}}^{nos} n_{lc}(t) \right)} \quad (A.5)$$

where, ΔV_- is the relative speed between the subject vehicle and the lead vehicle on the target lane; $I_{\Delta x}$ is an impact factor depending on both the remaining distance to the point at which the lane change must be completed and on a parameter λ^{nos} ; l_{gap} is the total gap length; and n_{lc} is the number of lane changes required to reach the target lane (Group 7, with 6 parameters: α^{nos} , $\beta_{\Delta V_-}^{nos}$, $\beta_{I_{\Delta x}}^{nos}$, λ^{nos} , $\beta_{l_{gap}}^{nos}$, $\beta_{n_{lc}}^{nos}$).

8. The application of the nosing model is also restricted by a maximum waiting time before nosing t_{max}^{nos} , a maximum and minimum distance for nosing, Δx_{max}^{nos} and Δx_{min}^{nos} , and a maximum yielding time t_{max}^{yield} for the lag vehicle (Group 8, with 4 parameters:

$$t_{max}^{nos}, \Delta x_{max}^{nos}, \Delta x_{min}^{nos}, t_{max}^{yield}).$$

9. The courtesy yielding alternative is modelled as a fixed probability: p_0^{cyield} , p_1^{cyield} , p_2^{cyield} and p_3^{cyield} are the probabilities to yield to none, one, two and three vehicles when tagged as MLC (Group 9, with 4 parameters: p_0^{cyield} , p_1^{cyield} , p_2^{cyield} , p_3^{cyield}).
10. A high share of the simulation stochasticity comes from the driver population heterogeneity: the acceleration model error terms for the car following and free flow behaviour follow a normal distribution with mean zero and standard deviation σ_{cf}^{acc} , σ_{cf}^{dec} and σ_{ff} respectively; the headway threshold, which rules the choice between car-following and free flow acceleration models, is obtained from a truncated normally distributed with parameters μ_{dv}^h and σ_{dv}^h , and lower and upper bounds lb_{dv}^h and ub_{dv}^h . Alternatively, the desired speed from Group 3 can be simplified as a normally distributed factor (with parameters μ_{DS} and σ_{DS} of the local speed limit (Group 10, with 10 parameters: σ_{cf}^{acc} , σ_{cf}^{dec} , σ_{ff} , μ_{dv}^h , σ_{dv}^h , lb_{dv}^h , ub_{dv}^h , μ_{DS} , σ_{DS}).
11. The target gap acceleration model captures the behaviour of drivers who target a lane change and already chose the corresponding target gap. This formulation is part of the integrated model proposed by Toledo (2003):

$$a^{TG} = \alpha_g^{TG} \left[D^{TG} (t - \tau)^{\beta_D^{TG}} \cdot \exp \left(\beta_{\Delta V_+}^{TG} \Delta V_+(t) + \beta_{\Delta V_-}^{TG} \Delta V_-(t) \right) \right] + \varepsilon_g^{TG}(t) \quad (\text{A.6})$$

where, D^{TG} is the distance to the to the desired position for the target gap TG ($TG \in \{\text{backward, adjacent, forward}\}$) and has different formulations for each of the possible TG but only depends on one parameter β_{DP} (see Toledo (2003) for details); ΔV_+^{TG} and ΔV_-^{TG} are the positive and negative relative target lane leader speeds; τ is the driver reaction time; and $\varepsilon_g^{TG} \sim N \left(0, (\sigma^{TG})^2 \right)$ is the random error term (Group 11, with 13 parameters: β_{DP} , α_g^{fwd} , β_D^{fwd} , $\beta_{\Delta V_+}^{fwd}$, $\beta_{\Delta V_-}^{fwd}$, σ^{fwd} , α_g^{bck} , β_D^{bck} , $\beta_{\Delta V_+}^{bck}$, $\beta_{\Delta V_-}^{bck}$, σ^{bck} , α_g^{adj} , σ^{adj}).

12. The gap acceptance model evaluates the adjacent gaps in the target lane model and decides to switch lanes immediately or not. The adjacent gap is split into lead and lag gaps which both need to be acceptable for the lane change action. A gap is acceptable if it is greater than the corresponding critical gap, which mean is modelled as a random variable following a lognormal distribution Ahmed (1999),

Toledo (2003):

$$\ln \left(G_n^{l,c,r}(t) \right) = \alpha^l + \beta_{\Delta V_+}^l \Delta V_+^l(t) + \beta_{\Delta V_-}^l \Delta V_-^l(t) + \beta^{EMU} EMU^l(t) + \alpha_v^l v_n + \varepsilon^l(t) \quad (\text{A.7})$$

where, $G_n^{l,c,r}$ is the critical l (with $l \in \{lead, lag\}$) gap; ΔV_+^l and ΔV_-^l are the positive or negative speed difference between the subject vehicle and the l vehicle on the target lane limited by a threshold ΔV_{max} ; EMU^l is the expected maximum utility of the target gap l ; v_n is the individual specific error term; and $\varepsilon^l \sim N\left(0, (\sigma^l)^2\right)$ the random error term (Group 12, with 8 parameters: α^{lead} , α^{lag} , $\beta_{\Delta V_+}^{lead}$, $\beta_{\Delta V_+}^{lag}$, $\beta_{\Delta V_-}^{lead}$, $\beta_{\Delta V_-}^{lag}$, σ^{lead} , σ^{lag}).

13. At the top of the drivers' decision tree is the lane choice model. Modelled as a discrete choice problem, the probability of choosing a target lane is computed through a logit formulation using the following utility function Toledo (2003) :

$$\begin{aligned} U^{TL} = & \alpha^{TL} + \beta_{RML}^{TL} \delta_{RML} + \beta_{V_l}^{TL} V_l(t) + \beta_{\Delta x}^{TL} \Delta x(t) + \beta_b \delta_b + \beta_h \delta_h(t) \\ & + \beta_k \delta_k(t) + \beta_{tail}^{TL} \delta_{tail}(t) + [\Delta x_{exit}(t)]^{\theta^{MLC}} \sum (\beta_{nlc,i} \delta_{nlc,i}(t)) \\ & + \beta_{next} \delta_{next} + \beta_{add} n_{add}(t) + \beta_{gap} EMU^{TL}(t) + \alpha_v^{TL} v_n + \varepsilon^{TL}(t) \quad (\text{A.8}) \end{aligned}$$

where, α^{TL} is a constant parameter for the target lane TL (with $TL \in \{\text{left, current, right}\}$); δ_{RML} is a dummy variable equal to one if TL is the right-most-lane; V_l is the speed of the lead vehicle on TL ; Δx is the gap between the lead and subject vehicles; δ_h is a dummy equal to one if the traffic density in TL is higher than a threshold k_{ceil} ; δ_b and δ_h are dummy variables equal to one on the presence of bus and heavy good vehicles in TL ; δ_{tail} is a dummy variable that captures drivers' tendency to move out of their current lane if they are being tailgate and it's equal to one if the backward gap is less than Δx_{floor}^{back} ; Δx_{exit} is the distance from the subject vehicle to the next exit; $\delta_{nlc,i}$ are idummy variables equal to one for each i number of lane changes required to reach TL , δ_{next} is a dummy for the need of exiting on the next off-ramp; n_{add} is a dummy for the number of lane changes required from the TL to the off-ramp; EMU^{TL} is the maximum utility of the available gaps in the TL given by the target gap model; v_n is the individual specific error term that captures correlations between observations over time and ε^{TL} the random error term (Group

13, with 17 parameters: α^{CL} , α^{RL} , β_{RML}^{TL} , $\beta_{V_l}^{TL}$, $\beta_{\Delta x}^{TL}$, β_b , β_h , β_k , k_{ceil} , β_{tail}^{TL} , Δx_{floor}^{back} , θ_{MLC} , $\beta_{nlc,1}$, $\beta_{nlc,2}$, $\beta_{nlc,3}$, β_{next} , β_{add}).

14. When a driver has decided to switch lanes, the target gap model captures the drivers' intention on the lane changing decision process, when the adjacent gap is rejected (25,26). The subject vehicle will then adjust its speed and position depending on the chosen target gap. Similarly to the lane choice model, the probability of choosing a target gap is modelled as a logit model using the following utility equation:

$$U^{TG} = \alpha^{TG} + \beta_{\Delta x_{TG}} \Delta x_{TG}(t) + \beta_{l_{TG}} l_{TG}(t) + \beta_{\delta_f} \delta_f(t) + \beta_{\Delta V_{TG}} \Delta V_{TG}(t) + \alpha_v^{TG} v_n + \varepsilon^{TG}(t) \quad (A.9)$$

where, Δx_{TG} is the distance to the target gap TG (with $TG \in \{\text{backward, adjacent, forward}\}$); l_{TG} is the effective gap length; δ_f^{TG} is a dummy for the presence of a front vehicle on the current lane; ΔV_{TG} is the relative gap speed; v_n is the individual specific error term; and ε^{TG} the random error term (Group 14, with 6 parameters: α^{fwd} , α^{bck} , $\beta_{\Delta x_{TG}}$, $\beta_{l_{TG}}$, β_{δ_f} , $\beta_{\Delta V_{TG}}$).

15. The origin and destination (OD) matrix is a key input on the variability of the simulation output. In this study the common stochasticity of the OD matrix was analysed by considering a common variance (σ_{OD}^2) for all OD paths and a distribution factor (β_{OD}), which determines the percentage of vehicles departing randomly (Poisson distribution instead of constant headway – Group 15, with 2 parameters: σ_{OD} , β_{OD})

Appendix B

Driving Behaviour Model

Parameters List & Numbering

Table B.1: List of MITSIMLab driving behaviour parameters

Param.	Description	Lower bound	Upper bound	Sensor calibrated	Trajectory calibrated
Reaction time (G1)					
1. μ_{RT}	Reaction time mean (s)	0.5	1.5	0.65	0.85
2. σ_{RT}	Reaction time standard deviation (s)	0.1	1.2	0.35	0.25
3. lb_{RT}	Reaction time lower bound (s)	0.0	0.5	0.35	0.30
4. ub_{RT}	Reaction time upper bound (s)	2.0	7.0	2.05	2.75
Car following CF (G2)					
5. Δx_{cf}^{min}	Minimum response distance (m)	2.0	6.0	5.5	2.5
6. h_{cf}^{lb}	Headway lower bound for CF (s)	0.2	0.8	0.5	0.8
7. α_{cf}^{acc}	Constant param. - CF acceleration	0.015	0.045	0.037	0.04
8. β_{cf}^{acc}	Speed param. - CF acceleration	0.1	0.9	0.593	0.74
9. γ_{cf}^{acc}	Headway param. - CF acceleration	-0.300	-0.125	-0.274	-0.205
10. δ_{cf}^{acc}	Density param. - CF acceleration	0.45	0.65	0.567	0.494
11. ρ_{cf}^{acc}	Speed difference param. - CF acc.	0.4	0.8	0.604	0.65
12. α_{cf}^{dec}	Constant param. - CF deceleration	-0.95	-0.02	-0.292	-0.374
13. γ_{cf}^{dec}	Headway param. - CF deceleration	-0.75	-0.05	-0.494	-0.65
14. δ_{cf}^{dec}	Density param. - CF deceleration	0.5	0.95	0.563	0.605
15. ρ_{cf}^{dec}	Speed difference param. - CF dec.	0.05	1.00	0.278	0.75
Free flow (G3)					
16. θ_{ff}	Density threshold - FF (v/km/lane)	15.0	23.0	22.0	18.55
17. α_{ff}	Constant param. - FF acceleration	0.05	0.45	0.129	0.296
18. β_{ff}	Constant param. - Desired speed	-25.0	-5.0	-5.254	-22.617
19. ρ_{ff}	Speed param. - Desired speed	0.50	0.75	0.726	0.746
20. δ_{ff}^k	Vehicle type param. - Desired speed	-2.00	-0.25	-1.055	-1.894
21. γ_{ff}	Density param. - Desired speed	5.0	10.0	5.425	8.936
Merging (G4)					
22. Δx_u	Upstream distance threshold (m)	25.0	100.0	76.5	99.277
23. Δx_d	Downstream distance threshold (m)	50.0	200.0	191.5	75.5
24. n_{max}	Max. number of vehicles in merging area	4.0	25.0	15	18
25. p_0	Probability of aggressive merging	0.1	0.6	0.585	0.187

Param.	Description	Lower bound	Upper bound	Sensor calibrated	Trajectory calibrated
Mandatory Lane change (G5)					
26. Δx_{lb}	Lower bound of distance to decision point	75.0	500.0	354	245
27. α_0^{MLC}	Constant param. for MLC	500.0	1000.0	987	1000
38. α_{nlc}^{MLC}	Number of lane changes param. for MLC	0.25	0.75	0.253	0.45
29. α_k^{MLC}	Density param. for MLC	0.75	1.25	0.804	0.75
30. Δt_{min}	Minimum time in lane in MLC (s)	0.75	1.50	1.120	1.05
Yield (G6)					
31. $p_{noyield}$	Prob. to yield if vehicle is not nosing	0.5	0.9	0.856	0.779
32. $p_{yesyield}$	Prob. to yield if vehicle is nosing	0.75	1.0	0.793	0.807
Nosing model (G7)					
33. α^{nos}	Constant param. - Nosing	-5.0	-2.5	-2.634	-4.050
34. $\beta_{\Delta V-}^{nos}$	Lead vehicle speed param. - Nosing	0.15	0.50	0.318	0.3611
35. λ^{nos}	Scale param. - Nosing	-0.06	-0.01	-0.028	-0.051
36. $\beta_{l_{\Delta x}}^{nos}$	Distance to critical decision point - Nosing	1.0	3.0	1.869	1.389
37. $\beta_{l_{gap}}^{nos}$	Sum of lead and lag gaps param. - Nosing	0.01	0.05	0.014	0.019
38. β_{nlc}^{nos}	Number of lane changes param. - Nosing	0.35	0.75	0.579	0.669
Nosing control (G8)					
39. t_{max}^{yield}	Maximum yielding time (s)	10.0	250.0	11	28
40. t_{max}^{nos}	Maximum waiting time before nosing (s)	15.0	200.0	32	19
41. Δx_{max}^{nos}	Maximum distance for nosing (m)	100.0	300.0	115	224
42. Δx_{min}^{nos}	Minimum distance for nosing (m)	10.5	25.0	15	12
Courtesy yielding probailities (G9)					
43. p_0^{cyield}	Prob. to yield to any vehicle	0.05	0.25	0.187	0.0549
44. p_1^{cyield}	Prob. to yield to up to one vehicle	0.5	0.9	0.677	0.881
45. p_2^{cyield}	Prob. to yield to up to two vehicles	0.05	0.20	0.112	0.172
46. p_3^{cyield}	Prob. to yield to up to three vehicles	0.01	0.05	0.016	0.013

Param.	Description	Lower bound	Upper bound	Sensor calibrated	Trajectory calibrated
Driver heterogeneity (G10)					
47. σ_{cf}^{acc}	Standard deviaton - CF acc. error term	0.5	1.5	1.25	1.10
48. σ_{cf}^{dec}	Standard deviaton - CF dec. error term	0.5	1.5	0.65	0.50
49. σ_{ff}	Standard deviaton - FF acc. error term	1.00	1.25	1.05	1.15
50. μ_{dv}^h	Headway threshold mean (s)	2.0	3.5	2.6	2.5
51. σ_{dv}^h	Headway threshold standard deviation	0.25	1.00	0.47	0.50
52. lb_{dv}^h	Headway threshold lower bound	0.0	0.5	0.50	0.50
53. ub_{dv}^h	Headway threshold upper bound	4.0	8.0	7.7	3.0
54. μ_{DS}	Desired speed add-on mean	-0.2	0.5	-0.13	0.26
55. σ_{DS}	Desired speed add-on standard deviation	0.025	0.25	0.02	0.19
Target gap acceleration (G11)					
56. β_{DP}	Desired position constant param.	0.50	0.75	0.655	0.735
57. α_g^{fwd}	Forward gap constant param.	0.2	0.6	0.547	0.526
58. β_D^{fwd}	Distance to desired position - fwd. gap	0.1	0.6	0.332	0.171
59. $\beta_{\Delta V_-}^{fwd}$	Positive speed difference - fwd. gap	0.03	0.10	0.030	0.034
60. $\beta_{\Delta V_+}^{fwd}$	Negative speed difference - fwd. gap	0.10	0.35	0.127	0.332
61. σ^{fwd}	Standard deviation - fwd. gap	0.25	0.75	0.482	0.564
62. α_g^{bck}	Backward gap constant param.	-0.75	-0.40	-0.453	-0.667
63. β_D^{bck}	Distance to desired position - bck. gap	-0.5	-0.2	-0.290	-0.231
64. $\beta_{\Delta V_-}^{bck}$	Positive speed diff. - bck. gap	0.05	0.10	0.096	0.080
65. $\beta_{\Delta V_+}^{bck}$	Negative speed diff. param.- bck. gap	-0.25	-0.05	-0.228	-0.192
66. σ^{bck}	Standard deviation - bck. gap	0.8	2.0	1.610	1.809
67. α_g^{adj}	Adjacent gap constant param.	0.05	0.20	0.157	0.065
68. σ^{aj}	Standard deviation - adj. gap	0.15	0.45	0.265	0.279
Critical gap model (G12)					
69. α^{lead}	Lead critical gap constant param.	0.5	2.0	1.358	1.373
70. $\beta_{\Delta V_-}^{lead}$	Negative speed difference - lead gap	-0.35	-0.1	-0.262	-0.285
71. $\beta_{\Delta V_+}^{lead}$	Positive speed difference param. - lead gap	-4.0	-1.5	-3.077	-2.643
72. σ^{lead}	Standard deviation error term - lead gap	0.75	1.75	1.162	1.684
73. α^{lag}	Lag critical gap constant param.	0.5	2.5	0.322	1.906
74. $\beta_{\Delta V_-}^{lag}$	Negative speed difference param. - lag gap	-0.15	0.00	-0.148	-0.128
75. $\beta_{\Delta V_+}^{lag}$	Positive speed difference param. - lag gap	0.2	0.7	0.210	0.319
76. σ^{lag}	Standard deviation error term - lag gap	0.5	1.0	0.607	0.936
77. ΔV_{max}	Maximum speed difference	2.0	6.0	2.2	5.3
Lane utility (G13)					
78. α^{CL}	Current lane constant param.	2.0	6.0	3.035	4.209

Param.	Description	Lower bound	Upper bound	Sensor calibrated	Trajectory calibrated
79. α^{RL}	Right lane constant param.	-0.5	-0.1	-0.485	-0.422
80. β_{RML}^{TL}	Right most lane dummy param.	-1.50	-0.75	-1.173	-1.350
81. $\beta_{V_i}^{TL}$	Front vehicle speed param.	0.03	0.10	0.061	0.095
82. β_b	Bus following dummy param.	-0.5	-1.5	-0.830	-1.298
83. $\beta_{\Delta x}^{TL}$	Front vehicle spacing param.	0.002	0.010	0.004	0.008
84. β_h	Heavy vehicle in target lane param.	-0.35	-0.15	-0.197	-0.270
85. β_k	Density in target lane param.	-0.015	-0.002	-0.015	-0.009
86. β_{tail}^{TL}	Tailgate dymmy param.	-5.50	-1.75	-3.017	-1.977
87. Δx_{floor}^{bck}	Back gap threshold for tailgate dummy (m)	5.0	15.0	7.25	13.0
88. k_{ceil}	Density threshold for tailgate dummy	15.0	23.0	21.5	16.6
89. $\beta_{nlc,1}$	One lane change required dummy param.	-3.5	-1.0	-1.631	-2.848
90. $\beta_{nlc,2}$	Two lane change required dummy param.	-6.5	-2.5	-6.336	-4.901
91. $\beta_{nlc,3}$	Each additional lane change required param.	-3.75	-1.25	-2.124	-2.750
92. β_{next}	Next exit, one lane change required param.	-2.00	-0.75	-1.46	-1.05
93. β_{add}	Next exit, each add. lanne change param.	-1.0	-0.5	-0.618	-0.6
94. θ_{MLC}	Distance to exit param.	-0.5	-0.15	-0.275	-0.309
Target gap (G14)					
95. α^{fwd}	Forward gap constant param.	-1.2	-0.3	-0.704	-0.413
96. α^{bck}	Backward gap constant param.	0.75	1.00	0.808	0.969
97. $\beta_{l_{TG}}$	Effective gap length param.	0.6	1.0	0.730	0.650
98. $\beta_{\Delta V_{TG}}$	Relative gap speed param.	-1.5	-1.0	-1.236	-1.188
99. $\beta_{\Delta x_{TG}}$	Distance to gap param.	-2.8	-1.8	-2.077	-2.425
100. β_{δ_f}	Front vehicle dummy param.	-2.2	-1.0	-1.614	-1.750
OD(G15)					
101. σ_{OD}^2	Variance of the OD matrix	0.0	0.15	0.139	0.087
102. β_{OD}	Distribution factor of the OD matrix	0.0	1.0	0.892	0.487

Table B.2: Numbering of parameters for the SA using loop-based data

Param.	Description	Variance based SA	Selected parameters
Reaction time (G1)			
1. μ_{RT}	Reaction time mean (s)	1	1
2. σ_{RT}	Reaction time standard deviation (s)	2	
3. lb_{RT}	Reaction time lower bound (s)	3	
4. ub_{RT}	Reaction time upper bound (s)	4	
Car following (G2)			
5. Δx_{cf}^{min}	Minimum response distance (m)	5	
6. h_{cf}^{lb}	Headway lower bound for CF (s)	6	
7. α_{cf}^{acc}	Constant param. - CF acceleration	7	2
8. β_{cf}^{acc}	Speed param. - CF acceleration	8	3
9. γ_{cf}^{acc}	Headway param. - CF acceleration	9	
10. δ_{cf}^{acc}	Density param. - CF acceleration	10	
11. ρ_{cf}^{acc}	Speed difference param. - CF acc.	11	
12. α_{cf}^{dec}	Constant param. - CF deceleration	12	4
13. γ_{cf}^{dec}	Headway param. - CF deceleration	13	5
14. δ_{cf}^{dec}	Density param. - CF deceleration	14	6
15. ρ_{cf}^{dec}	Speed difference param. - CF dec.	15	
Driver heterogeneity (G10)			
47. σ_{cf}^{acc}	Standard devaiiton - CF acc. error term	16	
48. σ_{cf}^{dec}	Standard devaiiton - CF dec. error term	17	
49. σ_{ff}	Standard devaiiton - FF acc. error term	18	
50. μ_{dv}^h	Headway threshold mean (s)	19	7
51. σ_{dv}^h	Headway threshold standard deviation	20	
52. lb_{dv}^h	Headway threshold lower bound	21	
53. ub_{dv}^h	Headway threshold upper bound	22	
54. μ_{DS}	Desired speed add-on mean	23	8
55. σ_{DS}	Desired speed add-on standard deviation	24	

Param.	Description	Variance based SA	Selected parameters
Lane utility model (G13)			
78. α^{CL}	Current lane constant param.	25	9
79. α^{RL}	Right lane constant param.	26	
80. β_{RML}^{TL}	Right most lane dummy param.	27	
81. $\beta_{V_l}^{TL}$	Front vehicle speed param.	28	
82. β_b	Bus following dummy param.	29	
83. $\beta_{\Delta x}^{TL}$	Front vehicle spacing param.	30	
84. β_h	Heavy vehicle in target lane param.	31	
85. β_k	Density in target lane param.	32	
86. β_{tail}^{TL}	Tailgate dymmy param.	33	
87. Δx_{floor}^{bck}	Back gap threshold for tailgate dummy (m)	34	
88. k_{ceil}	Density threshold for tailgate dummy	35	
89. $\beta_{nlc,1}$	One lane change required dummy param.	36	10
90. $\beta_{nlc,2}$	Two lane change required dummy param.	37	
91. $\beta_{nlc,3}$	Each additional lane change required param.	38	
92. β_{next}	Next exit, one lane change required param.	39	
93. β_{add}	Next exit, each add. lanne change param.	40	
94. θ_{MLC}	Distance to exit param.	41	11

Table B.3: Numbering of parameters for the SA using trajectory-based data

Param.	Description	quasi-OTEE	Variance based SA	Selected parameters
Reaction time (G1)				
1. μ_{RT}	Reaction time mean (s)	1	1	1
2. σ_{RT}	Reaction time standard deviation (s)	2	2	2
3. lb_{RT}	Reaction time lower bound (s)	3		
4. ub_{RT}	Reaction time upper bound (s)	4		
Car following CF (G2)				
5. Δx_{cf}^{min}	Minimum response distance (m)	5		
6. h_{cf}^{lb}	Headway lower bound for CF (s)	6	3	
7. α_{cf}^{acc}	Constant param. - CF acceleration	7		
8. β_{cf}^{acc}	Speed param. - CF acceleration	8		
9. γ_{cf}^{acc}	Headway param. - CF acceleration	9	4	
10. δ_{cf}^{acc}	Density param. - CF acceleration	10	5	
11. ρ_{cf}^{acc}	Speed difference param. - CF acc.	11		
12. α_{cf}^{dec}	Constant param. - CF deceleration	12	6	3
13. γ_{cf}^{dec}	Headway param. - CF deceleration	13		
14. δ_{cf}^{dec}	Density param. - CF deceleration	14	7	4
15. ρ_{cf}^{dec}	Speed difference param. - CF dec.	15		
Mandatory Lane change (G5)				
26. Δx_{lb}	Lower bound of distance to decision point	16		
27. α_0^{MLC}	Constant param. for MLC	17		
38. $\alpha_{n_{lc}}^{MLC}$	Number of lane changes param. for MLC	18		
29. α_k^{MLC}	Density param. for MLC	19		
30. Δt_{min}	Minimum time in lane in MLC (s)	20		
Nosing model (G7)				
33. α^{nos}	Constant param. - Nosing	21		
34. $\beta_{\Delta V_-}^{nos}$	Lead vehicle speed param. - Nosing	22		
35. λ^{nos}	Scale param. - Nosing	23		
36. $\beta_{l_{\Delta x}}^{nos}$	Distance to critical decision point - Nosing	24		
37. $\beta_{l_{gap}}^{nos}$	Sum of lead and lag gaps param. - Nosing	25		
38. $\beta_{n_{lc}}^{nos}$	Number of lane changes param. - Nosing	26		
Courtesy yielding probabilities (G9)				
43. p_0^{cyield}	Prob. to yield to any vehicle	27		
44. p_1^{cyield}	Prob. to yield to up to one vehicle	28		

Param.	Description	quasi-OTEE	Variance based SA	Selected parameters
$45.p_2^{cyield}$	Prob. to yield to up to two vehicles	29		
$46.p_3^{cyield}$	Prob. to yield to up to three vehicles	30		
Driver heterogeneity (G10)				
$47.\sigma_{cf}^{acc}$	Standard deviaton - CF acc. error term	31		
$48.\sigma_{cf}^{dec}$	Standard deviaton - CF dec. error term	32		
$49.\sigma_{ff}$	Standard deviaton - FF acc. error term	33		
$50.\mu_{dv}^h$	Headway threshold mean (s)	34	8	
$51.\sigma_{dv}^h$	Headway threshold standard deviation	35	9	
$52.lb_{dv}^h$	Headway threshold lower bound	36		
$53.ub_{dv}^h$	Headway threshold upper bound	37		
$54.\mu_{DS}$	Desired speed add-on mean	38	10	5
$55.\sigma_{DS}$	Desired speed add-on standard deviation	39	11	6
Lane utility (G13)				
$78.\alpha^{CL}$	Current lane constant param.	40	12	
$79.\alpha^{RL}$	Right lane constant param.	41		
$80.\beta_{RML}^{TL}$	Right most lane dummy param.	42		
$81.\beta_{V_i}^{TL}$	Front vehicle speed param.	43		
$82.\beta_b$	Bus following dummy param.	44		
$83.\beta_{\Delta x}^{TL}$	Front vehicle spacing param.	45		
$84.\beta_h$	Heavy vehicle in target lane param.	46		
$85.\beta_k$	Density in target lane param.	47		
$86.\beta_{tail}^{TL}$	Tailgate dymmy param.	48	13	7
$87.\Delta x_{floor}^{bck}$	Back gap threshold for tailgate dummy (m)	49		
$88.k_{ceil}$	Density threshold for tailgate dummy	50		
$89.\beta_{nlc,1}$	One lane change required dummy param.	51	14	8
$90.\beta_{nlc,2}$	Two lane change required dummy param.	52		
$91.\beta_{nlc,3}$	Each additional lane change required param.	53		
$92.\beta_{next}$	Next exit, one lane change required param.	54		
$93.\beta_{add}$	Next exit, each add. lanne change param.	55		
$94.\theta_{MLC}$	Distance to exit param.	56	15	9

Appendix C

Changes in MITSIM code

Simultaneous nosing was detected for the A44 case study. When the demand was very high (congested situations), and there were relatively short links between two interchanges, vehicles would have a higher difficulty in finding gaps to change lanes. the following module was added to the `TS_Vehicle::executeLaneChanging()` function in the `TS_LCModel.cc` file:

```
(...)
if (status(STATUS_LEFT)) {
    setFlag(FLAG_NOSING_LEFT);
} else {
    setFlag(FLAG_NOSING_RIGHT); }
// Start CLA 12/2011 - This fix the bug of the simultaneous
// nosing vehicles in side lanes causing deadlock
if (bv && bv->macroLeading_ == this && bv->flag(FLAG_NOSING) && dis2stop_ <=
theParameter->lcMinNosingDis()) {
    // Let me go
    bv->yieldVehicle_ = this;
    if (status(STATUS_LEFT)) {
        bv->unsetFlag(FLAG_NOSING); bv->setFlag(FLAG_YIELDING_RIGHT);
    } else {
        bv->unsetFlag(FLAG_NOSING); bv->setFlag(FLAG_YIELDING_LEFT);
    }
}
if (av && av->macroTrailing_ == this && av->flag(FLAG_NOSING) && dis2stop_ <=
theParameter->lcMinNosingDis()) {
    // Let him go
    yieldVehicle_ = av;
    if (status(STATUS_LEFT)) {
        unsetFlag(FLAG_NOSING); setFlag(FLAG_YIELDING_LEFT);
    } else {
        unsetFlag(FLAG_NOSING); setFlag(FLAG_YIELDING_RIGHT);
    }
}
// End CLA 12/2011
```

To extract the different detailed traffic variables presented in Chapter 3, a few changes were made in the trajectory output generation code. Five functions to help in the computation of these variables were declared in the `TS_Vehicle.h` file:

```
(...)
// Start CLA 2013 - Additional functions for trajectory output
float giveSpeedLead();
float retrieveLagGap();
float retrieveLeadGap();
float retrieveLagSpeed();
float retrieveLeadSpeed();
// End CLA 12/2011
```

These five functions allowing to compute the speed of the leading vehicle, the lag and lead gaps and vehicle speeds were defined in the `TS_Vehicle.cc` file:

```

(...)
// EDIT CLA-2103: Functions to Load data into trajectory file
// load speed of vehicle ahead
float
TS_Vehicle::giveSpeedLead()
{
    TS_Vehicle *front;
    float v0;
    if (leading_) {
        v0 = (leading_>currentSpeed_);
    } else if (nextLane_ && (front = nextLane_>lastVehicle())) {
        v0 = (front->currentSpeed_);
    } else {
        v0 = 0;
    }
    return (v0);
}
float
TS_Vehicle::retrieveLagGap()
{
    float bheadway=0; // lag headway
    // TARGET LANE
    TS_Lane *plane;
    if (status(STATUS_LEFT)) {
        plane = lane_>left();
    } else if (status(STATUS_RIGHT)) {
        plane = lane_>right();
    } else {
        return (bheadway); // No request for lane change
    }
    if (!plane) return (bheadway);
    if (isInIncidentArea(plane)) return (bheadway);
    // LAG VEHICLE (do not have to be in same segment)
    TS_Vehicle* bv = findFrontBumperFollower(plane);
    // LAG HEADWAY
    if (bv) {
        bheadway = bv->gapDistance(this);
    }
    return (bheadway);
}
float
TS_Vehicle::retrieveLeadGap()
{
    float aheadway=0; // leading headway
    // TARGET LANE
    TS_Lane *plane;
    if (status(STATUS_LEFT)) {
        plane = lane_>left();
    } else if (status(STATUS_RIGHT)) {
        plane = lane_>right();
    } else {
        return (aheadway); // No request for lane change
    }
    if (!plane) return (aheadway);
    if (isInIncidentArea(plane)) return (aheadway);
    // LEADING VEHICLE (do not have to be in same segment)
    TS_Vehicle* av = findFrontBumperLeader(plane);
    // LEADING VEHICLE IN TARGET LANE (must be in same segment).
    TS_Vehicle* front;
    if (av) {
        if (av->segment() == segment()) {
            front = av;
        } else {
            front = NULL;
        }
    } else {
        front = NULL;
    }
    // LEADING HEADWAY
    if (av) {
        aheadway = this->gapDistance(av);
    }
}

```

```

}
return (aheadway);
}
float
TS_Vehicle::retrieveLagSpeed()
{
float bspeed=0; // lag speed
// TARGET LANE
TS_Lane *plane;
if (status(STATUS_LEFT)) {
plane = lane_->left();
} else if (status(STATUS_RIGHT)) {
plane = lane_->right();
} else {
return (bspeed); // No request for lane change
}
if (!plane) return (bspeed);
if (isInIncidentArea(plane)) return (bspeed);
// LAG VEHICLE (do not have to be in same segment)
TS_Vehicle* bv = findFrontBumperFollower(plane);
// LAG Speed
if (bv) {
bspeed = bv->currentSpeed_;
}
return (bspeed);
}
float
TS_Vehicle::retrieveLeadSpeed()
{
float aspeed=0; // leading speed
// TARGET LANE
TS_Lane *plane;
if (status(STATUS_LEFT)) {
plane = lane_->left();
} else if (status(STATUS_RIGHT)) {
plane = lane_->right();
} else {
return (aspeed); // No request for lane change
}
if (!plane) return (aspeed);
if (isInIncidentArea(plane)) return (aspeed);
// LEADING VEHICLE (do not have to be in same segment)
TS_Vehicle* av = findFrontBumperLeader(plane);
// LEADING VEHICLE IN TARGET LANE (must be in same segment).
TS_Vehicle* front;
if (av) {
if (av->segment() == segment()) {
front = av;
} else {
front = NULL;
}
} else {
front = NULL;
}
// LEADING Speed
if (av) {
aspeed = av->currentSpeed_;
}
return (aspeed);
}
// Save trajectory record
void TS_Vehicle::saveTrajectoryRecord(ofstream &os)
{
float x = distance()/theParameter->lengthFactor();
float odometer = (mileage_ + segment()->length() - distance()) /
theParameter->lengthFactor(); // total distance traveled from origin (Angus)
if (theEngine->chosenOutput(OUTPUT_RECT_TEXT)) {
float t = theSimulationClock->currentTime();
os << Fix(t, (float)0.1);
} // time
// EDIT - CLA 2013

```

```

float gaphead=0;
if (gapDistance()<500){
gaphead=gapDistance();
}
// Added additional output for safety estimation
os << endc << code_ << endc // veh id
<< segment()->code() << endc // seg id
<< lane()->code() << endc // lane id
<< Fix(distance(), (float)0.1) << endc // dist from US seg end
<< Fix(currentSpeed(), (float)0.01) << endc // speed
<< Fix(accRate(), (float)0.001) << endc // acceleration
<< Fix(gaphead, (float)0.1) << endc // headway
<< Fix(giveSpeedLead(), (float)0.01) << endc // front speed
<< makeLaneChangingDecision() <<endc // LC status
<< Fix(retrieveLagGap(), (float)0.1) <<endc // Lag Gap
<< Fix(retrieveLeadGap(), (float)0.1) <<endc // Lead Gap
<< Fix(retrieveLagSpeed(), (float)0.01) <<endc // Lag speed
<< Fix(retrieveLeadSpeed(), (float)0.01) <<endc // Lead Speed
<< type() << endl; // vehicle type
}

// End CLA 2013

```